Biodegradable solvent cast films and solution electrospun meshes for the prevention of postsurgical adhesions

Dissertation zur Erlangung des naturwissenschaftlichen Doktorgrades der Julius-Maximilians-Universität Würzburg

vorgelegt von

Martina Keßler

aus Dachau

Würzburg 2015

Eingereicht bei der Fakultät für Chemie und Pharmazie am

_____

Gutachter der schriftlichen Arbeit

1. Gutachter: _____

2. Gutachter: _____

Prüfer des öffentlichen Promotionskolloquiums

1. Prüfer: _____

2. Prüfer: _____

3. Prüfer: _____

Datum des öffentlichen Promotionskolloquiums

_____

Doktorurkunde ausgehändigt am

_____

This work was conducted from February 2011 until October 2012 at the Department of Pharmaceutical Technology of the University of Regensburg and from November 2012 until June 2015 at the Department for Functional Materials in Medicine and Dentistry of the University Hospital of Würzburg under the supervision of Prof. Dr. Achim Göpferich and Prof. Dr. Jürgen Groll.

Angenehm sind die erledigten Arbeiten.
Marcus Tullius Cicero

Contents

Abbreviations and symbols

$	US Dollar
%	percent
[η]	intrinsic viscosity
£	British Pound
€	Euro
°	degree
°C	degree Celsius
µg	microgram
µL	microliter
µm	micrometer
4arm140, 4armPEG10k-*b*-PLA140k	4arm star-shaped poly(ethylene glycol)-*block*-poly(D, L-lactide)with PEG block of 10kDa and overall 140kDa PLA content
4arm70, 4armPEG10k-*b*-PLA70k	4arm star-shaped poly(ethylene glycol)-*block*-poly(D, L-lactide)with PEG block of 10kDa and overall 70kDa PLA content
4armPEG	4arm star-shaped poly(ethylene glycol)
8arm140, 8armPEG10k-*b*-PLA140k	8arm star-shaped poly(ethylene glycol)-*block*-poly(D, L-lactide)with PEG block of 10kDa and overall 140kDa PLA content
8arm70, 8armPEG10k-*b*-PLA70k	8arm star-shaped poly(ethylene glycol)-*block*-poly(D, L-lactide)with PEG block of 10kDa and overall 70kDa PLA content
8armPEG	8arm star-shaped poly(ethylene glycol)
Å	Ångstrom
ANOVA	analysis of variance
ASTM	American Society for Testing and Materials
c	concentration
CA	contact angle
$CDCl_3$	deuterated chloroform
cm	centimeter

CMC	carboxymethyl cellulose
COX-2	cyclooxygenase-2
D	shear rate
Da	Dalton
dL	deciliter
DMEM	Dulbecco's Modified Eagle Medium
DMF	N, N-dimethylformamide
DMSO	dimethyl sulfoxide
dn/dc	refractive index increment
DSC	differential scanning calorimetry
Đ	dispersity
E. coli	Escherichia coli
e.g.	exempli gratia, for example
FCS	fetal calf serum
FDA	Food and Drug Administration
g	gram
GPa	gigapascal
GPC	gel permeation chromatography
h	hour
HCl	hydrochloric acid
HEPES	4-(2-Hydroxyethyl)piperazine-1-ethanesulfonic acid
hPa	hectopascal
HPLC	high performance liquid chromatography
IU	international units
K	Kelvin
KCl	potassium chloride
kDa	kilodalton
kg	kilogram
KH_2PO_4	potassium dihydrogen phosphate

kV	kilovolt
L	liter
lin130, PLA65k-*b*-PEG10k-*b*-PLA65k	triblock poly(L-lactide-co-D, L-lactide)-*block*-poly(ethylene glycol)-*block*-poly(L-lactide-co-D, L-lactide) with PEG block of 10 kDa and overall PLA content of 130 kDa
lin70, PLA35k-*b*-PEG10k-*b*-PLA35k	triblock poly(L-lactide-co-D, L-lactide)-*block*-poly(ethylene glycol)-*block*-poly(L-lactide-co-D, L-lactide) with PEG block of 10 kDa and overall PLA content of 70 kDa
lin70rac	triblock poly(D,L-lactide)-*block*-poly(ethylene glycol)-*block*-poly(D, L-lactide) with PEG block of 10 kDa and overall PLA content of 70 kDa
lin90, PLA45k-*b*-PEG10k-*b*-PLA45k	triblock poly(L-lactide-co-D, L-lactide)-*block*-poly(ethylene glycol)-*block*-poly(L-lactide-co-D, L-lactide) with PEG block of 10 kDa and overall PLA content of 90 kDa
LMWH	low molecular weight heparin
M	molar
m	mass
MeOH	methanol
mg	milligram
MHz	megahertz
MIC	minimum inhibitory concentration
min	minute
mL	milliliter
mM	millimolar
mm	millimeter
M_n	number average molecular weight
MPa	megapascal
mPEG-PLGA	methoxy poly(ethylene glycol)-poly(L-lactide-co-glycolide)
M_w	weight average molecular weight
N	Newton

Na_2HPO_4	disodium hydrogen phosphate
NaCl	sodium chloride
NaN_3	sodium azide
NaOH	sodium hydroxide
nm	nanometer
NMR	nuclear magnetic resonance
NSAID	non-steroidal anti-inflammatory drugs
PAI	plasminogen activator inhibitors group
PBS	phosphate buffered saline
PCL	poly(ε-caprolactone)
PDLA	poly(D-lactide)
PDLLA	poly(D, L-lactide)
PEG	poly(ethylene glycol)
PenStrep	Penicillin Streptomycin
pH	negative logarithmic value of the hydrogen ion concentration
Ph.Eur.	Pharmacopoea Europaea, European Pharmacopoeia
PHB	poly(β-hydroxybutyrate)
pK_a	logarithmic constant of the acid dissociation constant
PLA	polylactide, poly(lactic acid)
PLGA	poly(lactide-co-glycolide)
PLLA	poly(L-lactide)
ppm	parts per million
PS	polystyrene
PTFE	polytetrafluoroethylene
PTMC	poly(1,3-trimethylene carbonate)
PVA	poly(vinyl alcohol)
PVAc	poly(vinyl acetate)
r	radius
RID	refractive index detector

ROP	ring opening polymerization
R_θ	Rayleigh ratio
s	second
SCAR study	Surgical and Clinical Adhesion Research study
SEM	scanning electron microscopy
SSP	solid state polymerization
Staph. aureus	Staphylococcus aureus
TFA	trifluoroacetic acid
T_g	glass transition temperature
tPA	tissue plasminogen activator
uPA	urokinase-like plasminogen activator
UV	ultraviolet
UV-VIS	ultraviolet-visible
V	volume
w_d	dry weight
w_i	initial weight
WST-1	water soluble tetrazolium salt, 2-(4-Iodophenyl)-3-(4-nitrophenyl)-5-(2,4-disulfophenyl)-2H-tetrazolium monosodium salt
wt%	percentage by weight
w_w	wet weight
η	viscosity
π	pi, ratio of a circle's circumference to its diameter

Chapter 1
Scope of the thesis

This chapter gives a short introduction to the background and aims of this thesis as well as an overview over the content of the particular chapters.

Intraperitoneal adhesions are fibrous tissue bands that connect usually separated tissues. These adhesions form as a consequence of trauma, inflammation or surgical interventions.[1] Since up to 93 % of the patients undergoing one or multiple operations develop intra-abdominal adhesions,[2–3] adhesion formation constitutes a huge postoperative problem. Most of the occurring adhesions are asymptomatic, however, the evolving problems for the few concerned patients are severe. The consequences include chronic abdominal and pelvic pain, small bowel obstructions as well as infertility in women and an increased risk of ectopic pregnancy. Moreover, surgical re-entries are aggravated by adhesions even if they cause no obstructions or other symptoms in the patient. Besides, due to the high incidence of adhesions, the costs for adhesiolysis are enormous emphasizing the need for potent and ideally cost-effective strategies for adhesion prevention. The most important factor in adhesion reduction is a neat surgical technique. A reduction of trauma and inflammation can be achieved by avoiding desiccation, minimizing tissue handling, reducing foreign material and using hemostatic agents. Therapeutic approaches include pharmacological therapy as well as barrier devices which physically separate the affected tissues. While until now the success of the application of pharmacological active substances has been limited, the implantation of physical barriers seems more promising. However, despite a broad variety of materials (natural and synthetic), material compositions and device morphologies on the market or under investigation, the ideal barrier device still has not yet been found.[1,4–8]

The scope of this thesis was the development of a synthetic barrier device made of modified poly(lactide) [PLA]. Solid PLA films (SurgiWrap®) are already successfully in clinical use due to the good biocompatibility and the biodegradability of the material resulting in non-toxic degradation products since lactic acid is naturally part of the metabolic circles of the human body. Considering the brittleness and stiffness of the films, the long degradation time of several months as well as the need for suturing, it gets clear that there is still the demand for optimization concerning handling by the surgeon and performance within the patient's body, though. Through a copolymerization with the biocompatible poly(ethylene glycol) [PEG], an improvement of the mechanical properties as well as the adjustment of the degradation to a more appropriate time frame was intended. Since PEG acts as plasticizer for PLA, softer and more flexible films should be obtained and the hydrophilicity of PEG should lead to a higher

water uptake and consequently shorter degradation times. Not only linear PLA-PEG-PLA triblock copolymers but also copolymers with branched PEG cores were synthesized since especially star-shaped block copolymers appear promising materials to tailor the barrier properties due to a supposed better anchorage of PEG resulting from more connecting points and consequently less washout effect, which potentially leads to a slower change of their properties during degradation.[9] Apart from investigations on solid films, PLA and the synthesized PEG-PLA copolymers were also processed via solution electrospinning. The resulting meshes were examined regarding effects of polymer architecture and composition on their properties as well. While the general advantage of the massive films towards meshes might lie in an easier handling for the surgeon, for solution electrospun meshes less polymer is required and consequently implanted into the patient than for films of similar thickness. Moreover, their erosion results in softer fragments potentially causing less tissue irritations and inflammation. In addition, the porous morphology could be further beneficial regarding permeability for relevant molecules since penetration of nutrients to and waste removal from the affected locations is important for wound healing.[10] Cell proliferation and cell adhesion tests were performed to evaluate the influence of material composition and morphology on the behavior of cells. With the intention to combine the prevention strategy barrier device with the approach of pharmacological treatment and to reduce infections and consequently inflammation, electrospun meshes and solvent cast films were loaded with the antibacterial drug triclosan and drug release as well as antibacterial efficacy was investigated. Since most of the currently available anti-adhesion barriers need to be fixed by suturing which additionally induces adhesion formation,[11] a further requirement on an ideal barrier is to stay in place without fixation. To achieve this, bilateral membranes with mucoadhesive alginate on one side were prepared and investigated.

Chapter 2 gives an overview over the pathomechanisms and consequences of adhesion formation as well as over prevention strategies. Furthermore, an introduction to the theoretical background of the used polymers, their properties and their processability to films and electrospun meshes is provided. The materials used for the conducted experiments and a precise description of the implementation of the experimental methods can be found in ***Chapter 3***. In ***Chapter 4,*** the synthesized PEG-PLA copolymers as well as the also used PLA

(Resomer® LR708) are characterized. ***Chapter 5*** summarizes the results of the experiments with solid polymer films. Thereby, the outcomes of contact angle measurements, swelling and degradation studies, mechanical tests as well as of an *in vitro* release study and an agar diffusion test with triclosan loaded films are shown and discussed. The establishment of an appropriate solution electrospinning process for the investigated polymers, the results of the experiments with the established meshes and a comparison of the obtained mesh properties with those of the films regarding surface properties, swelling, degradation, mechanical testing and drug release are presented in ***Chapter 6.*** Moreover, the outcomes of cell proliferation and cell adhesion tests with meshes and films are discussed. In ***Chapter 7,*** the potential benefit of solution electrospun meshes as cohesion promoter for bilateral membranes with one smooth PLA side and one bioadhesive alginate side is outlined. The results of the investigations concerning the processability, cohesion and bioadhesion of bilayered and trilayered bilateral membranes are summarized and discussed. Finally, ***Chapter 8*** gives a brief summary of the outcomes of this work and an outlook on future perspectives.

Chapter 2
Theoretical background

In this chapter, the pathomechanisms as well as the consequences of the formation of intraperitoneal adhesions are outlined and general strategies for their prevention are presented. Furthermore, the theoretical background to the polymers used in this work, their processing to films as well as electrospun meshes and further modifications is given.

2.1 Intraperitoneal adhesions

2.1.1 Peritoneal wound healing and adhesion formation

Adhesions are abnormal fibrous connections between tissue surfaces which are usually separated. The formation of peritoneal adhesions (***Figure 2.1***) can have various origins, for example be congenital or caused by inflammation. In most cases, however, adhesions are induced by tissue trauma through surgical interventions and actually occur in up to 93 % of the patients who underwent one or multiple operations as found in a post-mortem[2] and in a prospective study.[3] Until now, the pathomechanism is not known in detail yet. Generally, it is believed that adhesions develop due to a reduced fibrinolytic activity in the peritoneal cavity compared to normal wound healing so that an undesired fibrin clot persists and further on leads to the various possible complications.

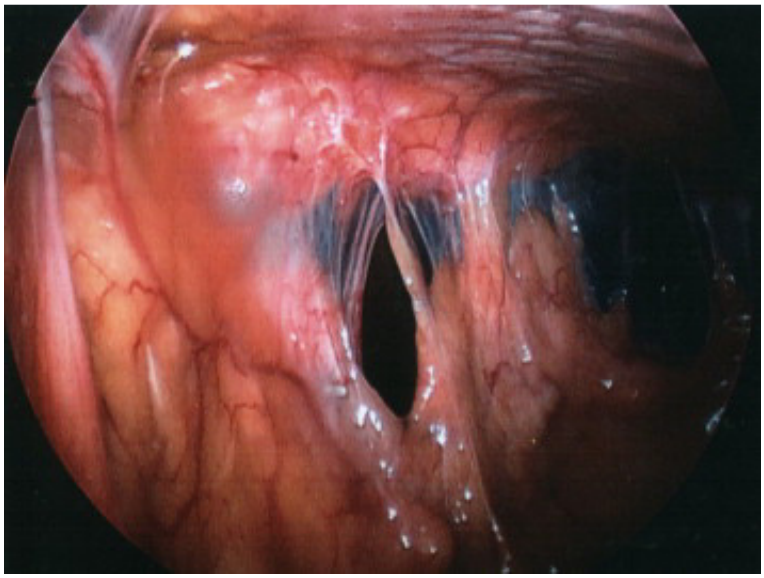

Figure 2.1 *Vascularized abdominal wall adhesions. (Reprinted from lit.[12] with permission from Elsevier)*

The intact peritoneum is a serous membrane which covers the organs and walls of the abdominal and pelvic cavity and which is composed of a monolayer of mesothelial cells on a basal membrane and an underlying vascularized loose connective tissue. The mesothelial cells on top are responsible for the secretion of peritoneal liquid to ensure unrestricted gliding of adjacent tissues within the peritoneal cavity and for the transport of molecules between the peritoneal cavity and the blood circulation.[1,5,13] When the peritoneum

experiences damage these functions are no longer guaranteed and the mechanisms of wound healing come into effect. In contrast to wound healing of the skin, which starts from the edge of the wound[14] and thus the healing time depends on the size of the injury, wound healing of the peritoneum starts from several places all over the wound area and consequently results in a newly formed mesothelial cell layer within five to ten days regardless of the initial size of the injury.[15–17] A damage of the peritoneum generally leads to an inflammatory reaction as well as to the initiation of the coagulation cascade resulting in fibrin deposition[18] (***Figure 2.2***). The fibrin together with leukocytes, erythrocytes, platelets, clotting and growth factors forms a temporary fibrin gel matrix[7,19] which provisorily closes the wound. Under normal conditions, the fibrin gel matrix is degraded and removed within 72 hours by the fibrinolytic activity of the peritoneum, which is mainly driven by the activity of tissue plasminogen activator [tPA]. At the same time the repair of the damaged peritoneum to a durable intact cellular state occurs mainly under the influence of macrophages without an ensuing development of adhesions.[5,20] In case of ischaemia or larger damage like after surgery, the fibrinolytic activity of the peritoneum is reduced and the fibrin matrix remains in place. The persisting fibrin gel matrix can then result in sticky linkages between adjacent tissues. The migration of various cells like fibroblasts into the fibrous clot entailing the building of a collagenous matrix, vascularization and innervation finally leads to highly organized mature adhesions,[1,21] which can only be lysed by surgical dissection. According to studies in animals and humans, the reduced fibrinolytic activity in affected patients can be attributed to less tPA on the affected sites due to a reduced secretion and additionally to an enhanced activity of plasminogen activator inhibitors [PAI] which inhibit tPA and urokinase-like plasminogen activator [uPA] by binding.[20]

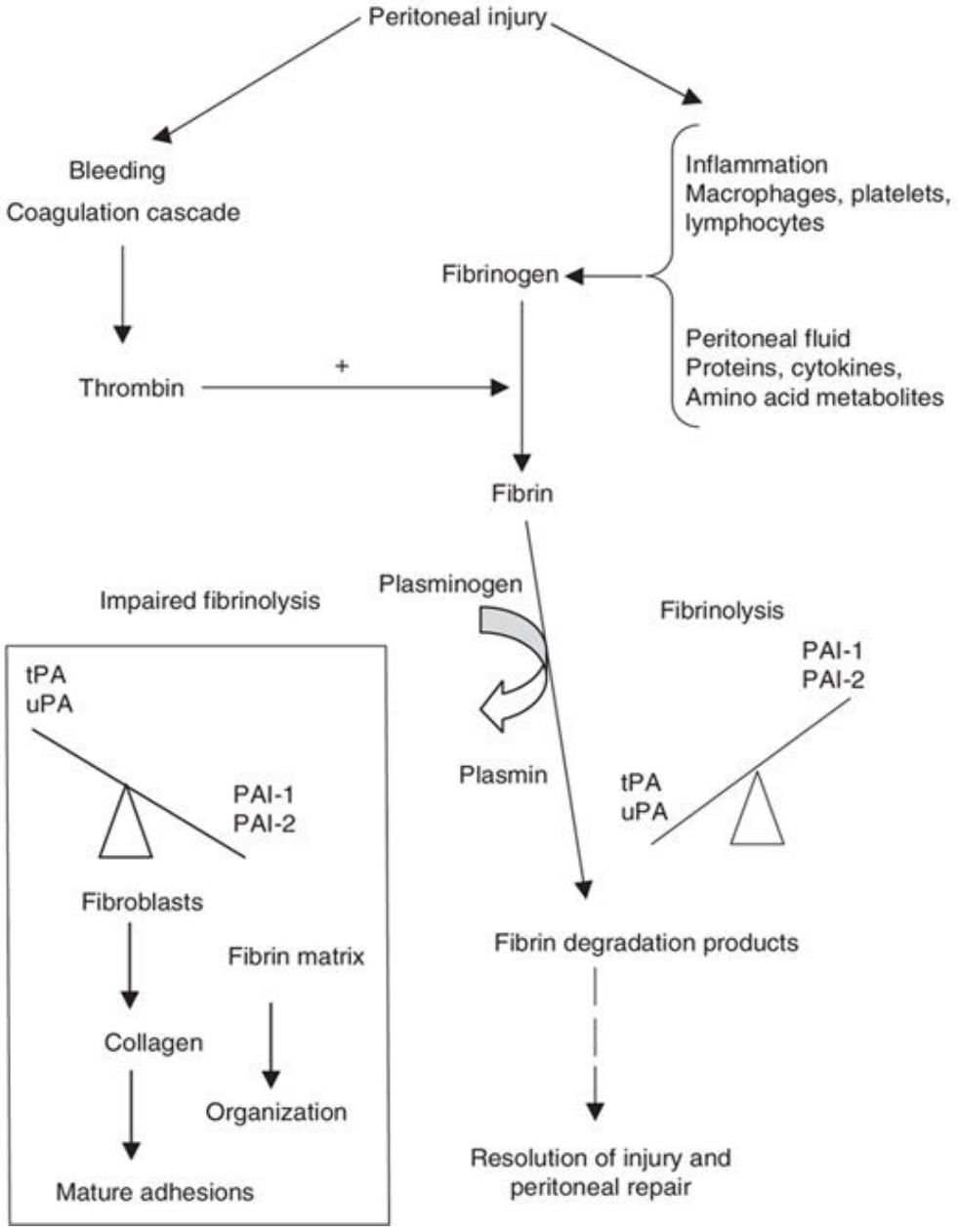

Figure 2.2 *Peritoneal wound healing and adhesion formation.*
PAI-1: plasminogen activator inhibitors group 1; tPA: tissue plasminogen activator; uPA: urokinase-like plasminogen activator.
(Reprinted from lit.[20]. © Canadian Medical Association (2007). This work is protected by copyright and the making of this copy was with the permission of the Canadian Medical Association Journal (www.cmaj.ca) and Access Copyright. Any alteration of its content or further copying in any form whatsoever is strictly prohibited unless otherwise permitted by law)

2.1.2 Adhesion-related consequences

Most occurring adhesions are asymptomatic, however, the few people experiencing consequences suffer from severe problems. In fact, it was found that adhesions are the most frequent cause of small bowel obstructions.[7,22–23] The obstructions arise both from adhesions connecting the small bowel with the small bowel itself and from adhesions between the small bowel and other adjacent peritoneal tissues.[3] Adhesions are also responsible for complications in the reproductive tract of women such as ectopic pregnancy and 15 % to 20 % of the cases of female infertility. Peritubal and intratubal adhesions can reduce the motility of the fallopian tube and the transportability of the ovum to the uterus.[19] Moreover, intrauterine adhesions can lead to obstructions of the tubal ostia of the uterine cavity and also reduce the endometrium necessary for the nidation of the embryo.[8] The role of adhesions as a cause of chronic abdominal and pelvic pain is controversially discussed since studies could not supply unambiguous results yet. Surgical adhesiolysis was found to relieve pain, however, not necessarily more than diagnostic surgery alone. In addition, no relationship between the severity of adhesions and the intensity of pain could be found.[8,24-27] Kresch et al.[28] suggested that adhesions which reduce the motility of pelvic organs rather result in pelvic pain than adhesions without that effect. The impact both on the patients' health with increased morbidity and on the amount of work for surgeons and healthcare providers was demonstrated by several clinical studies which investigated hospital readmissions related to adhesions.[29–32] In the Surgical and Clinical Adhesion Research [SCAR] study[29–30] hospital readmissions within ten years following open abdominal or pelvic operations were examined showing that more than 5 % of the readmissions were directly related to adhesions. Regarding only the open gynecological procedures in 8849 women,[30] the highest readmission risk was assessed after surgery on the ovary (7 %). The SCAR-3 study[32] revealed a 5 % adhesion-related risk of readmission after lower abdominal surgery (excluding appendicectomy) within five years after surgical intervention. Thereby, the highest readmission risk was found for patients who underwent panproctocolectomy (15.4 %) or ileostomy surgery (10.6 %). Moreover, patients younger than 60 years showed a higher readmission risk than older patients. Even if the present adhesions from previous surgery do not cause pain or result in other symptoms, they still increase the surgical workload when it comes to surgical reentries. A required adhesiolysis

prior to the actual surgical procedure is time consuming and significantly prolongs the operation time by a median of 18 minutes.[33]

The economic consequences of the adhesion-related hospital stays were put into figures for different countries. Ray et al.[34] calculated the total financial burden of hospitalization and surgeon charges for adhesiolysis in the USA in the year 1994 with $ 1.3 billion, which was less than in the year 1988 ($ 1.44 billion in total, thereof alone $ 1.2 billion for adhesiolysis in the lower abdomen). The difference cannot be attributed to a decrease of the hospitalization rate, though, but to a shorter average time of the hospital stays in 1994. Tingstedt et al.[35] estimated expenses of € 39.9 million to € 59.5 million per year for adhesion-related treatments in Sweden. This estimation was based on an extrapolation of the costs for selected patients with adhesion-related small bowel obstructions in the Lund University Hospital to the whole of Sweden. The calculated expenses thereby included the costs for anesthesia, surgery, ward, radiology and outpatient care. A study at Colchester General Hospital (Colchester) and Joyce Green Hospital (Dartford) in the UK from Menzie et al.[36] revealed average expenses of £ 4677.41 per operative treatment and £ 1606.15 per non-operative treatment per patient with adhesion-related small bowel obstruction. Moreover, they noted that roughly 2 % of the annual total bed occupancy of an average district general hospital could be ascribed to these adhesion-related cases. More recent numbers are lacking, however, both these financial calculations and the impairments to the patients' health, which the formation of adhesions bring along, make clear the importance to find potent strategies for the prevention of postsurgical adhesions, especially in high-risk patients as well as for complicated surgical procedures.

2.1.3 Strategies for the prevention of postsurgical adhesions

2.1.3.1 Surgical technique

A neat surgical technique, which keeps the inflicted trauma to the peritoneum to a minimum, is essential to reduce the formation of adhesions. Minimizing trauma can be achieved by careful tissue handling, the avoidance of desiccation and, in consideration of the above-described theory of adhesion formation, a best possible limitation of factors leading to or enhancing the activation of the coagulation cascade and an inflammatory reaction.[4] Thus, it is highly recommended to avoid blood and ischemia in the peritoneal cavity by putting surgical tools (clamps, retractors, forceps) only on locations intended for later dissection, by non-closure of the peritoneum as well as by the implementation of adequate hemostasis.[19] Moreover, exposure to foreign bodies like glove powder,[37–38] suture materials, gauze lint or substances from the digestive tract should be minimized to reduce inflammation and consequently adhesion formation.[39] The question if laparascopy results in less adhesion formation compared to open surgery is not fully resolved yet because there is no standardized system to score adhesions, which aggravates the evaluation and comparison of studies. Theoretically, and also supported by several studies,[40–42] laparoscopic procedures should be advantageous compared to open surgery due to reduced trauma by smaller incisions and more gentle tissue handling and due to reduced foreign body exposure and less desiccation owing to a closed abdominal cavity.[43] However, it was also shown that the pneumoperitoneum generated during laparoscopy can lead to a damage of the peritoneum promoting adhesion formation.[44–45]

2.1.3.2 Pharmacological treatment

Pharmacological treatment is one of the main research approaches with regard to adhesion prevention. Based on the underlying pathomechanism of adhesion formation, investigations are mainly directed to anti-inflammatory drugs, fibrinolytics and anticoagulants. As anti-inflammatory drugs, corticosteroids[46–48] as well as different classical non-steroidal anti-inflammatory drugs [NSAID][49–51] and selective cyclooxygenase-2 [COX-2] inhibitors[52–53] were tested. These agents showed some efficacy in animals, however, their clinical use is restricted due to the increased risk of bleeding related to NSAIDs and the property of corticosteroids to also diminish wound healing.[6] Fibrinolytics such as the plasminogen

activators streptokinase, urokinase and alteplase successfully reduced adhesion formation in animals and hemorrhages occurred only in rare cases.[54–60] Although there have been done some promising trials in humans, further research and controlled clinical trials are necessary to assess the pharmacokinetics of these agents after intraperitoneal application and their influence on postoperative bleeding and wound healing.[60–61] Heparin and low molecular weight heparin [LMWH] were also under investigation since their anticoagulant effect prevents the formation of fibrin clots and consequently should theoretically also prevent the formation of adhesions. Some preventive effects could be observed in animal studies,[62–64] however, the few human trials with heparin solutions did not result in a reduction of adhesion formation in comparison to the control group.[65] Moreover, the application of anticoagulants is always accompanied by an increased risk of intra-abdominal bleeding.[63] Apart from drugs directly associated with the pathways of adhesion formation, various other agents like growth factors and growth factor inhibitors were investigated with regard to wound healing and modulation of inflammation or fibrotic processes. Antibiotics were administered systemically as well as locally with varying success to reduce peritoneal inflammation due to bacterial contaminations associated with the surgical entry or the reason of the surgical procedure.[65–68] The generally quite limited efficacy of antibiotics but also of other pharmacological active agents may be partly attributed to the mainly conducted way of drug application. Not only systemic but also the local intraperitoneal delivery of saline drug solutions results in an only short duration of effectiveness at the intended site of action and relatively high drug amounts within the rest of the body. The relatively high permeability of the peritoneum to water and small molecules quickly leads to an elimination of the drugs into the blood stream[69] so that the drugs' mechanisms of action also come into effect on unintended locations. A more controlled drug delivery at the target location by an advanced drug delivery system other than a saline solution should significantly enhance the efficacy of the drugs on adhesion formation and decrease the systemic side effects.[65] Hence, to date no satisfyingly effective and safe pharmacologic treatment exists to reduce postoperative adhesions and further extensive research and randomized controlled clinical trials are required.

2.1.3.3 Physical barrier devices

Currently, a more successful strategy for the prevention of postsurgical adhesions is the application of several differently constructed barrier devices. The purpose of such devices is to physically separate the wound site from the adjacent tissues and organs or from the abdominal wall temporarily during the time of wound healing to prevent adhesion formation by avoidance of contact between the susceptible surfaces. Although the general concept is simple, there are several nontrivial requirements an ideal barrier should fulfill (***Table 2.1***). It

Table 2.1 *Requirements for barrier devices.*

Requirements for an ideal barrier device for the prevention of postsurgical adhesions
• biocompatibility
• effective separation of the affected tissues throughout the critical time of peritoneal healing
• biodegradability
• appropriate mechanical properties for surgical handling and *in vivo* performance
• self-adhesiveness without the need for fixation
• permeability for nutrients and waste dispatch
• cost-effectiveness

should be biocompatible provoking as little foreign body reactions and inflammation with all the already mentioned consequences as possible. Ideally, the barrier material is also biodegradable so that it can be completely absorbed by the body requiring no further surgical intervention to remove it. As the device has to efficiently separate the affected tissues and completely cover the site of injury over the time of wound healing, its fragmentation should not start until peritoneal wound healing is completed.[1] Moreover, the barrier should possess appropriate mechanical properties. While the mechanical stability of constructs intended for tissue engineering for example has to be oriented on the properties of the natural structures which they are supposed to substitute,[70–72] in case of an application as physical barrier for the prevention of post-surgical adhesions it is redundant for the device to mimic any anatomical structure, but important to guarantee an appropriate stability both for an uncomplicated handling and insertion by the surgeon during open as well as laparoscopic surgery with enough strength to withstand suturing and for a satisfactory performance inside the patient's body during the subsequent wound healing

phase. The application thereby ideally should be possible without the need for fixation with sutures since suturing additionally promotes adhesion formation.[11] Further beneficial for peritoneal healing within the patient's body is a certain molecular permeability to allow the sustenance with nutrients and waste dispatch.[10] In addition, an optimal barrier device should be cost-effective and not exceed a certain price. Wilson et al.[73–74] calculated the cost-effectiveness of anti-adhesion products in 2002 and again in 2007 based on the readmission costs of 2006. According to these calculations, the application of a € 130 product in the UK clearly saves costs over a 10-year period compared to readmission expenditures whereas a more expensive product of € 300 would not pay off.

Since the ideal barrier device has not yet been found and the ideal physicochemical properties of barriers for highest efficiency within the peritoneum are not known exactly yet, various materials and morphologies of devices have been investigated or brought to market. Thus, both nature-derived and synthetic polymers have been used. The investigated nature-derived materials are mostly based on polysaccharides like hyaluronic acid, cellulose, dextran, chitosan or alginate since they proved good biocompatibility in other biomedical applications. However, the necessary extraction and purification steps make them expensive and they additionally possess a higher level of biological contaminations such as viruses or pyrogens than synthetic polymers. Synthetic polymers like poly(lactide) [PLA] are advantageous because their composition and molecular weight can be controlled and consequently their properties can be adjusted within a broad range.[75–76] By using synthetic polymers, best possible removal of organic solvents used during synthesis is crucial to minimize solvent residues in the material, which can otherwise negatively affect cells during the application.

Commonly, the barrier devices are distinguished according to their physical state in liquids, gels and solid barriers (***Table 2.2***). The liquid products can be applied both during an open procedure and laparoscopically and are usually applied after the operation by simple instillation into the abdominal cavity. The intended principle for these fluids to separate the affected tissues is hydroflotation meaning that the organs float in the instilled solution without fatal contact. However, low viscosity crystalloid solutions such as normal saline or

Table 2.2 *Selected barrier devices for the prevention of postsurgical adhesions.*

Liquid barriers	• normal saline solution • Ringer's lactate solution • 32 % dextran 70 solution (Hyskon®) • 4 % icodextrin solution (Adept®) • 0.4 % sodium hyaluronate solution in PBS (Sepracoat®) (withdrawn)
Hydrogels	• two-component system of poly(ethylene glycol) [PEG] solutions (SprayShield®, SprayGel®) • auto-crosslinked hyaluronan gel (Hyalobarrier®) • calcium chloride stabilized gel made of polyethylene oxide and carboxymethyl cellulose (Intercoat®/Oxiplex®) • 0.5 % ferric hyaluronate gel (Intergel®) (withdrawn)
Solid barriers	• sodium hyaluronate/carboxymethyl cellulose film (Seprafilm®) • oxidized regenerated cellulose membrane (Interceed®) • poly(lactide) film (SurgiWrap®) • 100 % collagen type I membrane (CollaGUARD®) • non-degradable expanded polytetrafluoroethylene membrane (Preclude®)

Ringer's lactate solution resulted in little success because of the large resorptive capacity of the peritoneum leading to a residence time of the liquid barrier shorter than the peritoneal wound healing.[77] An elongation of the residence time and prolonged retention of liquid in the peritoneal cavity could be achieved by the use of high molecular weight polymer solutions like a 32 % dextran 70 solution (Hyskon®), a 4 % icodextrin solution (Adept®) or a 0.4 % sodium hyaluronate solution in PBS (Sepracoat®). However, the usefulness of the 32 % dextran 70 solution is questionable due to several side effects like abdominal pain, edema, dyspnea or allergic reactions and the additionally contradictory results regarding adhesion reduction.[78–81] By now the 4 % icodextrin solution (Adept®) is the only FDA approved liquid barrier for the prevention of postsurgical adhesions caused by gynecological laparoscopy.[82] Its efficacy regarding adhesion reduction in comparison to Ringer's lactate solution was proven by Brown et al.[83] in a double-blind, randomized, controlled human study. Sepracoat®, different than the other solutions, was already applied prior to the surgical procedure. This approach aims at the prevention of the formation of *de novo* adhesions at locations not directly affected by the surgical procedure by reducing tissue trauma through protective tissue precoating with the solution. Its efficacy was confirmed by both animal studies and a randomized, blinded, placebo-controlled study with

277 women.[84–85] However, the product did not get US approval and was voluntarily withdrawn from the European market for economic reasons.

Similar to liquid barriers, gels can be applied both during open and laparoscopic procedures. Beneficially, their residence time on the site of injury is generally longer than of the liquid products leading to a higher efficiency. A further positive property ascribed to gels for an application as barrier devices is the fact that they can be evenly spread over large surfaces and perfectly adapt to the shape of the affected tissues. Thus, especially sprayable *in situ* cross-linkable hydrogels are advantageous regarding laparoscopic procedures and hardly accessible wound sites since after spraying they gel exactly in adaptation to the tissue geometry without the need for the surgeon to handle the tissue. Consequently, the trauma to the tissue is reduced.[65,75] One example of a sprayable *in situ* cross-linkable gel is a two-component system of PEG solutions with modified end groups (amines and *N*-hydroxy succinimidyl esters) (SprayShield®, a modified version of SprayGel®) which react within seconds to a hydrogel.[86] Its effectiveness was confirmed in clinical trials, however, only with a small number of patients.[87–88] Further marketed products with demonstrated effectiveness in clinical trials are auto-cross-linked hyaluronan gel (Hyalobarrier®) and a calcium chloride stabilized gel made of polyethylene oxide and carboxymethyl cellulose [CMC] (Intercoat®/Oxiplex®).[89–92] These products cannot be sprayed but are applied to the affected wound location via a canula applicator already as ready-made gels, which also allows for a laparoscopic application. Intergel®, a 0.5 % ferric hyaluronate gel was voluntarily withdrawn from the market because complications like postoperative pain, foreign body reactions and tissue adherence were reported.[93] Due to the superior handling characteristics, current investigations concerning gels are mainly directed towards *in situ* forming systems based on different gelation mechanisms without the need for additional cross-linking agents such as thermosensitive poly(ε-caprolactone)-poly(ethylene glycol)-poly(ε-caprolactone)[94–95] and methyl cellulose-based hydrogels[96] gelling at body temperature or a chitosan-hyaluronic acid based hydrogel gelling after a Schiff's base cross-linking reaction between amino groups and aldehyde groups of the modified polymers.[97]

The currently clinically most successful barrier devices for the prevention of post-surgical adhesions are solid films and membranes.[65] These devices are applied at the end of the operation and positioned in adequate size over the affected wound sites where adhesions are likely to form. Depending on the texture and properties of the devices, they are either self-adhesive or a further fixation by sutures or staples is required to keep them in place. Laparoscopic application of solid films or membranes generally is more difficult than of liquids and gels, however, yet possible for some of the available devices. The most widely used and also FDA approved solid barriers are Seprafilm® and Interceed®. Seprafilm® is a transparent, bioabsorbable film consisting of sodium hyaluronate and CMC, which does not need further fixation, *in vivo* turns into a gel and is fully degraded and eliminated within 28 days.[98] Its adhesion preventive effectiveness in open abdominal and pelvic procedures was demonstrated in several randomized controlled clinical trials. Laparoscopic application of Seprafilm® is very limited because of the difficult handling and brittleness of the film, however, is possible for certain procedures and with a decent application technique.[99–100] Interceed® is a membrane of oxidized regenerated cellulose, which assumes a gelatinous texture after application, covers the wound site without further fixation and which is absorbed within two weeks. Its effectiveness was also shown in several randomized controlled clinical studies but is limited in the presence of blood so that adequate hemostasis is required prior to its application though.[1,101–104] Apart from Seprafilm® and Interceed®, other biodegradable products like CollaGUARD® or Surgiwrap® are in clinical use for the prevention of postsurgical adhesions. CollaGUARD® is a membrane consisting of 100 % collagen type I and can be applied both in laparotomy and laparoscopy.[105] SurgiWrap® is a relatively stiff, transparent film made of 70:30 poly(L-lactide-co-D, L-lactide), which has to be fixed on the injured site by sutures. It maintains its mechanical strength over eight weeks meaning throughout the entire critical time of wound healing, but degrades very slowly over more than 24 weeks. The film can be used both during open and laparoscopic procedures and its efficacy was demonstrated in animal studies[106–109] as well as in some human patients.[110–111] Randomized controlled human trials are still lacking, though. Besides biodegradable membranes, also a non-degradable expanded polytetrafluoroethylene [PTFE] membrane (Preclude®) proved its adhesion reducing properties in animals and human trials

and consequently is in clinical use. However, its applicability is limited since it has to be removed again in a second surgical intervention.[112–114]

Current research concerning solid barrier devices includes impermeable films[115–116] but also electrospun meshes[117–119] of various materials.

2.1.3.4 Combinations of a barrier device with pharmacological active substances

Considering the need for a more controlled drug delivery on the target site and the large pool of materials and morphologies available to create an anti-adhesion barrier, a logic outgrowth of the research concerning adhesion prevention is to combine the already mentioned research approaches of a physical barrier and the pharmacological treatment to combination devices. By drug loading a barrier device the advantages of each approach could be united by minimizing the shortcomings of each prevention method alone.[65] Consequently, several researchers have investigated the benefit of loading viscous solutions,[120] hydrogels,[121–126] electrospun meshes[127–131] or films[132] with drugs with regard to a reduction of adhesion formation. Moreover, the efficacy of marketed products like Seprafilm®[133–134] and Interceed®[102] in combination with drugs was examined. In animal studies, most of the investigated combinations showed positive results regarding reduced adhesion formation and many of the combination devices even fared better than each single treatment (if investigated as a reference) as desired. Consequently, the combinational approach of a barrier device with pharmacological active substances seems promising for further investigations. Thereby, the challenges for an optimized combination system will be to determine the appropriate drug amount and release rate for intraperitoneal application and to realize the ideal drug behavior in a barrier device with an optimal degradation rate for maximal preventive success and minimized undesired side effects.

2.2 Poly(lactide) based barriers for adhesion prevention

2.2.1 Poly(lactide)

For biomedical applications such as barrier devices for the prevention of postsurgical adhesions, biodegradable polymers have gained increasing interest. As already mentioned, synthetic polymers are superior to modified biopolymers regarding non-immunogenicity and the possibility to tailor and reproduce the desired properties. One of the most widely studied and used group of synthetic biodegradable polymers for surgical applications are aliphatic polyesters of α-hydroxy acids such as poly(lactide) or poly(glycolide). Thereby, poly(lactide) or poly(lactic acid) (***Scheme 2.1***), the aliphatic polyester of lactic acid, is the most attractive biodegradable polyester due to several reasons. PLA is not only hydrolytically cleavable into non-toxic degradation products since lactic acid is part of the natural metabolic cycles such as the citric acid cycle, but the monomer lactic acid for PLA synthesis can also be gained from cheap renewable sources like corn or sugar beets, making it also an inexpensive and ecofriendly polymer. Moreover, it can easily be processed and thus is used for many different applications such as suture materials, wound dressings, microspheres for drug delivery or screws, plates and fibers for bone restoration as well as for tissue engineering applications, since its properties can be widely adapted by varying the stereochemistry, molecular weight, copolymerization or the method of polymer processing.[135–136]

2.2.2 Synthesis of PLA

The monomer lactic acid possesses a chirality center and consequently an *R* (D-lactic acid) and *S* (L-lactic acid) configuration (***Scheme 2.2***).[137] It can be obtained both biologically and chemically. Since with chemical methods the stereoregularity cannot be controlled and only

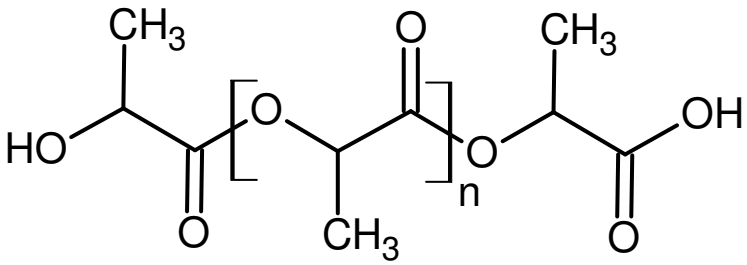

Scheme 2.1 *Structure of poly(lactide).*

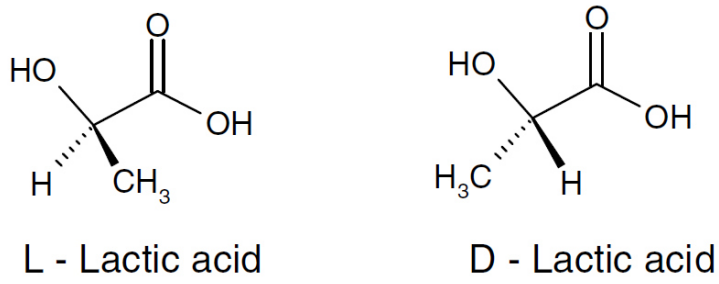

Scheme 2.2 *The two configurations of lactic acid. (Reprinted from lit.[136] with permission from Elsevier)*

the racemate of D- and L-lactic acid is received, for commercial production generally a biotechnological process is preferred. While in humans naturally only the L-isomer is formed, by bacterial fermentation depending on the chosen bacterium, both enantiopure D- and L-lactic acid can be produced. For the fermentation of the preferably used L-lactic acid typically strains of Lactobacilli are used.[138] Starting from the monomer, there are several synthesis routes for the polymerization of PLA (***Figure 2.3***). Unless chain coupling agents are used, the route of direct polycondensation is rather limited to the synthesis of very low molecular weight PLA since the necessary complete removal of water to achieve high molecular weights is quite difficult to realize. The required high reaction temperature and the reduced pressure for the removal of the water result in undesired side reactions like transesterifications known as back biting, which hinder polymer chain growth but promote

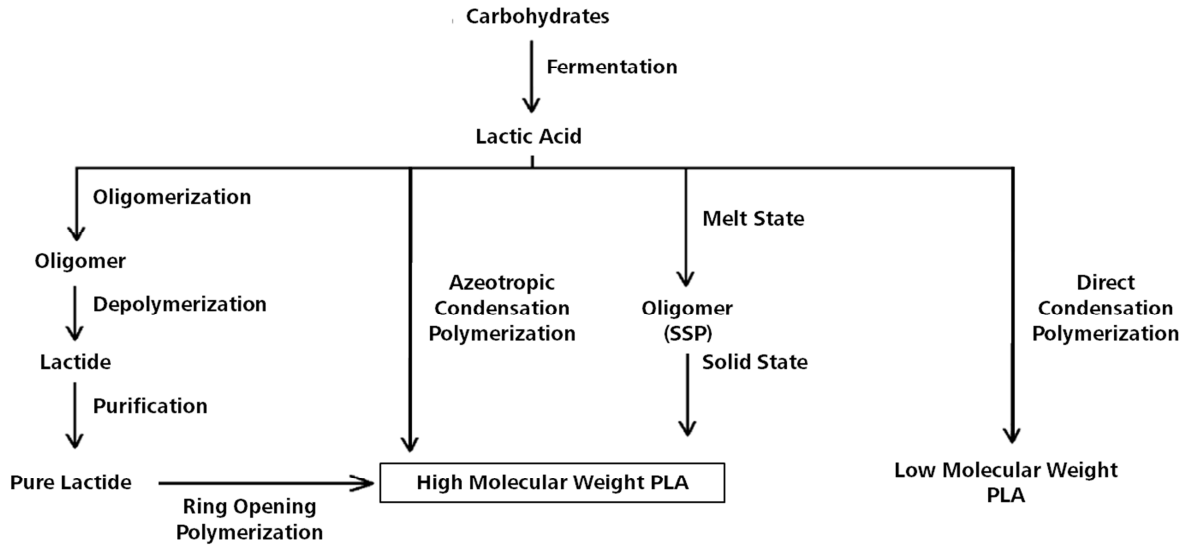

Figure 2.3 *Synthesis routes of PLA. (Modified from lit.[136] with permission from Elsevier)*

polymer decomposition by formation of the cyclic dimer lactide. In addition, in this process the stereoregularity cannot be controlled very accurately. Higher molecular weights with more than 300,000 Da can be achieved by azeotropic polycondensation. In this method, the disturbing water formed during the condensation reaction is removed azeotropically from the reaction mixture with an organic solvent, ideally with an aprotic solvent with a high boiling point, e.g. diphenylether. The organic solvent is recycled and brought back to the reaction mixture. This reaction can be realized below the melting temperature of the PLA leading not only to high molecular weights due to the prevention of depolymerization but also the racemization through the process is restricted.[136,139–140]

Another polymerization method to synthesize PLA is the ring opening polymerization [ROP], which was first reported by Carothers et al..[141] In this method, not lactic acid but its cyclic dimer lactide is used as educt. Lactide is obtained by depolymerization of low molecular weight PLA at high temperature and reduced pressure in the presence of a catalyst.[142] Due to the stereoisomerism of lactic acid, the dimer exists in three different forms, (R, R)-lactide (D-lactide), (S, S)-lactide (L-lactide) and (R, S)-lactide (*meso* lactide) (***Scheme 2.3***). An equimolar mixture of (R, R)-lactide and (S, S)-lactide is also termed *racemic* lactide.[137] Depending on the used isomeric form and polymerization mechanism, various compositions and molecular weights of PLA are achieved. An anionic ROP of PLA works best with alkali metal alkoxides as initiator. Due to the high basicity of the alkoxide the lactide can be deprotonated and reprotonated again, which entails racemization. Moreover, the deprotonated lactide can promote a chain transfer reaction so that generally stereoisomerism is difficult to control

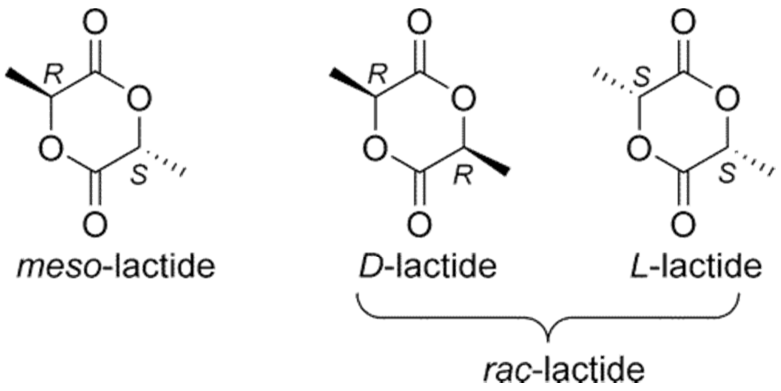

Scheme 2.3 *The three stereoisomers of lactide. (Reprinted with permission from lit.[135]. Copyright (2004) American Chemical Society)*

and the molecular weight, which can be achieved, is limited, though.[143–144] However, Jedlinski et al.[145] was successful in polymerizing L- and D, L-lactide via an anionic ROP with limited racemization with potassium methoxide as initiator. A cationic ROP can be carried out only with few initiators like trifluoromethanesulfonic acid or methyl triflate. Since the reaction is conducted at high temperature, it also results in racemization of the monomers. To achieve an optically pure polymer with a reaction according to this mechanism, temperatures below 50 °C are necessary, which reduces the reaction rate as well as the molecular weight which is possible to obtain.[146–147] Consequently, a ROP via coordination-insertion mechanism (***Scheme 2.4***) is the preferred and most widely studied polymerization method for PLA with high molecular weight and controlled stereochemistry. This reaction is conducted in the presence of covalent metal alkoxides with free p or d orbitals, which behave like weak Lewis acids, such as the alkoxides of tin, zinc, magnesium, titanium or zirconium. The first step of the mechanism is a coordination of the metal atom with one of the oxygen atoms of the carbonyl groups of the lactide. Through this coordination step the electrophilicity of the carbonyl group of the lactide is increased, which entails, together with the also increased nucleophilicity of the alkoxy group of the initiator, an insertion of the lactide into a metal-alkoxide bond while the acyl-oxygen bond of the lactide is cleaved. With this method, stereoisomerism and molecular weights can be controlled and also high

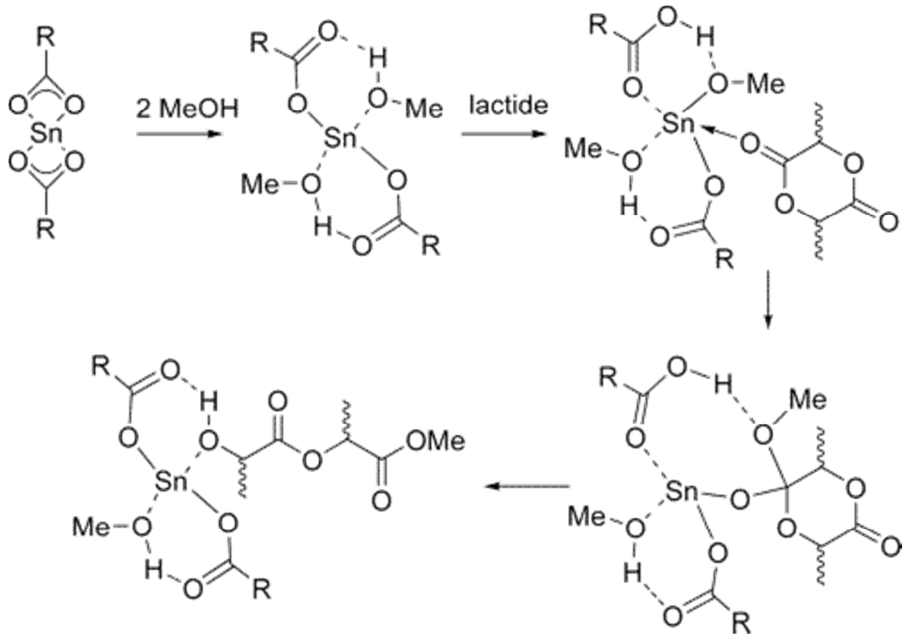

Scheme 2.4 *Coordination-insertion mechanism of PLA synthesis with methanol as coinitiator. (Reprinted with permission from lit.[135]. Copyright (2004) American Chemical Society)*

molecular weights can be successfully achieved.[144,148–149] Thereby, tin(II)2-ethylhexanoate is the preferably used initiator especially in combination with an initiating alcohol compound, which accelerates the reaction and improves the control over the reaction. This initiator is superior to other metal alkoxides due to its solubility in organic solvents and in the melt of the monomers, its high reactivity and the possibility to achieve high molecular weights. Moreover, it has been FDA approved as food additive. However, one should be aware that tin compounds are cytotoxic and therefore exposure in biomaterials should be minimized.[135]

Apart from the polymerization methods starting from the monomer lactic acid or the dimeric lactide, PLA can also be synthesized based on a relatively low molecular weight pre-polymer by solid state polymerization [SSP]. Thereby, the pre-polymer is heated to a temperature above the glass transition temperature but below the melt temperature. By-products of the reaction are removed by reduced pressure or by flushing with inert gas. This polymerization process is advantageous because there is no need for organic solvents and hardly any side reactions occur due to the low reaction temperature. High molecular weights can be achieved, however, the reaction time to obtain a certain molecular weight is distinctly longer than for reactions in melt or solution.[136,150]

Depending on the route of synthesis and the used educts, PLA is throughout literature either referred to as poly(lactide) or poly(lactic acid).

2.2.3 Properties of PLA

Depending on the stereosequence, PLA possesses quite variable properties. Pure poly(L-lactide) [PLLA] and pure poly(D-lactide) [PDLA] are semicrystalline, brittle polymers. PLLA is more widely studied and used since its monomer and degradation product L-lactic acid is the naturally occurring stereoisomer in humans. The PLLA polymer is crystalline to around 37 %, has a glass transition temperature [T_g] between 55-65 °C and a melting point of around 175-180 °C, depending on the molecular weight, molecular weight distribution as well as thermal history of the sample. Since this polymer has a high tensile strength of 50-70 MPa, a high modulus of around 5 GPa and a low elongation at break of around 4 %, it possesses optimal mechanical properties for load-bearing devices like orthopaedic screws and resorbable sutures.[151–154] In contrast, the optically inactive poly(D, L-lactide) [PDLLA] with its random stereosequence is amorphous. Consequently, the polymer's T_g is between

55-60 °C and the mechanical strength is significantly lower than that of PLLA.[152] However, it was found that amorphous PLA samples maintain their initially lower mechanical strength over a longer time period upon degradation in aqueous medium than semicrystalline PLA samples, which can probably be attributed to a higher stress susceptibility of PLA and occurring microcracking.[155] By controlling the ratio of D- and L-lactyl units of the polymer, the properties and crystallinity can be varied. Thus, the crystallization temperature is lower the lower the content of the L-isomer within PLLA and as soon as PLLA contains more than 12 % of the D-isomer, like the 70:30 poly(L-lactide-co-D, L-lactide) (Resomer® LR708) used for the manufacturing of SurgiWrap®, the polymer becomes amorphous.[156–157]

In contrast to the degradation of several other polymers, enzymatic degradation only plays a minor role for PLA, but the degradation is mainly controlled by the present amount of water.[158] The degradation of the PLA chain mainly occurs by hydrolytical cleavage of the ester bonds resulting in new carboxylic and hydroxylic end groups of the formed breakdown products. The ester hydrolysis accordingly proceeds to form shorter molecule chains, oligomers and lactic acid. Generally, the hydrolysis of PLA is believed to follow a quite random scission along the polymer chain, however, Shih[159] found a slightly faster cleavage of chain-ends than of internal ester-bonds at least under acidic conditions. Within the body, the finally obtained degradation product lactic acid enters the citric acid circle where it is metabolized into water and carbon dioxide. Probably due to its natural participation in human metabolism, no accumulation of the degradation products could experimentally be found in the essential organs, underlining the non-toxicity of the material and its degradation products.[160] Devices made of PLA typically undergo bulk erosion meaning that during application and after water contact the degradation and loss of low molecular compounds is not restricted to the surface and thus reducing the size of the device (surface erosion), but resulting in a constant dimension of the device with hardly any mass loss over a certain time. This behavior is due to an occurring hydrolysis all over the device resulting from a quite quick diffusion of water in relation to the PLA degradation.[161–162] In contrast to the classical bulk erosion model of a homogenously occurring degradation, Li et al.[155,158] found a heterogeneous degradation behavior for PLA with a faster chain scission rate in the center of the device than on the surface. This finding is generally explained by an autocatalytic effect

of the increasing number of acidic carboxylic end groups in the center of the device which further catalyze the ester cleavage. As long as the polymeric layer on the surface is impermeable for the occurring inner degradation products, hardly any mass loss occurs and the number of catalytically active carboxylic end groups steadily increases. As soon as the surface layer becomes permeable for the inner degradation products, water-soluble oligomers from the center diffuse out of the device and mass loss occurs. This concept was confirmed by further investigations[163] demonstrating a faster degradation with increasing thickness of a PLA device and a consequently longer diffusion path for the acidic degradation products out of the device maintaining a more acidic environment in the core of the device. Apart from the thickness of the device, the end group of the polymer, the molecular weight and the degree of crystallinity also influence the degradation. Depending on the used polymerization initiator, either carboxylic end groups (uncapped) or alkyl end groups due to esterifications (capped) are generated on the polymer terminus. Due to a faster water uptake and the catalytic activity of the uncapped carboxylic groups promoting autocatalysis, test specimens with uncapped chain ends degrade initially faster than polymers with capped ends. Thereby, the lower the initial molecular weight, the faster the complete molecule is degraded to soluble breakdown products and the more carboxylic end groups accelerate the degradation, at least at the beginning, leading to shorter degradation times.[164–165] Crystalline regions degrade slower than amorphous domains due to a higher resistance to the essential water uptake. Interestingly, fully amorphous PLA can also start to crystallize during degradation in aqueous medium, which can be explained by increased chain mobility and the formation of polymer pieces of similar stereosequence, which are able to crystallize then.[153,155,166] Due to the extreme hydrophobicity and crystallinity of pure PLLA, the complete *in vivo* degradation and excretion can take more than two years for high molecular weight polymers, which is only beneficial in loadbearing applications. Thus, the faster degradation rate of PDLLA makes amorphous polymers much more attractive for drug delivery applications[152] and together with the above-mentioned longer maintenance of the mechanical properties upon hydrolytic degradation also more useful for an application as barrier device for the prevention of postsurgical adhesions. Consequently, for the commercial PLA films (SurgiWrap®) an amorphous PLA containing 30 % of the D,L-lactide is used as standard material. For further optimizing the material properties regarding

mechanical properties and a shorter degradation time, modifications of the polymer by copolymerization with PEG, further increase of the content of D-lactyl units and a reduction of the molecular weight were conducted and investigated in this work.

2.2.4 Modification with PEG

Modifications of PLA have been extensively studied to tune the properties of the polymer for disposable or biomedical applications which do not require a high rigidity and slow degradation rate. By either blending or copolymerizing PLA with other materials, its poor hydrophilicity can be improved and the degradation much better controlled and accelerated. Moreover, with appropriate plasticizers the brittleness of the PLA can be overcome in applications for flexible polymer devices. Thereby, the examined PLA modifications for various applications include blends with poly(β-hydroxybutyrate) [PHB],[167] poly(vinyl acetate) [PVAc],[168] chitosan,[169–170] starch,[171–173] poly(ε-caprolactone) [PCL][174–176] and copolymers like poly(lactide-co-glycolide) [PLGA][177–179] or random and block copolymers made of lactide and ε-caprolactone.[180–182] In this work, the focus lay on modifications of PLA with poly(ethylene glycol) [PEG] (***Scheme 2.5***) in order to use a hydrophilic and water-soluble plasticizer. PEG of all molecular weights is hydrophilic (but still soluble in organic solvents), flexible, non-toxic and biocompatible. It has long been used in the pharmaceutical industry[183] and has already been examined for biomedical applications and drug delivery as blends or diblock and triblock copolymers with PLA for various applications in form of

linear PEG **4armPEG (pentaerythritol core)** **8armPEG (tripentaerythritol core)**

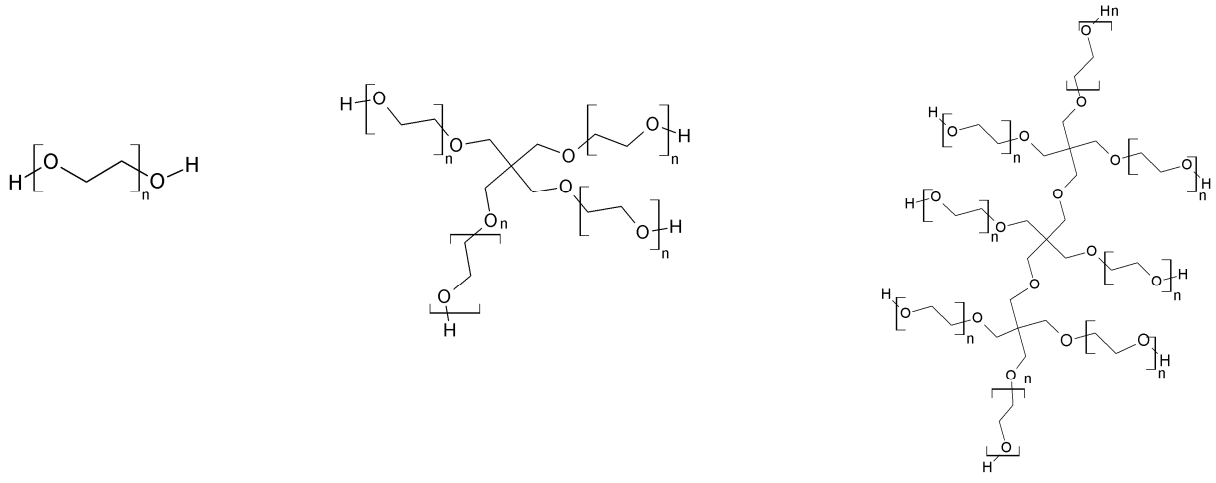

Scheme 2.5 *Structure of poly(ethylene glycol) with different geometries.*

Microspheres,[184] nanoparticles,[185–187] hydrogels,[188–189] films[190–191] or electrospun meshes.[192-194] Investigations with PEG blended PLA resulted in intended altered properties regarding degradation rate due to a higher water uptake and mechanical properties but also with a fast washout of the water-soluble PEG.[195–196] As PEG-PLA block copolymers (***Scheme 2.6***) also influence both the degradation and the mechanical properties of the material to shorter degradation times and a higher flexibility and ductility but with less washout effect,[197] a copolymerization with PEG is a very promising tool to tailor the properties of PLA based devices for the prevention of postsurgical adhesions as shown in former studies (by our group).[196] Since during aqueous ageing of PEG-PLA block copolymers ester cleavage preferentially occurs at the ester bond between PEG and PLA, PEG with more junctions to the PLA chains is longer retained.[9] Accordingly, star-shaped PEG-PLA block copolymers were investigated in addition to linear copolymers with the intention of an even extended retention of PEG within the matrix due to more connecting points and a longer maintenance of the mechanical properties during aqueous ageing. Analogous to pure PLA, PEG-PLA can be synthesized via ROP after the coordination-insertion mechanism with tin(II)2-ethylhexanoate as initiator with control over the stereochemistry. Thereby, due to its hydroxyl end groups, PEG functions as coinitiator instead of an added alcohol and via the PEG/lactide feed ratio and the used stereoisomer of lactide the molecular weight and the polymer composition can be exactly controlled.[198] The finally occurring PEG is non-biodegradable and its renal filtration is dependent on the used molecular weight. PEG with molecular weights below 8 kDa seems to be rapidly cleared without any restriction of the glomerular filtration. The elimination of PEG with molecular weights between 8 kDa and 30 kDa was found to be size-dependent whereas above a molecular weight of 30 kDa the filtration is extremely restricted independent on the exact molecular weight.[199] Due to the

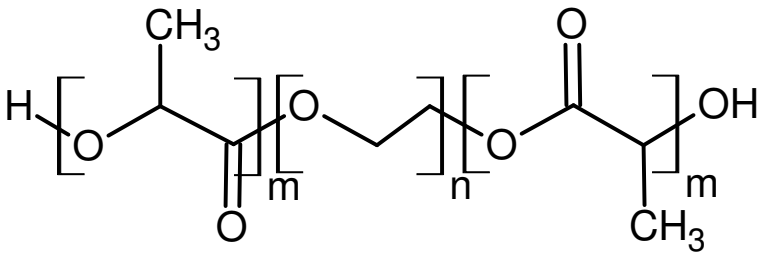

Scheme 2.6 *Structure of a PLA-PEG-PLA triblock copolymer.*

smaller hydrodynamic radius of branched PEG, even higher molecular weights could be excreted than for the linear PEG.[200] Hence, to ensure a potential fast renal elimination, only PEG with a molecular weight of 10 kDa was used for the copolymers evaluated in this work.

2.2.5 Process optimization of the manufacturing of PLA based barrier devices

2.2.5.1 Blown film extrusion

The marketed product SurgiWrap® is manufactured by blown film extrusion of a high molecular weight 70:30 poly(L-lactide-co-D, L-lactide) (Resomer® LR708) with an intrinsic viscosity of about 5.5 g/dL. This continuous process is used since it allows a solvent free film fabrication[201] and is convenient for large scale production. A typical set-up for an extrusion process is shown in ***Figure 2.4***. The raw polymer is filled into a hopper and from there fed by gravitational force into the barrel of the extruder. There, a rotating screw transports the polymer through the heated barrel. During the transport, the material is both molten and permanently mixed resulting in an ideally uniform polymer melt at the exit of the barrel. The polymer melt is filtered to remove contaminants such as parts from packaging material, metal abrasion from the extruder or residues of other polymers owing to cross-contaminations before entering a die which determines the shape of the final polymeric

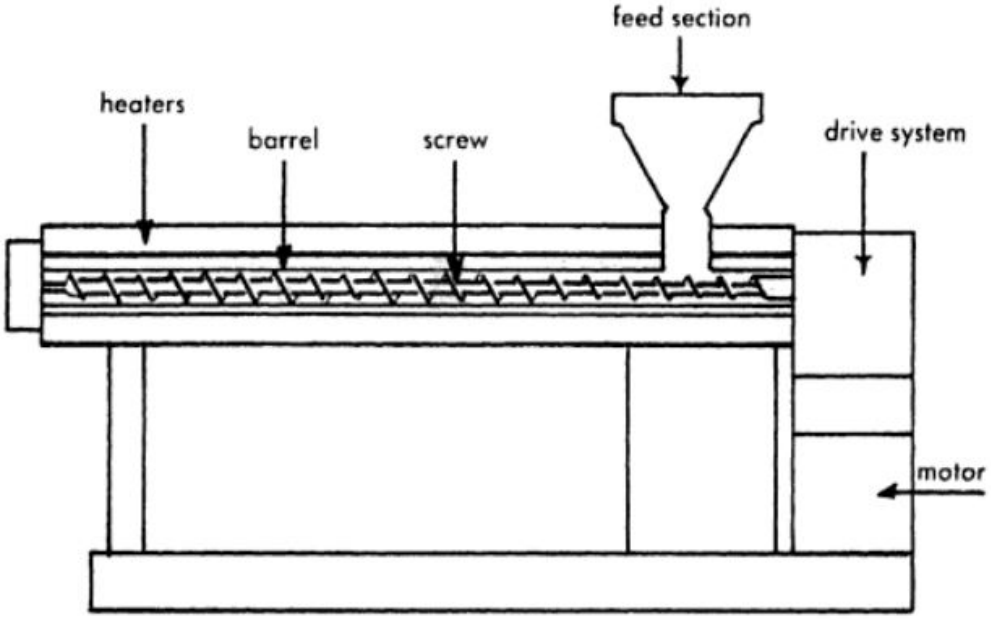

Figure 2.4 *Extrusion set-up. (Reproduced from lit.[202] with permission of CRC Press LLC via Copyright Clearance Center)*

construct. In case of the manufacturing of thin films by a blown film process, often an annular die is used to generate a polymer tube (***Figure 2.5***). Through this tube, an airflow is blown leading to an expansion of the tube and to a further thinning of the film. To cool the film and to control the expansion of the film, cooling air is blown against the outside of the tube as well. The inner airflow leads to a stretching of the blown polymer along two axes. Consequently, the speed of rotation of the nip rolls at the end of the tube has to be higher than the output speed of the die to control the process. Typically, the ratios of the die output speed to the rotational speed of the nip rolls and of the final to the initial diameter of the tube are between 2:1 and 5:1. The tube collapses when it arrives at the nip roles and is usually slit in line into two sheets and finally wound up.[202] Owing to the blowing and drawing procedure, the final films are thinner than the initially emerging tube and the polymer chains are highly oriented along the machine direction. These molecular alignments lead to

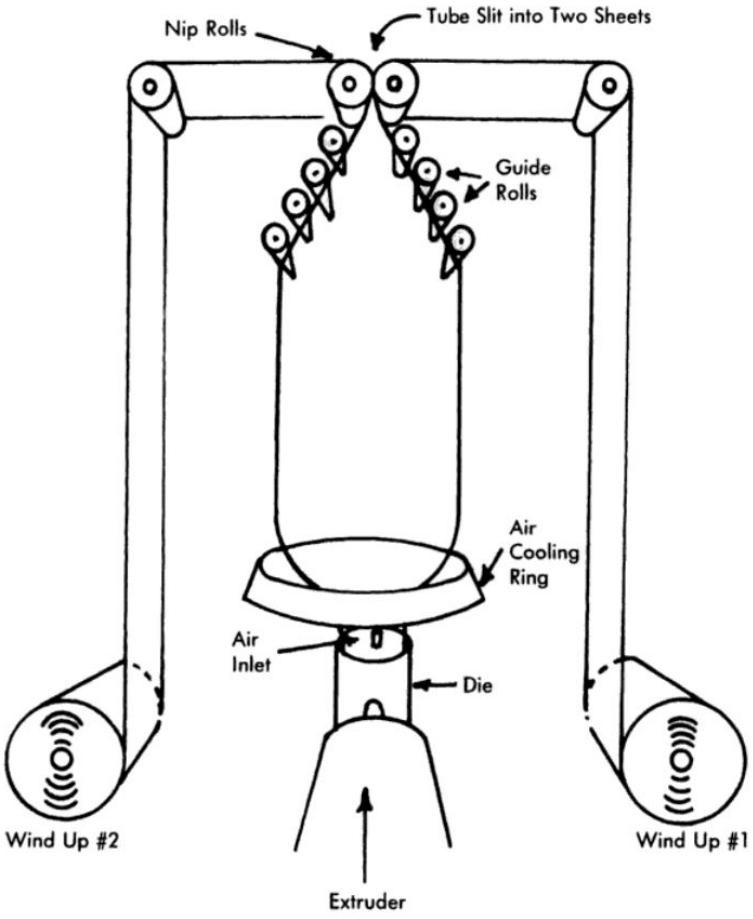

Figure 2.5 *Set-up for the fabrication of blown films. (Reproduced from lit.[202] with permission of CRC Press LLC via Copyright Clearance Center)*

anisotropic thermal and mechanical properties of the films. Thus, shrinkage upon heat treatment preferentially occurs in one direction and the mechanical strength of the film varies from machine to transverse direction. Owing to the thermal stress during the process, the molecular weight of the polymer is reduced. For the fabricated PLA, a reduction of the initial intrinsic viscosity to half of the value upon extrusion was found, which is further diminished by the subsequent sterilization process. Present moisture further entails the depolymerization of polyesters during extrusion. Hence, to achieve as little weakening, breaking or tearing of the film as possible during extrusion, a dry and high molecular weight polymer is preferred.[196,201–202]

2.2.5.2 Solvent film casting

For the alternative solvent film casting, a viscous polymer solution is prepared, poured into a film applicator with defined gap clearance and drawn with constant speed to ensure consistent thickness and texture throughout the entire casting length (***Figure 2.6***). Upon evaporation of the solvent, the polymer chains become entangled, intermediately come into a gel state and finally form a solid film after further drying.[203] Therefore, a certain molecule size is necessary since only high molecular weight polymers are capable to coalesce and provide sufficient cohesive strength to form stable films.[204] Thereby, the initial solvent

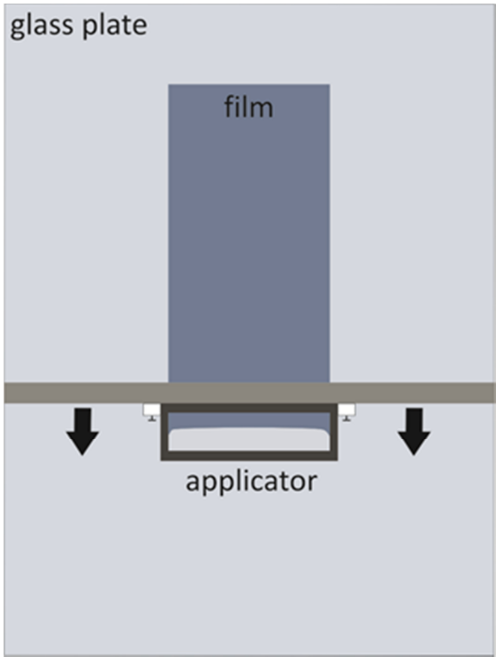

Figure 2.6 *Film casting process.*

evaporation rate depends only on the vapor pressure at the given casting temperature, the surface area to volume ratio as well as on the rate of air flow over the surface (***Figure 2.7***). With proceeding drying, the solvent evaporation becomes also dependent on the present polymer amounts since viscosity and T_g increase and the free volume decreases so that solvent evaporation depends on the diffusion of the solvent molecules to the surface of the films by passing the free volume holes. With further solvent evaporation, the evaporation rate more and more decreases due to a further decreased free volume.[205] Finally after sufficient drying, a solid film is obtained with only few residual solvent.

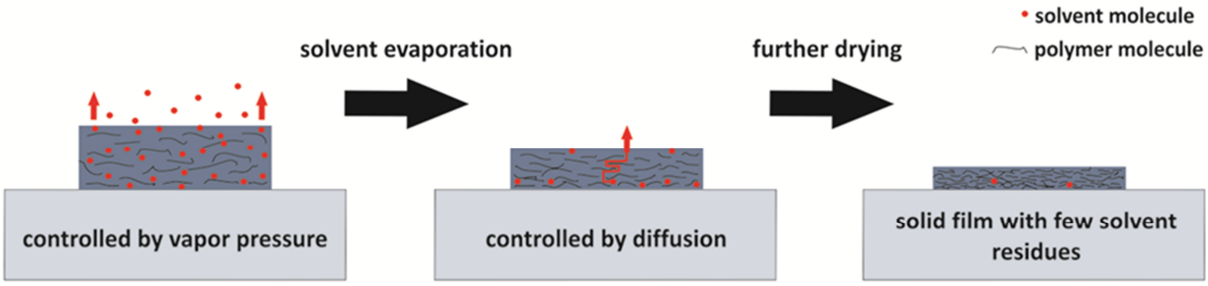

Figure 2.7 *Solvent evaporation and film formation after casting a polymer solution onto a glass plate.*

To achieve even spreading of the casting solution on the glass plate and consequently to ensure the formation of a uniform film, an adequate coating of the glass plate has to be identified prior to film casting. Here the chemical constitution of the casting solution and the used polymer play a major role for the necessary type of glass treatment. In case of a huge chemical difference the solution will not spread on the substrate but instead drip off, so that no adequate polymer film will be obtained. If the chemical similarity is too high, the casting solution will spread but the dried films stick heavily to the glass plate and cannot be detached without damage. The thickness of the resulting films can be easily controlled by the concentration of the casting solution and the gap clearance of the film applicator. Since this process is carried out with polymer solutions and not with polymer melts, intense anisotropic effects like for hot melt extruded films are not to be expected as only minor mechanical stresses are applied. A further advantage of this method is the complete lack of thermal stress on the polymer. Due to the simplicity of the method, solvent cast films are manufactured either with the described film applicator, by industrial in-line processing on a belt line or by simple casting of the polymer solutions into moulds. The obtained films find

use in various applications like photographic films, films for electronic applications[206] or as medical films like orodispersible buccal films.[207] Since solvent film casting can be carried out with significantly lower polymer molecular weights than hot melt extrusion, it is suitable not only for the high molecular weight PLA, but also for the PEG-PLA copolymers with renal reclearable PEG blocks and molecular weights ranging from 80-150 kDa which are evaluated in this work.

2.2.5.3 Solution electrospinning

The process of electrospinning was first patented by Formhals in the 1930s[208] but did not gain broad interest until Reneker et al.[209–210] took up the issue in the 1990s. The electrospinning process can be seen as a variation of electrospraying since both processes are based on the concept of jet formation from a polymer solution by application of a high voltage. While electrospraying is conducted with solutions of low viscosity resulting in individual particles due to a break-up of the jet (Rayleigh instability), during electrospinning sufficient polymer chain entanglements occur for the maintenance of a continuous jet and finally a continuous polymer fiber. This effect is achieved by using polymer solutions of higher viscosity.[211–212] The instrumental set-up for solution electrospinning basically consists of a metallic needle for the feed of the polymer solution from a syringe, a high voltage power supply and a grounded collector (***Figure 2.8***). To ensure a constant and controllable feeding rate often a syringe pump is installed to move the plunger.

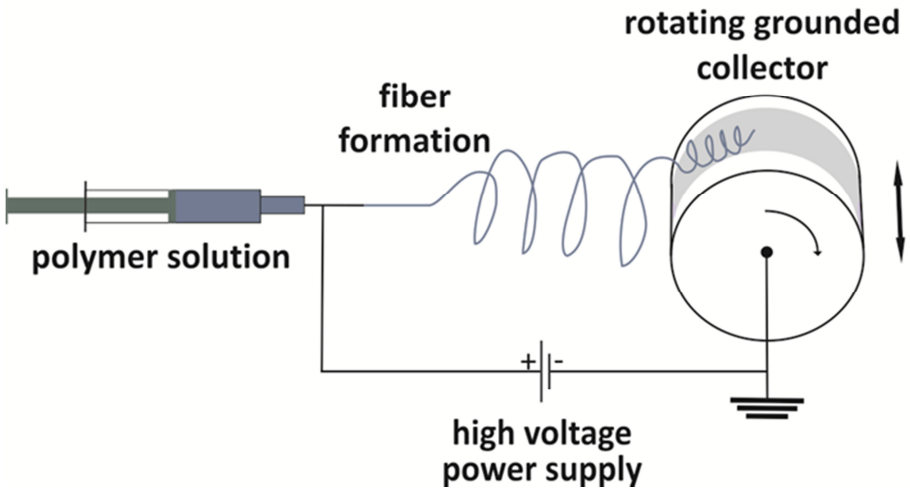

Figure 2.8 *Solution electrospinning set-up with rotating collector drum.*

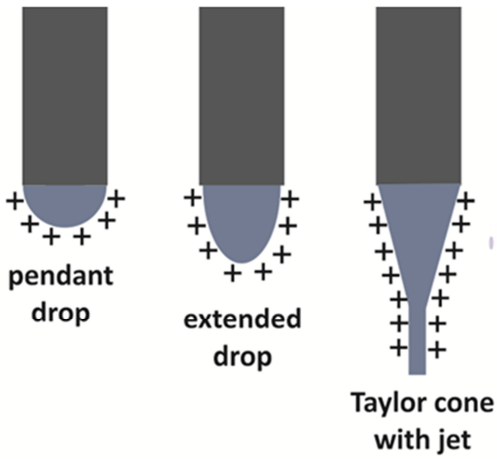

Figure 2.9 *Taylor cone and jet formation emerging from a pendant drop under application of a high voltage. (Modified from lit.[211] with permission from Elsevier)*

In the process, the needle serves as an electrode to transfer electrical charge onto the polymer solution. The induced charges on the surface of the polymer solution repel each other and generate shear stresses opposite to the direction of the surface tension. If the electrical field is high enough, the charged polymer drop on the needle tip is able to overcome the surface tension, the pendant drop is more and more extended into a conical shape and at a critical voltage a charged jet is ejected from the tip of the so-called Taylor cone[213] (***Figure 2.9***). The charged polymer jet is then accelerated towards the grounded collector. Over the distance from the needle tip to the collector, the polymer jet is more and more stretched and the organic solvent from the jet evaporates. Finally, the polymer is deposited on the collector in form of solid and generally randomly oriented fiber. With this technique, very thin fibers with diameters in the range from few nanometers to few micrometers and high mechanical strength can be fabricated from both natural and synthetic polymers.[211,214] The fiber diameter and morphology can be influenced by process parameters such as the concentration of the polymer solution, the applied high voltage, the feeding rate, the needle-collector distance, the used solvent and its volatility or the conductivity of the solution.[214] With different collector types such as a simple metal plate, a rotating disk, a rotating drum or a rotating wire drum various fiber assemblies can be achieved.[215] In addition, the fibers can be further functionalized or drug loaded by various electrospinning approaches or further treatments after the actual electrospinning process.[216] Due to the simplicity of the process set-up, its versatility and adaptability and the ability to

produce nanoscale fibers, which makes this method in many cases superior to other methods for fiber fabrication, solution electrospinning has found wide use in many different applications. Thus, electrospinning is employed for example for electrical and optical applications, filter materials as well as for biomedical applications like tissue engineering, drug delivery systems or wound dressings[211,214,217] and was also investigated regarding adhesion preventing barriers.[128] Limitations of solvent cast films such as brittleness (depending on the polymer) and impermeability can be overcome by using electrospun meshes with high porosity and controllable pore size.[128] The small size of the pores usually prevents cells from passing through the mesh,[218] which is desired for an adhesion preventing device. The mesh porosity can be quite advantageous since it is beneficial for peritoneal healing if nutrients can pass the barrier and waste can be dispatched.[10]

2.2.6 Modifications of PLA based barrier devices

2.2.6.1 Drug loading with triclosan

Combinational products of a barrier device with a pharmacologically active substance seem superior towards simple barrier devices like already mentioned (see 2.1.3.4). A drug loading with antibiotics is meant to reduce occurring peritoneal inflammation due to microbial contaminations. Therefore, investigations with films and meshes with the antibacterial substance triclosan were also performed in this thesis. The drug triclosan (***Scheme 2.7***) chemically is a lipophilic chlorinated biphenyl ether with a pK_a of 8.1 and a very poor water solubility of 0.01 g/L at 20 °C.[219–220] It has broad-spectrum antibacterial activity by being effective against both gram-positive bacteria such as Bacillus subtilis, Mycobacterium smegmatis, Staphylococcus aureus [Staph. aureus] and gram-negative bacteria such as Escherichia coli [E. coli], Salmonella typhimurium, Shigella flexneri and is also effective against funghi. In contrast to former assumptions of an only non-specific perturbation of the

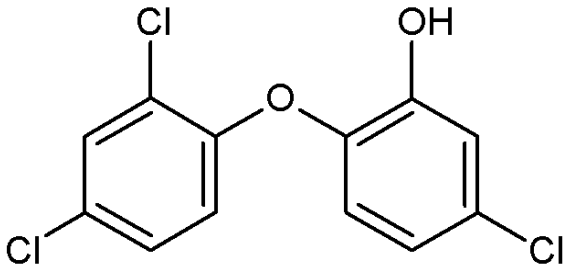

Scheme 2.7 *Structure of triclosan.*

cell membrane analogous to other agents from the chemical family of chlorinated phenols, like triclocarban or pentachlorophenol,[221] meanwhile a more specific mechanism of action was found via studies with E. coli. Thus, triclosan is able to block the bacteria's lipid biosynthesis by inhibition of the enoyl-acyl carrier protein reductase which is responsible for the catalysis of the terminal step in the fatty acid synthesis cycle.[222–224] This enzyme is essential not only in the investigated E. coli but also for many other bacteria including gram-positive bacteria, which are generally more affected by triclosan than gram-negative ones. This lower effectiveness is ascribed to efflux pumps of gram-negative bacteria like in Pseudomonas aeruginosa which pump drugs actively out of the cell. At low doses triclosan is bacteriostatic due to the already described specific enzymatic inhibition whereas high doses of triclosan are bactericidal owing to an additional non-specific targeting of the cell membrane.[221,225] Due to its antimicrobial activity triclosan has been widely used in consumer products such as toothpaste, shampoo, deodorants, toilet and hospital hand soaps, medicated cosmetics, footwear, textiles or toys.[220,226–227] The use of triclosan has long been considered safe since studies demonstrated its relative non-toxicity, non-carcinogenicity, non-mutagenicity, and non-teratogenicity.[228–229] It is furthermore also in clinical use as antimicrobial coating for surgical sutures (Vicryl Plus®) with the intention to reduce surgical site infections by inhibiting bacterial contamination of the suture since triclosan is also effective against Staphylococcus aureus, Staphylococcus epidermidis and even their methicillin-resistant counterparts, which are the main causes of surgical site infections.[229–231] The safety and antiinfective efficacy of the accordingly coated suture material was confirmed by safety studies regarding cytotoxicity, skin irritation, pyrogenicity and intramuscular tissue reactions.[229] This data makes triclosan a very promising candidate for the drug loading of barrier devices for the prevention of postsurgical adhesions as well. For future use especially in intracorporal applications, further investigations on the bacterial resistance and liver-toxicity have to be done and followed, though. It was found that for E. coli strains with a mutation in the gen encoding the target enzyme enoyl-reductase of the specific triclosan mechanism, the minimum inhibitory concentration [MIC] is significantly increased. However, the found resistances to triclosan in E. coli but also in other bacteria like Staph. aureus are restricted to low-level resistances. Since the nonspecific mechanisms of action still work out, the actual clinical relevance of these resistances is questionable.[223,232-233] Lately,

Yueh et al.[234] in contrast also reported a promotional effect of triclosan on the proliferation of hepatocytes, fibrogenesis and oxidative stress as well as on hepatocarcinogenesis in mice suggesting that this mechanism may be relevant in humans as well. However, this presumed liver tumor promoting activity of triclosan in humans has neither be confirmed nor confuted yet.

2.2.6.2 Self-adhesive devices by one-sided modification

As already mentioned, one of the requirements of an ideal barrier device is that it does not have to be sutured to stay in place since suturing additionally would promote adhesion formation. However, many of the investigated and already marketed materials and devices including PLA based polymer films have to be fixed to ensure their anti-adhesive activity at the site of defect. To overcome this need for fixation, efforts have been made by several researchers to modify one side of the barrier device to make it self-adhesive to the wound site whereas the other side is intended for the separation from adjacent tissues. The investigated approaches include structuring of one side, increasing the porosity of the barrier and coating one side with a bioadhesive material. Thus, honeycomb patterns were introduced to PLA films and successfully resulted in higher bioadhesive strengths than flat films.[235] For poly(vinyl alcohol) [PVA] membranes it was found that both a coating with CMC and an increase of the surface roughness by either imprinting of textures or increasing the porosity by a lyophilization method were more bioadhesive than the simple smooth PVA membranes.[236] The company Medisse will request CE approval in 2015 for its FlexiSurge Adhesion barrier, a non-porous smooth poly(1,3-trimethylene carbonate) [PTMC] film coated with a sticky FlexiTac 3 coating (not precisely described) making it self-adhesive.[237] Moreover, a fibronectin coated cross-linked collagen-hyaluronic acid membrane was brought onto a mPEG-PLGA film, which both led to a device lasting on the wound site during the time of peritoneal wound healing and to a promotion of wound healing.[238] Cho et al.[239-240] investigated self-adhesive alginate based adhesion prevention membranes both as single alginate film and in combination with an additional adhesive layer of an electrospun collagen mesh and also achieved good results. The used alginate (***Scheme 2.8***) is a brown algae-derived water-soluble polysaccharide composed of α-L-guluronate and

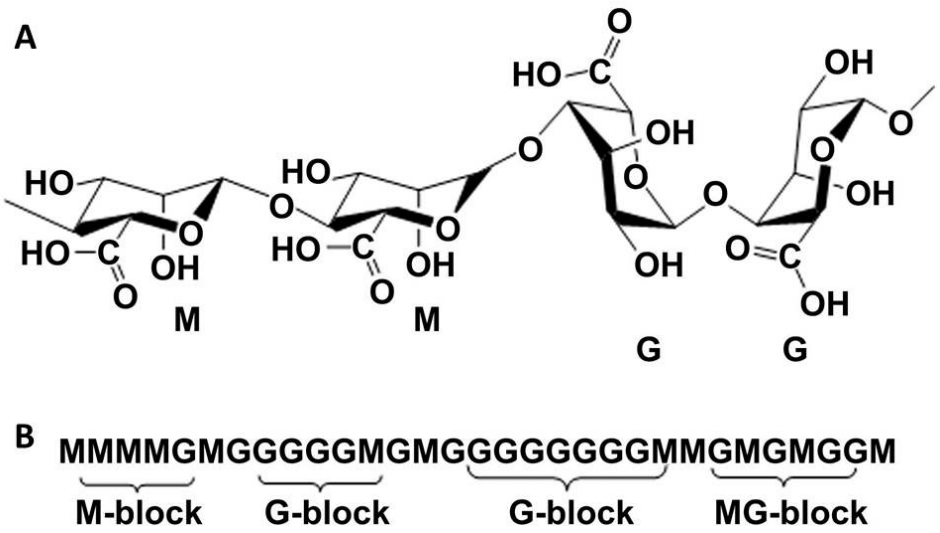

Scheme 2.8 *Exemplary illustration of chain conformation (A) and block structure (B) of the polysaccharide alginate consisting of the monomers α-L-guluronate(G) and β-D-mannuronate (M). (Modified from lit.[242] with permission from Elsevier)*

β-D-mannuronate. This copolymer consists of various blocks consisting of only α-L-guluronate, only β-D-mannuronate or alternating sequences of both monomers.[241] It is mucoadhesive due to the formation of hydrogen bonds with glycoproteins from the mucin-type. The mucoadhesion of alginate is dependent on the degree of cross-linking and amount of free carboxylic acid functions. Thus, un-cross-linked alginate possesses stronger adhesive properties than cross-linked alginate. This is why the applied extent of cross-linking should be carefully controlled. Owing to its proven biocompatibility, alginate has been widely investigated for biomedical applications mainly in form of hydrogels for drug delivery or tissue regeneration but also as wound dressings for superficial wounds because of its property to maintain a moist environment on the wound site and consequently promote wound healing.[20,243] Due to the promising mucoadhesive properties and the biocompatibility of alginate, in this work, bilateral PLA/alginate membranes were investigated with the intention to create self-adhesive devices for the prevention of postsurgical adhesions. The combination of the lipophilic PLA with an additional hydrophilic polymer layer could moreover be beneficial for modified drug delivery from this second layer, providing completely different release kinetics than lipophilic polymer films. The challenge for the manufacturing of such a bilayered device is to overcome the easily possible separation of those two chemically different layers due to the limited cohesion forces. For this purpose,

electrospun meshes were investigated as intermediate cohesion promoter between PLA and alginate. By direct electrospinning onto the PLA film, the fibers merge with the film and create a modified contact surface where the alginate solution can infiltrate into and consequently sort of anchor the alginate film on the PLA film. Thereby, chemical analogousness of the electrospinning polymer to the lipophilic PLA facilitates the merging of the fibers with the PLA film while a more hydrophilic polymer promotes the infiltration of the hydrophilic alginate. To both stay chemically as close as possible to the PLA film and be able to adapt the hydrophilicity to the best possible tailored device, PLA as well as PLA-PEG-PLA triblock copolymers with varying PEG content and PLA composition (synthesis with 70:30 L-lactide:D, L-lactide or 100 % D, L-lactide) were used for electrospinning. Since the pore sizes of the fibers are very small, the infiltration of the alginate solution may not only depend on the chemical properties of the applied fibers but also on the viscosity of the alginate solution, for what reason different concentrations of alginate (3 %, 5 %) were examined as well to find an appropriate combination to enable infiltration of the alginate solution and result in maximum adhesion to the PLA film.

Chapter 3
Materials and methods

In this chapter, the materials which were used for an accurate implementation of the experiments as well as a precise description of the applied methods are given.

Parts of this chapter are published or have been submitted:

M. Kessler, J. Groll, J. Tessmar

Application of linear and branched poly(ethylene glycol)-poly(lactide) block copolymers for the preparation of films and solution electrospun meshes

Macromolecular Bioscience, under review

M. Kessler*, E. Esser*, J. Groll, J. Tessmar

Bilateral PLA / alginate membranes for the prevention of postsurgical adhesions

Journal of Biomedical Materials Research Part B: Applied Biomaterials, accepted

*equally contributing authors

3.1 Materials

PLA (Resomer® LR708) was a generous gift from Boehringer Ingelheim (Ingelheim am Rhein, Germany). Polylactide-*block*-poly(ethylene glycol)-*block*-polylactide consisting of a 10 kDa PEG block with a PLA block of about 35 kDa on each side [PLA35k-*b*-PEG10k-*b*-PLA35k; lin70] (HWL73) was obtained from Polymaterials (Kaufbeuren, Germany). Poly(D, L-lactide-co-glycolide) [PLGA] (Resomer® RG504) was purchased from Evonik (Essen, Germany). Mesofol® was from Biomet (Berlin, Germany).

For synthesis, linear PEG10k (Fluka, Buchs, Switzerland), 4armPEG10k (pentaerythritol core) and 8armPEG10k (tripentaerythritol core) (both from JenKem Technology, Plano, USA) as well as racemic D, L-lactide, L-lactide, tin(II) 2-ethylhexanoate, methylene chloride, methanol, acetone and diethyl ether (all from Sigma-Aldrich, Steinheim, Germany) were used. Toluene was purchased from Alfa Aesar (Karlsruhe, Germany).

Deuterated chloroform [$CDCl_3$] for ^{1}H-NMR analysis was purchased from Sigma-Aldrich. Chloroform from Carl Roth (HPLC grade, Karlsruhe, Germany) or amylene stabilized chloroform from Fisher Scientific (HPLC grade, Loughborough, UK) was used for GPC analysis.

For film casting, Sigmacote® (Sigma-Aldrich), methylene chloride (VWR International GmbH, Darmstadt, Germany), alginate PROTANAL® LF 10/60 FT with a guluronic acid content of 60-70 % (FMC BioPolymer, Sandvika, Norway), glycerine 87 % (AppliChem, Darmstadt, Germany) and Water Blue (Fluka, Buchs, Switzerland) were used.

For solution electrospinning, dimethyl sulfoxide (DMSO, anhydrous ≥ 99.9 %, Sigma-Aldrich), acetone (CHROMASOLV® Plus, HPLC ≥ 99.9 %, Sigma-Aldrich), N, N-dimethylformamide (DMF, anhydrous ≥ 99.8 %, Sigma-Aldrich) and methylene chloride (VWR International GmbH) were used.

Triclosan (Irgasan) was purchased from Sigma-Aldrich. Trifluoroacetic acide [TFA] (Sigma-Aldrich) and acetonitrile (HPLC grade, Sigma-Aldrich) were used for HPLC analysis.

Sodium chloride [NaCl], potassium dihydrogen phosphate [KH_2PO_4], disodium hydrogen phosphate [Na_2HPO_4] and potassium chloride [KCl] for the preparation of phosphate buffer pH 7.4 and pH 5.5 were all purchased from Merck.

Bacto™ Tryptone, Bacto™ Yeast Extract and Bacto™ Agar and Muller Hinton Agar for the preparation of LB agar plates and Mueller Hinton agar plates were purchased from BD Biosciences (Erembodegem, Belgium). For inoculation, Staph. aureus ATCC® 25923™ or

Staph. aureus RN4220 were used. For cell culture tests L929 mouse fibroblast (ATCC® CCL-1™), Accutase™ (PAA GmbH, Cölbe, Germany), Cell Proliferation Reagent WST-1 (Roche Diagnostics, Mannheim, Germany), Dulbecco's Modified Eagle Medium (DMEM part number 31966-021, Invitrogen™ Life Technologies, Darmstadt, Germany), Penicillin-Streptomycin (10000 IU/mL-10000 g/mL part number 15140-144, Invitrogen™ Life Technologies), HEPES 1 M (Invitrogen™ Life Technologies), Fetal Calf Serum (FCS, part number 10270-098, Invitrogen™ Life Technologies) and Isoton-III diluent (part number 8448044, Beckmann Coulter GmbH, Krefeld, Germany) were used. Furthermore, a LIVE/DEAD® Viability/Cytotoxicity Assay Kit consisting of a calcein AM solution (4 mM in anhydrous DMSO) and ethidium homodimer-1 solution (2 mM in DMSO/water 1:4 v/v) was purchased from Life Technologies (Darmstadt, Germany).

The used water was always Milli-Q (Merck Millipore, Darmstadt, Germany) water or distilled water.

3.2 Synthesis of PEG-PLA copolymers

PEG-PLA block copolymers with varying PEG content and polymer geometry were synthesized via standard ring opening polymerization of lactide with PEG10k of different geometry and with tin(II) 2-ethylhexanoate as catalyst (***Scheme 3.1***). Lactide and PEG were separately dissolved in toluene and a water/toluene azeotrope was distilled off the solutions using a dean stark trap to remove water traces. The water-free PEG and lactide solutions were united and the catalyst was added. The reaction mixture was refluxed overnight under a nitrogen flow and the toluene was removed with a rotary evaporator. The residue was dissolved in methylene chloride and the solvent was removed with a rotary evaporator in two or three repetitions. The polymer was then precipitated either from a viscous solution in methylene chloride into a mixture of iced ether/methanol (60/40) or from a viscous solution in acetone into iced water, filtrated and lyophilized. Synthesized were the triblock copolymers PLA45k-*b*-PEG10k-*b*-PLA45k [lin90] and PLA65k-*b*-PEG10k-*b*-PLA65k [lin130] with 70 % L-lactide and 30 % D, L-lactide as this ratio was also used for the synthesis of PLA35k-*b*-PEG10k-*b*-PLA35k [lin70] (HWL73 from Polymaterials) and the pure PLA (Resomer LR708 from Boehringer Ingelheim). Furthermore, a triblock PLA35k-*b*-PEG10k-*b*-PLA35k [lin70rac],

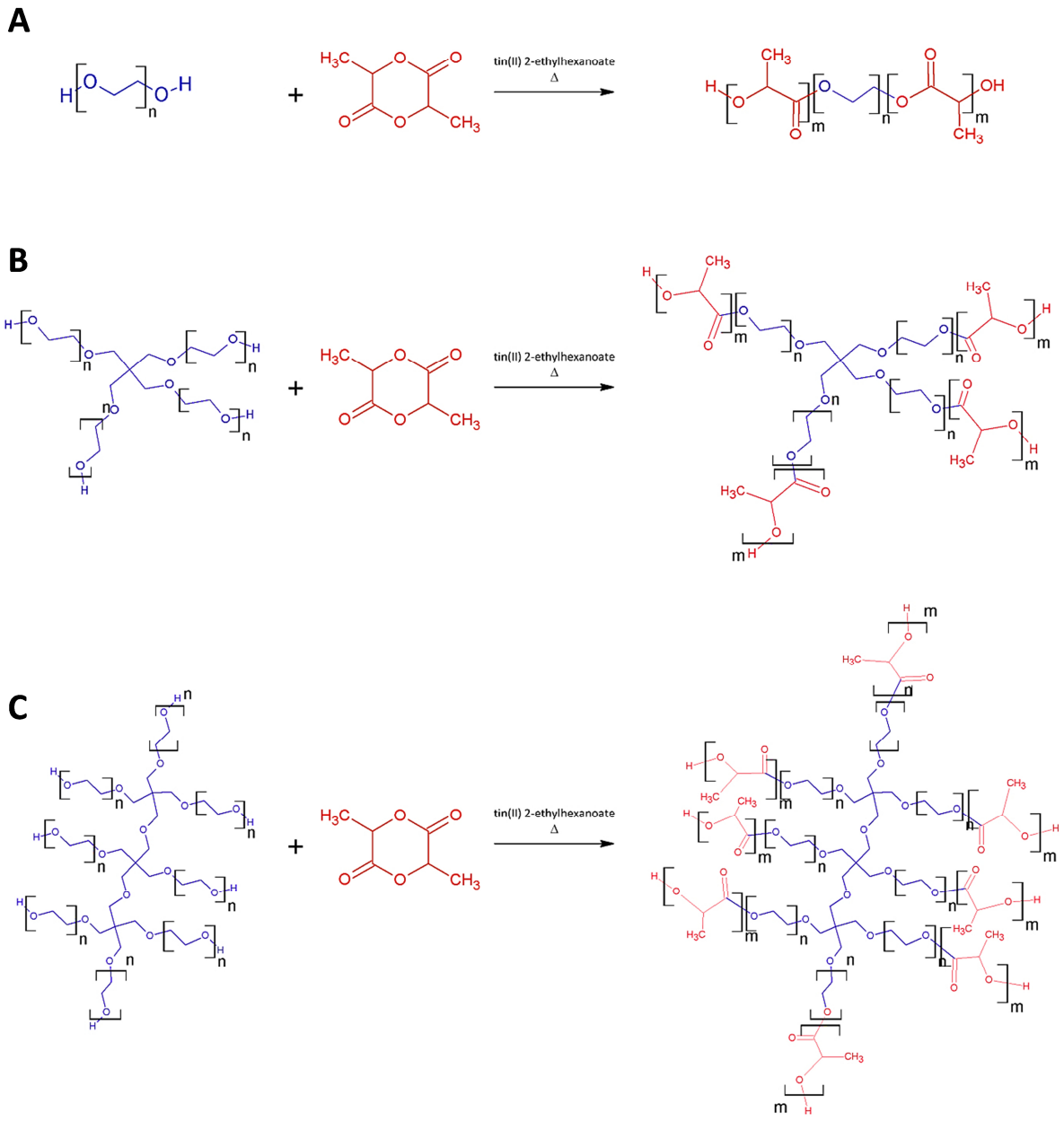

Scheme 3.1 *Reaction scheme of ring opening polymerization of linear triblock (A), 4arm star-shaped (B) and 8arm star-shaped (C) PEG-PLA.*

a 4armPEG10k-*b*-PLA70k [4arm70], a 4armPEG10k-*b*-PLA140k [4arm140], an 8armPEG10k-*b*-PLA70k [8arm70] and an 8armPEG10k-*b*-PLA140k [8arm140] were synthesized completely with 100 % racemic D, L-lactide. The front part of the abbreviation of the polymers used in the following chapters signifies the geometry of the PEG10k core, while the terminal number in the abbreviation of the polymers signifies the total molecular PLA content in kDa. The terminus rac stands for synthesis with racemic lactide and mainly serves to distinguish between the linear triblocks with similar molecular weights but with different PLA

composition. Since all of the star-shaped copolymers were synthesized with racemic PLA, these polymers are not further labelled with rac. The resulting copolymers were characterized via GPC, ^{1}H-NMR and DSC with regard to molecular weight and glass transition temperature. The measurements were carried out like described in 3.5.

3.3 Processing to potential polymeric barrier devices

3.3.1 Preparation of solid films

Solid films were fabricated by a solvent evaporation method using a film applicator (Erichsen Coatmaster 509 MC or 510, Hemer, Germany). Therefore, viscous polymer solutions were prepared, poured into a film applicator with defined gap clearance and drawn with constant speed to ensure consistent thickness and texture throughout the entire casting length (***Figure 3.1***).

PLA and PEG-PLA films for the experiments were prepared by solvent casting on Sigmacote®-coated glass plates. Therefore, the polymers were dissolved in methylene chloride in appropriate concentrations. To achieve films with a thickness of 20 µm (based on the commercially available thickness of SurgiWrap®), a 4 wt% PLA solution was cast with a gap clearance of 700 µm and a drawing-down speed of 5 mm/s, while 27 wt% solutions were prepared for the investigated PEG-PLA copolymers and cast with a gap clearance of 120 µm at 5 mm/s. The films were allowed to dry overnight under a fume hood at room temperature and were then stored under vacuum prior to use to remove residual solvent. Film thickness was determined with a microprocessor coating thickness gauge (MiniTest 600 or 650, ElektroPhysik, Cologne, Germany).

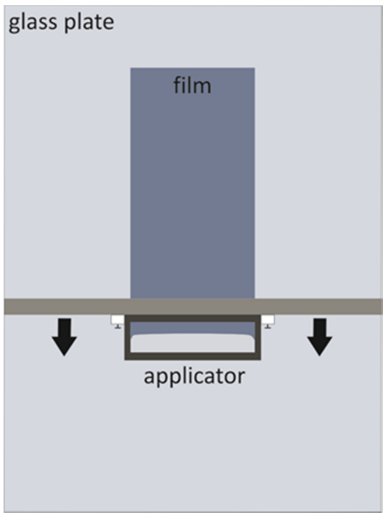

Figure 3.1 *Film casting process.*

Alginate films were cast on uncoated glass plates from a 3 wt% or 5 wt% solution in water with 3 % or 5 % glycerol as additive. A film applicator was used with a gap clearance of 700 µm and a drawing-down speed of 5 mm/s. After casting, the films were dried overnight under a fume hood at room temperature.

3.3.2 Preparation of solution electrospun non-woven meshes

Solution electrospinning was carried out with a process set-up like illustrated in ***Figure 3.2***. A polymer solution was placed in a syringe and fed through a needle (inner diameter: 0.4 mm) with a syringe pump at a constant feeding rate. Then a high voltage was applied and the electrospun fibers were collected on a grounded rotating collector drum (diameter: 6 cm; width: 10 cm) with additional reciprocating motion, which was positioned at a distance of 15 cm from the needle tip.

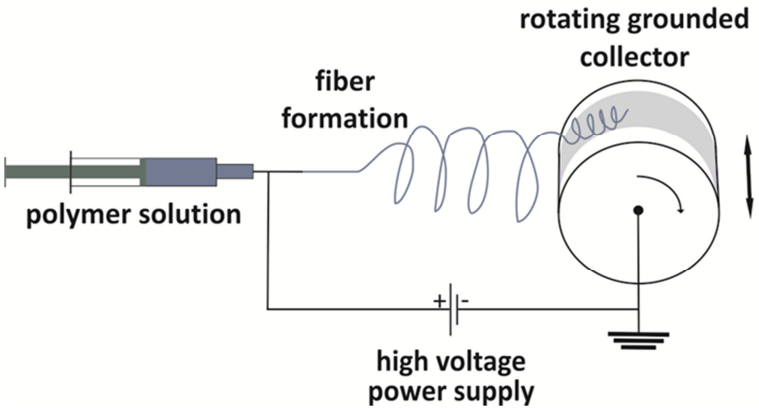

Figure 3.2 *Solution electrospinning set-up.*

To produce non-woven meshes for the experiments, solution electrospinning was mainly carried out with solutions in acetone/DMSO (90:10 % (v/v)) at room temperature. Thereby, concentrations in the range of 28-44 % (m/V) were prepared for the PEG-PLA copolymers, 28 % (m/V) for PLGA and concentrations of 3-7 % (m/V) for PLA. The electrospinning process was then conducted with a feeding rate of 0.5 mL/h and a high voltage of 12 kV. In addition, PLA solutions in DMF or methylene chloride were tested for electrospinning. Therefore, a high voltage of 12-14 kV and a feeding rate of 0.5-1.5 mL/h were used. After electrospinning all meshes were stored under vacuum overnight to remove residual solvent and subsequently in a refrigerator prior to use. The resulting fiber morphology and fiber diameters were examined via SEM as described under 3.4.2.

3.3.3 Preparation of bifunctional PLA/alginate membranes

3.3.3.1 Solvent casting of PLA/alginate bilayers

20 µm thick PLA films were cast on Sigmacote®-coated glass plates as described under 3.3.1 and allowed to dry overnight under a fume hood at room temperature. To prepare bilayers consisting of a PLA film and an alginate film, an alginate solution was cast directly on top of the dry PLA film (***Figure 3.3***). Therefore, solutions of 3 wt% or 5 wt% alginate in water with equal amounts of glycerol as additive were prepared and then cast with a gap clearance of 700 µm and a drawing-down speed of 5 mm/s. To be able to distinguish between the layers, the alginate solutions were stained with Water Blue before casting. The bilayers were dried overnight at room temperature before use.

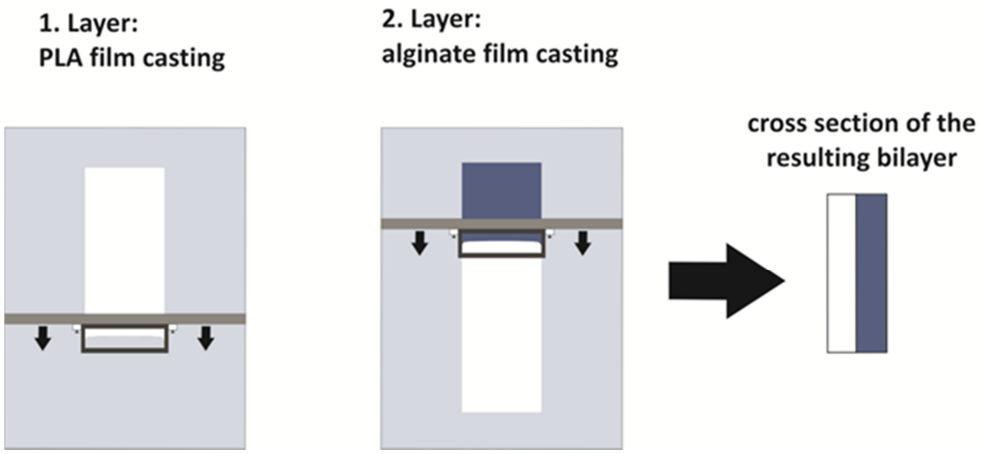

Figure 3.3 *Fabrication of bilateral PLA/alginate membranes consisting of a PLA and an alginate layer.*

3.3.3.2 Preparation of PLA/mesh/alginate trilayers

20 µm thick PLA films were cast on Sigmacote®-coated glass plates as described under 3.3.1 and dried under a fume hood overnight. To apply an electrospun mesh as intermediate second layer, a dried PLA film was tightly wrapped around a collector drum and solution electrospinning was carried out with polymer solutions of PLA, lin130, lin70 or lin70rac in acetone/DMSO (90:10 % (v/v)) as described under 3.3.2. The fibers were collected on the film covering the rotating collector drum and the film/mesh bilayers were stored under vacuum overnight to remove residual solvent (***Figure 3.4***). To apply the alginate layer, a 3 wt% or 5 wt% alginate solution in water with 3 wt% or 5 wt% glycerol was prepared. The alginate

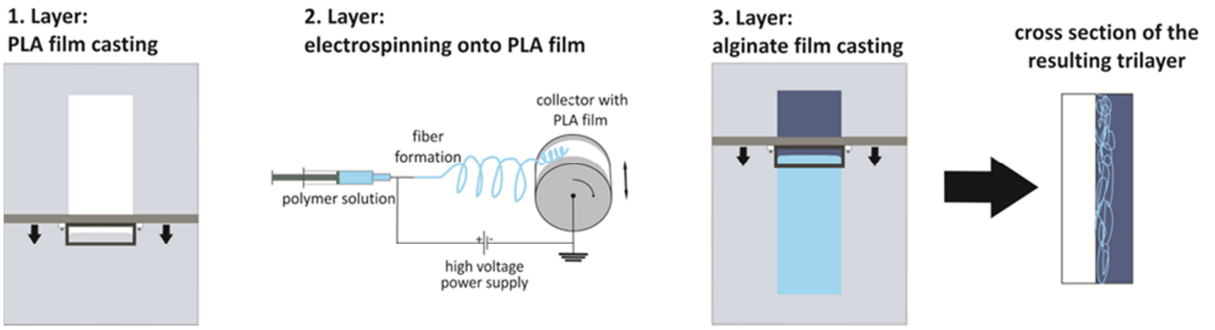

Figure 3.4 *Fabrication of bilateral PLA/alginate membranes consisting of a PLA film, a solution electrospun mesh and an alginate layer.*

solution was then cast on top of the solution electrospun mesh with a gap clearance of 700 µm and a drawing-down speed of 5 mm/s. Subsequently, the entire membrane was allowed to dry overnight at room temperature.

3.4 Determination of surface properties

3.4.1 Contact angle measurements

Contact angles of solvent cast films and solution electrospun meshes were determined at room temperature (24 °C) with a Contact Angle System (OCA 20, Data Physics Instruments GmbH, Filderstadt, Germany) equipped with a TD-DE/3 electronic multiple direct dosing system (Data Physics Instruments GmbH) and a CCD camera from IDS (Imaging Development Systems GmbH, Obersulm, Germany) with a maximal resolution of 768 × 576 pixel using a static sessile drop method. A water droplet of 3 µL was generated with a dosing rate of 1.0 µL/s from a 500 µL Hamilton Syringe. A minimum of three droplets was measured on different locations of each sample and assessed via an ellipse fitting. To reveal eventual changes over time, the contact angle of each droplet was determined immediately and once again two minutes after initial water contact with dry as-spun meshes and as-cast films. Additional samples were allowed to swell overnight in NaCl-containing phosphate buffer pH 7.4 (Ph. Eur. 6.0) containing 0.05 % NaN_3. After dry-blotting, contact angles of the swollen samples were determined analogous to the as-fabricated samples initially and two minutes after initial droplet contact.

3.4.2 Scanning Electron Microscopy [SEM]

The samples to be investigated were pretreated by gold sputtering (EMITECH K550 sputter coater, Quorum Technologies, West Sussex, United Kingdom) to minimize charging effects. For the acquisition of SEM images, a Digital Scanning Microscope DSM 940 from Carl Zeiss Microscopy GmbH (Oberkochen, Germany) was used at an accelerating voltage of 5 kV. For further evaluations of fiber morphology, fiber diameters were additionally determined with Image J Software by arithmetic averaging of a minimum of 50 fibers.

Investigated were dry as-spun meshes with and without drug loading, meshes after degradation, meshes after mechanical testing and meshes after dry incubation at 37 °C for predetermined time periods (0.5 h, 2 h, 4 h, 24 h).

3.4.3 Light microscopy/stereomicroscopy

A stereomicroscope (Zeiss Discovery V20, Carl Zeiss Microscopy GmbH, Oberkochen, Germany) was used to visualize the individual layers of the prepared bilateral bilayers and trilayers in cross-sectional images.

3.5 Further analytical methods

3.5.1 Nuclear Magnetic Resonance spectroscopy [^{1}H-NMR]

For molecular weight estimations of the raw polymers and of films and meshes during degradation, ^{1}H-NMR spectra were recorded at 300 MHz using a Bruker Avance 300 or a Bruker Fourier 300 (Bruker Corporation, Billerica, USA). For the measurements, the material was dissolved in $CDCl_3$ at concentrations of 10-20 mg/mL with added trimethylsilane [TMS] as internal standard. The obtained spectra were assessed with WIN-NMR or ACD/NMR Processor Academic Software. The integrated signal of the methine protons of the lactyl repeating unit at 5.15 ppm was set in relation to the singlet at 3.65 ppm corresponding to the methylene protons of the PEG repeating unit for the calculation of polymer composition and molecular weight estimations.

3.5.2 Gel Permeation Chromatography [GPC]

Molecular weights (M_w, M_n) and dispersity ($Đ = M_w/M_n$) of the raw polymers and degraded films and meshes were determined in chloroform via a standard calibration relative to polystyrene standards [PS] (Merck) using either a system from Shimadzu (Duisburg, Germany) consisting of a SCL-10A VP system controller, a SIL-10AD VP autoinjector, a LC-10AT VP pump, a FCV-10AL VP degasser, a RID-10A refractive index detector (RID, run at 40 °C) and a CTO-10AC VP column oven (run at 40 °C), equipped with a Phenogel™ 5 µm linear (2) LC column (300 × 7.8 mm, 100-10000 kDa) (Phenomenex, Aschaffenburg, Germany) or a system from Jasco (Easton, USA) consisting of a RI-2031 Plus refractive index detector, a PU-2080 Plus pump, a DG-2080-53 3 Line Degasser, a AS 2055 Plus autosampler and a LC Net II/ADC, equipped with a SDV linear M 5 µm column (300 × 8 mm, 100-10000 kDa) (PSS Polymer Standards Service GmbH, Mainz, Germany), whereby column oven and RID were run at 25 °C. The data was recorded with Class-VP™ or Jasco ChromPass Chromatography Data Software. The samples were dissolved in chloroform (8-15 mg/mL) and filtered through PTFE filter membranes with a pore size of 0.45 µm before injection. Degassed chloroform was also used as mobile phase with a flow rate of 1.0 mL/min.
The measurements with the different GPC systems were conducted in a way to achieve best possible comparable results. Measurements for a direct comparison of polymers and samples were performed on the same apparatus.

To gather further information about the degree of branching of the PEG educts (linPEG10k, 4armPEG10k, 8armPEG10k) and selected synthesized copolymers (lin70, 4arm70, 8arm70), in addition to the conventional method a triple detection method was conducted. The analysis was conducted on an OmniSEC GPC system from Malvern Instruments (Worcestershire, England) with a Viscotec Triple Detector Array (TDA-MAX-305 with RI, light scattering and viscosity detector) equipped with a ViscoGel T6000M column, a ViscoGel T2500 and a guard column. The samples were dissolved in chloroform (1.25 mg/mL) and filtered through a 0.45 µm nylon filter before use. The measurements were run with an injection volume of 100 µL, a flow rate of 1.0 mL/min and a column and detector temperature of 35 °C. Acetone instead of the sample solvent chloroform was used as eluent to achieve enhanced RI and LS detector sensitivities since the RI increment dn/dc is

increased due to a lower RI of acetone in comparison to chloroform (Solvent Enhanced Light Scattering GPC). The data was recorded and processed with OmniSEC software.

Weight average molecular weights M_w were determined from light scattering via the simplified Zimm equation

$$\frac{Kc}{R_\theta} = \frac{1}{M_w} \tag{3.1}$$

where K is a sample dependent constant, c is the concentration of the sample and R_θ is the Rayleigh ratio. By splitting each chromatogram into i equidistant slices, for each slice M_w [M_i] was calculated according to the already mentioned Zimm equation and the polymer concentration c_i was determined by the RI detector. With those parameters, the number average molecular weight M_n and the weight average molecular weight M_w of the sample were calculated by

$$\bar{M}_n = \frac{\sum (c_i M_i)}{\sum c_i} \tag{3.2}$$

$$\bar{M}_w = \frac{\sum (c_i M_i^2)}{\sum (c_i M_i)} \tag{3.3}$$

For the determination of branching of the samples, the g-factor was calculated by

$$g = \left(\frac{[\eta]_{br}}{[\eta]_{lin}} \right)_M^{\frac{1}{\varepsilon}} \tag{3.4}$$

where ε was set to 0.75, $[\eta]_{br}$ is the intrinsic viscosity of the branched polymer with the number of arms to be calculated and $[\eta]_{lin}$ is the intrinsic viscosity of corresponding linear polymer with similar molecular weight, both determined with the viscosity detector. Based on the calculated g-factor, the number of arms f of the star-shaped polymers was calculated by an equation derived from Zimm and Stockmeyer

$$g = \frac{3f - 2}{f^2} \tag{3.5}$$

3.5.3 Differential Scanning Calorimetry [DSC]

Thermal analysis of raw polymers, as-spun meshes and as-cast films for direct comparison were measured in non-hermetic aluminium pans (pierced lid) with a DSC 204 F1 Phoenix 240 from Netzsch (Selb, Germany) with a heating rate of 5.0 K/min from -50 °C to 210 °C under a nitrogen flow (70 mL/min). Samples were heated twice and T_g was determined from the second heating run with Proteus® Analysis Software.

Degraded mesh and film samples were either analyzed in non-hermetic aluminium pans with a DSC 204 F1 Phoenix 240 with a heating rate of 10 K/min from -50 °C to 210 °C or in hermetic aluminium pans with a DSC from TA Instruments (Eschborn, Germany) in modulated mode (amplitude: 0.32 °C, period: 60 s) from -45 °C to 210 °C with a heating rate of 2 °C/min under a nitrogen flow (65 mL/min). Each sample was heated twice and T_g was determined from the second heating run with TA Instruments Universal Analysis Software.

The measurements with the different DSC systems were conducted in a way to achieve best possible comparable results. Measurements for direct comparison were performed on the same apparatus.

3.5.4 Rheological characterizations of electrospinning solutions

Rheological investigations of the polymer solutions used for electrospinning were conducted at 20 °C on a Physica MCR301 (Anton Paar Germany GmbH, Ostfildern-Scharnhausen, Germany) using plate-plate measuring geometry (PP25, 25 mm diameter) with a gap of 0.5 mm and a sample volume of 500 µL. An ascending shear rate was applied and the resulting viscosity and shear stress were determined. The measurements were conducted in triplicate and assessed with RheoCompass™ Software.

3.5.5 Statistical analysis

One way and two way analysis of variance [ANOVA] was performed with SigmaPlot 12.0 (Systat Software GmbH, Erkrath, Germany). In order to evaluate the statistical significance of the individual values, a post-hoc Tukey test was used as a pairwise multiple comparison procedure whereby a p value < 0.05 was considered statistically significant.

3.6 Mechanical evaluations

All mechanical tests were conducted on a universal testing machine (Instron 5542, Pfungstadt, Germany or Zwick Z010, Zwick GmbH & Co. KG, Ulm, Germany) with a 100 N (Zwick) or 60 N (Instron) load cell. The resulting diagrams of a minimum of five test specimens per sample were recorded with Bluehill® or testXpert II Software. The measurements with the different texture analyzers were conducted in a way to achieve best possible comparable results. Measurements for direct comparison were performed on the same apparatus.

3.6.1 Tensile test

Tensile properties were determined uniaxial via a standard tensile test (basic principle from ASTM D882-02[244]). The test was carried out with 5 cm × 1 cm strips of dry 20 µm thick as-cast films, dry 20 µm thick as-spun meshes and the marketed product Mesofol® at different temperatures to characterize the behavior of samples both at surgery temperature (20 °C) and at body temperature (37 °C). An additional test temperature of 30 °C was set up with the intention to further visualize the influence of the different glass transition temperatures of the investigated polymers. The measurements were conducted with biplane grips at a crosshead speed of 100 mm/min and a gauge length of 3.0 cm. The resulting load – strain diagrams were recorded until the specimen ruptured and tensile strength was calculated by

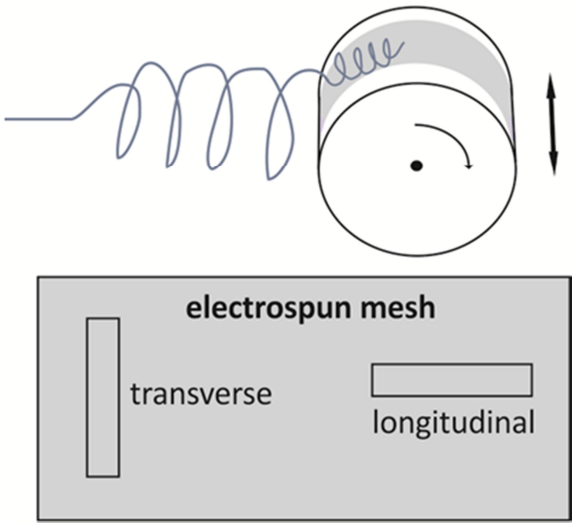

Figure 3.5 *Illustration of the cutting direction of solution electrospun meshes used for tensile testing. Longitudinal direction means alongside the rotating direction of the drum around its axle. Transverse direction means alongside the reciprocating motion of the drum.*

dividing the load by the original cross-sectional area of the sample. Thereby, the entire cross-sectional area of the mesh specimen was utilized for calculations as an accurate determination of the actual polymer fiber cross-section bearing the load is rather difficult. For conditioning purposes, the solid films were held at test temperature for two hours before measuring. In contrast, the electrospun meshes were exposed to the respective test temperature only for two minutes prior to the test to avoid coalescence of the individual fibers at elevated temperature. Furthermore, the meshes were investigated both in longitudinal and transverse direction (***Figure 3.5***) to evaluate the influence of eventual fiber orientation due to fiber deposition on a rotating collector on the mechanical properties. After conducting the test, eventual changes in fiber morphology were examined via SEM.

The tensile properties of bilateral PLA/alginate membranes (bi- and trilayers) were determined at room temperature (24 °C) with 5 cm × 5 cm strips as test specimens. The test specimens were fixed on each side between one plane and one convex grip. Then the test was carried out at a crosshead speed of 12.5 mm/min and a gauge length of 3.5 cm until the sample ruptured. The resulting load – strain diagrams were recorded and assessed.

3.6.2 Puncture test

A puncture test[207,245–246] was carried out with 5 cm × 5 cm squares of 20 µm thick films and meshes. Thereby, a metal puncture probe with a hemispherical end (diameter: 1 cm) was run through the test specimen, which was fixed on a metal sample holder with a cylindrical hole of 2.5 cm diameter (***Figure 3.6***). The measurements were conducted at a test velocity of 10 mm/min and the resulting load - displacement diagrams were recorded until the specimen was perforated. As it is rather impossible to correctly define the area affected by the metal probe for a determination of puncture strength, the load to puncture was used for analysis, which corresponds to the maximum load. The elongation to break was approximatively calculated based on the concept of Radebaugh et al.[245] from the displacement d at the point of specimen failure by

$$\text{elongation to puncture (\%)} = \frac{\sqrt{r^2+d^2} - r}{r} * 100 \qquad (3.6)$$

where r is the radius of the cylindrical hole (***Figure 3.6***).

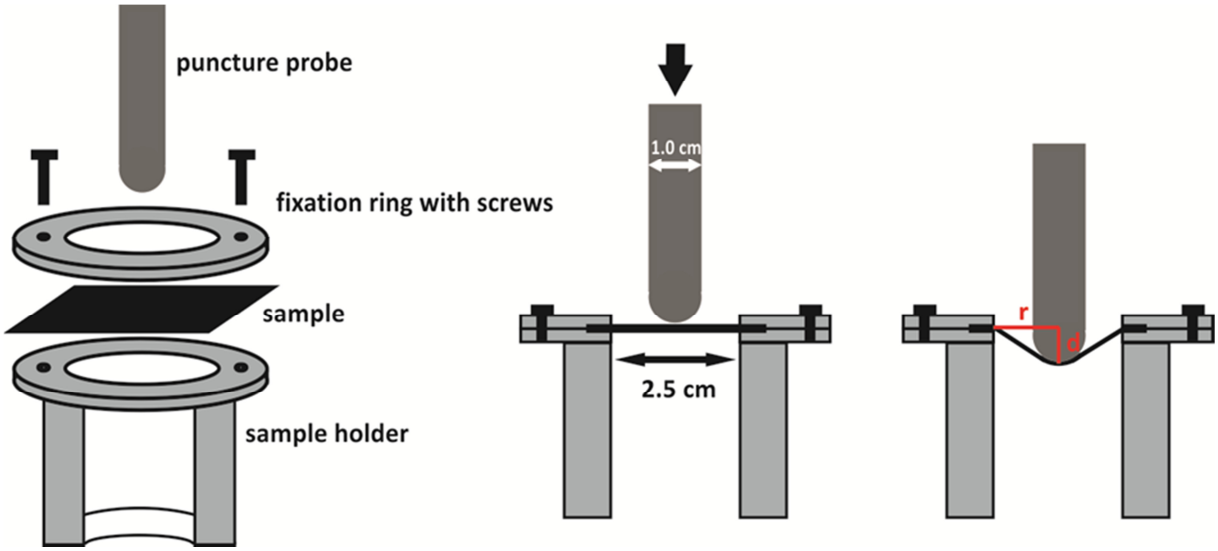

Figure 3.6 *Puncture test set-up.*

Analogous to the tensile test, the puncture test was performed with dry as-cast films and dry as-spun meshes at 20 °C, 30 °C and 37 °C. The solid films were conditioned at test temperature for 2 h prior to the test and the electrospun meshes for 2 min. Additional samples were incubated at 37 °C in NaCl-containing phosphate buffer pH 7.4 (Ph. Eur. 6.0) containing 0.05 % NaN_3. At predefined time points (4 h, 24 h, 1 week) samples were removed, dry blotted and tested at 37 °C to evaluate the mechanical properties upon degradation. The zero value was determined at 37 °C after dipping the sample for 5 s in phosphate buffer pH 7.4 and subsequent dry blotting. Moreover, the puncture test was conducted at 20 °C with sterilized film samples to evaluate the polymer stability towards electron beam irradiation.

3.6.3 Suture pullout test

To determine the maximum axial force that a cast film or electrospun mesh is able to withstand before a surgical suture is pulled out of the suture hole, a suture pullout test was performed according to a test report from the first film manufacturer MacroPore ("Test Report Tensile and Suture Pullout Properties of SupraFoil Implant Material"), which was oriented on the suture pullout test from Yamada et al.[247] The test was conducted at 20 °C to mimic surgery conditions with dry 5 cm × 2 cm squares of 20 µm films as well as 20 µm or

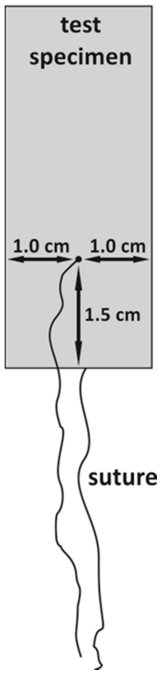

Figure 3.7 *Positioning of the surgical suture in the test specimen.*

40 µm thick meshes as test specimens and a 3-0 polyglactin 910 suture (Vicryl ethicon; Johnson and Johnson, 4×45, 2 Ph.Eur, 4PG2543Y). The suture was drawn through the test specimen at a distance of 1.5 cm from the edge of the narrow end and 1 cm from both sides like illustrated in ***Figure 3.7***. The upper clamps of the universal testing machine were positioned at a distance of 5 cm from the lower clamps. The test specimen was then fixed by the upper clamps and the loose ends of the suture were fixed by the lower clamps in the way that the suture was hanging without any tension between clamps and test specimen. The test was carried out with a crosshead speed of 50 mm/min and load was recorded until the suture was pulled out of the test specimen. The maximal achieved load was considered as suture pullout force and used for data analysis.

3.6.4 T-peel test

To study the cohesion between the individual layers of bilateral PLA/alginate membranes, a t-peel test (basic principle from ASTM D1876-08[248]) was conducted at 24 °C with 5 cm × 1 cm strips cut out of the bi- and trilayers prepared like described under 3.3.3. Each test specimen was pre-separated at one end for a length of 1 cm. Prior to the test, the

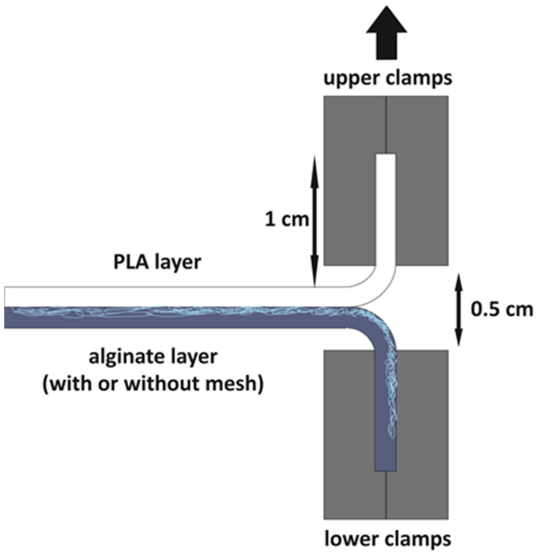

Figure 3.8 *Performance of t-peel test.*

biplane clamps of the universal testing machine were positioned at a distance of 0.5 cm. The PLA layer was fixed by the upper clamps of the universal testing machine and the alginate layer respectively alginate layer with mesh was fixed on the lower clamps like illustrated in ***Figure 3.8***. The upper grip was then driven upwards at a crosshead speed of 250 mm/min and the load was recorded until the layers were completely separated. The average load was calculated as the average of load taken from 5 mm to 60 mm head movement and the peel strength was determined by dividing the average load by the width of the test specimen.

3.6.5 Bioadhesion test

A bioadhesion test was performed at 24 °C with the bilateral PLA/alginate membranes prepared like described under 3.3.3 in comparison to a single PLA film, which was solvent cast like described under 3.3.1. Since there is no agreed standard test method for the evaluation of bioadhesive strength,[249] a test set-up was constructed which was best possible tailored to the intended application of the membranes as physical barrier device for adhesion prevention. 5 cm × 1 cm strips were cut out of the membranes and used as test specimens. The particular test specimen was fixed on the bottom of a metal probe with a resulting measuring surface of one square centimeter. The bilateral membranes were fixed on the metal probe with the alginate layer along the outside so that the adhesion strength of the alginate side could be determined. As biological surface to test the bioadhesive strength on the exterior of natural tissue served a piece of small intestine of a male domestic pig (eight weeks old, 18 kg), which was fixed outside up on a sample holder. Prior to use, the small intestine was stored in PBS pH 7.4 containing 5 mL/100 mL PenStrep to avoid bacterial growth and putrefaction. To achieve similar test conditions for all samples, the fixed piece of small intestine was sprinkled with PBS containing PenStrep prior to each measurement. To carry out the measurement, the metal probe with the attached membrane sample was driven downwards to make and hold contact with the exterior of the intestine with a compressive load of 0.1 N. After 30 s contact time, the metal probe was raised from the intestine with a crosshead speed of 0.5 mm/s and the resulting load was recorded until the test specimen was completely separated from the intestine. Bioadhesive strength was calculated by dividing the required maximum load to detach the membrane from the intestine by the contact area.

3.7 Swelling and degradation studies

3.7.1 Swelling and degradation of solid films

For degradation studies simulating normal body conditions, 20 µm thick film disks (diameter: 2 cm) were used as test specimens (***Figure 3.9***) and incubated over eight weeks at 37 °C in 10 mL NaCl-containing phosphate buffer pH 7.4 (Ph. Eur. 6.0) containing 0.05 % NaN_3 to avoid bacterial growth. Every week, four samples of each polymer were removed and rinsed with water to remove buffer salts. Then the samples were dry blotted and weighed to determine the wet weight for swelling calculations. Afterwards, the disks were lyophilized and weighed again to determine the dry weight for mass loss calculations. The dry specimens were then further analyzed via ^{1}H-NMR, GPC and DSC like described under 3.5 to evaluate changes during degradation. Untreated polymer film disks served as references for week zero. The water uptake was calculated by

$$\text{swelling (\%)} = \frac{(W_w - W_d)}{W_d} \times 100 \tag{3.7}$$

and the remaining mass upon degradation was determined by

$$\text{remaining mass (\%)} = \frac{W_d}{W_i} \times 100 \tag{3.8}$$

where W_w is the weight of the swollen specimen, W_d is the dry weight after lyophilization and W_i is the initial weight of the sample prior to buffer contact. The swelling was calculated related to the dry weight since this calculation determines most accurately the water uptake of the material present at any time point.

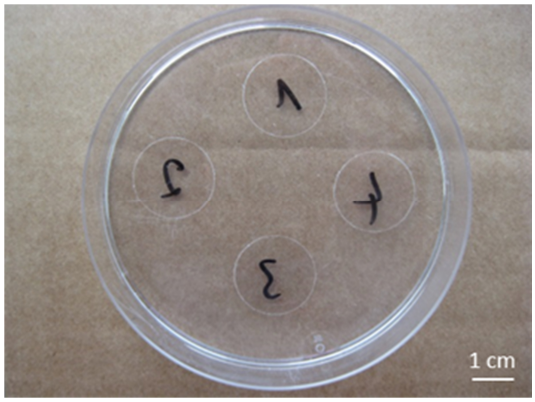

Figure 3.9 *Exemplary test specimens of 4arm140 film.*

Apart from the study at pH 7.4, degradation studies were also performed analogous in phosphate buffer pH 5.5 R (Ph. Eur. 7.0) containing 0.05 % NaN_3 to simulate inflammatory conditions since mostly an acidic pH can be found at sites of inflammation partly with values partly below pH 6.0.[250–251] A pH of 5.5 was chosen to cover worst case conditions.

3.7.2 Swelling and degradation of electrospun meshes

The swelling and degradation studies of solution electrospun meshes were conducted under similar conditions as the studies with solvent cast films. Mesh specimens were incubated over eight weeks at 37 °C in NaCl-containing phosphate buffer pH 7.4 (Ph. Eur. 6.0) containing 0.05 % NaN_3 to simulate physiological conditions and besides weighing of the samples in initial, wet and dried state to determine water uptake and mass loss, further analytical methods (GPC, ^{1}H-NMR, DSC) were applied at predetermined time points to reveal occurring changes during degradation. Analogous to the experiments with films, the swelling and remaining mass were calculated according to the equations (3.7) and (3.8).
In addition to the measurements that were performed with the films as well, SEM images of degrading non-wovens were recorded to visualize eventual changes in fiber morphology. Moreover, mesh samples were sized to determine the extent of shrinkage.

For the determination of shrinkage, 20 µm thick mesh disks (diameter: 2 cm) (***Figure 3.10***) were used in triplicate as test specimens because of an easy handling and an accurate determination of the change of the mesh dimension. After rinsing with water and lyophilizing, SEM images to evaluate the fiber morphology were recorded with these

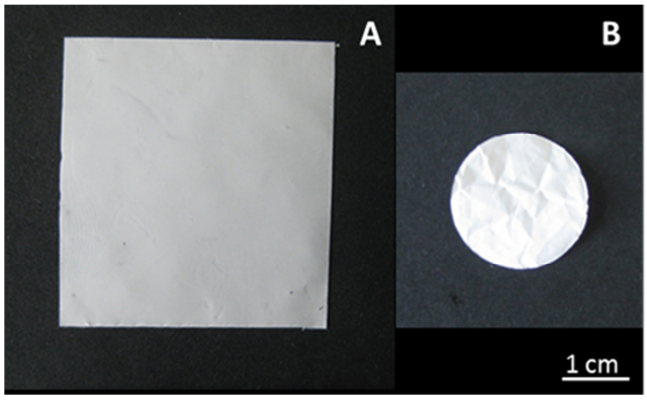

Figure 3.10 *Initial appearance of a 4 cm × 4 cm square (A) and a disk (diameter: 2 cm) (B) test specimen for mesh degradation.*

samples as well. For the determination of swelling, mass loss and for further analysis via GPC, ^{1}H-NMR and DSC, 20 µm thick 4 cm × 4 cm mesh squares served as test specimens to obtain sample masses high enough for accurate weighing and providing sufficient material for the applied analytical methods since the meshes had distinctly lower weights than films with comparable thickness.

3.8 Cell culture tests

3.8.1 WST-1 assay/Cell adhesion test

Cell adhesion and cell viability tests were performed in 24-well plates in quadruplicate with film and mesh disks (diameter: 2 cm) that were fixed on the bottom of the wells with stainless steel cylinders (inner diameter: 1.1 cm). For the experiment, mesh and film disks of PLGA, PLA and lin70rac were used. The PS bottoms of the cell culture plates were used as references. The samples were first washed with PBS pH 7.4 (8.0 g NaCl, 0.2 g KH_2PO_4, 2.8 g Na_2HPO_4, 0.2 g KCl ad 1,000 mL water). Then 1.0 mL L929 mouse fibroblast cell suspension (100,000/mL) in DMEM medium (with added 10 % FCS, 1 % PenStrep, 1 % HEPES) was added to each well and the well-plates were incubated at 37 °C under 5 % CO_2 for one, three or seven days. For the WST-1-based assay, the medium was aspirated and 0.5 mL WST-1 reagent were added to each well and incubated for 30 min. The absorbance of 200 µL supernatant was measured in duplicate with a Tecan spectrafluor plus plate reader (Tecan, Männedorf, Switzerland) at 450 nm and a reference wavelength of 690 nm. For cell counting of the adhered cells, the cells were washed twice with 1.0 mL PBS pH 7.4 before 0.5 mL Accutase® were added and the well-plates were incubated for 10 min to detach the cells. After homogenizing the suspension, 100 µL were mixed with 10 mL CASYton and the cells were counted with a CASY model TT cell counter (Roche Diagnostics GmbH, Penzberg, Germany). The results were calculated per surface area related to the highest occurring PS value.

3.8.2 Live/Dead cell viability assay

The live/dead cell viability assay was carried out in 12-well plates with film and mesh disks (diameter: 2 cm) which were fixed on the bottom of the wells with stainless steel cylinders (inner diameter: 1.1 cm). For the experiment, film and mesh disks of PLGA, PLA and lin70rac were used. The PS bottoms of the cell culture plate served as a reference. The samples were washed with PBS. Subsequently, 1.0 mL DMEM medium was put around the steel cylinder in each well and 1.0 mL L929 mouse fibroblast cell suspension (100,000/mL) in DMEM medium (with added 10 % FCS, 1 % PenStrep, 1 % HEPES) was added to each well inside of the steel cylinder. Then, the well-plates were incubated at 37 °C under 5 % CO_2. At predetermined time points (one, three and seven days after cell seeding), the samples were washed twice with PBS and 300 µL of the staining solution was added. The staining solution consisted of 20 µL calcein AM solution and 5 µL ethidium homodimer solution in 10 mL PBS. After 30 min incubation at room temperature under exclusion of light, the staining solution was aspirated and the samples were analysed with a fluorescence microscope (Axio Imager M1, Carl Zeiss Microscopy GmbH, Oberkochen, Germany) with filter set 20 (item number 488020-9901-000) and filter set 10 (item number 488010-9901-000) from Carl Zeiss Microscopy GmbH. Living cells were stained with calcein resulting in a green fluorescence. Red fluorescence of ethidium homodimer indicates dead cells.

3.9 Drug release studies with triclosan

3.9.1 Preparation of drug loaded films and meshes

The loading dose of the polymer films was oriented on the MIC of triclosan on Staph. aureus (0.025-1 mg/L[233]) as well as on the drug content of the Vicryl® plus suture material (12-60 µg/m[229]).

3.9.1.1 Preparation of triclosan loaded films

For drug release studies, 20 µm thick PLA and PEG-PLA films as well as drug-free PLA films with triclosan containing PEG-coating were prepared with a triclosan loading of 1 µg, 25 µg or 50 µg triclosan per test specimen (disks with 2 cm diameter). For the preparation of PLA and PEG-PLA films with triclosan, 4 wt% PLA or 27 wt% PEG-PLA was dissolved in appropriate stock solutions of triclosan in methylene chloride. The solutions were cast on Sigmacote®-

coated glass plates with a film applicator at a drawing-down speed of 5 mm/s. A gap clearance of 700 µm was used for the PLA solutions and a gap clearance of 120 µm for the PEG-PLA solutions. After casting, the films were dried overnight under a fume hood at room temperature and subsequently stored under vacuum to remove residual solvent. Film thickness was determined with a microprocessor coating thickness gauge after drying.

PEG-coated PLA films with 1 µg or 10 µg triclosan per disk were prepared by casting a solution of 0.5 g PEG400 and 1.0 g PEG4000 in 1.5 mL appropriate triclosan stock solution in methylene chloride with a gap clearance of 90 µm and a drawing down-speed of 5 mm/s onto a 20 µm thick PLA film.

As film disks (diameter: 2 cm) were used as test specimens for the *in vitro* drug release study as well as for the agar diffusion test, the intended drug content was calculated as $mass_{triclosan}$/disk.

$$\frac{mass_{triclosan}}{disk} = \frac{mass_{triclosan}}{casting\ solution} \times \frac{r_{disk}^2 \times \pi}{length_{film} \times width_{film}} \tag{3.9}$$

All triclosan loaded films were protected against light during storage to prevent photodegradation of the triclosan.[252]

3.9.1.2 Preparation of triclosan loaded meshes

Solution electrospinning was carried out with 4 % (m/V) PLA or 24-32 % (m/V) PEG-PLA solutions in a mixture of a triclosan stock solution in acetone and DMSO (90:10 % (v/v)) with 12 kV and a feeding rate of 0.5 mL/h on a rotating collector drum (diameter: 6 cm; width: 10 cm) with additional reciprocating motion which was masked to a width of 7 cm for PLA or a width of 8 cm for PEG-PLA to achieve a defined area and a preferably evenly high mesh with a consistent drug content. As disks (diameter: 2 cm) were used for agar diffusion tests the intended drug content (25 µg) was calculated as $mass_{triclosan}$/disk.

$$\frac{mass_{triclosan}}{disk} = \frac{mass_{triclosan}}{spinning\ solution} \times \frac{r_{disk}^2 \times \pi}{2\pi r_{drum} \times width_{masked\ drum}} \tag{3.10}$$

Besides meshes that were drug loaded by electrospinning, drug-free electrospun meshes were impregnated with triclosan after the spinning process. Therefore, mesh disks (diameter: 2 cm) were sprinkled twice with 20 µL of a solution of triclosan in absolute ethanol (0.625 mg/mL) to achieve a triclosan content of 25 µg/disk. The ethanol was allowed to evaporate before use to avoid bacterial inhibition due to the still present ethanol. To make sure that the fibers withstood the ethanolic treatment, dried ethanol sprinkled meshes were examined via SEM before conducting further investigations.

All triclosan loaded meshes were protected against light during storage to prevent photodegradation of the drug.[252]

3.9.2 *In vitro* triclosan release study

The *in vitro* release of triclosan was investigated in triplicate from 20 µm thick films of 8arm70, 4arm70, lin70rac, lin70 and PLA using film disks (diameter: 2 cm) as test specimens, each containing about 25 µg of triclosan. Furthermore, the release from a PEG coated PLA film containing about 10 µg per disk was investigated (higher detection accuracy compared to 1 µg per disk). As triclosan is poorly soluble in water (0.002 mg/mL at 30 °C) as well as in buffer pH 7.4 (0.004 mg/mL at 30 °C),[253] a mixture of absolute ethanol and NaCl-containing phosphate buffer pH 7.4 (Ph. Eur. 6.0) containing 0.05 % NaN_3 (25:75 % (v/v)) was used both as release medium and as solvent for the calibration solutions. After adding 5 mL pre-warmed release medium to each disk, the glasses with the samples were stored at 37 °C in a shaking water bath. The glasses were tightly sealed to avoid solvent evaporation and were protected from light to prevent photodegradation.[252] At predetermined time points, 300 µL were taken from each sample for HPLC analysis and replaced with 300 µL fresh pre-warmed release medium. HPLC analysis was performed on a system from Shimadzu (Duisburg, Germany), consisting of a Knauer degasser, an auto injector SIL-AD VP, a liquid chromatograph LC-10AT, a FCV-10AL VP, a column oven CTO-6A, UV-VIS spectrophotometric detector SPD-10AV and a system controller SCL-10A VP, equipped with a Jupiter 5u C18 column (300 Å, 250 × 4.6 mm) (Phenomenex, Aschaffenburg, Germany). The methods of Sanches-Silva et al.[226] and Chedgzoy et al.[254] were adapted to the used system so that a gradient elution method with acetonitrile with 0.1 % TFA as mobile phase A and Millipore

water with 0.1% TFA as mobile phase B was used. The TFA was used as additive to protonate the triclosan and ensure a quantitative detection. Mobile phase A was raised from 55 % to 65 % within the first 12 min, then kept constant at 65 % for 3 min and was finally lowered to 55 % within 1 min. The retention time of triclosan was 12.9 min. To clean the column, the total time of each run was 20 min. Each analysis was conducted with an injection volume of 100 µL, a flow rate of 1.0 mL/min, a column oven temperature of 30 °C and UV-detection at 280 nm. Chromatograms were recorded and assessed with Class-VP™ Software. For the determination of the triclosan concentration, calibration solutions of triclosan in the release medium ranging from 0.1 µL/mL to 5 µL/mL were prepared by diluting a stock solution of 10 mg triclosan that was first dissolved in 25 mL absolute ethanol and then filled up to a total of 100 mL with NaCl-containing phosphate buffer pH 7.4 (Ph. Eur. 6.0) containing 0.05 % NaN_3. The release rate was calculated cumulatively in percent related to the average initial triclosan content per disk.

To determine the average initial drug content per disk and to check whether the triclosan was distributed homogenously within the film, three film disks per polymer film from different locations of the film were degraded by adding 2 mL 1 M NaOH and storing the mixture at 37 °C overnight. 1.85 mL 1 M HCl for neutralization and 1.15 mL release medium were added. The so-treated samples were analyzed via the above-described HPLC method and the triclosan contents per disk of each polymer film were averaged.

At the end of the release study, film residues were rinsed with water, lyophilized and treated like the film disks for the determination of initial drug content in order to evaluate the residual drug content.

3.9.3 Agar diffusion test

Agar diffusion tests for the comparison of films of polymers with different geometry and PEG content were carried out with triclosan loaded films of 8arm70, 4arm70, lin70rac and PLA as well as PEG-coated PLA films with triclosan within the PEG layer. Film disks (diameter: 2 cm) were put on Mueller-Hinton agar plates (38 g Mueller Hinton agar, 1,000 mL water), which were inoculated with a suspension of Staph. aureus (ATCC® 25923™) in sterile NaCl solution

(0.5 McFarland). After 24 h incubation at 37 °C, the agar plates were examined and the size of the inhibition zones was determined.

Agar diffusion tests to compare the efficacy and its duration of triclosan loaded meshes to triclosan loaded films were carried out on LB agar plates (2 g yeast extract, 4 g tryptone, 2 g NaCl, 6 g Bacto Agar, 400 mL water) that were inoculated with 100 µL overnight culture of Staph. aureus RN4220. Film and mesh disks (diameter: 2 cm) as test specimens were placed on the agar plates and were incubated at 37 °C for 24 h. The inhibition zones were determined and the samples were carefully transferred to fresh inoculated agar plates every 24 h until no inhibition could be observed anymore or until the membranes started to fragment and could not be further transferred. The test was conducted with PLA, lin70rac and 4arm140 triclosan loaded films, meshes with triclosan loaded during electrospinning and electrospun meshes that were impregnated with triclosan containing 25 µg triclosan per disk each. The experiment was conducted in quadruplicate. Triclosan-free polymer film and mesh disks (diameter: 2 cm) served as references.

The inhibition of each polymer disk was calculated by

$$\text{inhibition} = \frac{(i-d)}{2} \tag{3.11}$$

where i is the diameter of the entire inhibition zone of a single disk averaged from measurements in horizontal and vertical direction and d is the current diameter of the disk also averaged from measurements in horizontal and vertical direction. With this calculation, both an occurring shrinkage of the meshes and slight extensions of the films due to swelling were taken into account.

To determine the initial drug content per mg mesh or film, 4 cm × 4 cm squares (three per polymer) were weighed and subsequently degraded in 2 mL 1 N NaOH each overnight at 37 °C and the absorption at 292 nm of 200 µL per well was measured in a 96 well UV Star® microplate (Greiner Bio-One GmbH, Frickenhausen, Germany) with a microplate reader (Tecan Infinite 200, Tecan, Männedorf, Switzerland). The drug concentration was calculated

via a calibration curve with calibration solutions of triclosan in 1 M NaOH ranging from 20 µg/mL to 100 µg/mL. Based on these measurements, the average triclosan content per mg mesh or film was determined and used to determine the drug contents of the disks used for the agar diffusion via the masses of the disks.

Chapter 4
Characterization of PLA and the synthesized PEG-PLA block copolymers

In this chapter, the utilized polymers for further processing to solid films and solution electrospun meshes are characterized and presented. The results of ^{1}H-NMR, GPC and DSC analysis of the purchased PLA as well as the synthesized PEG-PLA block copolymers with different composition and polymer architecture regarding molecular weight, molecular weight distribution and thermal properties are discussed. Apart from conventional analysis, GPC triple analysis was performed with linear and branched PEG as well as with PEG-PLA block copolymers with different branching at equivalent molecular weight to gain further information about the number of polymer arms.

Parts of this chapter have been submitted:

M. Kessler, J. Groll, J. Tessmar

Application of linear and branched poly(ethylene glycol)-poly(lactide) block copolymers for the preparation of films and solution electrospun meshes

Macromolecular Bioscience, under review

4.1 ^{1}H-NMR analysis

^{1}H-NMR analysis revealed the approximate composition and number average molecular weight of the synthesized PEG-PLA copolymers. ***Figure 4.1*** shows a typical ^{1}H-NMR spectrum of a PEG-PLA block copolymer using the example of lin70rac. The absence of lactide monomer peaks and the appearance of the polymeric peaks indicate a successful polymerization. Characteristically, the methine protons of the lactyl repeating unit appear at a chemical shift of 5.15 ppm, the methylene protons of PEG at 3.65 ppm and the methyl protons of the PLA blocks at 1.57 ppm. The methine protons adjacent to the hydroxylic end groups of the PLA blocks and the PEG methylene protons next to the ester bond connecting PEG and PLA block appear between 4.20 and 4.40 ppm.[255] Due to the higher number of end groups and esters between PLA and PEG block with an increasing number of polymer arms, the intensity of this signal increased with increasing branching of the polymers. However, an accurate end group analysis was not possible for the investigated polymers due to the used

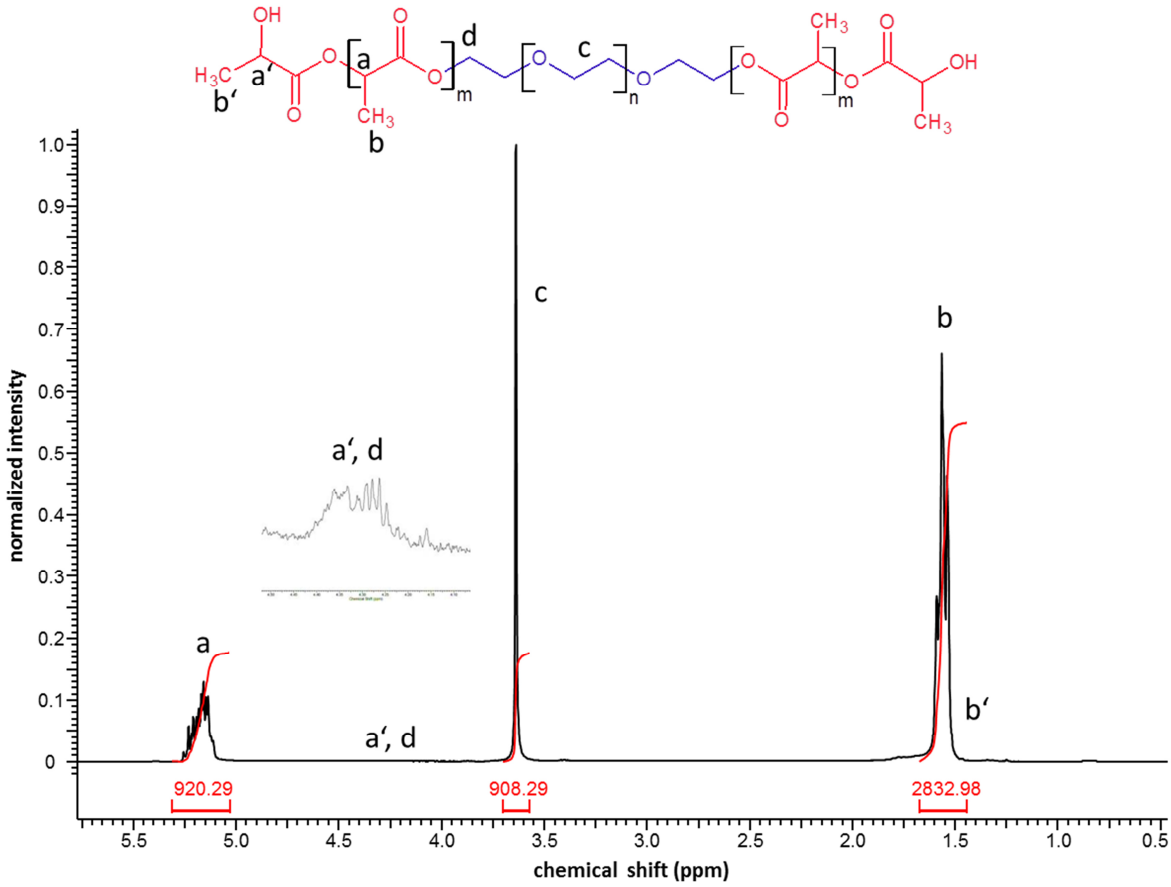

Figure 4.1 *^{1}H-NMR spectrum of lin70rac.*

high molecular weights. PEG contents and molecular weights were calculated by setting the integral of the methine protons of the PLA main chain in relation to the methylene protons of the PEG block. In ***Table 4.1*** and ***Table 4.2*** the determined approximate number average molecular weights and PEG contents for the synthesized linear and star-shaped PEG-PLA block copolymers are listed, illustrating that the targeted PEG contents and PLA chain lengths were achieved by the synthesis within an adequate accuracy.

Table 4.1 *Molecular weight and PEG content of linear copolymers synthesized with 70 % L-lactide and 30 % racemic lactide according to ^{1}H-NMR.*

polymer	$PEG_{calculated}$ (%)	M_n	PEG (%)
lin70	12.50	70161	14.25
lin90	10.00	93219	10.73
lin130	7.14	145064	6.89

Table 4.2 *Molecular weight and PEG content of star-shaped copolymers synthesized with racemic lactide according to ^{1}H-NMR.*

polymer	$PEG_{calculated}$ (%)	M_n	PEG (%)
lin70rac	12.50	77680	12.87
4arm70	12.50	79768	12.54
8arm70	12.50	77464	12.91
4arm140	6.67	142408	7.02
8arm140	6.67	146152	6.84

4.2 GPC analysis

GPC analysis was performed not only to gain information about the success of the polymerization and about the molecular weights but also about the dispersity and the degree of branching of the investigated polymers. GPC analysis in chloroform via conventional calibration relative to PS standards confirmed the successful polymerization and intended increasing molecular weights for the linear triblock copolymers from lin70 to lin130 (***Table 4.3***). The chromatograms showed monomodal peaks with a medium molecular weight distribution and no traces of low molecular weight by-products, PEG or impurities. For the purchased PLA a distinctly higher molecular weight with a broad molecular weight distribution was determined as expected.

Table 4.3 *Weight average molecular weight [M_w], number average molecular weight [M_n] and dispersity of linear PLA and PEG-PLA triblock copolymers determined by GPC via standard calibration method.*

polymer	M_w	M_n	Đ (M_w/M_n)
lin70	62482	33359	1.87
lin90	68116	32443	2.01
lin130	72108	37980	1.90
PLA	1078542	338598	3.19

Concerning the star-shaped block copolymers, the GPC chromatograms also showed only single peaks and higher molecular weights for 4arm140 and 8arm140 than for lin70rac, 4arm70 and 8arm70 as desired as well (***Table 4.4***). Thereby, broader molecular weight distributions were determined than for linear copolymers. Despite similar molecular weights of lin70rac and 8arm70 and a slightly higher molecular weight for 4arm70 according to ^{1}H-NMR analysis, the determined molecular weight via GPC decreased with an increasing number of arms. Since molecular weight determination via conventional GPC is based on the hydrodynamic radius of the molecules and a similar trend was obtained for the pure linear and branched PEGs used for synthesis as well, this trend can be attributed to the generally smaller hydrodynamic radius of polymers with increasing branching.

Table 4.4 *GPC results for star-shaped PEG-PLA block copolymers determined by standard calibration method.*

polymer	M_w	M_n	Đ (M_w/M_n)
lin70rac	79827	27760	2.88
4arm70	77406	21800	3.55
8arm70	76831	20722	3.71
4arm140	121350	31987	3.79
8arm140	121870	41548	2.93

The GPC analysis of pure linear and branched PEG10k and of linear and star-shaped PEG-PLA block copolymers via solvent enhanced light scattering GPC with samples dissolved in chloroform but acetone as eluent and triple detection with a RI, light scattering and viscosity detector resulted in deviating values compared to conventional GPC since the determination of molecular weights was based on light scattering and not on the different hydrodynamic

radii compared to PS. The results are listed in ***Table 4.5***. Moreover, in contrast to conventional GPC, for both the pure PEG polymers and the PEG-PLA copolymers narrow molecular weight distributions were detected, which was attributed to the molecular weight determination using the light scattering detector. The branching calculations based on the intrinsic viscosities of linear and branched polymers yielded an average number of arms of 4.1 for 4armPEG10k and of 8.4 for the 8armPEG10k, which confirms the number of arms specified by the manufacturer. 5.4 average arms were determined for the 4arm70 and 10.7 for the 8arm70. This calculation indicates that the desired branching of the polymers was maintained. The slightly higher calculated average number of arms compared to the pure PEG might be attributed to the higher difference of the molecular weights between the branched copolymers and the linear copolymer than between linear and branched PEG since the calculation is the more accurate the more exact the molecular weights correspond.

Table 4.5 *GPC results of PEG and PEG-PLA copolymers determined by triple detection method.*

polymer	**M_w**	**M_n**	**Đ (M_w/M_n)**
linear PEG10k	12373	12092	1.02
4armPEG10k	11197	11098	1.01
8armPEG10k	11640	11538	1.01
lin70	36728	34300	1.07
4arm70	61177	44846	1.36
8arm70	75210	62255	1.21

As the differing results concerning molecular weights and dispersity of the investigated polymers by the conventional calibration method and the triple detection method underline, the results of GPC analysis extremely depend on the applied method and system used for the measurements. Thus, it is highly recommended to use the same system and method for direct comparison of polymers, especially in case of evaluations concerning different batches of the same polymer, to ensure best possible validity.

4.3 DSC analysis

Thermal analysis via DSC revealed glass transition temperatures but no melting or crystallization peaks for both the PLA and the PEG-PLA block copolymers indicating that the initial polymers for further processing were totally amorphous (***Figure 4.2***). Comparing the linear polymers, decreasing T_g was determined with decreasing PLA chain length and increasing PEG content (***Table 4.6***). This can be attributed to the plasticizing effect of PEG and moreover to the overall decreasing molecular weight as postulated by Flory and Fox.[256] With lower molecular weight, the sample consists of shorter polymer chains with more chain ends than for a similar polymer with higher molecular weight. The chain ends disturb the local order of the material leading to less density and a higher free volume, which consequently lowers T_g. For the star-shaped PEG-PLA block copolymers, a similar dependence of T_g on the PEG content and molecular weight was observed as the 4arm140 and the 8arm140 polymer showed higher T_g than their counterparts with shorter PLA chains. A lower T_g for the star-shaped polymers than for the corresponding linear polymer like described by other researchers[9,257] was not observed. In contrast, T_g was slightly higher for the 8arm than for the 4arm polymers.

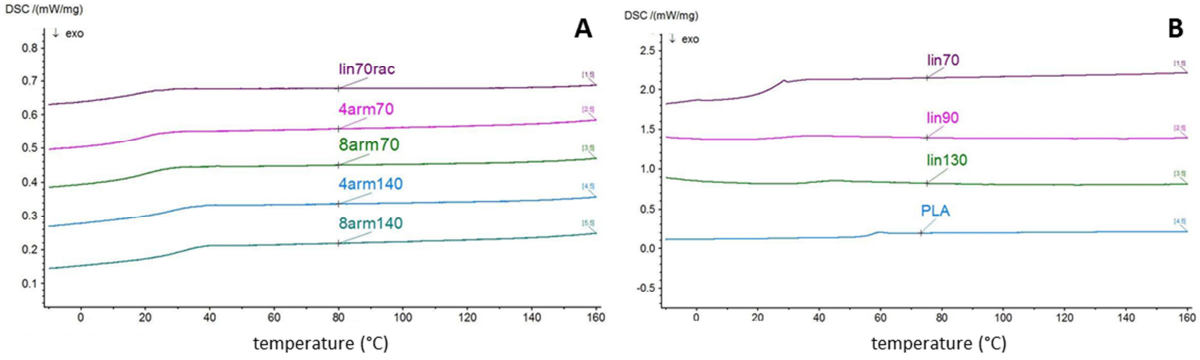

Figure 4.2 *DSC thermograms of star-shaped PEG-PLA copolymers (A) and linear polymers (B) displaying only glass transitions.*

Table 4.6 *Glass transition temperatures determined from the second heating run.*

linear polymers	**T_g (°C)**
lin70	24.4
lin90	28.2
lin130	35.8
PLA	56.1
star-shaped copolymers	**T_g (°C)**
lin70rac	20.2
4arm70	18.3
8arm70	20.4
4arm140	28.9
8arm140	30.7

4.4 Summary and conclusions

In conclusion, ^{1}H-NMR and GPC analysis confirmed that the desired polymers for further processing were successfully achieved by standard ring opening polymerization. PLA-PEG-PLA triblock copolymers synthesized with 70 % L-lactide and 30 % racemic lactide were gained within an adequate range for the targeted PLA chain lengths and molecular weights. DSC measurements revealed decreasing T_g with increasing content of plasticizing PEG and decreasing molecule size. PLA-PEG-PLA triblock copolymers and star-shaped PEG-PLA block copolymers with 4arm and 8arm PEG core and synthesized with 100 % racemic lactide were also obtained with the desired molecular weight. GPC analysis with triple detection indicated the desired average number of arms both for the starting substances 4armPEG10k and 8armPEG10k and the resulting star-shaped PEG-PLA copolymers. T_g of branched polymers depended more on the PEG content and PLA chain length than on the number of arms.

Chapter 5
Evaluation of solvent cast polymer films

In this chapter, the results of the investigations on solvent cast films processed from the previously described synthesized PEG-PLA copolymers and PLA regarding an application as physical barrier device for adhesion prevention are presented and discussed. The plasticizing effect of PEG both within linear copolymers and within the star-shaped copolymers was explored by conducting different mechanical tests. The experiments included not only measurements with dry as-cast films but also with sterilized and with degraded samples to ensure a constant quality of the investigated or implanted films. Furthermore, the extent of swelling and the degradation behavior of the PEG-PLA copolymer films, influenced by the polymer architecture and different contents of the hydrophilic PEG, were examined to identify trends and to tailor the film properties. A further studied drug loading of the prepared films may lead to a more efficient barrier with less systemic side effects of the drug due to a strictly localized drug delivery. To evaluate differences in drug release behavior of the solvent cast films of differently composed PLA and PEG-PLA copolymers and to determine their efficacy, polymer films were loaded with the antibiotically active triclosan and subsequently an *in vitro* drug release study as well as an agar diffusion test were conducted and are discussed in this chapter as well.

Parts of this chapter have been submitted:

M. Kessler, J. Groll, J. Tessmar

Application of linear and branched poly(ethylene glycol)-poly(lactide) block copolymers for the preparation of films and solution electrospun meshes

Macromolecular Bioscience, under review

5.1 Surface properties - Contact angle measurements

Water contact angles were determined to evaluate the wettability and hydrophilicity of 20 µm thick polymer films made of PLA and the different synthesized PEG-PLA copolymers. ***Figure 5.1A*** shows a typical image of a water droplet with its reflection on a polymer film immediately taken after contact, which was then utilized for the determination of the contact angle. For the polymer films made of linear polymers, the differences between the polymer films were only very small. Nevertheless, a significant decrease of the immediately taken contact angles could be determined from the PLA film (77.2°) to the lin70 film (68.2°) with the highest PEG content (***Figure 5.1B***). Since a surface is considered the more hydrophilic the smaller the water contact angle is, the results confirm that with increasing content of hydrophilic PEG the hydrophilicity of the films increased like expected. Concerning the contact angles two minutes after the first contact, only a slight decrease could be observed, which was probably rather due to starting evaporation of the water droplet than due to material effects like swelling or unfolding.[258]

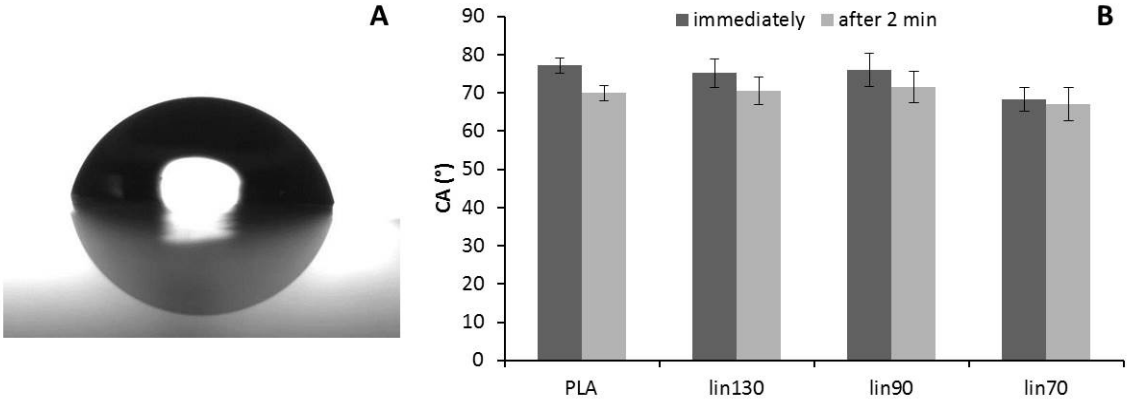

Figure 5.1 *Water droplet on lin90 film immediately after contact (A) and contact angles of dry as-cast linear polymer films measured immediately and two minutes after contact with the water droplet (B).*

Regarding the polymer films made of star-shaped PEG-PLA block copolymers, analogous to the linear polymer films, only slight decreases of the water contact angles were received between the measurements immediately after contact and the measurements two minutes afterwards (***Figure 5.2***). Higher contact angles and consequently a higher surface hydrophobicity could not be detected with elevated PLA content like for the linear polymers

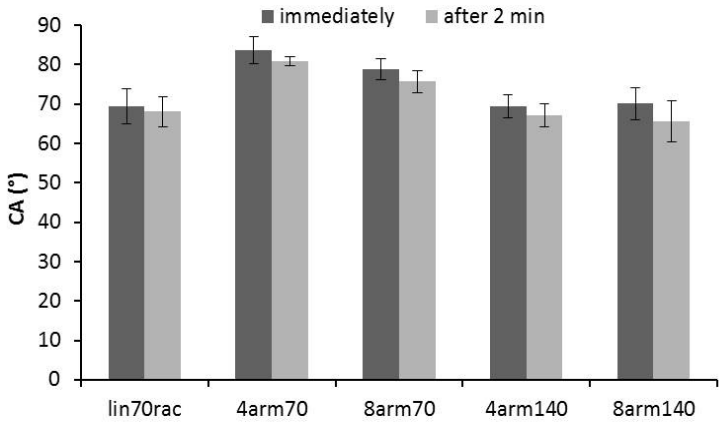

Figure 5.2 *Contact angles of dry as-cast star-shaped polymer films measured immediately and two minutes after contact with the water droplet.*

and like expected. In contrast, the 4arm140 film and the 8arm140 film showed lower contact angles than the 4arm70 and the 8arm70 film. The linear lin70rac film turned out to be more hydrophilic than the films made of branched polymers with equivalent molecular weight, probably due to a better accessibility of the PEG segment for water by having only two arms of the lipophilic PLA shielding the PEG core.

5.2 Mechanical properties

To evaluate the mechanical properties depending on the contained amount of plasticizing PEG and the chosen polymer architecture, a tensile test, a puncture test as well as a suture pullout test were conducted. The results of the measurements highly depended on the glass transition temperature of the particular polymer (***Table 5.1***)**.** The glass transition itself describes the change from a glassy state to the rubbery state when a material is heated. With increasing temperature, a massive increase of the molecular mobility occurs, which is often explained with the theory of free volume according to which a particle within a glass-forming material needs sufficient free volume into which it can move to enable motion within adequate time. With increasing temperature, the density of the material decreases facilitating it for the particle to find enough free volume to move.[259] Using differential scanning calorimetry the glass transition is determined as the step in heat capacity, which is measured during the second heating run. As a consequence, the outcomes of all mechanical tests are highly dependent on the chosen test temperatures, which were varied to describe the behavior as native film as well as at the application site.

Table 5.1 *Glass transition temperatures of polymer films determined from the second heating run of DSC measurements.*

linear polymers	**T_g (°C) film**
lin70	25.9
lin90	27.8
lin130	34.4
PLA	57.0
star-shaped copolymers	**T_g (°C) film**
lin70rac	19.5
4arm70	20.9
8arm70	19.4
4arm140	30.3
8arm140	33.5

5.2.1 Tensile test

A tensile test for the determination of the materials' tensile properties was conducted to investigate the plasticizing effect of PEG with a common method to characterize a material and to evaluate the influence of the test temperature on the experimental outcomes. Generally for dry tested as-cast films, with increasing test temperature an increasing strain at break and a decrease of the tensile strength was observed. This can be attributed to the above-mentioned higher mobility of the polymer chains at elevated temperatures especially by overstepping T_g. With respect to the particular test temperature and their T_g, each polymer film showed various tensile properties like illustrated exemplarily on the load – strain diagrams of 8arm140 films in ***Figure 5.3***. At low temperature (20 °C) well below T_g the polymer film was very brittle and tore already after little deformation. At elevated temperature (30 °C) the polymer film showed ductile properties. After an initial stage of reversible elastic deformation, a first stress maximum (yield point) occurred after which the film experienced plastic deformation and also necking of the sample was observed. During the stage of plastic deformation, the polymer chains undergo parallel alignment before after full alignment the samples rupture. By overstepping T_g (37 °C), the polymer films showed highly elastic properties, with increasing tensile strain the force to extend the film increased until failure of the sample.[260–261] Depending on T_g and the polymer composition, test specimens showed either a different mechanical behavior for all tested temperatures like in

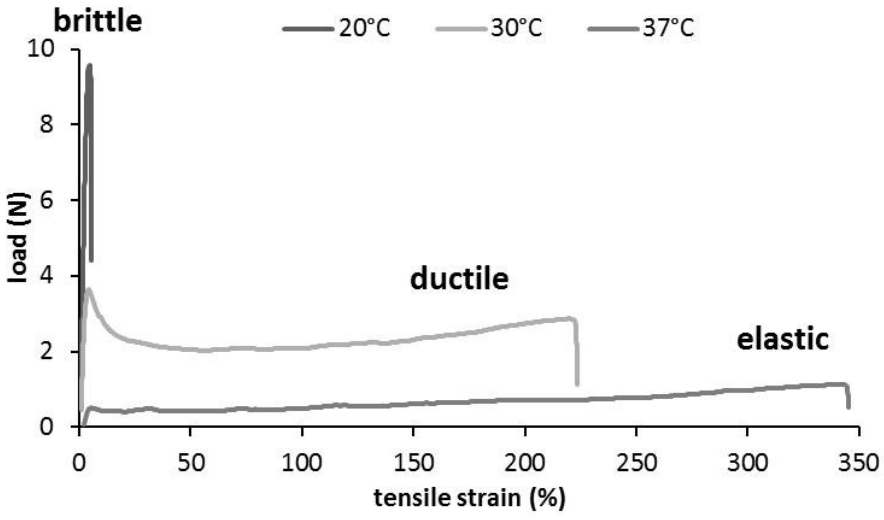

Figure 5.3 *Load – strain diagrams of dry 8arm140 films obtained at different test temperatures.*

case of 8arm140 or only one or two of the shown types of load-strain curves. As the maximum load of the sample sometimes occurred at the yield point and sometimes at the point of break, depending on the polymer and the test temperature the tensile strength was obviously calculated from varying stages of the test but represents always the maximum stress the films could withstand without rupture.

By comparing the films of different polymers to each other, it was observed for the linear polymers that with increasing PEG content the tensile strength of the films decreased whereas the strain at break increased (***Figure 5.4***). While films of the pure PLA and the lin130 were quite stiff at all tested temperatures with relatively high tensile strengths, the lin90 films were only stiff at 20 °C and showed distinctly higher strains at break at elevated temperatures. The lin70 with the highest PEG content was relatively flexible at all temperatures and also withstood the lowest tensile forces. This can be attributed to the significantly decreasing T_g with increasing PEG content, since PEG serves as plasticizer leading to a higher chain flexibility at the same test temperature. Since tensile strength

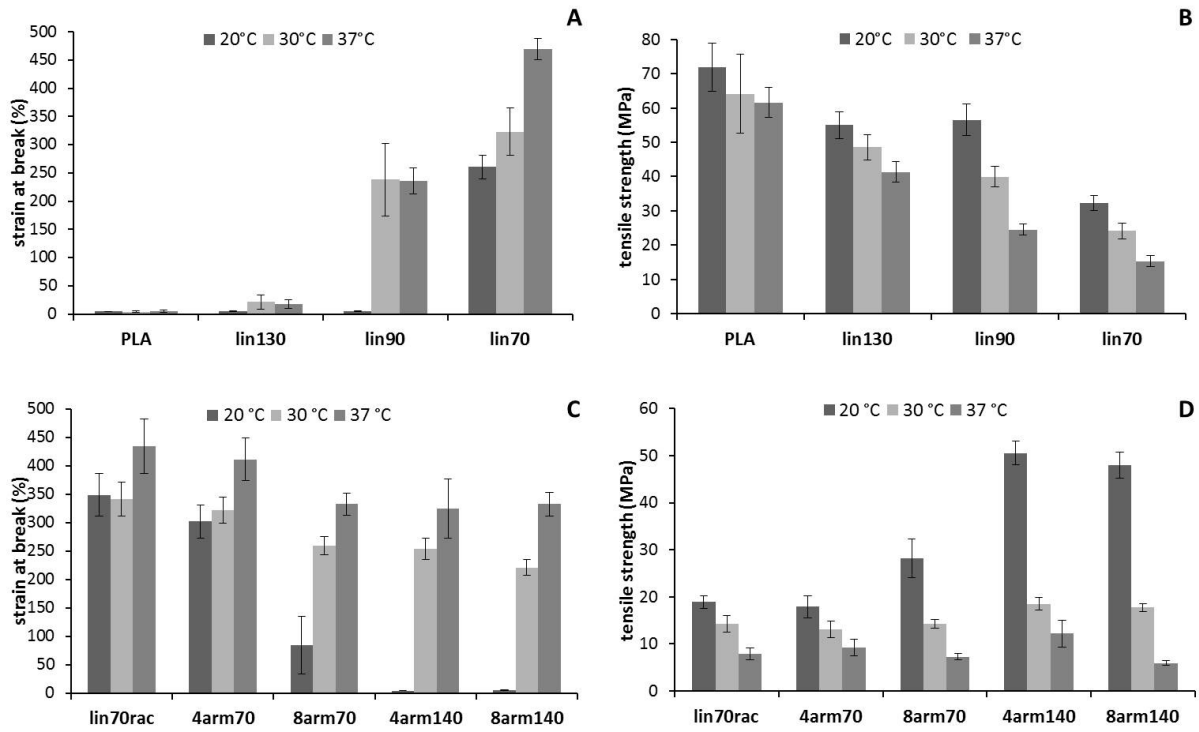

Figure 5.4 *Strain at break and tensile strength at different temperatures for linear polymer films (A, B) and star-shaped copolymer films (C, D).*

depends, apart from the general chemical structure, also on the molecular weight of the polymer,[262] the increased tensile strength of the polymers with lower PEG content may additionally be caused by the higher molecular weights of these polymers since the reduction of the polymers' PEG content was mainly generated by synthesizing longer PLA chains on the same PEG10k core. Regarding the star-shaped copolymers, the tensile properties were not only related to T_g but also to the used branching of the polymers. Analogous to the linear copolymers, for the polymers with higher PEG content and consequently lower T_g (lin70, 4arm70, 8arm70) higher strains at break and lower tensile strengths were determined than for the polymers with lower PEG content and higher molecular weight (4arm140, 8arm140), especially at 20 °C, which is around T_g of the polymers with 12.5 % PEG but clearly below T_g of 4arm140 and 8arm140. Despite about the same values for T_g, different mechanical properties were obtained for films prepared of star-shaped copolymers with similar molecular weights but a various number of arms. The strain at break values decreased with an increased branching whereas hardly any difference occurred for the tensile strength. The shorter length of the chains of the polymer arms with increasing branching together with a higher segment density[263] and less chain mobility due to more chain entanglements[264] probably made a sliding of the molecule chains difficult and led to an earlier failure of the samples.

Concerning applicability as barrier for adhesion prevention, the required mechanical properties for a best suited device are still unknown and consequently undefined. As body motion leads to non-uniform forces on the barrier device[10] the main problem is probably that the forces that impact on the barrier device are very difficult to determine. To get an impression of possible adequate properties and a classification of the investigated polymers though, the tensile test was conducted with the marketed product Mesofol® (40 µm thick poly(lactide-co-ε-caprolactone) film) as well. ***Figure 5.5*** shows that the tensile properties of Mesofol® were in about the same range as those of the lin70 and lin70rac film indicating that the achieved tensile properties will not hinder a successful application. Precise comparisons with results from other researchers are despite the common usage of tensile tests difficult due to distinct variations in test parameters, like extension rate or test temperature, which

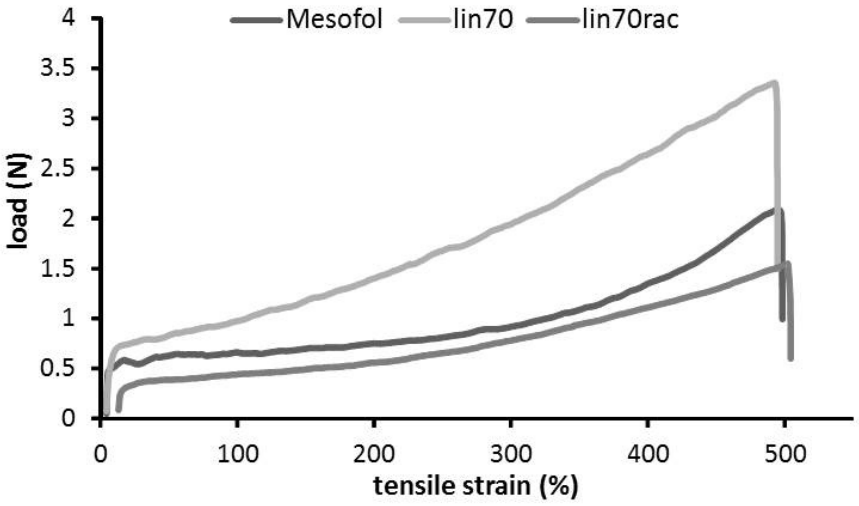

Figure 5.5 *Load – strain diagrams of Mesofol® at 37 °C in comparison to lin70 and lin70rac.*

massively influences the experimental outcomes.[261] However, the reports provide information about the general order of magnitude of the mechanical properties, which were considered appropriate. Yamaoka et al.[76] investigated membranes both made of different copoly(ester-ether) composed of PLLA and Pluronic® and of pure PLLA with obtained tensile strengths from 40 to 57 MPa and tensile moduli between 740 and 1200 MPa. They stated that the increased flexibility of the membranes with increased Pluronic® content had a positive effect on adhesion prevention since adhesion formation may be promoted also by a mechanical stimulus. By implanting a material with high flexibility the mechanical stimulation of the surrounding tissue is reduced and consequently adhesions minimized. Other researchers implanted PVA membranes[236,265] in animals with strains at break up to 500 % in wet state, meaning potentially during the application in the body, and distinctly lower values in the dry state, which is the state during application by the surgeon. They also recommended a sufficient flexibility so that the membrane is able to adapt to body movements and does not break with occurring deformations but proposed a certain stiffness and stability for an easy and accurate application procedure. Regarding the here investigated PEG-PLA films, tensile properties were in about the same range as the described devices so that it can be assumed that, except from the very brittle and stiff PLA and PEG-PLA with low PEG content, the investigated PEG-PLA films provide sufficient flexibility and tensile strength for a very promising application. By varying the device's T_g via an adapted PEG content,

strain at break varied from about 5 to 350 % at a test temperature of 20 °C so that depending on the intended application procedure and desired properties of the surgeon for an easy application, either polymer films with a high flexibility or a certain stiffness at surgery temperature can be created both still providing the desired high flexibility at the later present body temperature (strain at break 37 °C > 220 %).

5.2.2 Puncture test

Various set ups of puncture tests are often used to determine the puncture resistance of protective clothes like surgical gloves to medical needles[266] or in the food industry to verify the textural properties and quality of food,[267–269] but the idea of a puncture test was also adapted by some groups to determine the puncture properties for medical applications like orodispersible and buccal films[207] or polymeric film coatings of tablets.[245–246,270] Radebaugh et al.[245] found that the puncture test allowed a greater differentiation of the elongation of different polymer films than the tensile test as higher ratios of the elongations to puncture/break of a polymer film to a reference film were obtained with the puncture test than with the tensile test. Consequently the puncture test was not only a useful complementation to the tensile test due to additional findings regarding resistance to deformation by puncture, but it also turned out to be a versatile tool to differentiate films that showed similar results during the tensile test. Since during body motion also not only

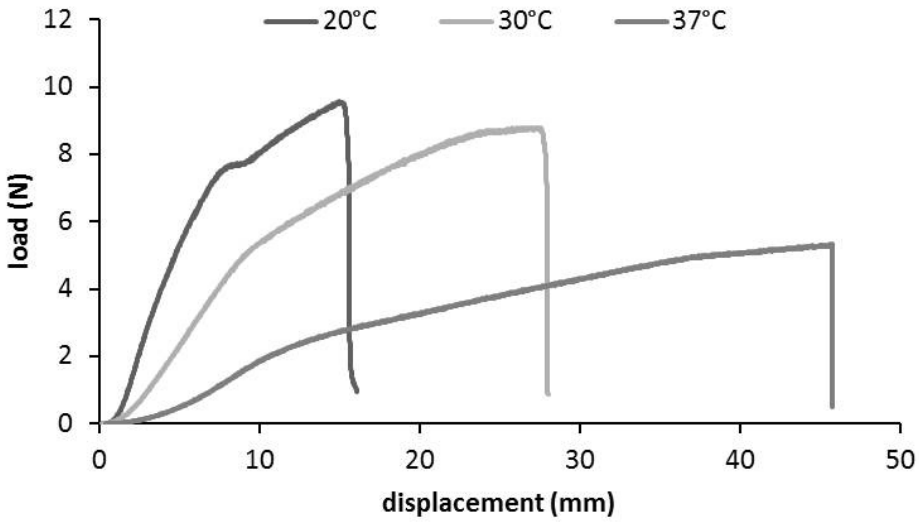

Figure 5.6 *Load – displacement diagrams of dry 8arm140 film obtained at different temperatures.*

tensile forces occur, besides a tensile test a puncture test was conducted to additionally determine the resistance to deformation by puncturing the films. Typical load – displacement diagrams are exemplarily illustrated in ***Figure 5.6*** with 8arm140 films. With increasing displacement the load increased and at the maximum load the films finally ruptured. After an initial steep ascent of the curve, the slope noticeably decreased after an inflection point probably due to a relaxation of the film to the applied stress[246] or due to a first crack or damage of the film.[271] Similar to the tensile test, generally with increased test temperature the maximum load decreased whereas the elongation to puncture increased.

For the linear polymers with increasing PEG content generally the elongation to puncture increased significantly (***Figure 5.7A***). The higher values of the PLA film compared to the lin130 may be due to its massively higher molecular weight and longer polymer chains. The load to puncture values did not correlate with the PEG content but were distinctly higher for the pure PLA film than for the copolymers, probably due to the massively higher molecular weight as well (***Figure 5.7B***). For the star-shaped block copolymers both an influence of the

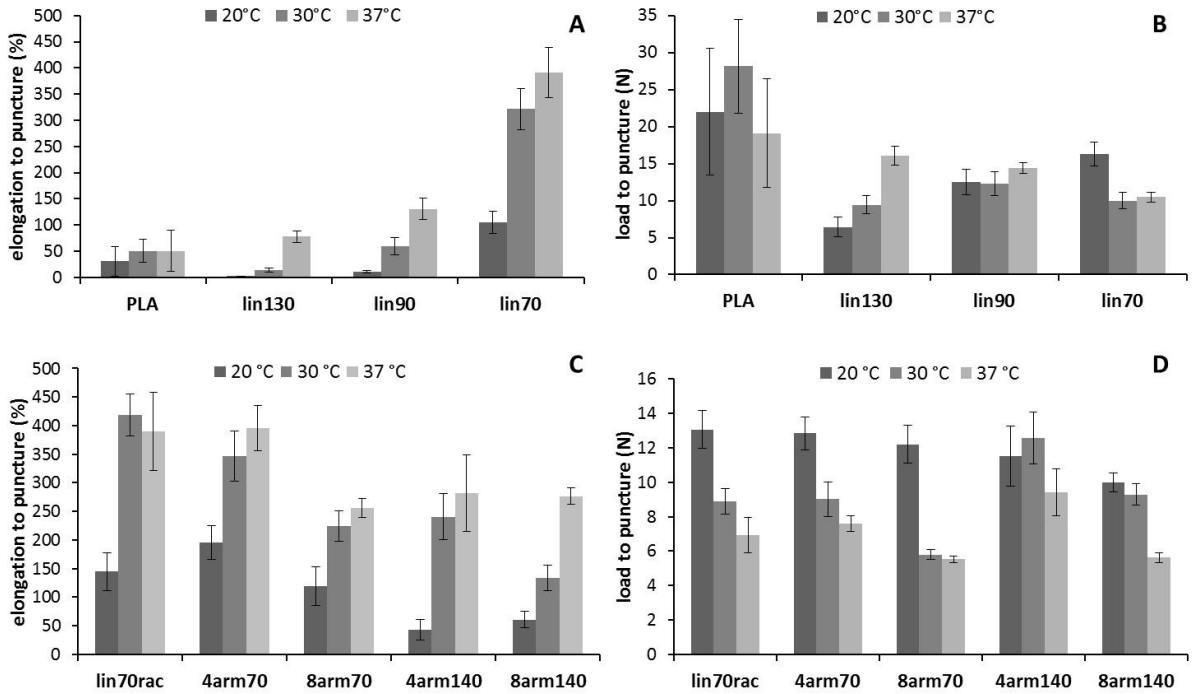

Figure 5.7 *Elongation to puncture and load to puncture of linear (A, B) and star-shaped (C, D) PEG-PLA block copolymer films.*

PEG content and branching was observed for elongation to puncture as well as for maximum load (***Figure 5.7C, D)***. With increasing PEG content and shorter PLA chains the films were longer stretched but withstood lower forces. Increased branching of the PEG-PLA copolymers led to a decrease of the elongation to break values, but in contrast to the tensile test a slight decrease of the load to puncture for polymers with similar molecular weights occurred. Moreover, the PEG content and molecular weight dependent higher resistance to the applied force for the branched polymers with prolonged PLA chains was clearly visible also at elevated temperature. In summary, these results generally reflect the same trends as found by the tensile test but with different absolute values and a finer differentiation between the polymers, which confirms that the puncture test not only is a versatile method to characterize polymer films but also has the ability to detect differences between samples that do not appear during tensile test. The test results again indicate that the linear polymers with very low PEG content are distinctly less flexible and consequently probably less suitable for an application as barrier device than the polymers with elevated PEG contents, which exhibit high and sufficient elongation values.

The puncture test was additionally used to determine the mechanical properties of the polymer films during degradation to evaluate their stability during application especially regarding differences between films made of polymers with various architectures. During the storage in buffer pH 7.4, thin film strips such as the test specimens for the tensile test tended to curl and also suffered along the edge leading to predetermined breaking points, which ultimately led to inaccurate tensile test results. The alternative puncture test, where the measurements are conducted in the center of the test specimen, appeared to be a more reliable method since the actual shape of the edges of the films after incubation in phosphate buffer pH 7.4 at 37 °C is irrelevant for the test results. Concerning the load to puncture, again a consistent decrease with increasing PEG content and with an increasing branching could be observed over the investigated degradation time but with a general decrease of the absolute values. However, the reduction of the maximum forces the films could withstand was quite small so that a good stability of the films during application can be expected (***Figure 5.8B***). The elongation to puncture massively decreased over time for all investigated polymer films (***Figure 5.8A***). Thereby, the values of star-shaped copolymers with

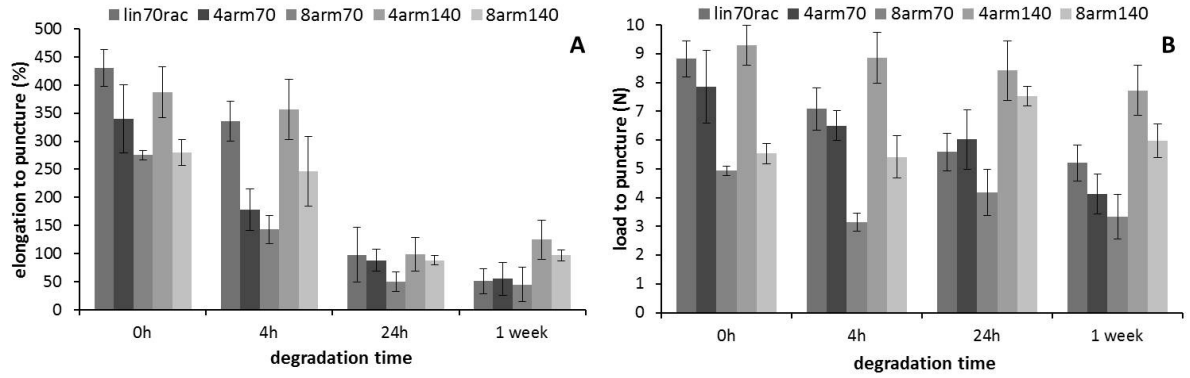

Figure 5.8 *Puncture properties of star-shaped PEG-PLA block copolymer films during degradation in phosphate buffer pH 7.4 at 37 °C.*

similar molecular weights approximated after one week, which may be attributed to a longer retention of the plasticizing PEG within higher branched polymers due to more connecting points that anchor it.[9] In contrast to the beginning of the degradation and to dry films, after 24 h higher elongations to puncture were obtained for the polymer films with low PEG content than for the polymer films with high PEG content implying that the 4arm140 and the 8arm140 film maintained their initial mechanical properties to the highest extent among the investigated polymers. This may be attributed to a slower washout of degradation products due to higher chain lengths and a better anchorage of the PEG due to branching.

Since medical devices need to be sterilized before implantation to avoid infections in patients,[272] an appropriate sterilization method for the particular device has to be found to ensure maintenance of adequate material properties upon sterilization. Thereby, the most commonly applied sterilization methods dry-heat sterilization and autoclaving are not suitable for medical devices of aliphatic polyesters as those polymers are sensitive to both heat and moisture, which is reflected in plastic deformation and degradation. Chemical sterilization with ethylene oxide is also not ideal as the gas might not permeate the entire device and moreover toxic residues may remain.[273–274] In the end, sterilization with electron beam or γ-irradiation is the most widely used method because of short sterilization times and relatively small effects on the polymer devices. However, depending on the chemistry of the polymer chains, chain scission or cross-linking reactions occur, which alter the chemical composition and thereby also change the mechanical properties of the device.[275] To evaluate

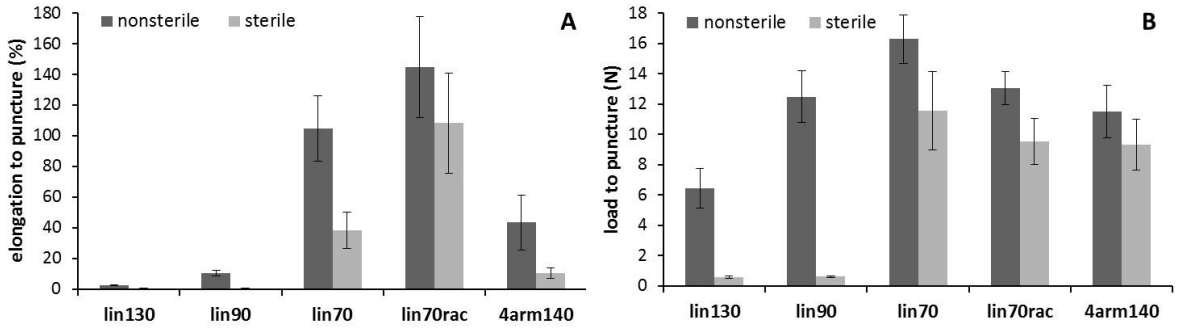

Figure 5.9 *Elongation to puncture (A) and load to puncture (B) at 20 °C of selected polymer films after sterilization via electron beam irradiation.*

how much the mechanical properties of the developed PEG-PLA films suffer upon sterilization, films of selected polymers were sterilized via electron beam irradiation and a puncture test was conducted with samples of the sterilized films. A massive decrease both of the elongation to puncture and the load to puncture was observed for lin130 and lin90 indicating little stability towards electron beam irradiation (***Figure 5.9***). The 70:30 L-lactide:D,L-lactide chain copolymers with the highest PEG content (lin70) showed less losses of the mechanical properties, however, the linear racemic version of the polymer (lin70rac) showed both less loss of elongation and load to puncture than the lin70. The tested 4arm140 film also turned out to be quite stable upon electron beam irradiation especially regarding the load that the film could withstand. With the smallest losses especially in load to puncture for the lin70rac and the 4arm140 film it can be concluded that both racemic PLA chains and a high PEG content in the polymers increased the mechanical stability towards sterilization via electron beam irradiation.

5.2.3 Suture pullout test

Many medical devices (e.g. pacemakers, heart valves, breast implants) start to move within the body without fixation, which can lead to significant problems for the patient.[10] In case of non-adhesive barrier devices also a complete coverage of the site of injury during the critical stages of wound healing is not ensured without a fixation so that barriers are usually sutured or fixed with staples to stay in place and remain effective. Therefore, it is quite important that the applied films withstand the forces occurring during suturing by the surgeon. With the conducted suture pullout test the maximum axial forces that can be applied to the film until the surgical suture is pulled out of the suture hole were determined.

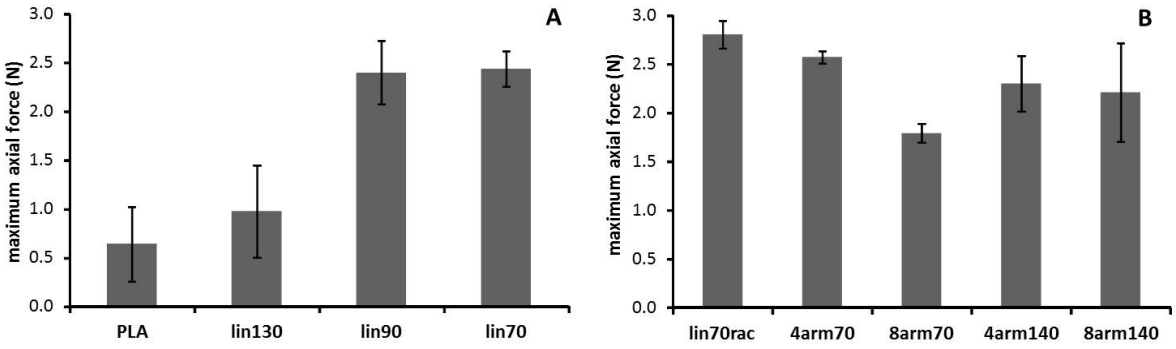

Figure 5.10 *Results of the suture pullout test of linear polymer (A) and star-shaped copolymer (B) films.*

Concerning the linear copolymers, an increasing PEG content of the polymer led to an increased suture pullout force (***Figure 5.10A***) in contrast to the tensile and puncture test where with increasing PEG content the films withstood lower loads. This finding can probably be attributed to the brittleness of the polymer films with high PLA content. By examining the shape of the suture holes generated during the experiment, for the PLA film samples a thin straight line can be recognized for all test specimens illustrating that the surgical suture was neatly sliding through the films without further deformation of the specimens due to the high brittleness of the film (***Figure 5.11***). With slightly increased PEG content (lin130) still for two test specimens the suture neatly slid through the film. However, three specimens tore sideways so that the films were separated into two pieces to finally pull out the suture. The linear polymer specimens with 10 % and 12.5 % PEG content and a higher elasticity of the material showed a higher resistance towards the surgical suture so

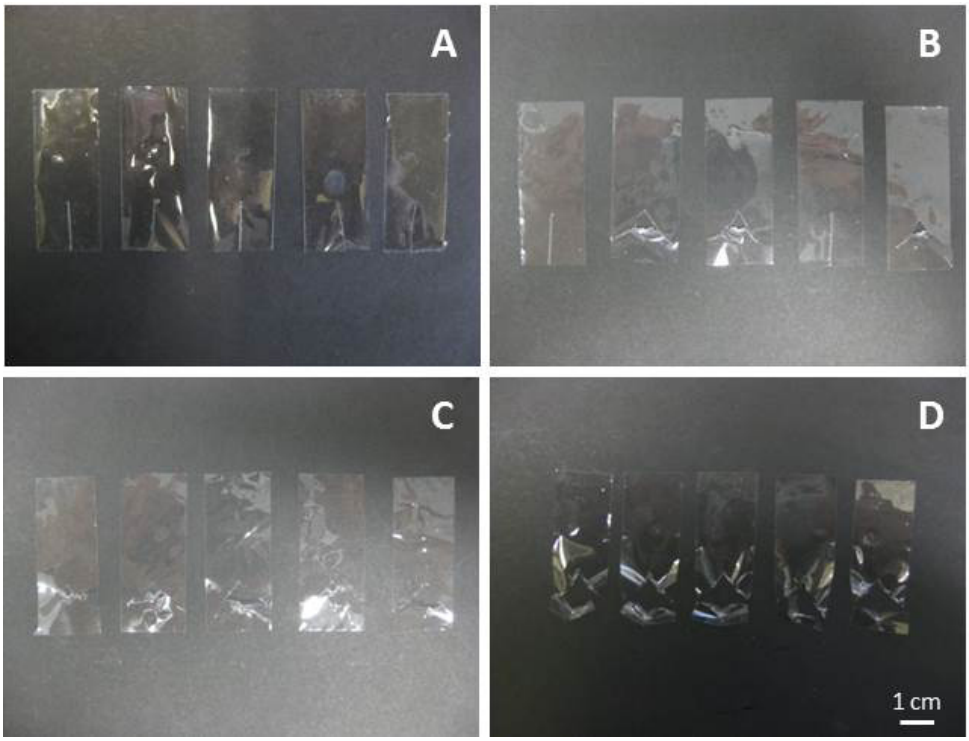

Figure 5.11 *Film test specimens after suture pullout test made of PLA (A), lin130 (B), lin90 (C) and lin70 (D).*

that a neat sliding of the suture through the film was prevented and all test specimens tore sideways with a separation of the film.

For films made of star-shaped PEG-PLA copolymers a dependence of the maximum force on the number of arms could be observed. For polymers with equivalent molecular weights and PEG content, a higher branching resulted in a lower maximum force (***Figure 5.10B***). This might be attributed to the phenomenon already discussed for the tensile test in 5.2.1, that higher branching results in shorter polymer chains and aggravates sliding of the chains along each other, consequently leading to a faster rupture of the film, which occurred sideways like described for the linear copolymers with elevated PEG content. With increased PLA content (elongated PLA chains) a lower load was necessary to pull out the suture due to a higher brittleness of the films analogous to the linear copolymers. Since all of the investigated PEG-PLA films showed higher maximum loads than the PLA film already in clinical use, which can successfully be sutured, good suture pullout properties and local residence in the body can be expected.

5.3 Swelling and degradation studies

Over an investigated degradation time of eight weeks, the PLA film samples macroscopically changed neither in dimension nor in optical appearance for both investigated pH values but stayed intact with consistent diameter and a transparent appearance. Hardly any water uptake (maximum 2 %) and no significant mass loss occurred and the molecular weight was reduced only to 78 % or 92 % of the initial molecular weight after eight weeks (***Figure 5.12***). In addition, DSC measurements of the degraded PLA samples resulted in no significant changes for T_g confirming the GPC results as in case of a massive reduction of the molecular weight and also with the presence of monomers or oligomers acting as plasticizer a decrease of T_g can be expected.[276–277] The findings of the slow degradation of the PLA film are in good accordance with descriptions in the literature that report long degradation times not only for semicrystalline PLLA[278] but also for long chained amorphous PDLLA.[279] The hydrophobicity of the PLA made it very difficult for water to penetrate into the film, which is necessary for the ester cleavage. In addition, chain scission within the high molecular weight of the used PLA led at the beginning to degradation products that were not small enough to be washed out of the film but large enough to keep the integrity of the film. Thereby, an increase of the acidity of the degradation media to pH 5.5 had no relevant influence on the degradation of the PLA film.

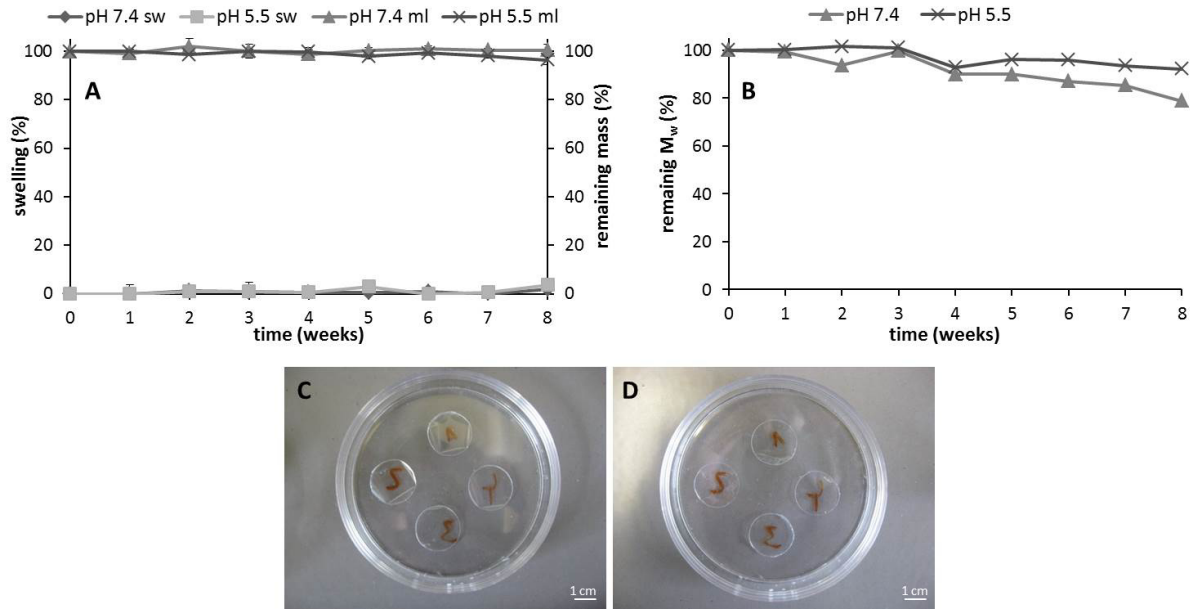

Figure 5.12 *Swelling and mass loss (A), molecular weight loss (B) and macroscopic appearance initially (C) and after eight weeks (D) of a PLA film during degradation.*

Macroscopically, the investigated PEG-PLA films kept their dimensions or experienced only slight extension due to swelling and stayed intact in buffer over the investigated eight weeks, but largely started at some point to fragment during removal, like clinically desired, so that a fragmentation can be expected *in vivo* due to the body movement. The starting point of fragmentation thereby depended both on the PEG content and the branching of the film polymer. Regarding the linear polymers with 70:30 L-lactide:D,L-lactide chains, the higher the PEG content the earlier the films started to fragment at pH 7.4. The copolymer films with the highest PEG content tore first already after three weeks and the lin90 with intermediate PEG content after six weeks, while the stiff lin130 did not rupture until week eight. The racemic lin70rac was more stable than the non-racemic lin70 as it stayed intact over seven weeks and also stayed transparent (but slightly opaque) while the lin70 turned completely white after several weeks (***Figure 5.13***). For the star-shaped PEG-PLA copolymer films, an increasing number of arms led to less stability and an earlier fragmentation of the films with similar molecular weights of the polymers. While the lin70rac showed first ruptures after seven weeks at pH 7.4, the 4arm70 and the 8arm70 films started to fragment already after six weeks and the 8arm70 films disintegrated in distinctly smaller fragments. In contrast to the trend of the linear copolymers, the films of star-shaped block copolymers with elongated PLA chains and consequently lower PEG content started to fragment earlier (week 4) than the films with higher PEG content.

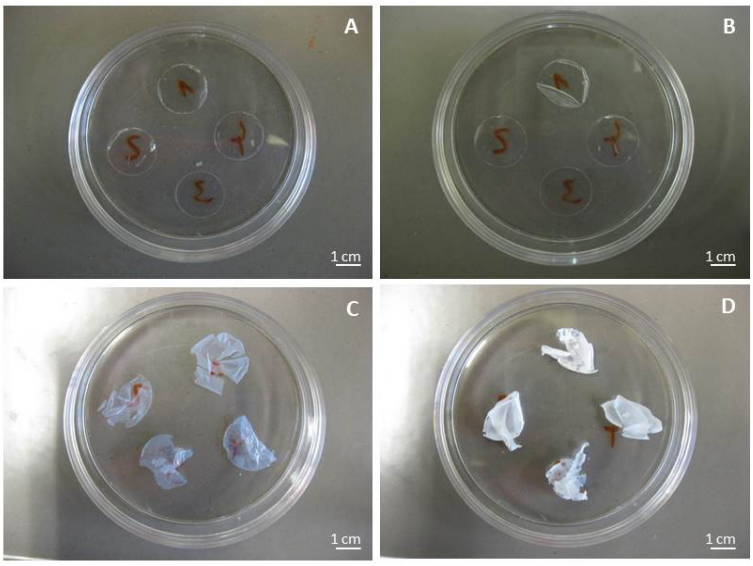

Figure 5.13 *Film specimens of lin70rac (A, C) and lin70 (B, D) before storage in phosphate buffer pH 7.4 (A, B) and after eight weeks incubation (C, D).*

The results of the swelling study at pH 7.4 of the linear PEG-PLA copolymer films are in good accordance with the contact angle measurements (see 5.1) because the ascertained increased hydrophilicity with increasing PEG content of the polymer was reflected by the extent of water uptake as well. The water uptake of all films was generally rather low, but with the consistent trend that the swelling was higher for polymers with a higher PEG content and a consequently higher hydrophilicity (***Figure 5.14***). Despite the occurring water uptake and the above-mentioned starting fragmentation during the investigated time, hardly any mass loss could be detected for all linear PEG-PLA copolymer films indicating that hardly any small molecules were washed out. However, GPC analysis revealed a massive decline of molecular weight to about 35 % of the initial weight for the triblock copolymers after eight weeks so that it can be concluded that the degradation products were despite a marked chain scission largely still not small enough to freely diffuse out of the films. Consequently, the disintegration of the films can be attributed to degraded molecules that could not maintain the integrity of the film rather than to a massive washout of water soluble degradation products. Thereby, the polymer film with the highest PEG content (lin70) probably started to fragment first because of shorter PLA chain lengths after the first ester cleavages.

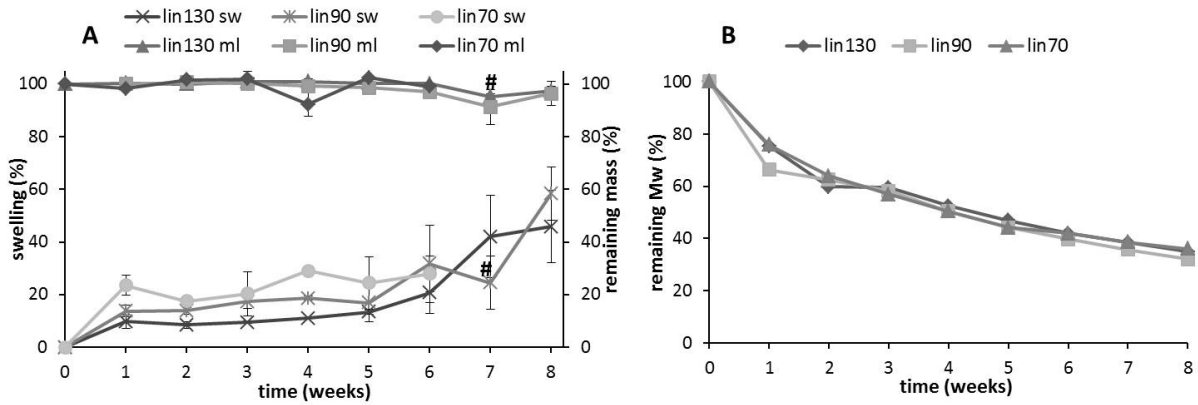

Figure 5.14 *Mass loss, swelling (A) and molecular weight loss (B) of triblock copolymer films determined at pH 7.4.*
 # indicates film fragmentation in small pieces that could not be weighed accurately.

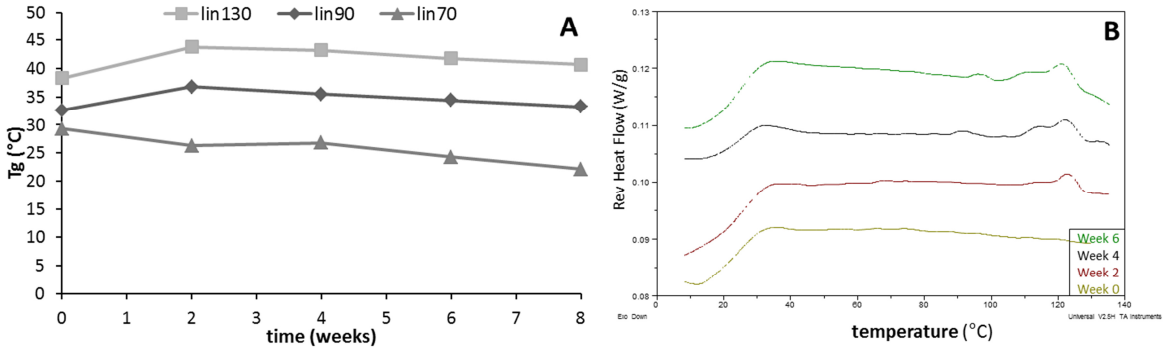

Figure 5.15 *T_g of linear polymer films (A) and DSC thermograms of lin70 film (B) over degradation time determined via second heating run.*

DSC analysis of the degraded films consistently displayed a lower T_g with higher PEG content and revealed only slight changes in T_g over time. A slight increase after the first week and a subsequent slight decrease (***Figure 5.15***) occurred probably because of the polymer degradation leading to a mixture of various smaller breakdown products that resulted in enhanced chain mobility. Although the initial as-cast films were totally amorphous, crystallization peaks occurred at 121 °C for lin70 after two weeks degradation indicating congregation of the segments and probably leading to the above described white appearance of the lin70 samples, due to formed crystallites.

Under inflammatory conditions at pH 5.5, the swelling study as well as the DSC measurements gave similar results as under pH 7.4 and no noteworthy mass loss occurred over the investigated eight weeks as well. In contrast, an enhanced molecular weight loss could be determined with increasing PEG content of the polymer as the decline of the

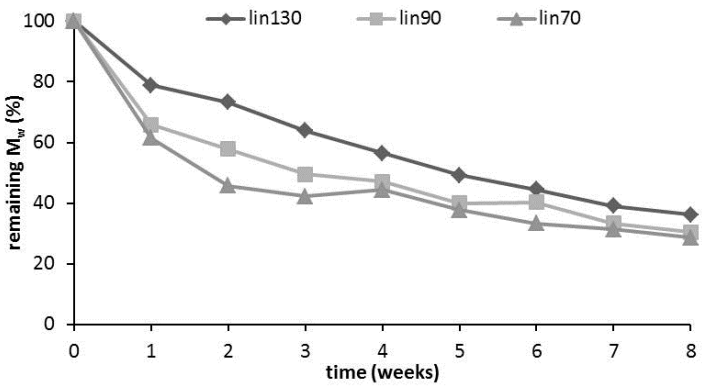

Figure 5.16 *Molecular weight loss of triblock films at pH 5.5.*

molecular weights of lin70 and lin90 was higher than at pH 7.4 (***Figure 5.16***). However, this was not manifested in an earlier disintegration of the films since the first signs of fragmentation occurred after the same time as for the films degraded at pH 7.4, which indicates that more acidic degradation conditions did not negatively influence the behavior of the films and that the films may also withstand an inflamed wound site.

Concerning the swelling and degradation of the films made of star-shaped PEG-PLA copolymers, except from the 8arm70 films, no decisive differences could be detected between "normal" physiological conditions (pH 7.4) and inflammatory conditions (pH 5.5) as well. The water uptake generally was low and depended both on the PEG content and on the branching of the polymers. Analogous to the linear triblock PEG-PLA copolymers, a higher swelling occurred for the star-shaped block copolymers with a higher content of the hydrophilic PEG (lin70rac, 4arm70, 8arm70) than for the polymers with elongated PLA chains and lower PEG content (4arm140, 8arm140) (***Figure 5.17***)**.** Comparing the copolymers with similar molecular weights but different architecture with each other, less water uptake was determined with increasing branching which can probably be attributed to a better accessibility for water of the PEG segment of the linear copolymer than for the PEG segment of the star-shaped block copolymers. The local average polymer density relatively increases with an increasing number of arms so that in terms of water uptake the star-shaped block copolymers resemble an impenetrable core from which the PLA arms arise.[200]

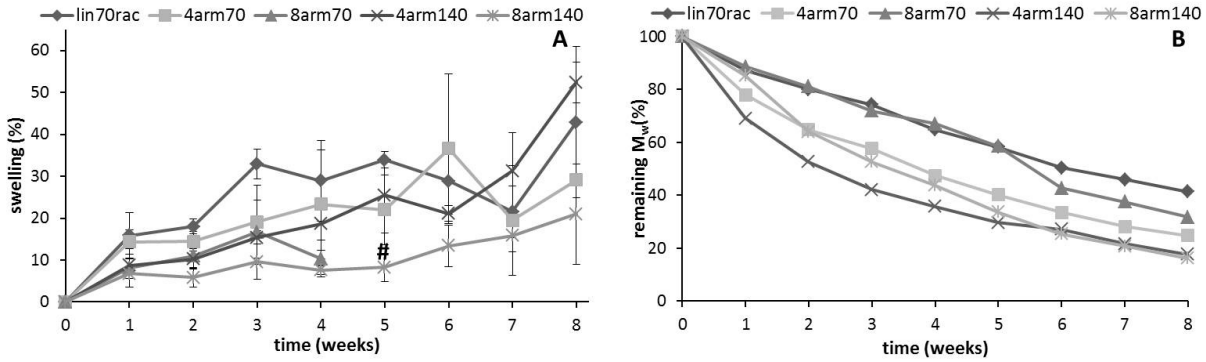

Figure 5.17 *Swelling at pH 5.5 (A) and molecular weight loss (B) at pH 7.4 of star-shaped PEG-PLA block copolymers.*
 # indicates film fragmentation in small pieces that could not be weighed accurately.

Like for the linear PEG-PLA copolymers, the molecular weights massively declined for the star-shaped block copolymers as well. A higher loss of molecular weight was determined for the branched PEG-PLAs than for the lin70rac with the highest losses for the polymers with elongated PLA chains (4arm140, 8arm140). Furthermore, with similar initial molecular weight in both cases the films made of 4arm-shaped copolymers experienced faster molecular weight losses than the comparable 8arm block copolymers. The faster molecular weight loss for the branched polymers than for the linear polymer with similar molecular weight may be due to the preferential ester cleavage of the ester bond between PEG and PLA. Due to reduced PLA chain lengths with an increasing number of arms, the ester cleavage led to smaller initial degradation products with increased branching of the block copolymers.[9] The smaller breakdown products resulted in the above-mentioned earlier fragmentation of the films with increasing branching of the polymer because the integrity of the film matrix could no longer be maintained. In case of the 8arm70 films, the polymer breakdown obviously soon led to small water soluble oligomers that diffused out of the film in the early stages of the experiment because a higher initial mass loss could be determined for the 8arm70 film than for the 4arm70 and the lin70rac. The results of the GPC analysis with the higher remaining molecular weight for the 8arm70 film than for the 4arm70 despite a faster fragmentation confirm a washout effect of the small breakdown products, which is further reinforced by ^{1}H-NMR analysis of the degrading film samples. These measurements revealed a relatively higher increase in PEG content over time with an increasing number of arms for the polymers with similar molecular weight referred to the initial films. This signifies both a washout of PLA oligomers and a longer retention of the hydrophilic PEG within the film matrix with an increased branching. In contrast to the other star-shaped copolymer films, the 8arm70 film disintegrated faster during incubation at pH 5.5 (week 4) than at pH 7.4 (week 6), which can be attributed to a distinctly higher molecular weight loss at pH 5.5 than at pH 7.4 for the 8arm70 film, which did not occur for the other polymers (***Figure 5.18***). The above-mentioned earlier fragmentation of the 4arm140 and the 8arm140 films may be due to the higher PLA content and higher glass transition temperature compared to lin70rac, 4arm70 and 8arm70, which generally made the films more brittle.

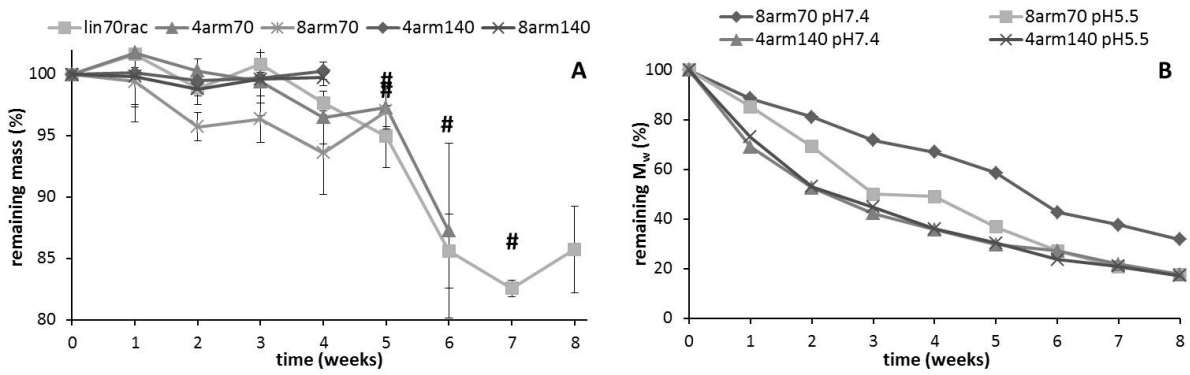

Figure 5.18 *Mass loss of star-shaped PEG-PLA block copolymer films at pH 7.4 (A) and molecular weight loss of 8arm70 and 4arm140 film at pH 7.4 and pH 5.5 (B).*
 # indicates film fragmentation in small pieces that could not be weighed accurately.

DSC measurements revealed only slight changes of T_g over time with a slight increase followed by a decrease probably due to the occurrence of small degradation products. In contrast to the films made of the linear copolymers synthesized with 70:30 L-lactide:D,L-lactide, no crystallization peaks occurred for both investigated pH values for the branched copolymers and only minor crystallization at week four for the lin70rac film indicating softer and more rapidly absorbed degradation products (***Figure 5.19***)**.**

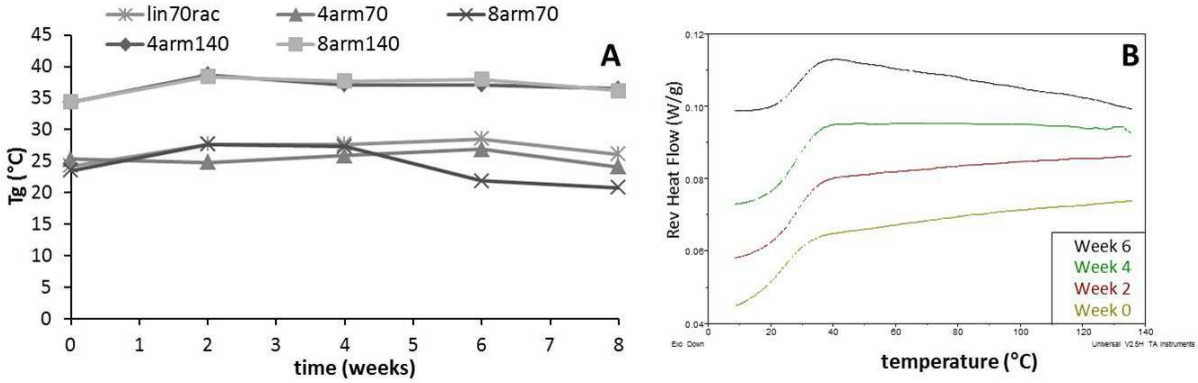

Figure 5.19 *T_g of branched polymer films (A) and DSC thermograms of lin70rac film (B) over degradation time determined via second heating run.*

5.4 Drug release study

The release behavior and the antibacterial efficacy of films loaded with the lipophilic triclosan were evaluated by an *in vitro* release study and agar diffusion tests on agar plates inoculated with Staph. aureus since Staph. aureus counts to the organisms mostly responsible for surgical site infections related to surgical procedures.[231] ***Figure 5.20*** shows the growth inhibition of Staph. aureus by films of different polymers with varying drug loading.

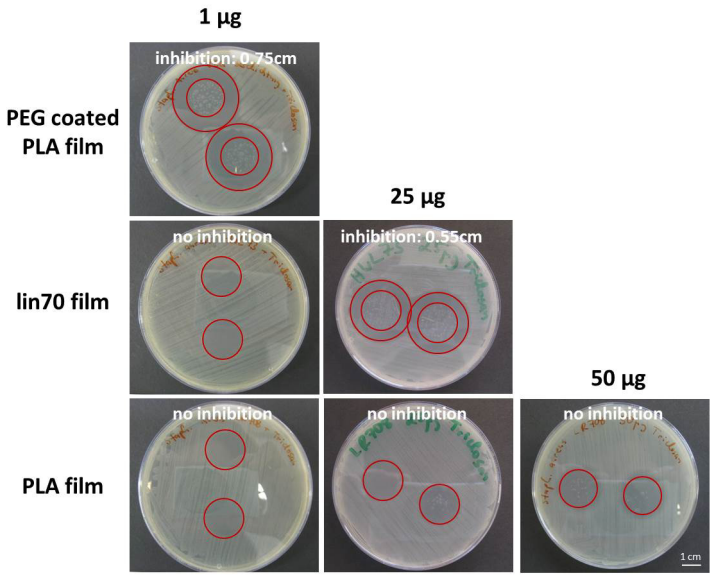

Figure 5.20 *Inhibition of Staph. aureus growth of PEG coated PLA film, lin70 film and PLA film disks loaded with different amounts of triclosan after 24 h incubation.*

While the PLA films with triclosan loaded PEG coating already led to an inhibition of 0.75 cm with only 1 µg triclosan per polymer disk, for films made of lin70 and PLA a loading with 1 µg was too low to inhibit bacterial growth. By increasing the drug content to 25 µg per disk, an antibacterial efficacy was observed for the lin70 films whereas for the PLA film no inhibition zone was obtained. A further increase of drug content to 50 µg per disk still did not result in visible inhibition indicating a very poor diffusion of the drug through the PLA matrix. A determination of the released triclosan over time via HPLC was in good accordance with the results of the agar diffusion test. While the PEG coating showed an immediate release with a detected release of 70 % already after ten minutes, a sustained release with elongated drug release was obtained for the lin70 film and a very slow release for the PLA film with lower drug release (***Figure 5.21***).

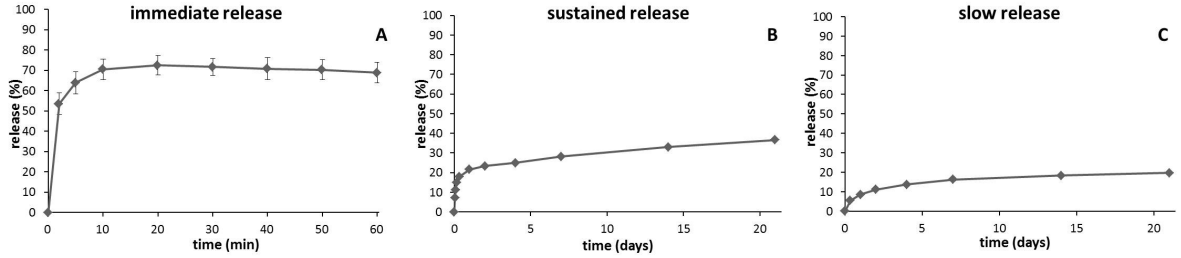

Figure 5.21 *In vitro release curves of PEG coating with 10 µg triclosan (A), lin70 film with 25 µg triclosan (B) and PLA film with 25 µg triclosan (C). For analytical reasons, the drug release from a 10 µg triclosan loaded PEG coating was used for the HPLC analysis.*

The differences between the polymer films regarding drug release behavior can be attributed to the varying contents of hydrophilic PEG. The initial burst for the release of triclosan of the PEG coating with an immediate release of virtually the entire contained drug was due to the immediate dissolution of the coating in the aqueous release medium. Owing to the hydrophilic nature of PEG, the coating was washed off the PLA film and consequently all the triclosan was released into the medium. This effect led to the antibacterial efficacy already with very low drug loading of 1 µg per disk. The lin70 film and the PLA film cannot be dissolved in water due to the lipophilicity and high molecular weights of the polymers. Therefore, drug release was significantly slower without a large burst as the triclosan release occurred by diffusion of the drug through the polymer matrix. Consequently, with a drug loading of only 1 µg per disk no inhibition of bacterial growth could be achieved. By enhancing the drug content to 25 µg per disk, in contrast to the PLA film, for the lin70 PEG-PLA an inhibition was obtained due to the contained hydrophilic PEG which led to a higher water uptake of the film (see 5.3) and as a consequence to a faster diffusion of the triclosan out of the film matrix. The lipophilicity and the very poor water solubility of triclosan led to a good miscibility of the triclosan with PLA and consequently a higher affinity to the PLA film than to the aqueous release medium. Together with the low water uptake of the PLA film this effect obviously hindered the triclosan extremely to diffuse so that diffusion through the PLA film was so slow that only low amounts were released over three weeks and even a drug loading with 50 µg per disk did not result in bacterial inhibition despite a released absolute amount of 2.3 µg within 24 hours for a loading with 25 µg as well as with 50 µg, which is more than the overall released 1 µg from the PEG coating.

To evaluate the influence of polymer branching on the release behavior and antibacterial efficacy, an *in vitro* release study and an agar diffusion test were conducted with polymer films made from lin70rac, 4arm70 and 8arm70. After 24 hours, with a determined inhibition of 0.55 cm each, no difference in antibacterial efficacy was observed with varying polymer architecture (***Figure 5.22***). This result was confirmed by HPLC analysis of the released triclosan amount since after one day with around 20 % of the initial drug content similar amounts were released for all samples. Over the following weeks, slight differences occurred regarding the released drug amount. With an increasing number of arms, an increasing amount of triclosan was released. In this case, the difference cannot be attributed to differences in water uptake since less swelling occurred with an increasing number of arms (see 5.3). The difference might be explained by the earlier fragmentation and consequently higher specific surface with increasing branching leading to a faster release. However, the overall release of between 27 % (lin70rac) and 31 % (8arm70) of the initial triclosan content after thirteen weeks was very low and differences only minor so that hardly any differences for an *in vivo* release and efficacy can be expected. With regard to the above described differences in release behavior and efficacy between PLA and PEG-PLA, a variation in triclosan release can rather be achieved by a variation of the overall content of the hydrophilic PEG than by a variation of the polymer architecture. By regarding the release curves over several weeks, it is furthermore remarkable that after an initial drug release of about 20 % the curves flattened and the release constantly proceeded over the following

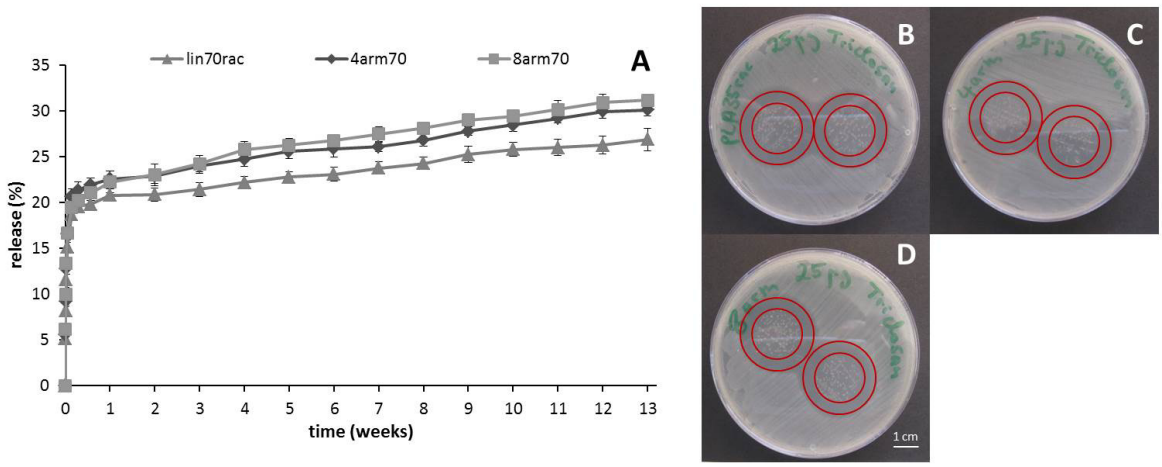

Figure 5.22 *In vitro release profiles determined via HPLC (A) and agar diffusion test of polymer films made of lin70rac (B), 4arm70 (C) and 8arm70 (D) loaded each with 25 µg triclosan per disk.*

weeks. Taking into account that the films were made of hydrolytically cleavable polymers and started to fragment after six to seven weeks (see 5.3), one would expect a two-stage release like manyfold described in the literature[280–282] for devices undergoing bulk degradation and illustrated in ***Figure 5.23***. The first stage is diffusion controlled with an initial burst release. With starting erosion or fragmentation of the matrix, an acceleration of the drug release with a second stage of fast release occurs. The obtained release curves without the second stage of fast release and only around 30 % release after thirteen weeks despite film residues which were only tiny pieces indicate that the lipophilic triclosan adhered strongly to the polymers fragments, which prevented a detectable soaring release into the medium because of film fragmentation. However, the differences in film fragmentation were manifested in slight differences in the absolute release values like already mentioned. Determinations of the residual drug content of the remaining material confirmed that the residuary triclosan was still in the tiny film pieces and not yet released or decomposed. As long as the drug content is high enough to lead to an efficacy, the achieved slow and constant release of the drug could be quite beneficial for applications which require a linear longterm release. The antibacterial efficacy over time of the here investigated polymer films and the benefit for an application as drug loaded barrier device for adhesion prevention were further investigated with additional agar diffusion tests in comparison to drug loaded electrospun meshes. The obtained results were therefore illustrated and discussed in ***Chapter 6***.

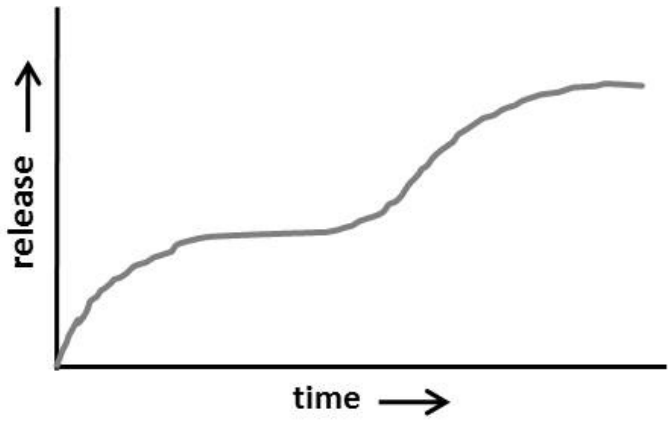

Figure 5.23 *Expected curve progression from a biodegradable drug eluting device undergoing bulk erosion.*

5.5 Summary and conclusions

In conclusion, it was shown that with a PLA modification using the hydrophilic PEG, the properties of solvent cast films can be triggered and consequently films were successfully tailored for an application as physical barrier device for the prevention of postsurgical adhesions. Due to the plasticizing effect of PEG on the PLA, the mechanical properties could be improved and designed for different applications. Films with high flexibility at body temperature (37 °C) and concurrent low or high flexibility at surgery temperature (20 °C) were achieved so that depending on the desired application procedure and its requirements a film with adequate properties for an easy application by the surgeon can be chosen, in either case providing appropriate flexibility within the patient's body to adapt to natural body and organ motion. A suture pullout test confirmed that the films withstand sufficient forces to stay appropriately fixed, indicating sufficient local residence stability to ensure a complete coverage of the site of injury during the time of wound healing.

The presence of hydrophilic PEG resulted in an increased hydrophilicity of the polymer films and consequently to an enhanced water uptake as well. This led together with lower molecular weights to a massively accelerated degradation of the films compared to pure PLA so that the degradation time was shortened from several months to four to six weeks. For drug loaded PEG-PLA films a faster initial release of the lipophilic antiseptic triclosan was achieved, which, in contrast to PLA films at the investigated drug contents, resulted in a successful growth inhibition of postsurgical adhesions causing Staph. aureus. With a pure PEG coating of PLA films, due to a burst release, the highest initial inhibition was obtained so that combinations of different polymer layers with different drug content for a modified release system seem promising as well.

By varying the polymer architecture using star-shaped PEG cores with different numbers of arms for polymer synthesis, the properties of the fabricated films could further be adapted. Polymer branching resulted in an earlier film fragmentation compared to linear polymers due to shorter initial PLA chains and consequently degradation products. However, a longer persistence of the mechanical properties over time was achieved because with a higher number of arms more connecting points to the PLA chains are provided, leading to a better

anchorage of PEG within the film matrix. Polymers with racemic PLA chains seemed superior to the polymers synthesized with 70 % L-lactide and 30 % D,L-lactide. Racemic films degraded in softer film pieces without occurring crystallization and showed a higher stability towards electron beam irradiation. This improved resistance towards the sterilization process is very crucial to ensure the film's quality since sterilization is stringently required before application.

Chapter 6
Evaluation of electrospun meshes particularly in comparison to films

In this chapter, the establishment of solution electrospun meshes of PLA and PEG-PLA copolymers is described and the results of the subsequent experiments with these meshes with regard to an application as physical barrier device are illustrated and discussed. Thereby, the special focus lies on the comparison with solvent cast films of the same polymers. For a best possible comparability, analogous to the films, 20 µm thick solution electrospun meshes were used unless otherwise stated and as far as possible similar experimental conditions were applied. Thus, also swelling and degradation studies as well as mechanical tests were conducted with regard to the influence of hydrophilic PEG and polymer architecture. Furthermore, an agar diffusion test with triclosan loaded meshes and films was carried out to evaluate the particular antibacterial efficacy of the different delivery devices. Cell culture tests were also performed to determine cell adhesion and viability on the differently structured surfaces.

Parts of this chapter have been submitted:

M. Kessler, J. Groll, J. Tessmar

Application of linear and branched poly(ethylene glycol)-poly(lactide) block copolymers for the preparation of films and solution electrospun meshes

Macromolecular Bioscience, under review

6.1 Establishment and surface properties of solution electrospun meshes

6.1.1 Concentration and solvent effects

Non-woven meshes of the previously synthesized PEG-PLA copolymers and the commercial high molecular weight PLA first had to be established for further investigations on the impact of the different manufacturing techniques. To obtain best possible uniform fibers and meshes that were good to handle, varying polymer concentrations and solvents were used for the solution electrospinning process. For all PEG-PLA copolymers, uniform cylindrical fibers could be obtained by electrospinning with a polymer solution in an acetone/DMSO mixture (90:10 % (v/v)). SEM images of electrospun 8arm70 solutions with varying polymer concentrations (***Figure 6.1***) exemplarily illustrate a concentration and a concomitant viscosity effect, which is already well-known for electrospinning of other polymers[283–285] and which was observed for the other investigated PEG-PLA copolymers as well. By applying a high voltage to a solution with low polymer concentration, no fibers but only beads were generated so that the process was rather electrospraying than electrospinning. This can be

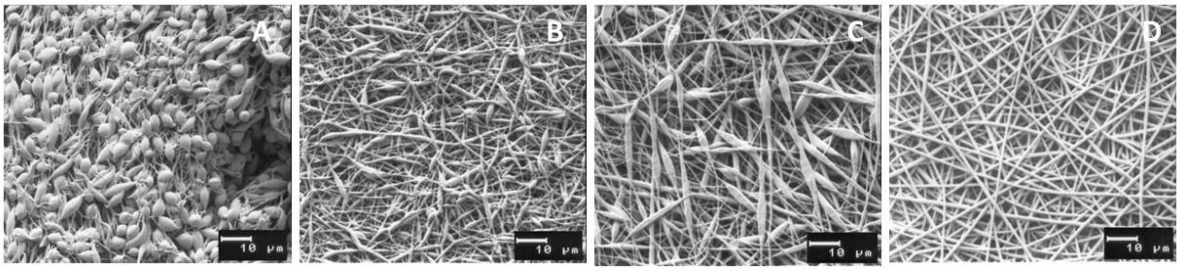

Figure 6.1 *SEM images of electrospun meshes of 28 % (A), 32 % (B), 36 % (C) and 44 % (D) 8arm70 solutions in acetone/DMSO.*

explained by insufficient molecule chain entanglements for the formation of a stable jet to create fibers and an occurring capillary breakup of the jet into droplets by surface tension known as Rayleigh instability. By increasing the polymer concentration, at first fibers with incorporated beads were obtained. The shape of the beads changed from spherical to a spindle-like appearance until with enough net charge density the beads became smaller and finally, with sufficient polymer concentration, continuous fibers without beads were obtained.[283,286–288] By further increasing the polymer concentration, fiber diameters increased. To achieve similar fiber diameters, concerning the linear triblock PEG-PLA copolymers, a lower polymer concentration was necessary for the lin90 than for the lin70.

For the lin130 an even lower concentration than for the lin90 led to similar fiber diameters (***Figure 6.2***). In this case, the results can be explained by the overall extended polymer chains and higher molecular weights with extended PLA chains which consequently enhanced the polymer solution viscosity and led to thicker fibers rather than by the varying PEG content of the polymers. Unless otherwise stated, in the following investigations with electrospun meshes of triblock copolymers, a 24 % solution of lin70, a 28 % solution of lin90 as well as a 32 % solution of lin130 in acetone/DMSO were used for the electrospinning process to achieve uniform fibers with diameters of 1.07 µm ± 0.21 µm. By using solely non-wovens with fiber diameters in the same range, occurring differences in the results of further experiments can be mainly attributed to the properties of the polymers rather than to differences in the achieved and applied fiber morphology.

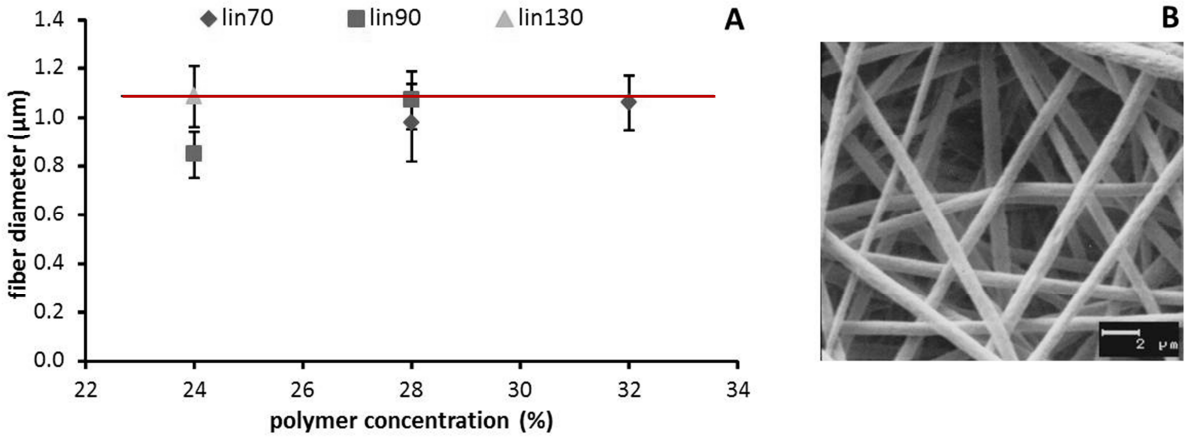

Figure 6.2 *Fiber diameters of triblock PEG-PLA copolymers at different polymer concentrations (A) and exemplarily a SEM image of a lin130 mesh processed with a 24 % polymer solution (B).*

Regarding the star-shaped PEG-PLA block copolymers with equivalent molecular weights, higher polymer concentrations were necessary to obtain uniform fibers without beads with increasing branching of the polymer (***Figure 6.3***)**.** Moreover, by applying the same polymer concentration, the higher the number of arms of the polymer the smaller the resulting fiber diameters were. These observations can be explained by the smaller hydrodynamic volume of the branched polymers due to a higher segment density resulting from the increased branching. Together with the branching points, which additionally prevent an overlapping of the molecule chains, this led to reduced and then insufficient chain entanglements

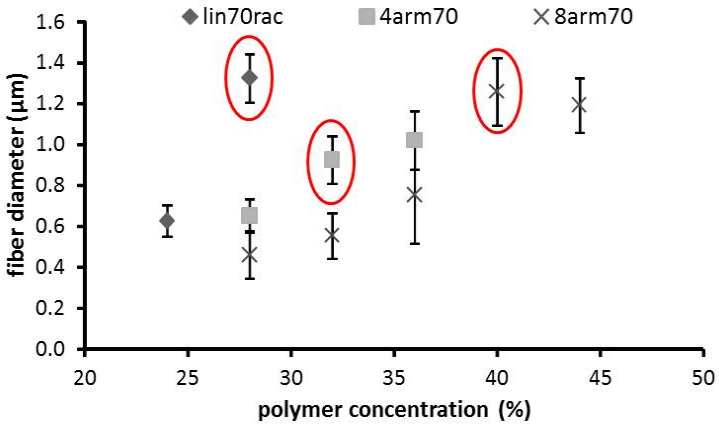

Figure 6.3 *Fiber diameters after electrospinning different concentrations of star-shaped block copolymers with equivalent molecular weights.*
indicates the lowest concentration leading to fibers without beads.

preventing the formation of a stable jet and consequently uniform fibers during the electrospinning process at concentrations which already led to a stable jet for the linear copolymer with similar molecular weight.[263] However, also the lowest concentration to generate fibers without beads not always led immediately to uniform fibers but meshes consisting of fibers of quite various diameters so that for the preparation of meshes for the following experiments electrospinning was partly carried out with slightly higher polymer concentrations in the spinning solutions. Unless otherwise stated, meshes for further investigations were processed with the concentrations given in ***Table 6.1*** and a fiber morphology that can be seen in ***Figure 6.4***. For the star-shaped copolymers with extended PLA chains (4arm140, 8arm140), lower concentrations were sufficient to achieve uniform fibers without beads than for their analogs with shorter PLA chains (4arm70, 8arm70) due to

Table 6.1 *Polymer concentrations of star-shaped PEG-PLA block copolymers in acetone/DMSO applied for electrospinning in the following experiments and resulting fiber diameters.*

Polymer	concentration (m/V %)	fiber diameter (µm)
lin70rac	28	1.32 ± 0.12
4arm70	32	0.93 ± 0.12
8arm70	44	1.19 ± 0.13
4arm140	24	1.03 ± 0.16
8arm140	32	1.30 ± 0.19

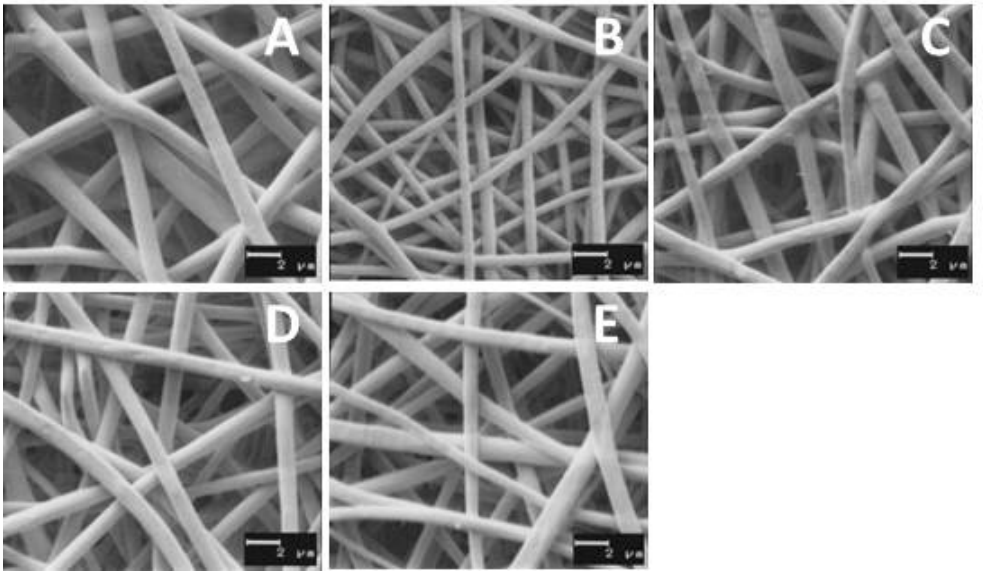

Figure 6.4 *SEM images of lin70rac (A), 4arm70 (B), 8arm70 (C), 4arm140 (D) and 8arm140 (E) meshes electrospun with concentrations given in* ***Table 6.1.***

higher hydrodynamic volumes and chain lengths facilitating chain entanglements and fiber formation. The fiber diameters of the non-woven meshes of the star-shaped block copolymers could not be as exactly brought onto the same value as the fiber diameters of the triblock copolymers, but in a narrow range that still allows drawing conclusions about the effects of the different polymers.

Electrospinning of solutions of the high molecular weight PLA was carried out in distinctly lower concentrations than the PEG-PLA copolymers due to the massively higher molecular weight of the polymer and the consequently higher viscosity of the resulting polymer solutions. Moreover, various different fiber morphologies were obtained based on the chosen solvent and the spinning conditions. By electrospinning PLA in acetone/DMSO the process did in contrast to the PEG-PLA copolymers not lead to uniform cylindrical fibers but resulted in flat ribbon-like fibers (***Figure 6.5A***). By varying the concentration of the polymer solution, the ribbon-like morphology of the fibers remained but despite the flat appearance the already mentioned phenomenon occurred that with increasing concentration the fiber diameter increased (***Figure 6.5B***). A variation of the applied high voltage and the feeding rate also did not change the fiber morphology but only the fiber diameter. Other researchers

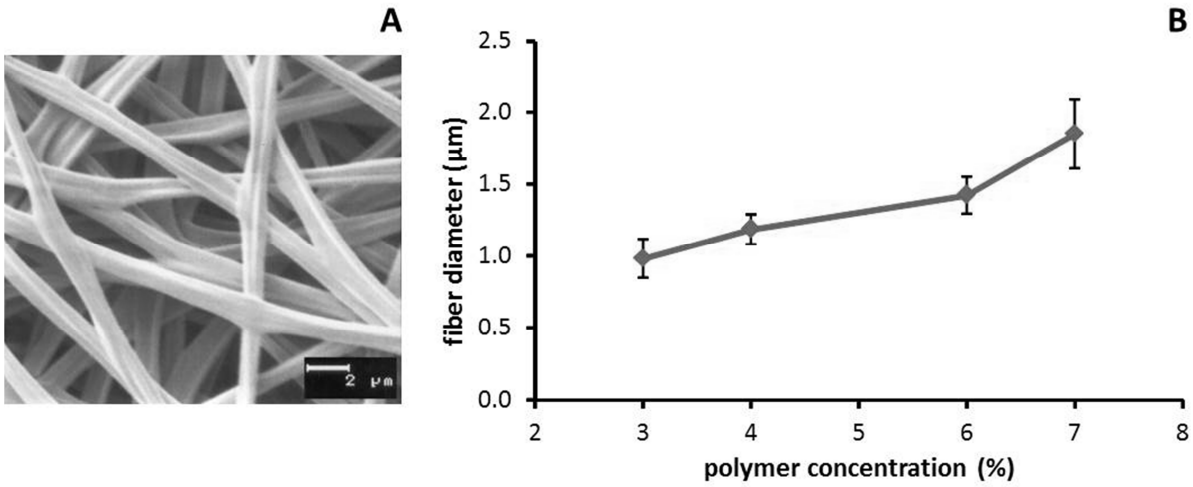

Figure 6.5 *SEM image of a PLA mesh made of a 4 % solution in acetone/DMSO (A) and fiber diameters of PLA meshes after electrospinning with different concentrations in acetone/DMSO (B).*

suggested that the ribbon-like morphology emerges when the solvent rapidly evaporates of the surface of the jet. Thus, the remaining solvent is partly trapped within the fibers as a thin polymer skin is formed on the jet. The fiber skins collapse and flatten through the atmospheric pressure when the solvent finally evaporates.[211,289] With the additionally investigated solution electrospinning in methylene chloride the obtained fibers were cylindrical but porous (***Figure 6.6A***). According to Bognitzki et al.,[290] who obtained porous PLLA fibers with electrospinning solutions in methylene chloride, the regular pore structure may be caused by a high solvent vapor pressure, especially since pore formation was reduced by using solvents with lower vapor pressure. They hypothesized a rapid phase separation during the electrospinning process whereby the pores were formed in solvent

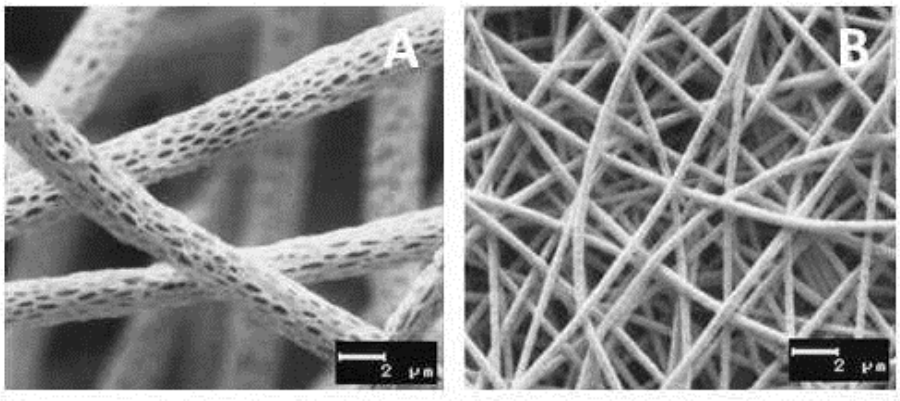

Figure 6.6 *SEM images of PLA meshes showing fiber morphologies after electrospinning of solutions in methylene chloride with 12 kV and 1 mL/h (A) or DMF with 12 kV and 0.5 mL/h (B).*

rich regions. Another explanation of pore formation on fibers during electrospinning is an effect called “breath figures”. Upon rapid solvent evaporation the cooling effect may lead to condensation of air moisture on the surface of the jet. When the jet is drying, pores are formed on the former position of the water droplets.[291] Electrospinning of PLA solutions in DMF with its distinctly lower vapor pressure (3.60 hPa at 20 °C[292]) than acetone (245 hPa at 20 °C[293]) and methylene chloride (470 hPa at 20 °C[294]) led to the desired cylindrical non-porous fibers (***Figure 6.6B***) for comparison with the PEG-PLA meshes. However, the resulting non-wovens were impossible to handle accurately for further experiments as no plane cohesive mesh could be obtained and the fibers were very sticky most likely due to residual solvent. Due to a similar behavior of the porous fibers, the following experiments were conducted with PLA meshes consisting of ribbon-like fibers. Unless otherwise stated, the here studied meshes were prepared by electrospinning a 4 % PLA solution in acetone/DMSO since this concentration led to the best mesh with the most comparable fiber diameters to the PEG-PLA meshes.

6.1.2 Rheology

Since a critical polymer concentration and consequently viscosity is necessary to achieve uniform fibers, rheological investigations on the solutions utilized for electrospinning were conducted to reveal exact relations between the particular viscosity of the investigated electrospinning solutions and fiber formation in order to facilitate the establishment of further polymer meshes. The results confirm that with increasing polymer concentration naturally the viscosity of the solution increased like illustrated in ***Figure 6.7A*** exemplarily on solutions of 8arm70. The measurements also revealed that for branched copolymers a higher concentration was necessary to achieve the same viscosity than for a linear copolymer with equivalent molecular weight due to the already mentioned smaller hydrodynamic volume of the branched polymers. The interesting and useful finding is that the viscosities and shear stresses of the concentrations yielding uniform fibers were all in the same range (***Figure 6.7B***). As a consequence of these findings, by knowing the rheological properties of polymer solutions with varying concentrations, it can be inferred on the appropriate polymer concentration that may lead to uniform fibers without time-consuming

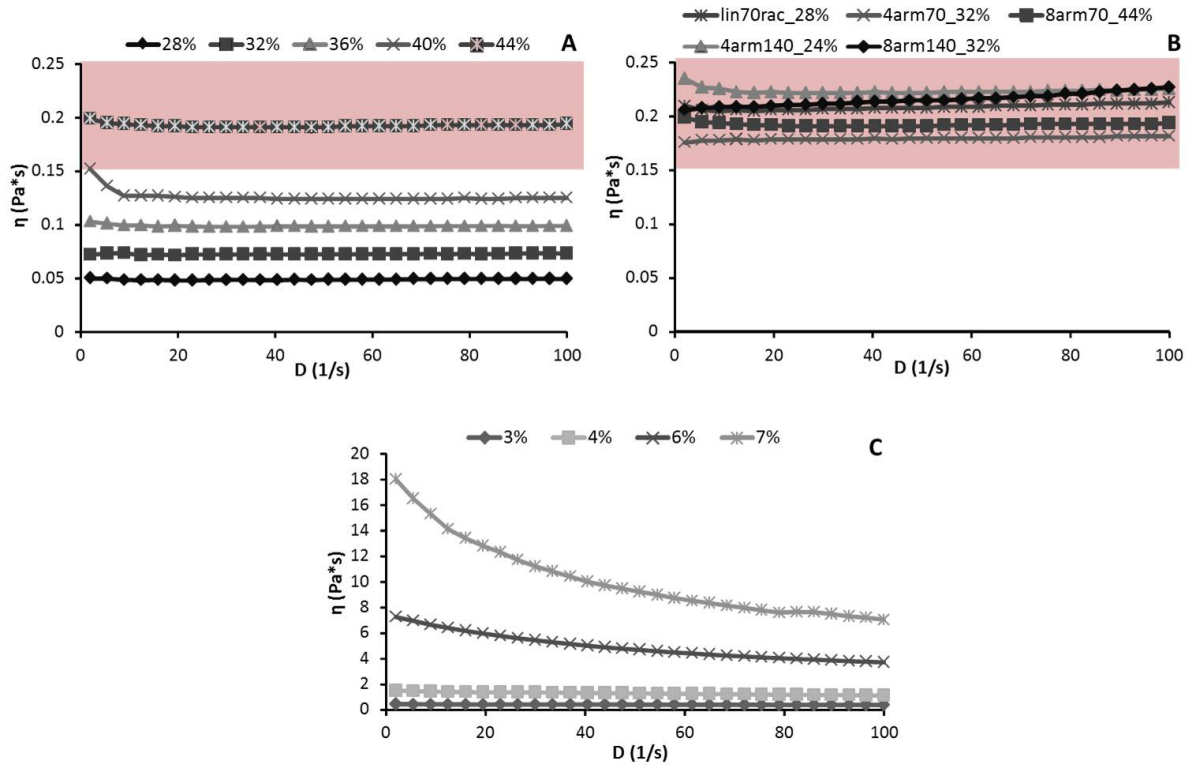

Figure 6.7 *Rheological properties of 8arm70 solutions in different concentrations (A), PEG-PLA solutions leading to uniform fibers (B) and PLA solutions (C) in acetone/DMSO.*
The red shading indicates the viscosity range where uniform fibers were generated.

electrospinning trials with subsequent SEM observations. However, the ideal range of viscosity is probably only valid for PEG-PLA copolymers or comparable polymers in a certain molecular weight range, since the viscosities of the also processed high molecular weight PLA massively differed from the values of the PEG-PLA solutions (***Figure 6.7C***).

6.1.3 Contact angle measurements

To get an idea of the surface wettability and hydrophilicity of the different meshes, water contact angles on the meshes were determined. By measuring the contact angles of dry meshes, no significant differences occurred between the different polymers in contrast to the also investigated films. Moreover, the initial contact angles of dry as-spun meshes were distinctly higher than those of the dry as-cast films of the same polymers like ***Figure 6.8*** exemplarily shows for the linear polymers. While the measured contact angles of films represent the particular hydrophilicity of the polymer, the very hydrophobic values of the meshes can rather be attributed to the fiber or mesh morphology than to the chemical

composition of the fibers, since it is known that surface roughness heavily influences the contact angle, which may be explained by two different models. For one thing, a higher surface roughness brings along an increase of the surface area of the material and consequently an increase of the surface energy in comparison to a smooth surface of the same material proposing a geometrical enhancement of hydrophobicity (Wenzel model[295]). For another thing, trapped air within the pores of the material below the droplet may lead to the effect that the water droplet is partially located on air so that the contact angle is measured of a surface composed of a solid material and air. With increasing surface roughness and air entrapment and consequently a decrease of the contact area between the droplet and the solid material the hydrophobicity increases (Cassie model[296]).[297–298]

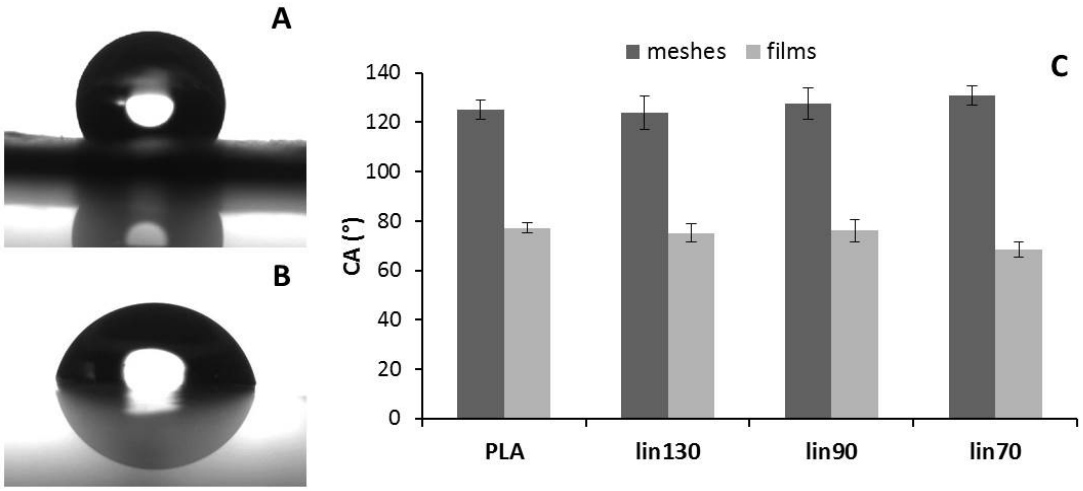

Figure 6.8 *Water droplet on lin90 mesh (A) and lin90 film (B) and results of determined water contact angles of dry as-fabricated linear polymer meshes and films (C).*

However, a varying wettability of the meshes of the different polymers could be observed by an iterated measurement two minutes after initial contact with the water droplet and especially by determining the contact angles of dry-blotted meshes that were pre-incubated overnight in phosphate buffer pH 7.4. After the long time in water contact the chemical composition of the different meshes came into effect, now exhibiting significant differences of the water contact angles. Depending on the content of the hydrophilic PEG within the linear polymers the water droplet partially infiltrated into the mesh. While the initial contact angles on the dry as-spun meshes hardly differed like already mentioned, after two minutes

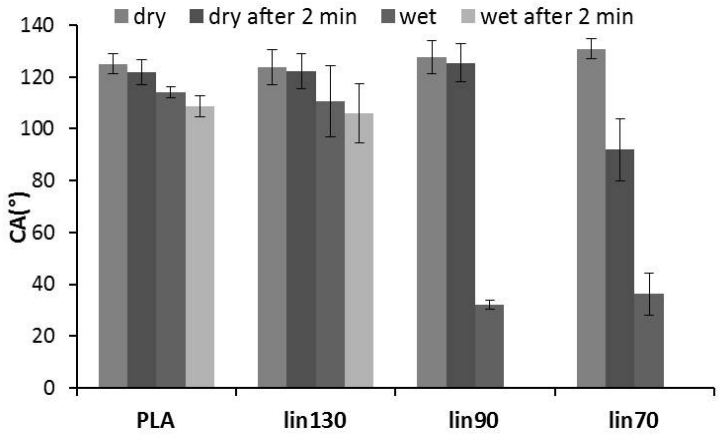

Figure 6.9 *Contact angles of dry and dry-blotted incubated meshes of linear polymers.*

the contact angle of the mesh with the highest PEG content (lin70) was massively lower than initially and also than the contact angles of the meshes with lower PEG content that were only slightly smaller after two minutes (***Figure 6.9***)**.** After the incubation in buffer overnight, further influences of the enhancement of the hydrophilicity through the incorporation of PEG became visible. The water droplets still did not penetrate into the PLA and the lin130 mesh immediately after dry-blotting and two minutes afterwards, but a complete infiltration of the water droplets into the meshes with higher PEG contents became clearly visible. For those polymer meshes, the contact angles immediately after dry-blotting were very small and the droplets were completely soaked up after two minutes.

For meshes prepared of the star-shaped PEG-PLA block copolymers, both a dependence on the PEG content and on the number of arms was detected. Thereby, the lin70rac showed the best wetting properties since in contrast to the other polymers already after two minutes on the dry mesh a diminution of the contact angle was observed (not shown) like for its 70:30 L-lactide: D, L-lactide analog. After incubating the meshes in buffer overnight, the immediate contact angles of the dry-blotted meshes of the polymers with 12.5 % PEG (lin70rac, 4arm70, 8arm70) were massively lower than those of the dry meshes (***Figure 6.10***). Despite similar molecular weights and PEG contents, thereby the contact angle was the higher the higher the number of arms of the polymer, probably due to a worse accessibility of the PEG core for water with an increasing number of PLA chains. However, after two minutes the water

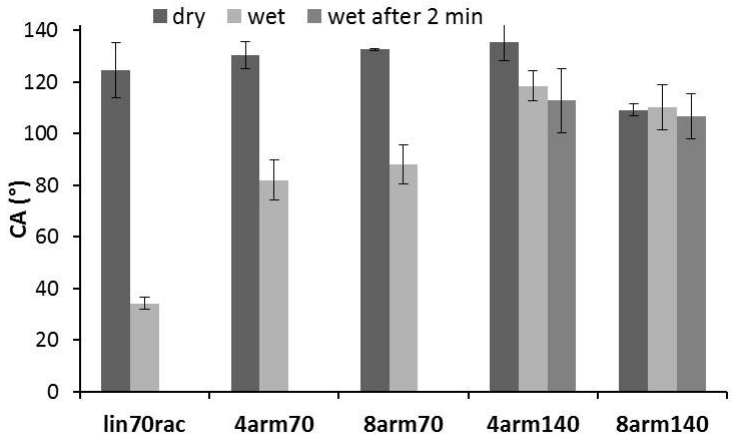

Figure 6.10 *Contact angles of dry and dry-blotted incubated meshes of star-shaped polymers.*

droplets were completely absorbed by all of the meshes with 12.5 % PEG. In contrast, the contact angles of the meshes of the polymers with elongated PLA chains (4arm140, 8arm140) only slightly decreased after buffer incubation and also no absorption of the water droplets into the meshes could be observed, but instead the droplets were still sitting on top of the meshes after two minutes. This relatively poor wettability may be attributed to the higher length of the hydrophobic PLA chains which prevents a rapid water infiltration by a shielding effect. In contrast to the meshes, for massive polymer films that were incubated in buffer overnight, the contact angles only slightly differed to those on dry films indicating that hardly a better spreading let alone an infiltration of the water droplets occurred during the shortness of the investigated time. The high density of the relatively hydrophobic polymers and consequently the massive surface character of the films made it difficult for water to penetrate into the polymer films.

6.2 Mechanical properties

To evaluate the mechanical properties of the established solution electrospun meshes, analogous to the methods applied to the solvent cast films a tensile test, a puncture test as well as a suture pullout test were conducted. In ***Table 6.2*** T_g of the meshes of the linear and star-shaped polymers were summarized since T_g highly influenced the results of the mechanical tests. Like for the polymer films, T_g of the polymer meshes decreased significantly with increasing PEG content of the polymer, while no obvious correlation

regarding the number of arms could be assessed. Generally, T_g of the electrospun meshes was higher than of the raw polymers and of cast films prepared of the same polymer (see ***Table 4.6*** and ***Table 5.1***), which can be attributed to the orientation and dense packing of the polymer chains resulting from the electrospinning process.[299]

Table 6.2 *Glass transition temperatures of polymer meshes determined from the second heat of DSC measurments.*

linear polymers	**T_g (°C) mesh**
lin70	25.7
lin90	35.0
lin130	41.0
PLA	55.1
star-shaped copolymers	**T_g (°C) mesh**
lin70rac	26.1
4arm70rac	21.2
8arm70rac	22.6
4arm140rac	36.5
8arm140rac	33.4

Prior to each measurement standardly the test specimens are conditioned for several hours at the particular test conditions.[244] However, an incubation of selected polymer meshes at 37 °C in air with subsequent SEM observation at defined time points showed that, depending on their T_g, the meshes suffered upon the temperature treatment and partly lost their fiber structure. For PLA meshes with a T_g clearly above 37 °C (T_g 55.1 °C) and for 4arm140 meshes with a T_g near the incubation temperature fibers did not noticeable change over several hours and showed a slight coalescence only after 24 h. In case of the lin70rac mesh with a T_g distinctly below 37 °C (T_g 26.1 °C) already after half an hour first signs of fiber coalescence appeared (***Figure 6.11***). After 24 h the lin70rac meshes had more a film-like appearance with almost no recognizable fiber structure anymore. Consequently, the electrospun meshes were only hold at test temperature for two minutes prior to the test to avoid a destruction of the fibers and to maintain the comparability between the different polymers. Moreover, the SEM images make clear that the meshes need to be stored cool to preserve the meshes from fiber coalescence and to keep the matrix integrity for subsequent tests.

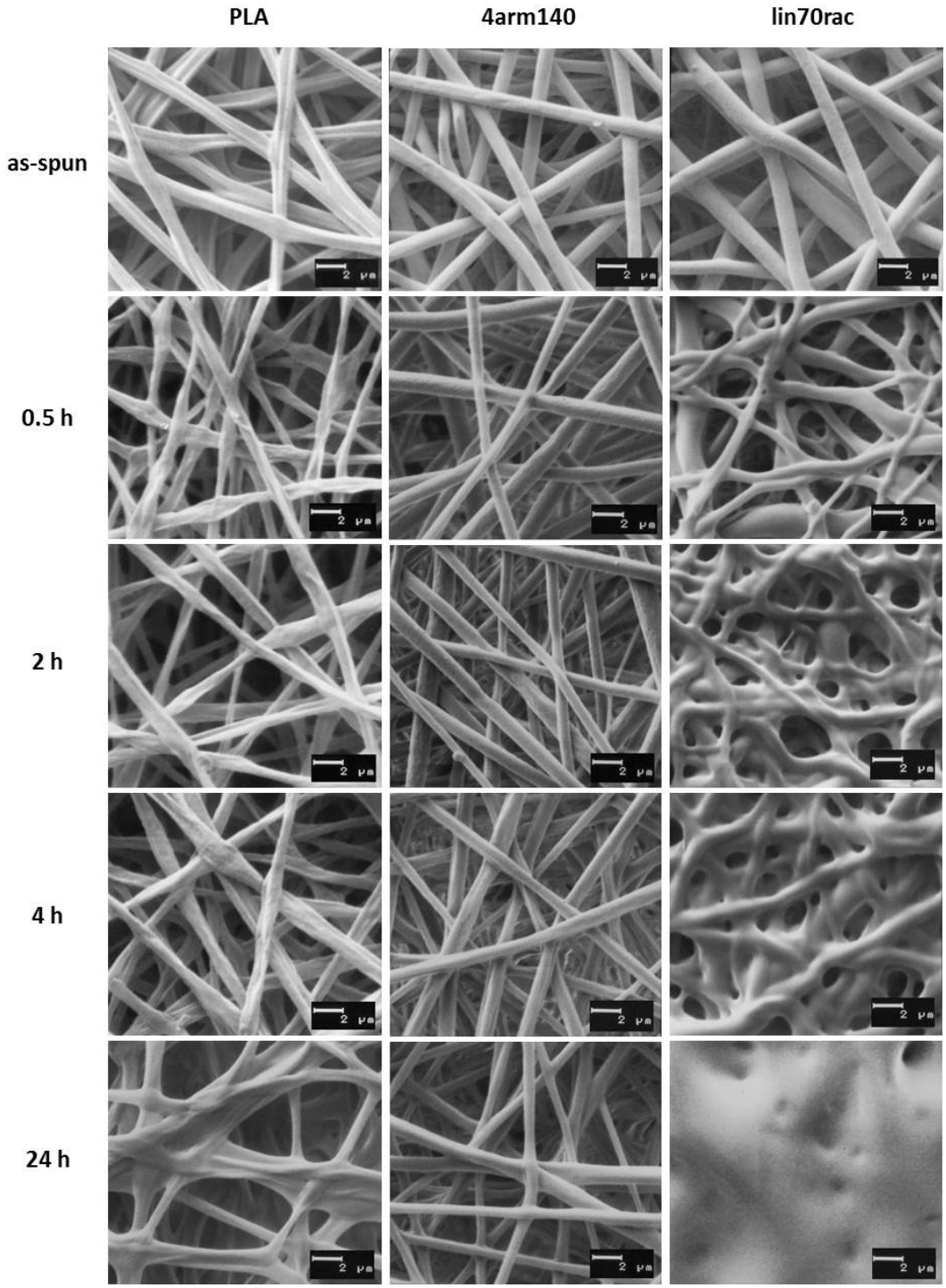

Figure 6.11 *Solution electrospun meshes of PLA, 4arm140 and lin70rac as-spun and after dry incubation at 37 °C.*

6.2.1 Tensile test

The tensile test was carried out in two ways for each polymer mesh, both with specimens cut in longitudinal direction as well as in transverse direction. The reason therefor was that during the electrospinning process with a rotating drum as collector a preferential fiber orientation may take place that influences the mechanical properties of the mesh. The implementation of the tensile test with test specimens in both cutting directions aimed both to the evaluation and quantification of the influence of fiber orientation and to the exclusion of falsifications of the results due to varying cutting directions within one test row. In general, the temperature also highly influenced the mechanical properties of the electrospun meshes. Both for all investigated polymers and in both cutting directions strain at break increased and the tensile strength decreased with increasing test temperature.

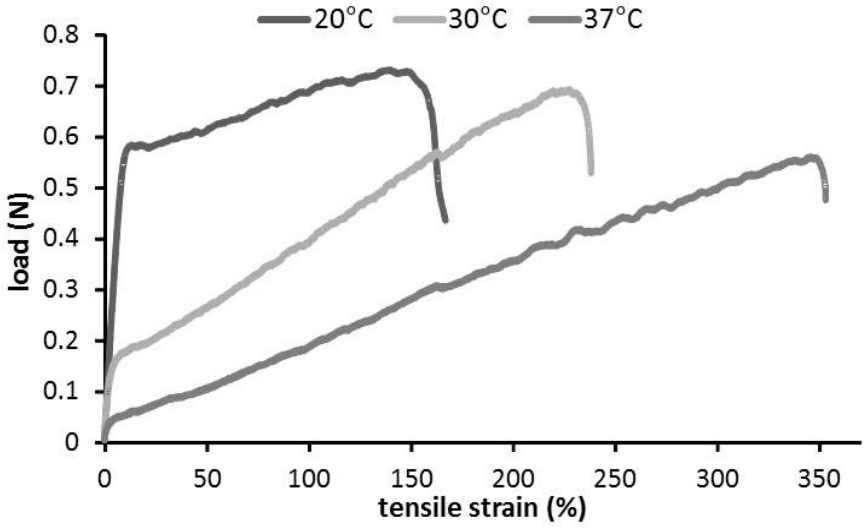

Figure 6.12 *Load – strain diagrams of 4arm70 mesh obtained at different test temperatures.*

Similar to the polymer films, this can be attributed to a higher mobility of the polymer chains at elevated temperatures especially by overstepping T_g. Depending on the particular test temperature and the polymer, each mesh resulted in various load – strain diagrams like exemplarily illustrated in ***Figure 6.12*** for a 4arm70 mesh. In contrast to the cast polymer films, none of the electrospun meshes was brittle and tore already after minor deformation (see films with high PLA content) but all meshes experienced a certain elongation owing to the fiber morphology. The meshes either exhibited ductile properties with a recognizable yield

point and subsequent plastic deformation (***Figure 6.12 20°C***) or at elevated temperatures showed elastic properties without a detectable yield point (***Figure 6.12 37 °C***). With increasing tensile strain the force to stretch the mesh increased until the samples finally ruptured.

By examining the results of the test specimens in different cutting directions, the test direction of the meshes turned out to be relevant. It is described in the literature that fiber alignment depends on the rotational speed of the collector drum and that the alignment of fibers affects the mechanical properties. By applying a rotational speed that concurs with the evaporation rate of the solvent, the fibers are deposited in an aligned manner on the collector drum whereby the alignment increases with an increasing rotation speed. With a rotational speed that is too high though, no continuous fibers can be obtained because the fiber jet is already torn apart by the take-up velocity.[211] From a mechanical point of view, uniaxial, aligned fibers evidently show different properties than randomly oriented fibers. The tensile strengths and modulus were found to be higher than for random fiber orientation by aligning the fibers in the direction of the applied load because then the applied force is distributed equally on all fibers. With a rotational speed which is lower than the fiber take-up speed fibers are collected randomly oriented on the rotating drum,[211] which furthermore favors evenly strong fiber meshes. In the electrospinning process of the meshes which were used in this study a low rotational speed was applied so that fibers appeared to be randomly oriented on SEM images. Nevertheless, for all test conditions and polymers, lower tensile strengths and higher strains at break could be determined for the specimens tested alongside the fiber jet and rotating direction of the collector drum (longitudinal) than for the mesh specimens in transverse direction (***Figure 6.13***)**.** Obviously the here obtained fibers still experienced a discreet orientation during the electrospinning process and the deposition on the collector drum. If the fiber orientation was caused by the rotation of the collector drum, mechanical properties would be expected contrary to the obtained results, with a higher tensile strength in longitudinal direction. The observed higher tensile strength in transverse direction might be caused by a preferential fiber orientation in transverse direction provoked by the typical behavior of the fiber jet to deposit on the closest location on the collector with low fiber density. As a consequence, at relatively low

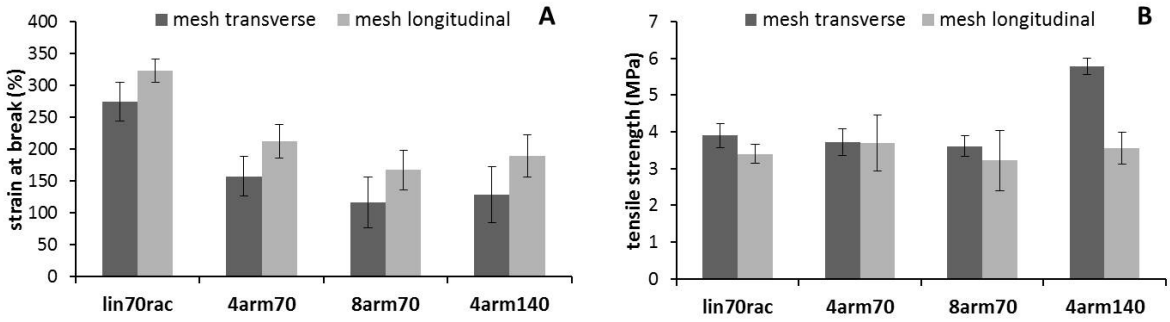

Figure 6.13 *Strain at break (A) and tensile strength (B) of solution electrospun meshes cut in longitudinal and transverse direction determined at 20 °C.*

rotational speeds of the drum the fibers were probably preferably deposited along the bending of the drum and thereby slightly oriented in transverse direction, which is additionally promoted by the reciprocating motion of the drum.

Despite the occurring differences in the results of mesh specimens with different cutting directions, similar trends were detected by comparing the different polymers to each other. Therefore, in the following only the results of the meshes cut in transverse direction are shown to illustrate the trends. Regarding the linear polymers, generally higher strains at break were determined with increasing PEG content due to the still observed plasticizing effect of PEG (***Figure 6.14A***). The tensile strength decreased for the same reason with increasing PEG content at 20 °C, while at 30 °C and 37 °C no obvious trend was observed (***Figure 6.14B***).

For the non-woven meshes of star-shaped copolymers, a dependence on the PEG content was determined as well. The meshes of the branched polymers with extended PLA chains and consequently lower PEG contents (4arm140, 8arm140) exhibited smaller strains at break and higher tensile strengths than the polymer meshes with 12.5 % at all investigated test temperatures (***Figure 6.14C, D***). At 20 °C, also a dependence on the number of arms was observed. At equivalent molecular weights, lower strains at break were determined with increased branching. Like already mentioned for the polymer films, this may be attributed to the shorter lengths of the polymer arms and less chain mobility due to more chain entanglements with increased branching, which leads to an earlier slipping of the molecule

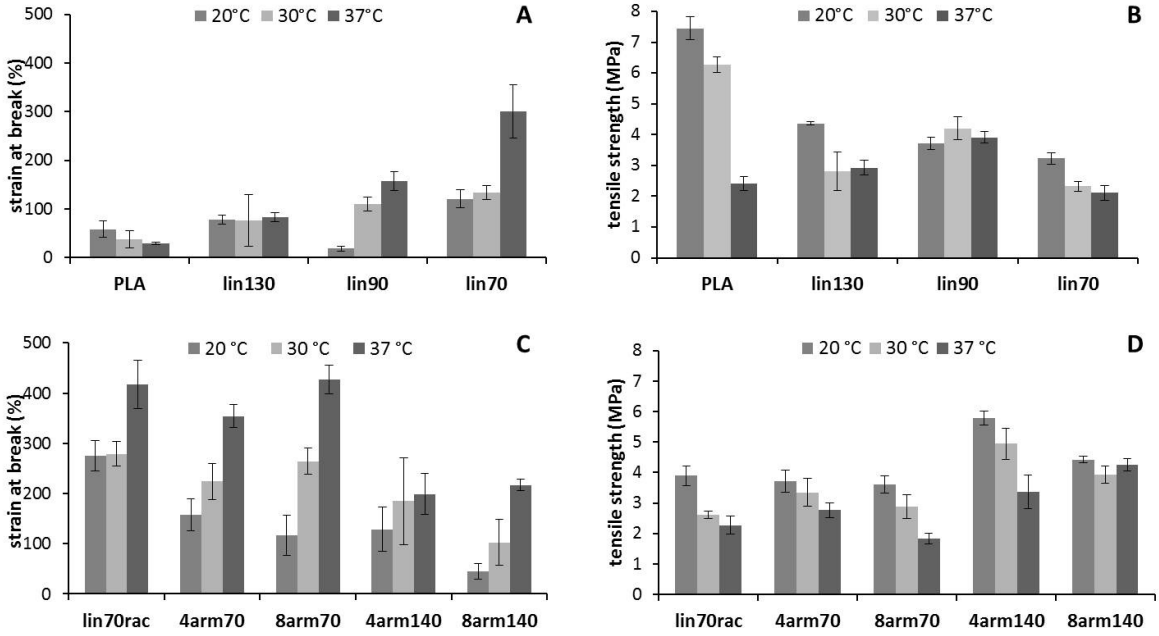

Figure 6.14 *Strain at break (A, C) and tensile strength (B, D) of electrospun meshes of linear polymers (A, B) and star-shaped copolymers (C, D) determined at different test temperatures.*

chains as well as rupture of chemical bonds and consequently of the sample. At elevated temperature, no clear trend was detected anymore.

SEM images of the meshes after conducting the mechanical test revealed significant changes in fiber morphology compared to the initial appearance. Partly a parallel alignment of the fibers both in longitudinal as well as in transverse direction caused by the applied tensile forces was observed (***Figure 6.15***). Moreover, despite the precaution to condition the samples for only two minutes at test temperature prior to the test to avoid coalescence, the fibers of the polymers with 12.5 % PEG obviously fused during the test at 37 °C, while the fibers of the polymers with lower PEG content and higher T_g remained individual fibers. As it is known that bonding points between the fibers affect the mechanical properties of electrospun meshes,[300] it can be assumed that the occurring fusion of the fibers during the test is responsible that at elevated temperatures no obvious trends in the mechanical properties could be detected like for the massive polymer films. After tensile testing at the lowest temperature of 20 °C, on the SEM images of the investigated meshes necking of single fibers made from the stiff polymers with high PLA content and T_g could be clearly recognized (***Figure 6.16***).

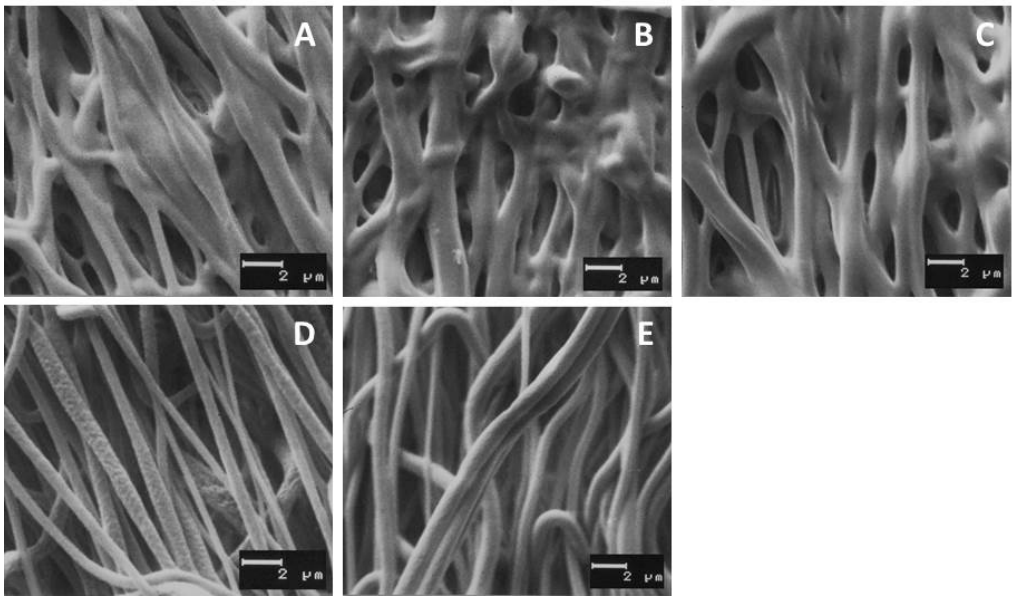

Figure 6.15 *SEM images of electrospun meshes of lin70rac (A), 4arm70 (B), 8arm70 (C), 4arm140 (D) and 8arm140 (E) after tensile testing in transverse direction at 37 °C.*

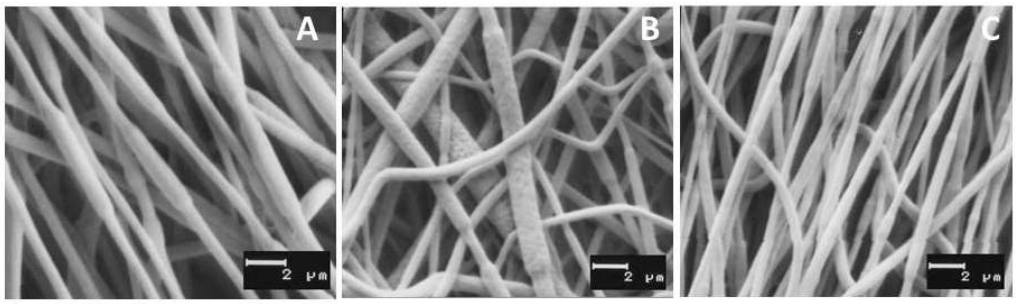

Figure 6.16 *SEM images of electrospun meshes of 4arm140 (A), 8arm140 (B) and lin130 (C) after tensile testing in transverse direction at 20 °C.*

This phenomenon of multiple necking of single fibers was also reported and explained by other researchers. Zussmann et al.[301] obtained multiple necking of their investigated electrospun PEO nanofibers directly after the electrospinning process without applying further mechanical stresses through a mechanical test. They attributed the observation to a stretching of the fibers by the rotating collector wheel since the necking phenomenon did not occur for fibers which were electrospun without tension on an aluminium plate. Liu et al.[302] explained the multiple necking of electrospun PMMA fibers after tensile testing by a heterogeneous distribution of the molecule chain entanglement density caused by the electrospinning process. Subsequently, the occurring segments with a low entanglement density can easier be elongated leading to the observed necking phenomenon.

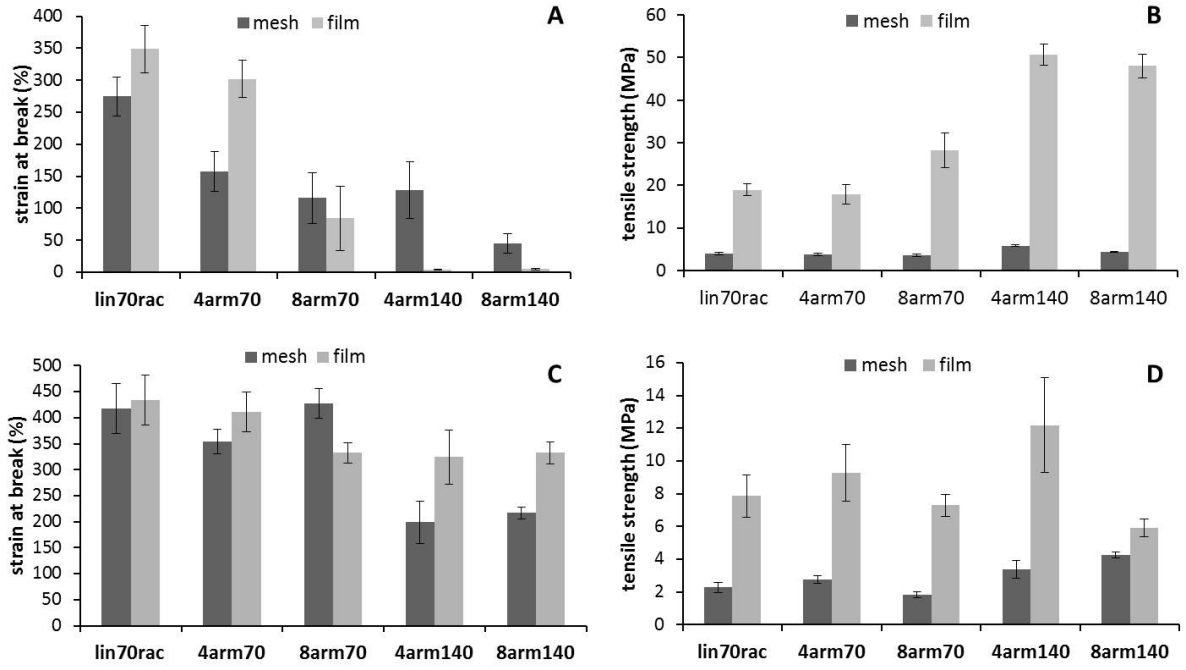

Figure 6.17 *Strain at break (A,C) and tensile strength (B, D) of star-shaped polymer films and electrospun meshes (transverse direction) determined at 20 °C (A, B) and 37 °C (C, D).*

The generally observed trends of the tensile properties of the meshes resembled the trends the solvent cast films of the same polymers displayed, but with divergent absolute values. Concerning strain at break, partly the respective meshes and partly the films displayed higher values in direct comparison. At the lowest applied test temperature of 20 °C the strains at break for polymers with high PEG contents were higher for the polymer films, whereas with lower PEG content higher strains at break were determined for the respective meshes (***Figure 6.17A***). Obviously the fiber structure promoted the extensibility of polymers with low plasticizer content in contrast to the massive films. At elevated test temperature, the effect of the fiber structure was diminished since strains at break were mainly higher for the films (***Figure 6.17C***). In contrast, the tensile strengths of the films were always way higher than that of the respective meshes, which can be explained by an overall higher polymer content and a higher polymer density with similar thickness of the sample that strengthens the implant device (***Figure 6.17B, D***).

6.2.2 Puncture test

Apart from the tensile test, a puncture test was conducted to additionally determine the resistance to deformation by puncturing the meshes. Since the cutting and clamping direction was irrelevant due to square-shaped test specimens and the application of a centrical force acting equally in all fiber orientations, the experiment was in contrast to the tensile test carried out in only one test row. The appearance of the resulting load – displacement diagrams from the measurements with the electrospun meshes is exemplarily shown in ***Figure 6.18*** on 8arm140 meshes. Similar to the diagrams of solvent cast films, the load increased with increasing displacement. Initially the curves steeply ascended until an inflection point from where on the slope decreased. Finally, at the point of maximum load the meshes ruptured. By increasing the temperature, due to an enhanced flexibility of the polymer chains, the elongations to puncture increased and the maximum loads decreased.

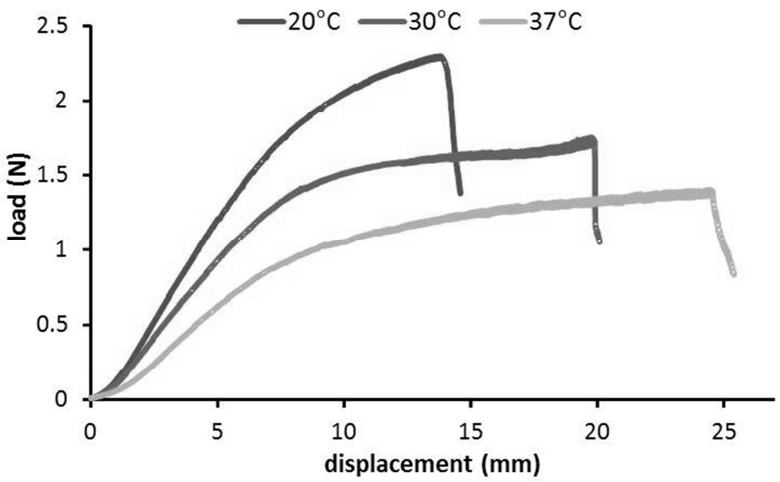

Figure 6.18 *Load – displacement diagrams of 8arm140 mesh obtained at different temperatures.*

The recognizable overall trends were similar to the results of the tensile test, but with a more distinct differentiation of the particular polymers over all investigated temperatures. The results of the linear PEG-PLA copolymers clearly display the plasticizing effect of PEG since at all test conditions the elongation to puncture was increased with increasing PEG content (***Figure 6.19***). The results of the meshes of pure PLA did not exactly fit in the trend, but this may be attributed to the massively higher molecular weight and molecule chain length of the utilized PLA making a direct comparison to the PEG-PLA copolymers difficult.

Apart from the generally higher strength of pure PLA in comparison to plasticized PLA, the massively higher molecular weight might have also led to the determined load to puncture values that were partly more than twice as high as the values of the PEG-PLA meshes (***Figure 6.19B***).

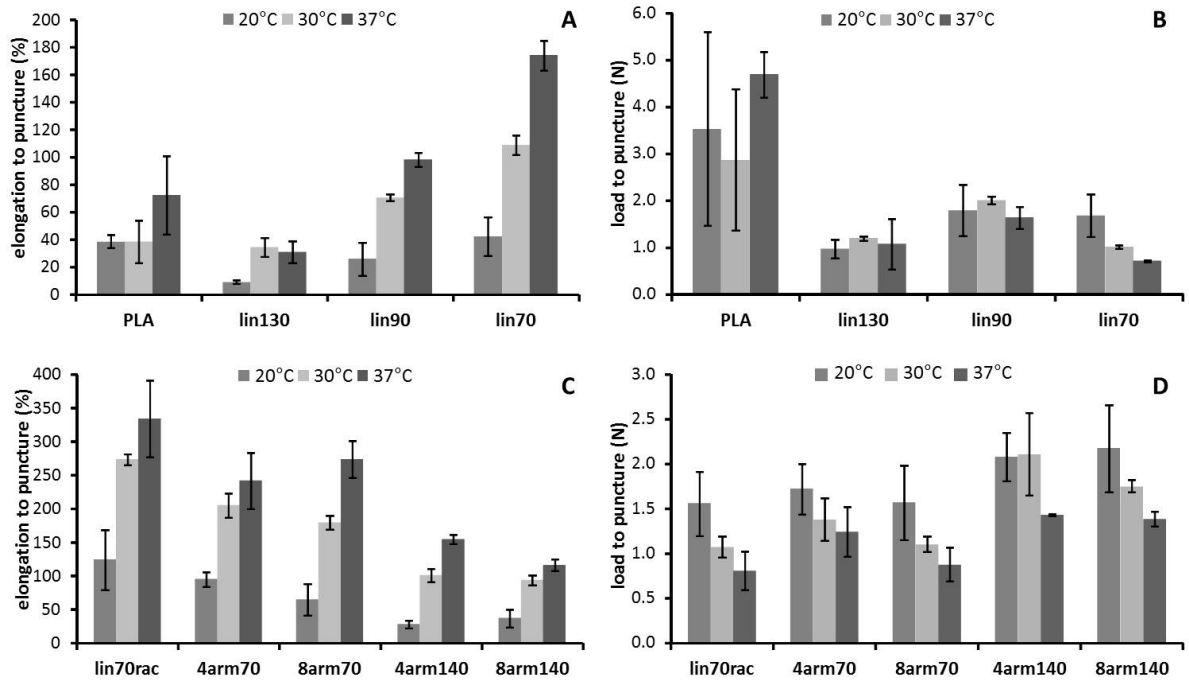

Figure 6.19 *Puncture properties of solution electrospun meshes of linear (A, B) and star-shaped polymers (C,D).*

The measurements with star-shaped copolymer meshes again showed a strong dependence not only on the PEG content but also on the number of arms. The loads to puncture depended apparently only on the PEG content since the differently branched polymers with equivalent molecular weights withstood similar loads in each case, but the polymer meshes with extended PLA chains exhibited higher loads than the polymer meshes with higher PEG content (***Figure 6.19D***). However, elongation to puncture both varied with the PEG content and the number of arms. The values generally decreased with increased branching and elongation of the PLA chains (***Figure 6.19C***).

Similar to the films, a puncture test was conducted with electrospun meshes after incubation in phosphate buffer pH 7.4 at 37 °C as well to study the behavior during application in the body. Prior to measuring at 37 °C, the meshes were removed from the buffer and dry blotted. Again the puncture test was preferred to a tensile test after degradation since similar trends were observed as with the tensile test but with a better differentiation of the polymers like already seen for the films. Moreover, the cutting direction is obviously irrelevant for the test and the shrinkage of the meshes does not affect the execution of the test, especially by incubating mesh pieces that are large enough even after shrinkage to allow both an accurate fixation of the samples in the sample holder and the coverage of the defined area to puncture. In contrast, the required 5 cm × 1 cm test specimen size for an accurate and comparable tensile test is almost impossible to achieve as owing to shrinkage either the width would be to low or the specimen too short for a fixation in the instrument's clamps. In ***Figure 6.20*** the results of the puncture test of degraded samples of 4arm140 meshes and lin70rac meshes are presented in comparison to degraded films of the same

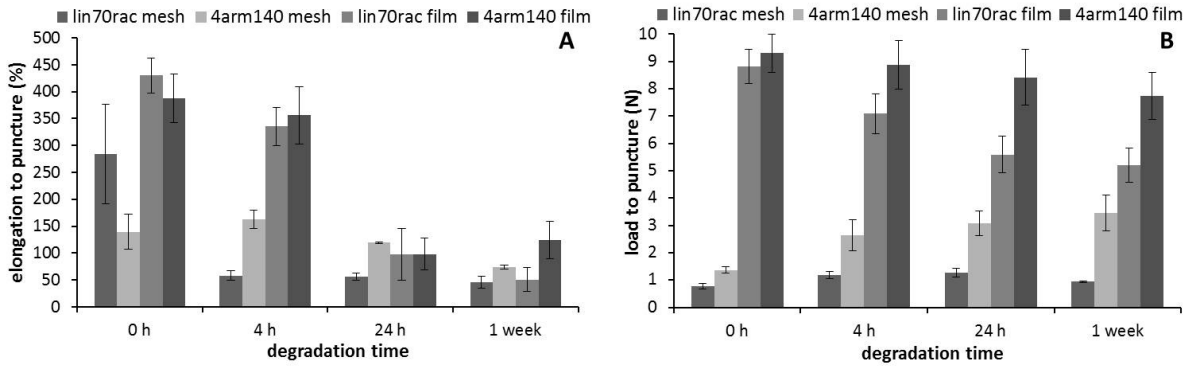

Figure 6.20 *Elongation to puncture (A) and load to puncture (B) of lin70rac and 4arm140 meshes and films during degradation in phosphate buffer pH 7.4 at 37 °C.*

polymers. Similar to the corresponding films, the elongation to puncture decreased for the investigated meshes exhibiting also the same reversion that after four hours incubation the elongation value of lin70rac was lower than that of 4arm140. However, resembling elongations to puncture were determined for the investigated films and meshes after one week since the decrease of elongation to puncture was massively higher for the films. The load to puncture of the meshes increased at the beginning of buffer incubation probably due to relatively increased polymer contents per test area due to shrinkage of the meshes.

Nevertheless, the loads still remained distinctly lower than the loads of degraded massive films, so that it remains questionable if the 20µm thick meshes alone could withstand an application in the body.

6.2.3 Suture pullout test

A suture pullout test was conducted to determine the maximum axial forces that can be applied until the surgical suture is pulled out of the suture hole of the mesh. Photographic images of the test specimens after the test demonstrate how the suture interacted with the meshes (***Figure 6.21***). While the suture neatly slid through the brittle films with high PLA content and the more flexible films tore sideways (see ***Figure 5.11***), all of the meshes tore

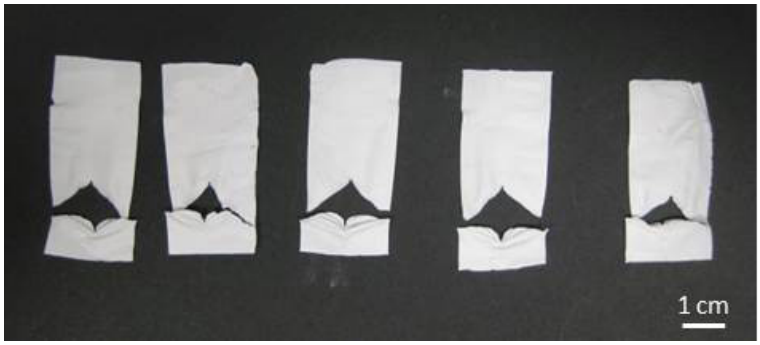

Figure 6.21 *Test specimens of lin70 mesh after suture pullout test.*

sideways before releasing the suture since the suture was caught by the mesh and did not slide through it. ***Figure 6.21*** exemplarily shows the test specimens of lin70 after conducting the suture pullout test. The resulting maximum pullout forces decreased for the linear polymers from PLA (0.71 N) to lin70 (0.29 N) and increased with branching of the polymers (by having similar molecular weights) and elongation of the PLA chains (4arm140, 8arm140) (***Figure 6.22***). The results display opposite trends than for cast films made of the same polymers (see ***Figure 5.10***) and can in that case probably rather be attributed to the fiber structure, the particular molecule size and branching than to the PEG content. The suture intertwines with the fibers so that the test might reflect the mechanical resilience of the particular fibers to lateral forces. Longer polymer chains and higher branching lead to more chain entanglements within the fibers and might consequently result in a higher resilience to lateral forces aggravating it for the suture to neatly slide through the mesh.

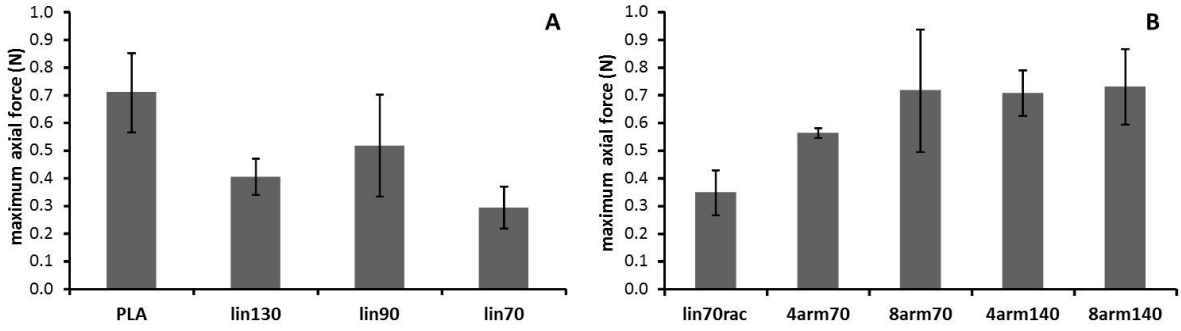

Figure 6.22 *Results of the suture pullout test of linear polymer (A) and star-shaped copolymer (B) meshes.*

According to surgeons, due to the weakness and relatively small thickness, suturing of a 20 µm mesh is very difficult and rather impossible so that a successful application of a monolayer is questionable. As a consequence, non-woven meshes with a thickness of 40 µm were also fabricated and subsequently a suture pullout test was conducted. ***Figure 6.23*** illustrates that the resulting pullout forces of the meshes were about three times higher than with half of the thickness so that in case of 4arm140 the pullout force even reached the same level as the corresponding film. The results indicate that with the twofold thickness the meshes can successfully be sutured.

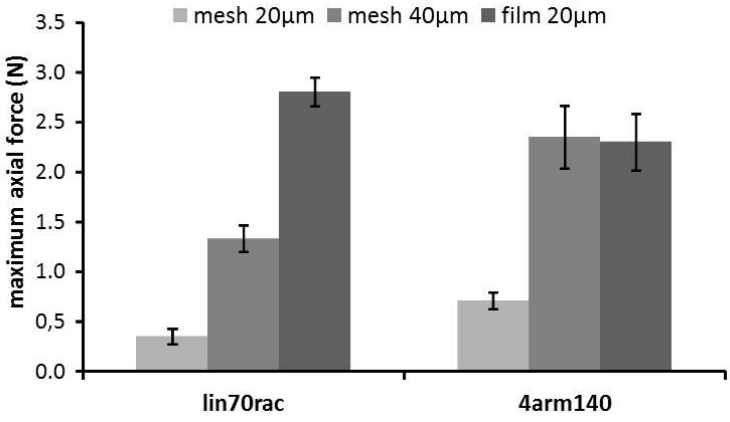

Figure 6.23 *Suture pullout forces of 20 µm and 40 µm thick meshes and 20 µm thick films.*

6.3 Swelling and degradation studies

Similar than for the films, electrospun meshes of PLA experienced hardly any changes over the investigated eight weeks incubation time. Thus, in the following only the degradation of PEG-PLA meshes is discussed. Macroscopically, the electrospun meshes of the linear copolymers started to tear earlier than the films but displayed the same trend since meshes started to fragment the earlier the higher the content of hydrophilic PEG in the mesh polymer was. Thus, the mesh with the highest PEG content (lin70) experienced first ruptures during removal from the buffer already after two weeks of incubation, while the lin90 stayed intact until week four and lin130 even until week eight. Additional differences were recognized concerning the appearance of the meshes and the handling. While the lin70 mesh was very soft and turned transparent immediately after buffer contact confirming a good wettability with water, the meshes with higher PLA content were stiffer and partly stayed white over several weeks indicating a much lesser wettability. Regarding the meshes of star-shaped PEG-PLA copolymers, similar to the linear copolymer meshes but in contrast to the films, the meshes with lower PEG content were stiffer in buffer and maintained stable and intact over a longer time period than meshes with higher PEG content. However, despite an overall higher PLA content than lin90 and lin130, the meshes exhibited no white parts in buffer but appeared completely transparent immediately after buffer contact indicating a better wettability. Furthermore, again an influence of the number of arms of the polymer and of the composition of the PLA chains with similar molecular weights could be observed. With increasing branching of the polymers, the meshes started to fragment faster. The 8arm70 mesh tore already after two weeks and the 4arm70 mesh after four weeks while the lin70rac mesh did not rupture until week six, which thereby also showed a higher stability than the lin70 polymer with PLA arms synthesized with 70:30 L-lactide:D, L-lactide. The influence of branching was observed for the polymers with elongated PLA chains as well. The 8arm140 mesh started to rupture after six weeks whereas the 4arm140 mesh remained intact until week eight. In general, longer PLA chains and a low PEG content led to meshes with longer stability probably because of a slower washout of the longer chained degradation products that stabilized the fibers and due to the higher stiffness through the high content of PLA in comparison to the soft meshes with higher PEG contents. Besides the softness, optical appearance and the start of fragmentation of the investigated meshes,

another phenomenon could be observed macroscopically. In contrast to the films, which maintained their dimension or experienced slight extension, the electrospun meshes shrank significantly upon incubation in phosphate buffer pH 7.4 at 37 °C. This effect can be explained by an occuring relaxation of the polymer chains of the fibers which underwent high alignment and orientation through the electrospinning process.[303–304]

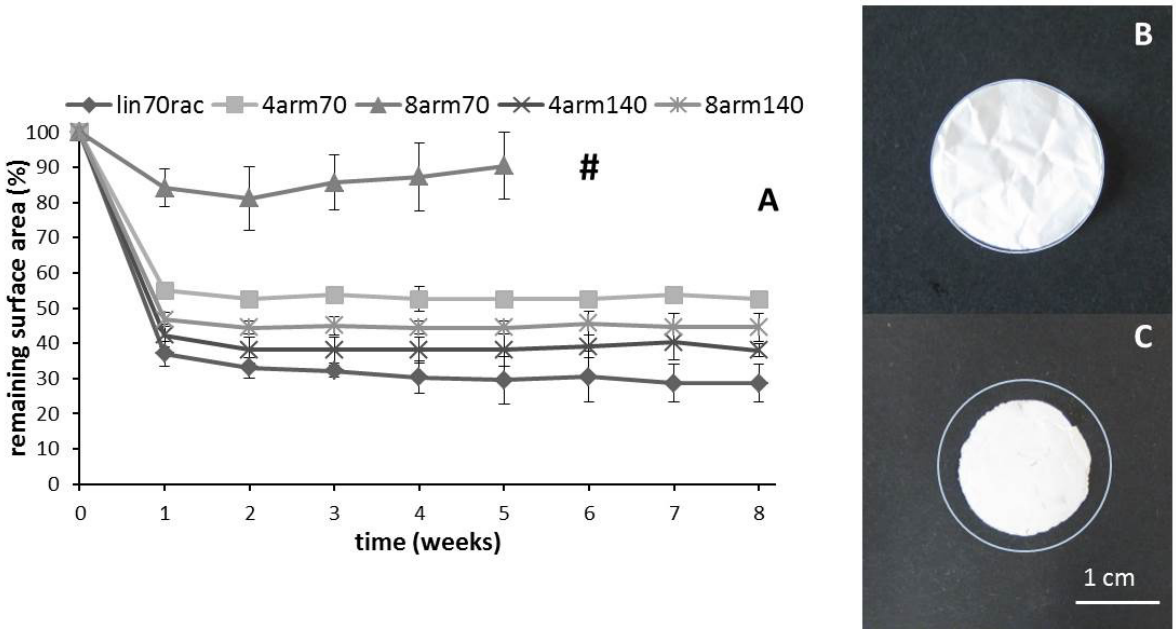

Figure 6.24 *Shrinkage of star-shaped PEG-PLA block copolymer meshes. A illustrates the remaining surface area of the meshes with proceeding incubation time. B shows an initial lin70rac mesh specimen and C the same test specimen shrunk after one week incubation.*
 # indicates fragmentation in small pieces so that an accurate measurement was not possible.
White circle indicates the original mesh dimension to visualize the dimension of shrinkage.

The meshes massively shrank immediately at the beginning of incubation in buffer at 37 °C and subsequently the remaining surface area largely plateaued until the end of the investigation indicating that the relaxation was a relatively fast process. Thereby, the extent of shrinkage depended on the polymer of which the meshes consisted as ***Figure 6.24*** illustrates for the star-shaped block copolymers. With increasing branching of the PEG core molecule less shrinkage occurred, while longer polymer chains led to a higher loss of the mesh dimension. The reason therefore probably was the higher flexibility of long and especially linear polymer chains leading to a higher alignment and orientation during the electrospinning process in comparison to the higher branched polymers, which consequently resulted in a higher shrinkage. At any rate, shrinkage is very unfavorable for an application as

barrier device since a complete coverage of the wound site may not be ensured. Hence, a way to overcome shrinkage ideally has to be found or at least a tolerable extent of shrinkage for the application has to be identified in further studies.

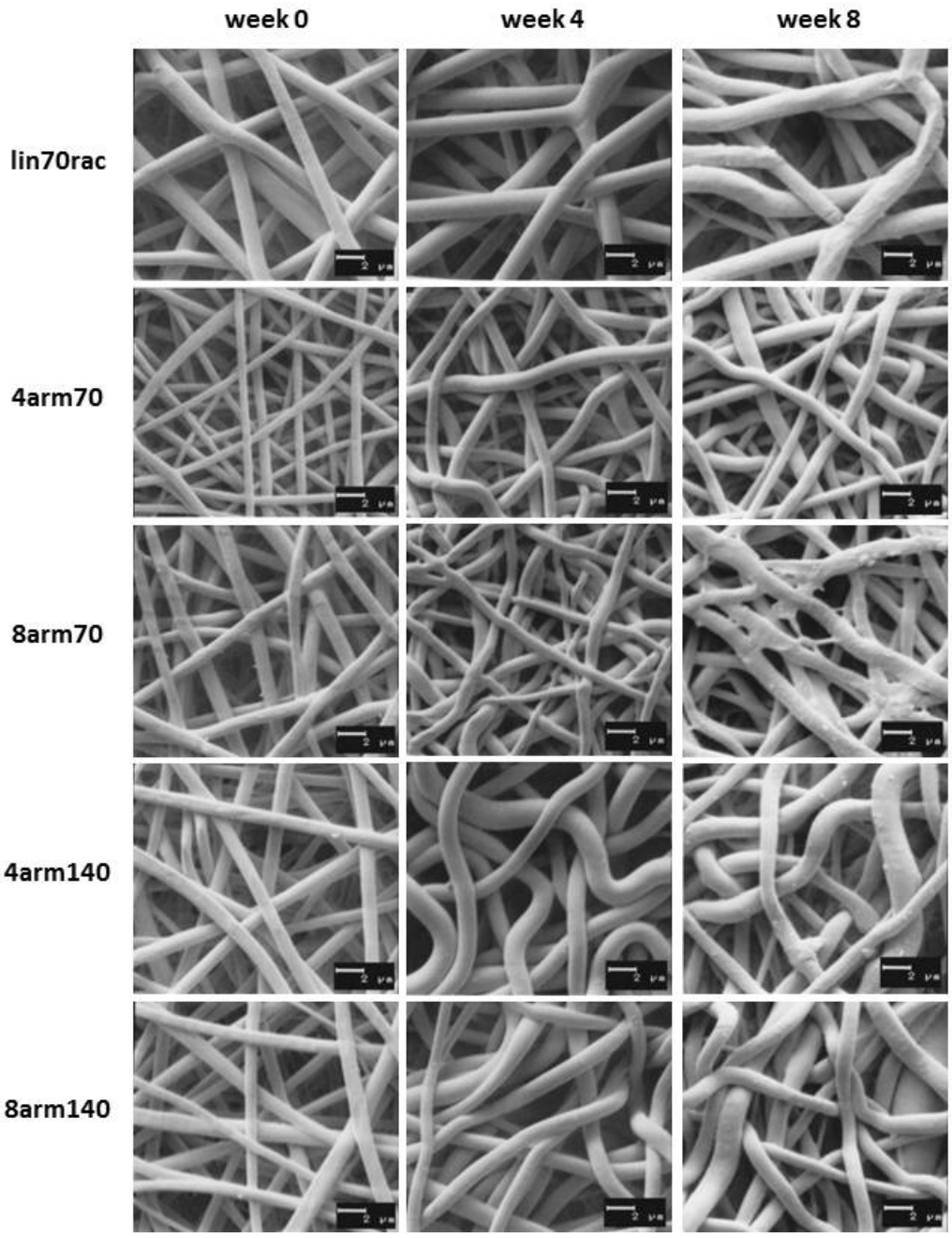

Figure 6.25 *SEM images of the initial mesh (week 0) and meshes after four weeks and eight weeks degradation made of lin70rac, 4arm70, 8arm70, 4arm140 and 8arm140. (identical magnifications)*

The observation of SEM images of the meshes revealed the morphology of the fibers during incubation in buffer. In contrast to the dry incubation at 37 °C (see 6.2), incubation in phosphate buffer pH 7.4 at 37 °C did not result in a coalescence of the fibers, but the fibers retained their shape and remained individual fibers over the whole investigated time frame (***Figure 6.25***). Only for the 8arm70 mesh a slight adherence occurred after eight weeks. Obviously incorporated water or buffer salts had a stabilizing effect on the fibers and prevented coalescence even for polymer fibers with a T_g way below the incubation temperature of 37 °C. Nevertheless, some obvious changes upon incubation in buffer were observed. The already mentioned relaxation of the fibers, which led to shrinkage of the meshes, could be recognized on the SEM images as well, since the fibers lost their stretched appearance and partly even started to curl over time. Moreover, for some polymers, e.g. for 4arm140 or 8arm140, increased fiber diameters could be observed probably due to a contraction of the fibers during shrinkage or due to swelling and also ageing phenomena such as indentations on the fibers emerged after several weeks (lin70rac). The fiber stability without coalescence may be advantageous for an application in adhesion prevention because the maintenance of the porosity of the meshes can, in contrast to solid devices, promote the supply of the wound area with nutrients which are necessary for an accurate wound healing.[10]

The swelling and degradation study of the electrospun meshes revealed a clear influence of the polymer composition and architecture on the extent of water uptake of the meshes. For non-wovens made of the linear copolymers, increasing swelling was obtained with an increasing content of hydrophilic PEG (***Figure 6.26A***). This is in good accordance with the above-described macroscopic sensation of white and transparent meshes and with the results of the contact angle measurements that showed lower water contact angles and a faster infiltration of the water droplet into the mesh with increased PEG content for dry-blotted meshes, which were incubated in buffer overnight (see 6.1.3). A dependence of the extent of swelling on the PEG content of the polymer could be observed for the meshes consisting of star-shaped PEG-PLA block copolymers as well, but also on the number of arms (***Figure 6.26B***). Thus, the meshes of polymers with elongated PLA chains and thereby less PEG

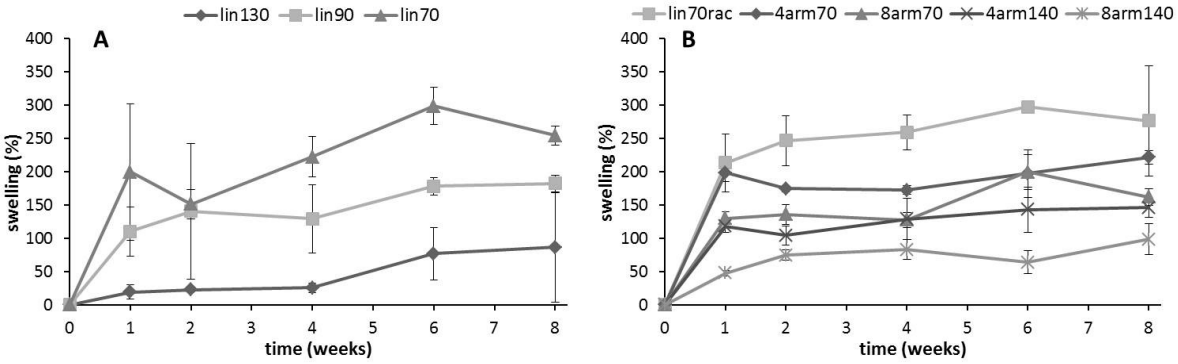

Figure 6.26 *Swelling of electrospun meshes of linear (A) and star-shaped (B) block copolymers.*

content (4arm140, 8arm140) showed less water uptake than the polymers with 12.5 % PEG (lin70rac, 4arm70, 8arm70).

Moreover, with similar PEG contents and molecular weights, the higher the branching of the polymer the less swelling was achieved for the mesh. These results are also in good accordance with the contact angle measurements since for the copolymers with 12.5 % PEG the water contact angles on dry-blotted meshes after buffer incubation decreased with an increasing number of arms and also the water droplets penetrated faster into the meshes with higher branching of the polymers, whereas the water droplets did not penetrate into the meshes of the polymers with elongated PLA chains within the investigated time (see 6.1.3). The effect that less swelling occurred with increased branching can for one thing be attributed to a worse accessibility of the star-shaped PEG cores than for a linear PEG core for water like already discussed for the films (see ***Chapter 5***). For another thing, the restricted mobility of branched polymers with more chain entanglements, while the linear polymer can diffuse freely,[264] may facilitate a PEG orientation towards the water phase within the fibers of the linear polymer and affect the overall swelling as well.

The GPC analysis of the degrading linear polymer meshes showed a massive loss of molecular weight to around 50 % of the initial molar mass for all investigated triblock copolymers (***Figure 6.27A***). The obtained curves for the lin130 and the lin90 were in accordance with the swelling study and the macroscopic findings as the lin90 with the higher PEG content and water uptake displayed an initially relatively higher molecular weight loss

leading to a faster fragmentation. The triblock with the highest PEG content (lin70) and swelling values did not result in the highest molecular weight loss like expected but the curve proceeded in the range of the lin130 mesh. However, the relatively high remaining molecular weight that was determined can be explained by an enhanced washout of small breakdown products in comparison to the lin90 and the lin130 as a distinctly higher mass loss occurred for the lin70 mesh than for the meshes made of the other triblock copolymers (***Figure 6.27B***). Due to a preferential ester cleavage of the esters between the PLA blocks and the PEG block and relatively shorter PLA chain lengths of the lin70 in contrast to the lin90 and the lin130, the degradation products were already in the first few weeks small enough to be washed out of the meshes and were not gathered by GPC analysis anymore, while the degradation products of lin130 and lin90 largely were still entrapped within the meshes due to higher molecular weights and consequently determined via GPC measurements.

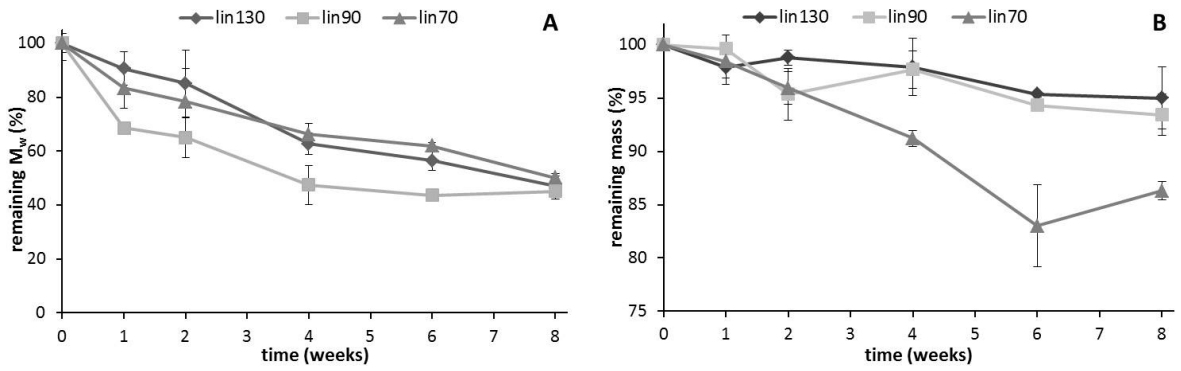

Figure 6.27 *Molecular weight loss (A) and mass loss (B) of linear triblock copolymer meshes.*

Regarding the star-shaped PEG-PLA block copolymers, a massive loss of molecular weight was determined as well (***Figure 6.28***). Thereby, different than expected, because the results seemed at first view contradictory to the swelling trend and the order of fragmentation of the meshes, for the branched copolymers with the highest molecular weights the highest molecular weight loss was detected. Moreover, for the copolymers with similar molecular weights less molecular weight loss was detected with an increasing branching of the polymer despite a faster fragmentation of the meshes. However, similar to the linear copolymer meshes, by regarding the mass loss of the meshes, these findings can be attributed to

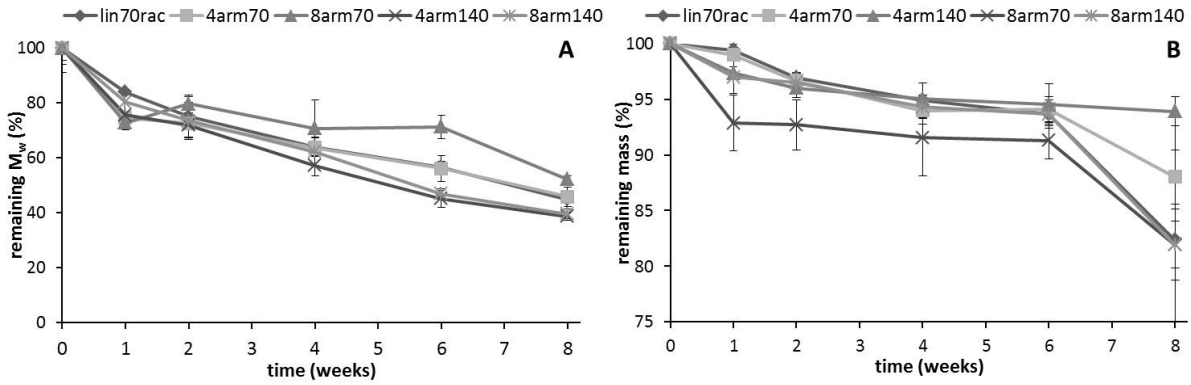

Figure 6.28 *Molecular weight loss (A) and mass loss (B) of star-shaped block copolymer meshes.*

varying washout effects. The highest mass loss occurred for the 8arm70 mesh due to the shortest PLA chains which could earlier be washed out than the degradation products of 4arm70 and lin70rac meshes and were not gathered by the later GPC analysis. The minor washout of the longer cleaved PLA blocks of the 4arm140 mesh may have led to a stabilization of the fibers and consequently to a longer matrix integrity. ^{1}H-NMR analysis of the remaining mesh fragments after eight weeks incubation generally revealed an increased PEG content within the meshes in comparison to the initial polymer. Thereby, with increasing branching of the polymers the increase of PEG content was relatively higher, indicating both a washout of mainly small PLA oligomers and an improved anchorage of PEG within the mesh by the usage of the different star-shaped PEGs.

Analogous to the films, DSC measurements of the meshes showed a slight increase of T_g during the first weeks with a subsequent slight decrease but with the overall consistent trend of lowered glass transition temperatures with increased PEG content (***Figure 6.29***). However, in contrast to the films, which partly showed crystallization phenomena, all investigated meshes were totally amorphous over the investigated time and only exhibited a detectable T_g. Thereby, T_g of the meshes was consistently higher than T_g of the corresponding films. Like already mentioned (see 6.2), the initial higher T_g of the meshes can be explained by the higher orientation and dense packing of the polymer chains caused by the electrospinning process. Obviously this orientation persisted over the degradation time in the polymer meshes.

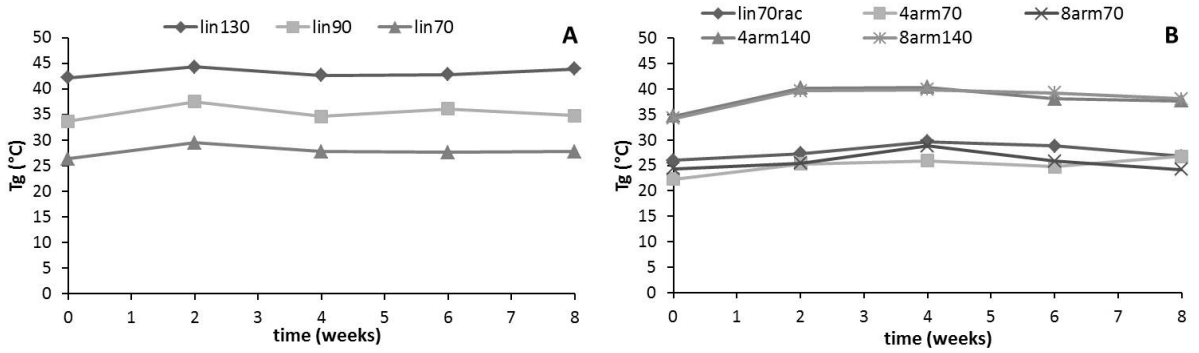

Figure 6.29 *T_g of linear (A) and branched (B) PEG-PLA block copolymer meshes over degradation at pH 7.4.*

In comparison to the massive films prepared of the same polymers and in comparable thickness, the electrospun meshes generally started to fragment earlier (exceptions: 4arm140, 8arm140) and in softer pieces. The swelling results of the electrospun meshes exhibited the same trends as the swelling study of the solvent cast films. However, with water uptakes up to nearly 300 % (lin70rac), the absolute values of the meshes were generally massively higher than those of the films and differences between the various polymers could be observed more marked (***Figure 6.30A***). The overall higher swelling of the meshes can obviously be explained by their high porousness in contrast to the massive films and the associated higher specific surface facilitating the infiltration of the buffer. As a consequence of the higher specific surface and the water infiltration, the polymers within the meshes were better accessible for hydrolytic ester cleavage than the polymers within the massive films leading to a higher mass loss and together with the overall lower polymer

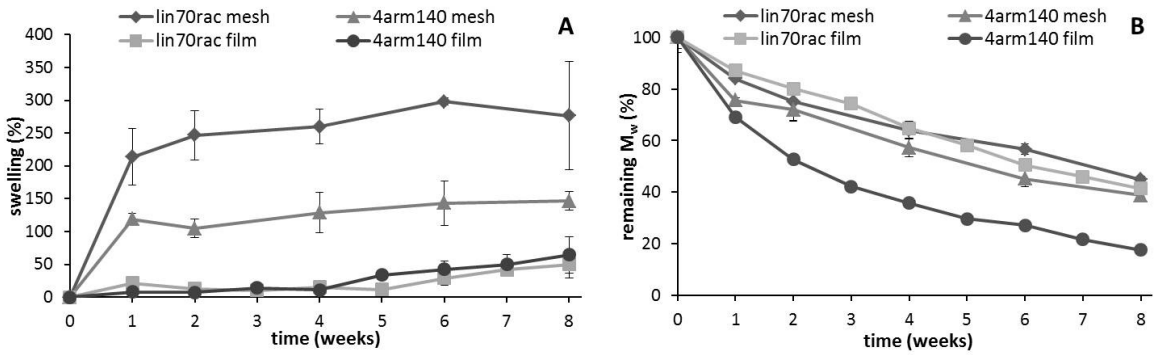

Figure 6.30 *Swelling (A) and molecular weight loss (B) of solution electrospun meshes in comparison to solvent cast films of selected polymer.*

content also leading to a faster fragmentation of the meshes in comparison to the films. However, despite a higher swelling, a higher specific surface and a higher mass loss in the first weeks, the expected faster molecular weight loss for the meshes could not be observed. The molecular weight loss of the meshes was either congruent or slower than the loss of the films (***Figure 6.30B***). This can probably be attributed both to a faster washout of the breakdown products of the meshes due to a higher porosity than the films that consequently were not gathered by GPC analysis of the residues and to an autocatalytic effect of the remaining acidic oligomers that influenced the degradation of the massive films[305] but did not affect the degradation of the meshes due to a shorter diffusion path for the degradation products out of the fibers and the whole meshes, respectively.[279]

6.4 Cell culture tests

Cell viability and cell adhesion tests of L929 mouse fibroblasts on both films and meshes of PLGA, PLA and lin70rac in comparison to a flat PS surface were performed to evaluate the anti-adhesive potential of films and meshes of the commercial PLA and especially the synthesized PEG-PLA lin70rac in relation to polymer surfaces which are known as good substrates for cell adhesion and proliferation. Thereby, an influence of the used polymer as well as of the surface morphology on cell attachment and morphology could be observed. ***Figure 6.31*** shows microscopic images of the cells 24 h after seeding onto polymer films and PS, giving a first impression of cellular behavior on the different polymer surfaces. While on the cast PLGA films similar to the PS reference a lot of cells were visible and the cells also spreaded nicely, a distinctly lower amount of cells could be observed on PLA as well as on PEG-PLA films. Moreover, cells on PLA and lin70rac films were spherical, on lin70rac even partially appeared as clusters, indicating poor cell adhesion on these surfaces so that the cells can easily be shook off. Instrument-based, analogous images of the investigated electrospun polymer meshes were not possible due to the intransparency of the investigated polymer meshes.

A live/dead staining of the seeded cells after one, three and seven days after cell seeding illustrates the viability of the cells on the different surfaces. The mainly visible green

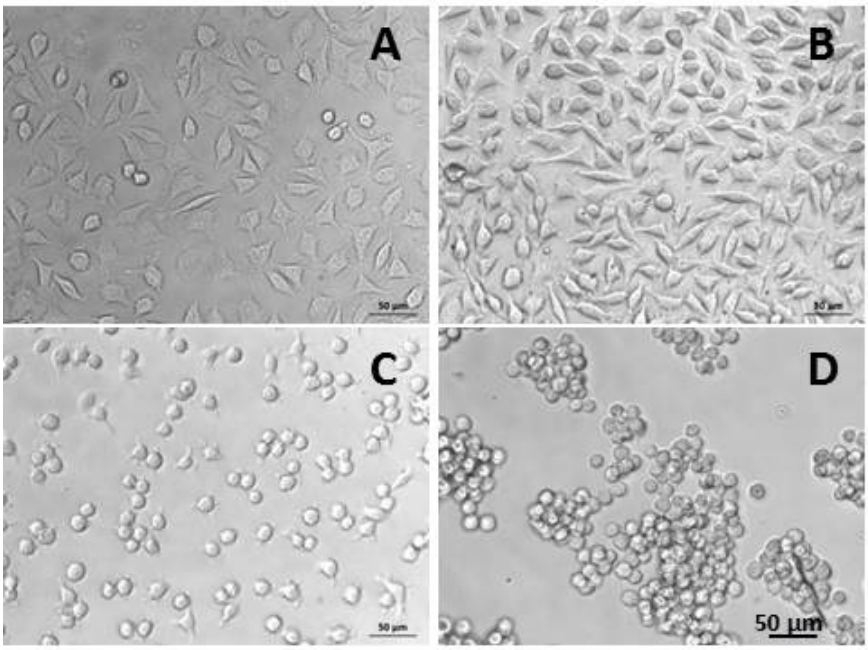

Figure 6.31 *Microscopic images of L929 cells on the PS reference (A) and on polymer films of PLGA (B), PLA (C) and lin70rac (D) 24 h after cell seeding (identical magnifications).*

fluorescence of living cells and the almost complete absence of red fluorescing dead cells confirmed the good biocompatibility of the investigated materials (***Figure 6.32***, ***Figure 6.33***). For polymer films, similar to the simple light microscopic images, distinctly denser cell colonization was observed for the PS reference and for the cast PLGA films as for the PLA films and the PEG-PLA films (***Figure 6.32***). With proceeding incubation time a good cell proliferation was visible on PS and the PLGA films with a very dense population after seven days. In contrast, less cells were observable on the PLA films and even less on the lin70rac films, confirming the anti-adhesive properties of the commercially available PLA film in contrast to cast PLGA films and furthermore illustrating the enhanced properties of a PEG-PLA film compared to the PLA film. The difference in cell attachment between the polymer films can be ascribed to their different chemical composition. PLGA in comparison to pure PLA possesses less hydrophobic methyl side groups, which generally leads to an enhanced hydrophilicity of PLGA compared to PLA. This compositional difference is in favor of better cell attachment.[306–307] On the other hand, the presence of sufficient PEG on a material's surface reduces protein adsorption, which is necessary for cell attachment.[190] Consequently, fewer cells attached and proliferated on the PEG-PLA film than on the PLA film.

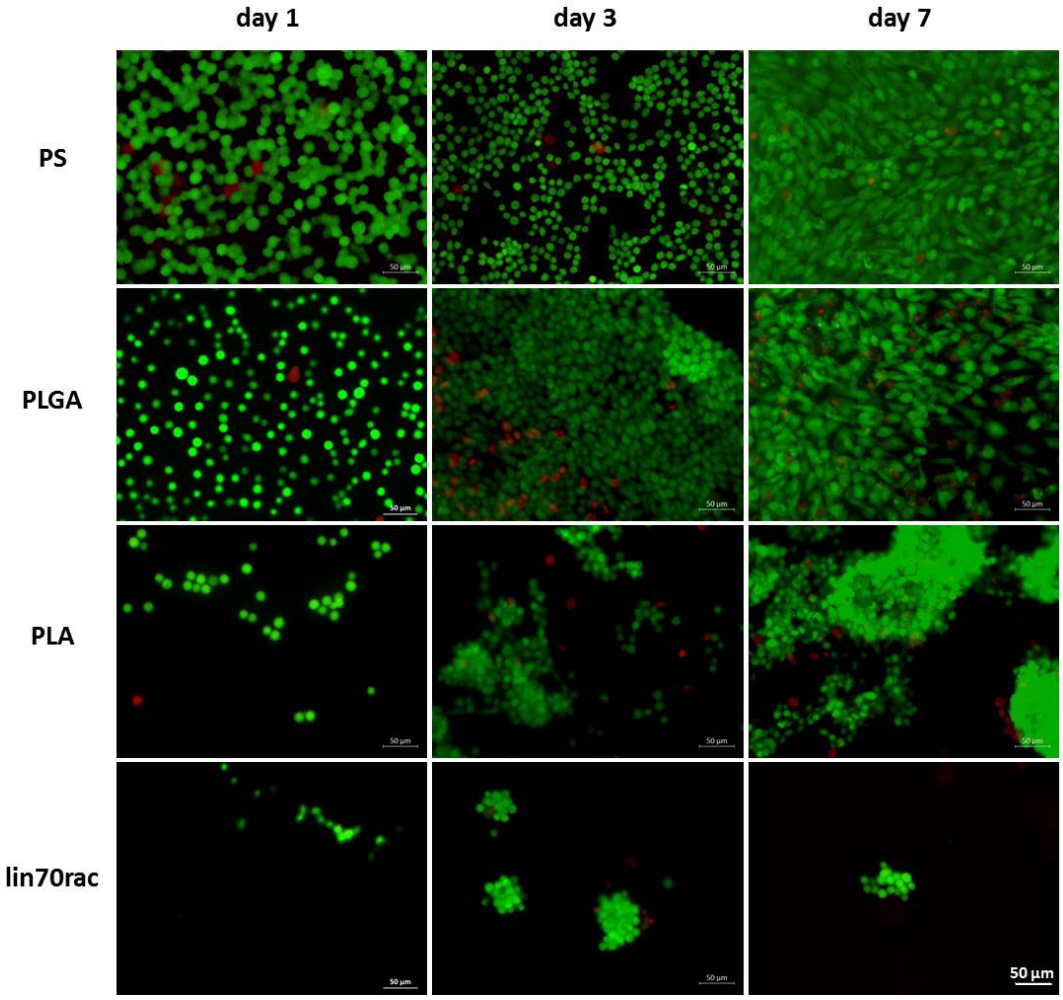

Figure 6.32 *Fluorescence images of L929 cells on polymer films and PS after live/dead staining on days 1, 3 and 7 after cell seeding (identical magnifications). Green fluorescence indicates living cells, red fluorescence dead cells.*

Regarding live/dead staining of electrospun meshes (***Figure 6.33***), analogous to the films almost solely green fluorescing living cells were visible. Similar to the PLGA films, PLGA meshes constituted good substrates for cell proliferation since a dense population was recognizable. In contrast to the corresponding polymer films, PLA meshes appeared similarly densely populated than PLGA meshes indicating a better cell adhesion on PLA fibers than on smooth PLA films. This finding can be attributed to the rough fiber morphology in contrast to the smooth film surface, since other researchers found that the surface morphology and porosity of a PLA substrate can highly influence cell attachment, cell morphology and cell proliferation.[308–310] On the more hydrophilic lin70rac meshes rarely any cells were visible after seven days illustrating again good anti-adhesive properties of PEG-PLA devices.

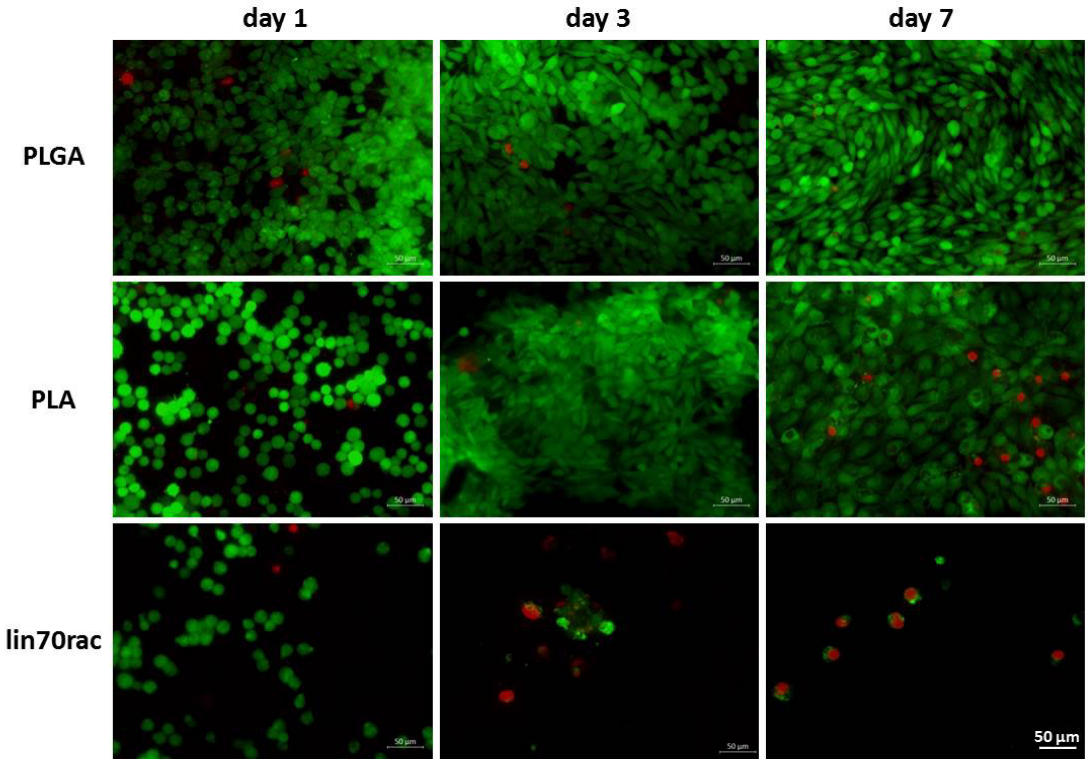

Figure 6.33 *Fluorescence images of L929 cells on polymer meshes after live/dead staining on days 1, 3 and 7 after cell seeding (identical magnifications)*

The WST-1 assay and the cell adhesion test (***Figure 6.34***) displayed similar trends as the microscopic images. For both films and meshes, L929 cells clearly adhered in higher numbers and consequently showed higher cell viability on PLGA devices than on PLA devices and especially on lin70rac devices on days one and three after cell seeding. After seven days, less cells were counted on most of the investigated devices and trends changed, probably because the cell layers were partly washed off the surfaces. This limits the value of long term

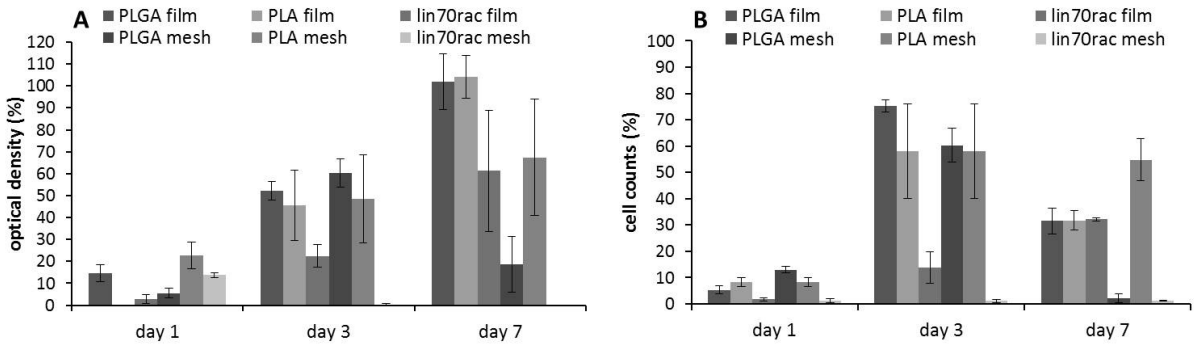

Figure 6.34 *Results of WST-1 assay (A) and cell counting (B) of films and electrospun meshes of PLGA, PLA as well as lin70rac in relation to the PS reference.*

biocompatibility testing on the anti-adhesive materials. As a result, the conducted cell culture tests confirmed the anti-adhesive potential of the marketed PLA films and revealed moreover that the properties could be further enhanced by using PEG-PLA copolymers both for the fabrication of solid films and electrospun meshes.

6.5 Drug release study via Agar diffusion test

Since via HPLC a release of only small amounts of triclosan from drug loaded films into the release medium was detected over many weeks due to an adherence of the drug to the polymers (see ***Chapter 5***), no *in vitro* release study was conducted for the electrospun meshes with an even larger surface area. Instead, a long-term agar diffusion test in comparison to drug loaded cast films was performed to gain immediate information about the antibacterial performance of the mesh based devices. A direct drug loading of electrospun meshes with triclosan by adding the drug to the electrospinning solution was not immediately successful, since the usually applied polymer concentrations for electrospinning did not lead to adequate fibers for PEG-PLA copolymers as ***Figure 6.35*** illustrates on the example of lin70rac. While electrospinning with a pure 28 % solution of lin70rac in acetone/DMSO usually leads to uniform fibers without coalescence, a 28 % solution of lin70rac with 0.26 % added triclosan led to irregular fused fibers. This morphology appeared probably due to a change of the charge conditions of the electrospinning solution which influenced the jet formation and fiber deposition.

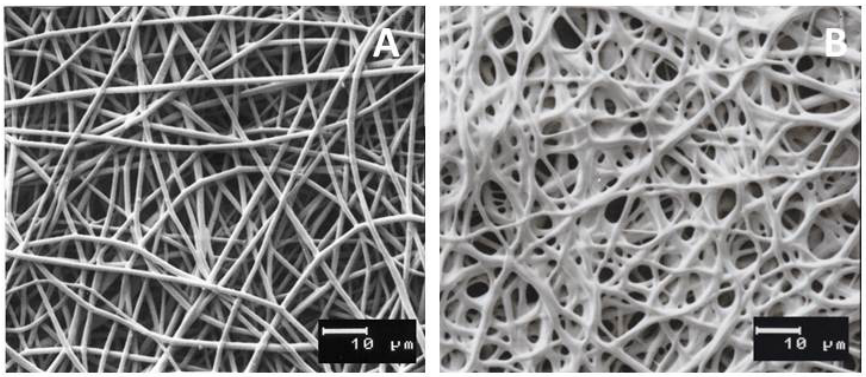

Figure 6.35 *SEM image of 28 % lin70rac mesh electrospun without (A) and with (B) triclosan in the electrospinning solution.*

By increasing the PEG-PLA polymer concentration of the triclosan containing electrospinning solution, uniform fibers without fusion were successfully obtained, which were then used for the following experiment (***Figure 6.36***). The electrospinning solution of PLA was less influenced by triclosan as additive since for the fabrication of triclosan loaded PLA meshes the usually used concentration of 4 % already led to uniform fibers without bonding points. The obtained fibers of the triclosan loaded meshes all had comparable fiber diameters of around 1.3 µm so that occurring differences during the agar diffusion test can be mainly attributed to differences in the chemical composition of the polymers rather than to the fiber morphology and the resulting surface area.

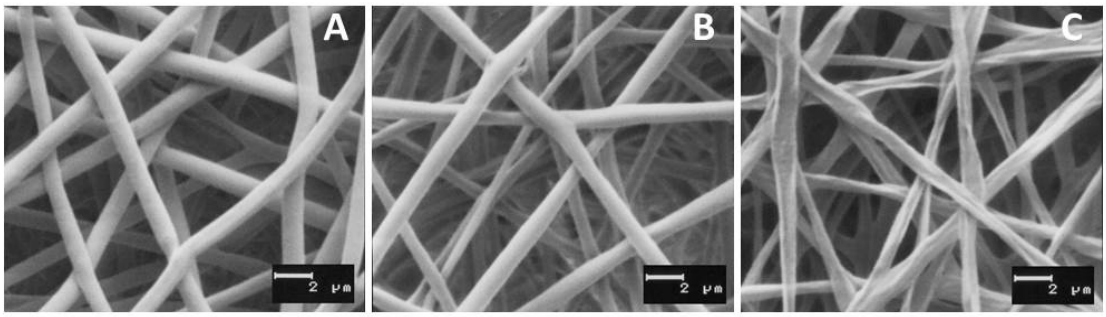

Figure 6.36 *SEM images of triclosan loaded electrospun meshes after electrospinning solutions with triclosan and 32 % lin70rac (A), 28 % 4arm140 (B) or 4 % PLA (C).*

Apart from the meshes loaded directly during the electrospinning process with triclosan, additional drug loaded meshes were fabricated by impregnating regular drug-free meshes with an ethanolic triclosan solution. While due to the very poor solubility of PLA in ethanol a change of the PLA fibers was not to be feared, for the more hydrophilic PEG-PLA copolymers the fiber morphology after impregnation was precautionally examined via SEM. ***Figure 6.37*** illustrates that the meshes suffered only slightly under the ethanolic treatment. Negligible shrinkage of the meshes occurred and the fibers appeared slightly denser than untreated, but the fibers were still uniform without fusion so that they could be used for the agar diffusion test.

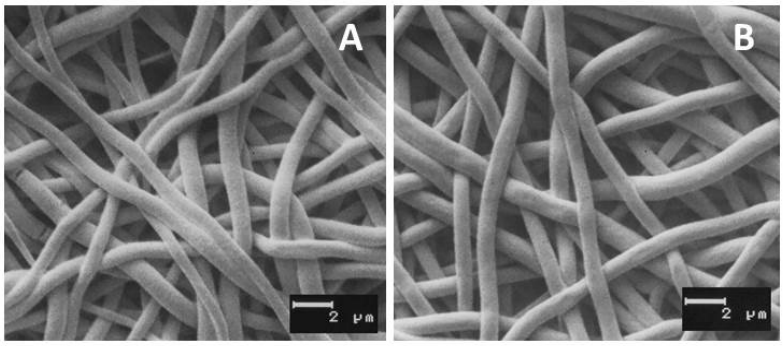

Figure 6.37 *SEM images of lin70rac mesh (A) and 4arm140 mesh (B) after ethanolic impregnation.*

Figure 6.38 shows photographic images of inoculated agar plates with the obtained inhibition zones from drug loaded meshes and films after 24 hours, where some of the trends (***Figure 6.39***) that were manifested over time were already visible. The antibacterial efficacy against Staph. aureus both depended on the chemical constitution of the polymer and on the fabrication of the drug loaded sample. The results of triclosan loaded films confirmed the *in vitro* release results determined via HPLC which revealed a faster drug release with increasing PEG content (see ***Chapter 5***). The agar diffusion test showed that with increasing PEG content of the films also a higher inhibition and a longer maintenance of the efficacy

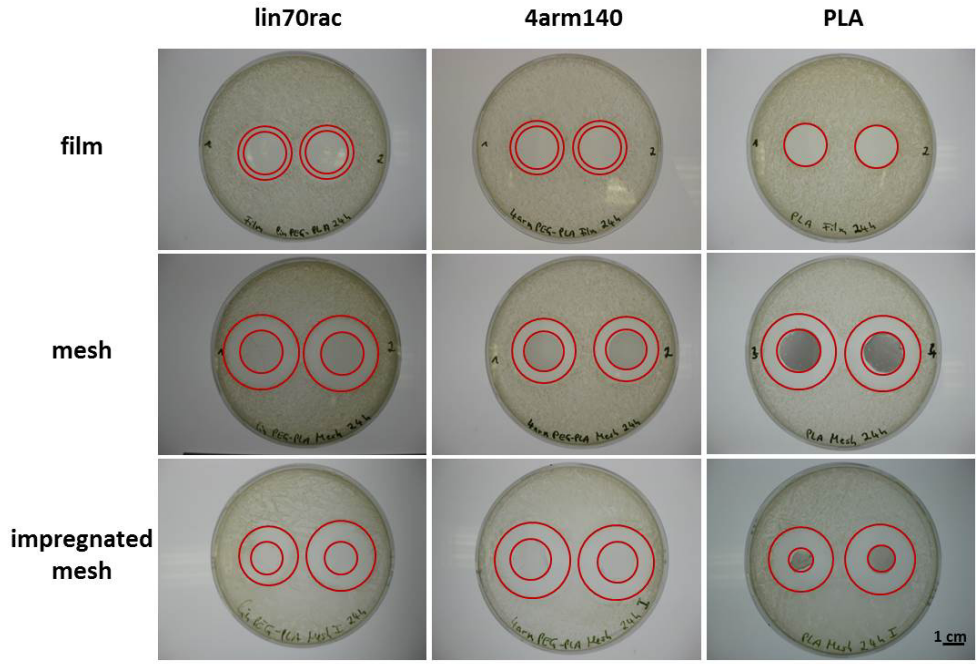

Figure 6.38 *Inhibition zones of triclosan loaded films and meshes after 24 h incubation.*

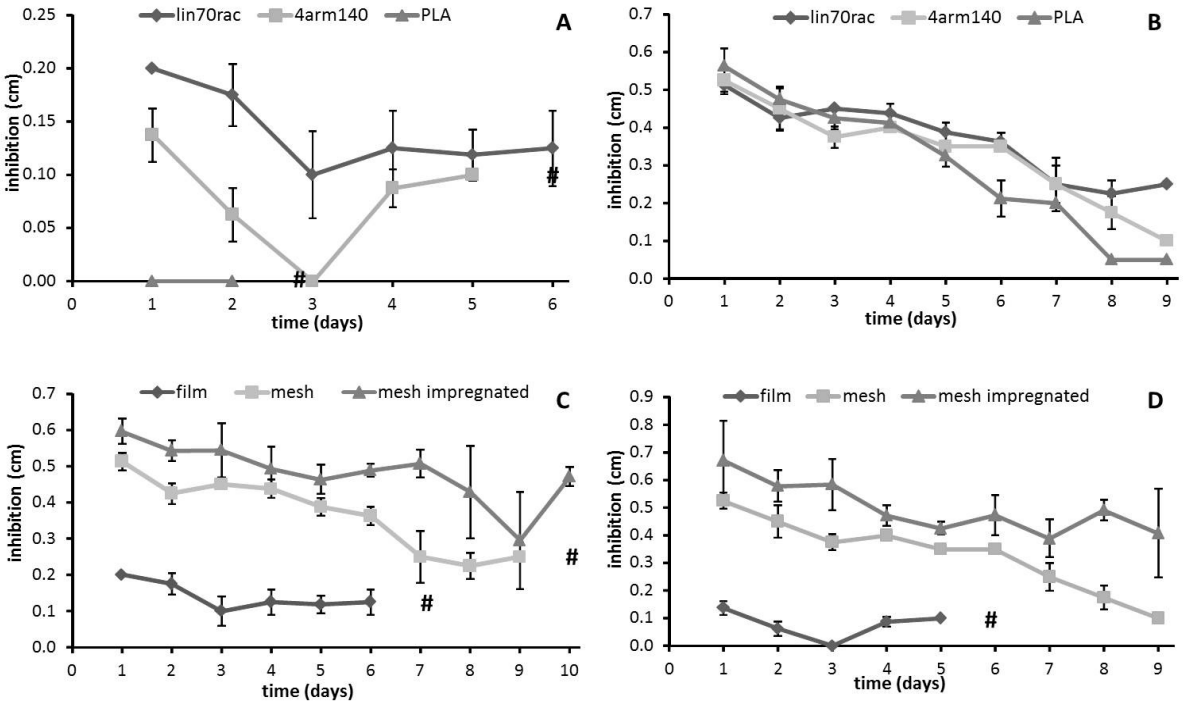

Figure 6.39 *Bacterial inhibition by triclosan loaded polymer films and electrospun meshes. The results of films (A) and meshes (B) of the different polymers both drug loaded during the manufacturing process as well as the comparison of loaded film, loaded mesh and impregnation loaded mesh of lin70rac (C) and 4arm140 (D) are shown. Each of the investigated devices contained around 25 µg triclosan per sample disk.*
 # indicates that no further inhibition was achieved.

occurred (***Figure 6.39A***). For the PLA film no bacterial inhibition was observed and for the lin70rac film a higher and with an efficacy over six days also a longer inhibition than for the 4arm140 film was determined. An influence of PEG content was also visible in the results of the electrospun meshes (***Figure 6.39B***). While during the first days of the test only slight differences between the polymers were measured, after five days the same trend as for the films became visible with higher bacterial inhibition with increasing PEG content until no more inhibition was detectable. This effect can be attributed to the hydrophilicity of PEG, which promoted water uptake and consequently facilitated drug diffusion out of the matrix. Comparing the manufacturing processes, drug loaded film and mesh as well as drug impregnated mesh of the same polymer, for all investigated polymers similar trends were observed like illustrated in ***Figure 6.39C, D*** for lin70rac and 4arm140. For the drug loaded electrospun meshes a higher inhibition as well as a longer efficacy against Staph. aureus was obtained than for the drug loaded films. Furthermore, the drug impregnated meshes resulted in distinctly larger inhibition zones than the meshes which were drug loaded during

the electrospinning process with at least the same duration of the antibacterial efficacy. The relatively poor efficacy of the films can be explained by the smaller specific surface and longer diffusion path combined with an occurring lower water uptake and higher polymer density in comparison to the meshes, which generally makes the release of the drug more difficult. The further enhanced efficacy of drug loaded meshes by impregnating drug-free meshes with an ethanolic triclosan solution can be attributed to a location of the drug mainly on the fiber surface in contrast to the electrospinning-loaded meshes where the drug should be distributed quite homogenously within the fiber. After seven to eight days, transferring the PEG-PLA meshes to fresh agar plates became more and more demanding since the meshes started to tear while removing them. Hence, the surrounding conditions also highly influenced the mechanical properties of the meshes since degradation studies in phosphate buffer pH 7.4 initially suggested longer stabilities.

6.6 Summary and conclusions

The synthesized different PEG-PLA copolymers and the also investigated commercial PLA could successfully be processed to uniform fiber meshes without fusion points by a solution electrospinning process. Apart from processing parameters like flow rate and high voltage, the choice of a suitable solvent as well as an adequate viscosity of the spinning solution were crucial in order to achieve fibers without incorporated beads or pores. With a sufficient PEG content the meshes showed high strains and elongations at break indicating a high flexibility, which is desirable for an appropriate performance within the patient's body. Different tensile properties of every electrospun mesh by testing in opposite cutting directions were revealed, which can be explained by the chosen motion of the rotating and reciprocating collector drum. These observed differences were nevertheless only minor, so that during application the implantation direction may not affect the performance of the whole mesh.

During degradation in phosphate buffer pH 7.4, elongation to puncture and after an initial increase the load to puncture also decreased but the mechanical properties were generally more stable over time than the mechanical properties of the solid films. However, the forces the 20 µm thick meshes withstood until they ruptured or until a surgical suture was pulled out of the suture hole were relatively low so that an application as individual monolayer

remains quite questionable. A suture pullout test with 40 µm thick electrospun meshes resulted in similar values as for the stable applicable solid films indicating that appropriate properties can be achieved with increased mesh thickness.

Initially, a massively higher surface hydrophobicity was determined for the electrospun meshes than for the solid film. This effect can be attributed to the higher surface roughness and was negated with time since with sufficient PEG content already after two minutes water started to infiltrate into the mesh. Due to the porosity of the meshes and the higher specific surface the swelling of the meshes was many times higher than the water uptake of the solid films and consequently the fragmentation of most meshes started earlier than film fragmentation of the same polymer as well. However, for some polymers still appropriate *in vitro* degradation times were found for 20 µm thick meshes and can probably further be adapted by using meshes with a higher thickness, which are anyway required for enhanced mechanical properties like already mentioned.

The occurring mesh shrinkage during buffer incubation at 37 °C of as-spun meshes may negatively affect the required coverage of the entire wound area so that either a modification of the electrospinning process to prevent mesh shrinkage or an appropriate preshrinking process has to be established, like since long been practiced in textile industry,[311] to ensure constant mesh dimensions during an application as monolayer. SEM observations of incubated meshes in dry and wet state in conjunction with the degradation study and mechanical tests made obvious that the meshes need to be stored dry and cool to not only preserve the meshes from degradation but also from fiber coalescence and to keep the matrix integrity.

The performed cell adhesion and viability tests confirmed the non-toxicity and the anti-adhesive potential of the clinically used PLA films and even more the enhanced properties of devices made of PEG-PLA copolymers. On both lin70rac films and meshes very few cells attached.

A long-term agar diffusion test revealed a longer inhibition of Staph. aureus growth on agar plates and also a higher efficacy of triclosan loaded meshes than of triclosan loaded films due to a higher specific surface and a shorter diffusion path for the drug out of the matrix. Meshes which were drug loaded by impregnating drug-free meshes with an ethanolic triclosan solution thereby showed an even enhanced efficacy in comparison to meshes which were drug-loaded directly during the electrospinning process. With the achieved antibacterial efficacy of more than one week especially the triclosan-loaded meshes appear a promising component for a drug eluting device in combination for example with a water soluble drug-loaded PEG coating like described in ***Chapter 5*** and a mechanically stabilizing film to obtain a device with a burst release for initial antibacterial efficacy and subsequent sustained release to fight persistent bacteria, which is generally recommended for local antibiotic delivery.[312] During the agar diffusion test the investigated meshes started to fragment substantially earlier than during the degradation studies in buffer indicating that the surrounding conditions (enzymes or agar components) highly influence the device performance. This makes obvious that a future *in vivo* animal study is inevitable for a conclusive evaluation of the properties of the investigated devices and their efficacy since additional factors like body motion and enzymes stress the membranes which cannot be simulated all-embracing in an *in vitro* model.

Chapter 7
Electrospun meshes as cohesion promoter for bilateral PLA/alginate membranes

In this chapter, the results of the investigations concerning the processability, cohesion and bioadhesion of bilayered and trilayered bilateral membranes with one smooth PLA side and one mucoadhesive alginate side are summarized and discussed. The bilayers simply consisted of an alginate film and a PLA film, whereas the trilayers additionally contained an electrospun mesh as intermediate cohesion promoting layer between the chemically different alginate and PLA. The well-established PLA film for adhesion prevention is supposed to keep the affected tissues glidingly separated, while the bioadhesive alginate side may prolong the residence time of the barrier at least long enough to keep the barrier in place during the time of fixation by sutures or staples to facilitate the surgical application or ideally long enough to cover the injured site for the entire duration of wound healing to get along completely without suturing since suturing additionally increases adhesion formation.[11]

Parts of this chapter are published:

M. Kessler*, E. Esser*, J. Groll, J. Tessmar

Bilateral PLA / alginate membranes for the prevention of postsurgical adhesions

Journal of Biomedical Materials Research Part B: Applied Biomaterials, accepted

*equally contributing authors

7.1 Optical evaluations

7.1.1 Contact angle measurements

To get an idea of the hydrophilicity of the polymers used for further processing to solution electrospun meshes as cohesion promoter between alginate and PLA film, contact angle measurements were conducted of solvent cast PLA and PLA-PEG-PLA films immediately after contact with a water droplet. Solvent cast films were used for this determination as contact angles of solution electrospun meshes measured immediately after water contact rather depend on the rough surface morphology than on the chemical composition of the fibers,[129,313] whereas the immediate contact angles on smooth films of different materials reflect the particular hydrophilicity as already mentioned in ***Chapter 6***. The resulting water contact angles showed only slight differences between the different polymers, but attested an increasing hydrophilicity with increasing PEG content as the contact angles decreased from about 77° to 69° from PLA to PLA-PEG-PLA with the highest PEG content though (***Figure 7.1***).

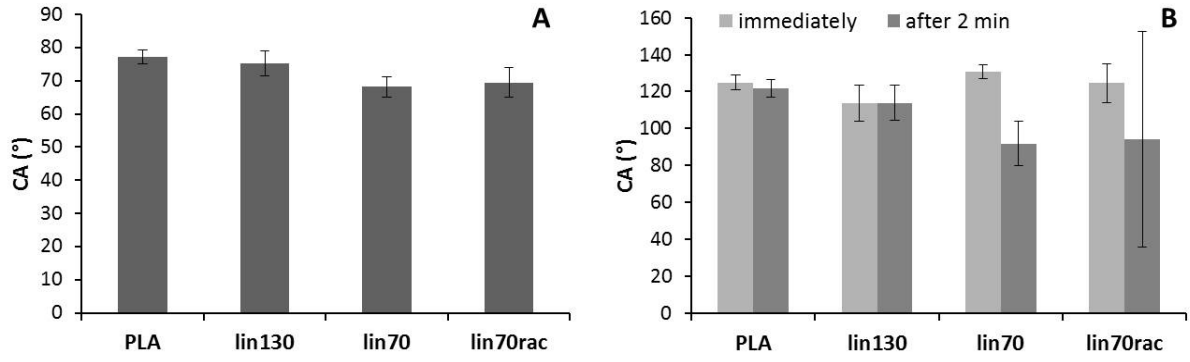

Figure 7.1 *Water contact angles of polymer films (immediately) (A) and solution electrospun meshes (B).*

In addition, contact angle measurements on solution electrospun meshes were conducted since repeatedly determined contact angles sometime after the first water contact are then mainly caused by the chemical composition of the fibers and reflect the infiltration of the droplet.[129] As a consequence, water contact angles of solution electrospun meshes were determined immediately after water contact and again two minutes after the initial water contact. The immediately determined contact angles of the meshes generally resulted in more hydrophobic values than those of the films due to the above-mentioned higher surface

roughness of the meshes. However, after two minutes the contact angles massively decreased depending on the PEG content indicating a better infiltration of the water droplet into the mesh with augmented PEG content.

7.1.2 Macroscopic and microscopic evaluations

For investigations with bilayers, the cast PLA films were unstained and consequently totally transparent and colorless, while the alginate solutions were stained with Water Blue prior to film casting on top of the PLA film to facilitate visual examinations. Directly cast onto the PLA film, the 3 % alginate solution immediately became narrower than the width of the film applicator after film casting, while the 5 % alginate solution spread much better and resulted in a bilayer with as-cast width after drying (***Figure 7.2***). While a dried alginate monolayer cast from a 3 % solution with a similar gap clearance is naturally thinner than a monolayer prepared of a 5 % alginate solution, the contraction of the 3 % solution on the PLA film led to similar final thicknesses (~45 µm) for both dry PLA/alginate bilayers so that occurring differences in the results between them in the following experiments were caused only by the manufacturing process and not by thickness effects.

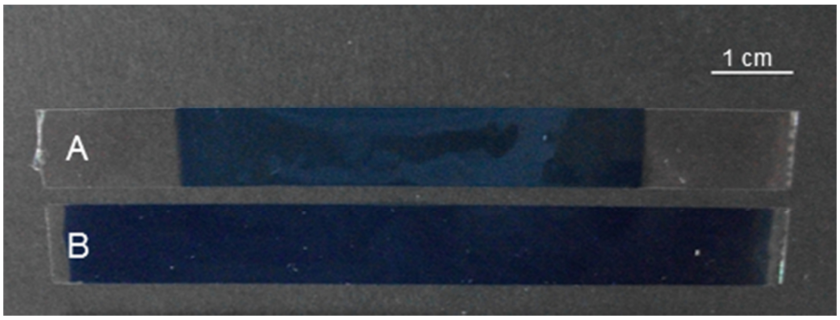

Figure 7.2 *Photographic image of bilayers prepared with a 3 % (A) or 5 % (B) alginate solution cast on top of a PLA film.*

By solution electrospinning onto the PLA film, uniform fibers were successfully generated for all investigated polymers as SEM images confirmed (***Figure 7.3***). Thereby, the resulting fibers on the film had slightly smaller diameters than electrospun fibers that were produced under analogous conditions with similar polymer solutions but electrospun directly onto the rotating collector drum without film (see ***Chapter 6***), but displayed the same shape. Ribbon-like fibers were formed by PLA while cylindrical shaped fibers were obtained for all PLA-PEG-

PLA copolymers having all similar diameters (***Table 7.1***) so that it can be assumed that the results of further investigations depended only on the chemical composition of the fibers rather than on structural effects.

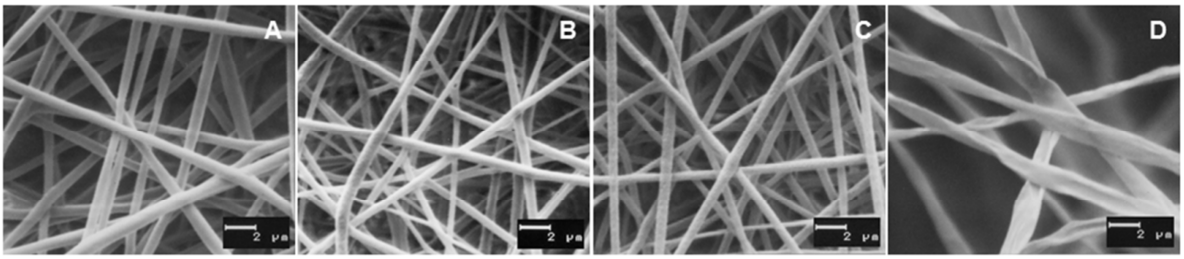

Figure 7.3 *SEM images of lin70rac (A), lin70 (B), lin130 (C) and PLA (D) fibers fabricated by solution electrospinning onto a PLA film.*

Table 7.1 *Fiber diameters of meshes directly electrospun onto a PLA film.*

	fiber diameter (µm)	
mesh polymer	**mean**	**standard deviation**
(A) lin70rac	0.904	0.109
(B) lin70	0.892	0.140
(C) lin130	0.913	0.086
(D) PLA	1.350	0.206

To visualize differences in the infiltration behavior of the alginate solution into the various electrospun meshes, like for the bilayer preparation, the alginate solution was stained with Water Blue before casting for the trilayer preparation as well. Photographic images of the dry trilayers from the upper side (alginate on top) and from the bottom (PLA film on top) show the extent and uniformity of the infiltration of the stained alginate solution into the mesh (***Figure 7.4***). The mesh on top of the transparent PLA film originally had a whitish appearance. After casting the alginate on top of the meshes, various steps of increasing translucency of the mesh occurred, depending on the actual chemical composition of the fibers. In good accordance with the contact angle measurements, with increasing PEG content of the mesh polymer, the infiltration obviously was facilitated due to an elevated hydrophilicity and a consequently better assimilation to the aqueous solution of the alginate. After alginate casting, the pure PLA fibers kept their whitish appearance and remained

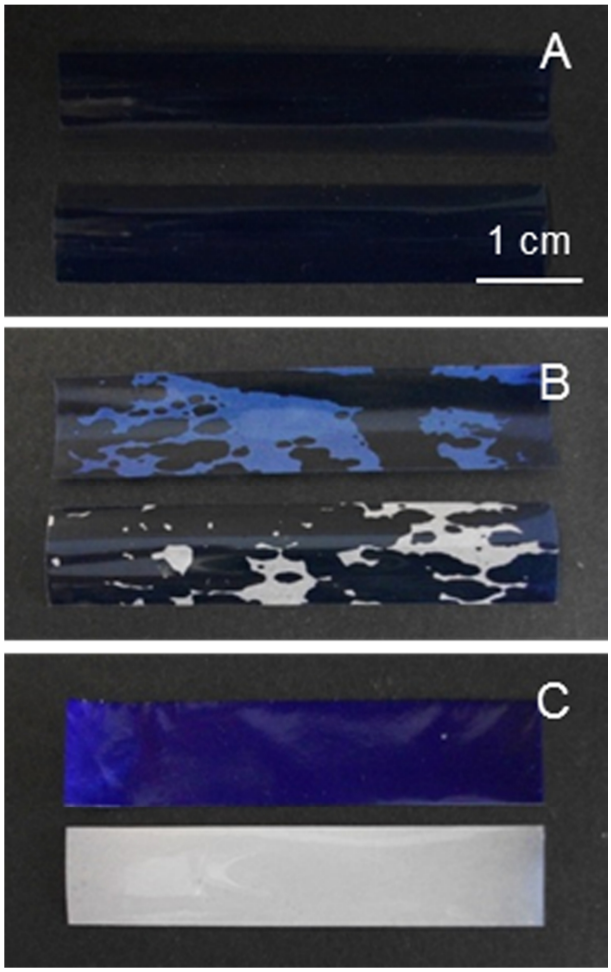

Figure 7.4 *Photographic images of trilayers after alginate casting: lin70rac mesh with 5 % alginate (A), lin130 mesh with 5 % alginate (B) and PLA mesh with 3 % alginate (C) on a PLA film. The upper sample shows the membranes with the alginate side on top, the lower sample the PLA film on top.*

completely untransparent, which indicated that hardly any infiltration of the alginate solution took place. Moreover, the dried alginate layer even started to dissociate from the PLA mesh. In contrast, the fiber layer made of the copolymers with the highest investigated PEG content (lin70 and lin70rac) became completely translucent indicating a good penetration of the alginate as the change in light refraction is indicative for the wettability of the polymer mesh. The PLA meshes appeared white when light was scattered at the air/fiber interface due to the lacking alginate infiltration, while light is not refracted and reflected on the material/fiber interface for a material with a more similar refractive index as the mesh polymer[314] than air, which was the case as soon as the alginate replaced the air between the PLA-PEG-PLA fibers. For trilayers with meshes of the copolymer with intermediate PEG content (lin130), the mesh layer partly turned transparent but some white spots remained

which displays infiltration properties in between those of the pure PLA and the copolymers with the highest investigated PEG contents.

On cross-sectional stereomicroscopic images of the trilayer membranes only two tight layers were recognizable with PLA-PEG-PLA fibers, while for the trilayers with PLA mesh a clear intermediate mesh layer without blue alginate traces was observed (***Figure 7.5***). Moreover, the above-described beginning separation of the layers of the trilayer with PLA mesh can be seen as well and confirmed the results of the macroscopic evaluations.

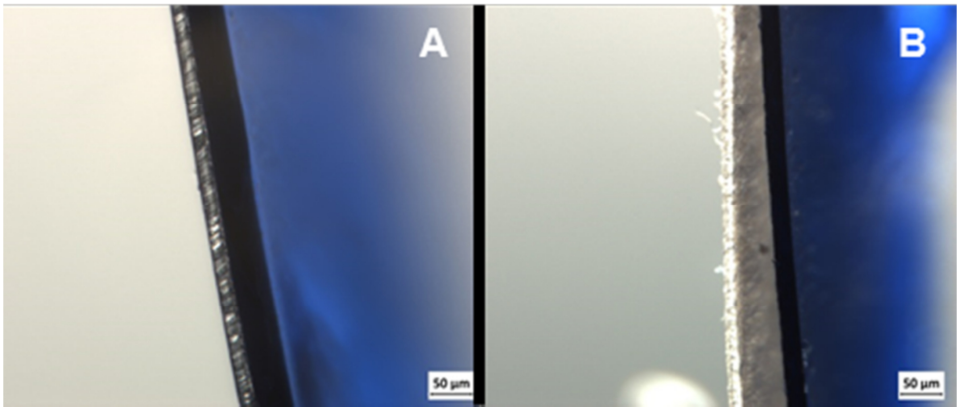

Figure 7.5 *Cross-sectional images of trilayers of a PLA film with a lin70rac mesh (A) or a PLA mesh (B) with a 5 % alginate layer on top.*

As a consequence, the use of PLA fibers on top of a PLA film as a mere surface modification of the PLA film without any chemical modification did not improve the cohesion between PLA film and alginate layer. To the contrary, since the alginate solutions did not infiltrate into the PLA mesh and the alginate layer was deposited loosely on top of the lipophilic mesh, the PLA mesh layer easily dissociated from the alginate layer due to an even worse spreading than on the smooth PLA film. For this reason, the trilayers with PLA mesh were excluded from the following mechanical and bioadhesive evaluations and only the promising membranes with PLA-PEG-PLA copolymer meshes were further investigated. Visually, hardly any difference between the membranes prepared with 3 % and with 5 % alginate solutions could be observed. Nevertheless, both types of samples were used for further investigations in the case that differences in manufacturing resulted in different mechanical or mucoadhesive properties.

7.2 Mechanical evaluations

A tensile test, a t-peel test as well as a bioadhesion test were performed on a universal testing machine with samples of the prepared PLA/alginate bilayers, the prepared trilayers with PLA-PEG-PLA meshes as intermediate layer between PLA film and alginate layer using a 3 % or 5 % alginate solution to create the alginate layer and partly also with alginate or PLA monolayers to expose relevant differences.

7.2.1 Tensile test

A standard tensile test was performed with rectangular test specimens (1 cm × 5 cm) to determine the tensile properties of the membranes and to evaluate both the enhancements of multilayers towards monolayers and potential beneficial effects of the intermediate meshes on the multilayer membrane stability. A PLA monolayer resulted in a distinctly higher maximum load than the alginate monolayers, whereby the alginate film cast from a 5 % solution withstood higher forces (4.7 N) than an alginate film cast from a 3 % solution (3.0 N) (***Figure 7.6***). This can be attributed to the higher thickness of the 5 % alginate film that occurred because of a higher solid content in dried state and because by casting on uncoated glass plates no contraction occurred in contrast to the casting of a 3 % alginate

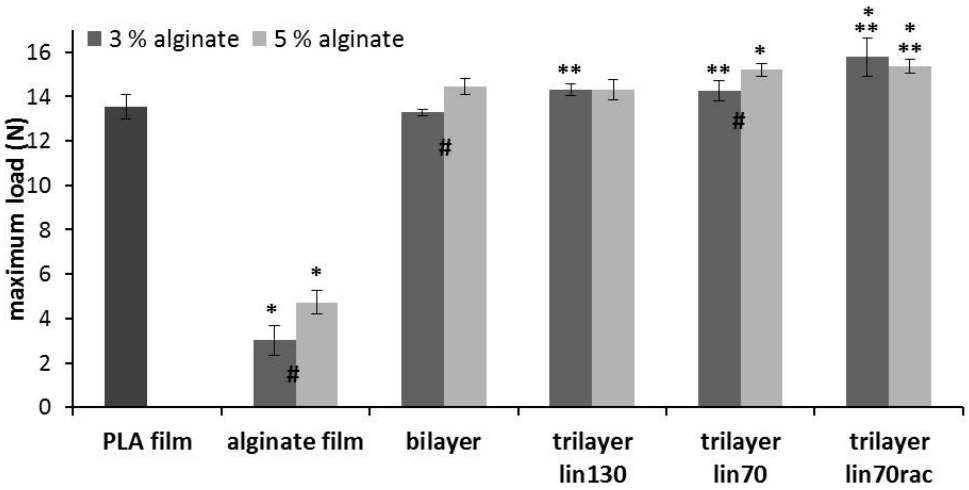

Figure 7.6 *Tensile properties of the prepared bilateral membranes as well as of PLA and alginate monolayers.*
***** *indicates a significant difference to the PLA film.*
****** *indicates a significant difference to the bilayer with similar alginate layer.*
# *indicates a significant difference between the respective coatings with 3 % or 5 % alginate solutions.*

solution onto a PLA film as already mentioned. By adding additional layers to the PLA film, the membranes naturally gained thickness and consequently maximum loads increased in comparison to a simple PLA film. Trilayers showed significant increases in maximum loads with increasing PEG content of the mesh and especially with racemic PLA chains in comparison to bilayers. The increasing tensile forces from bilayer to trilayer and with increasing PEG content and even with a change to racemic PLA parts within the mesh polymer of the trilayers may be attributed to the known phenomenon that fibers within another polymer phase stabilize the construct and consequently lead to improved mechanical properties.[315–316] This effect may be seen as a beneficial side effect to the desired application as improved mechanical properties facilitate surgical handling. In addition, these findings confirm the results of the optical evaluations which revealed a better infiltration of the alginate solutions into meshes with higher PEG contents. Since the trilayers with the highest PEG contents withstood the highest forces although pure meshes show lower maximum loads and tensile strengths with increasing PEG content due to the plasticizing effect of PEG (see ***Figure 6.14***), it can be concluded that the mesh properties itself hardly contributed to the tensile properties of the trilayers but that the meshes with the highest PEG contents were best embedded in the alginate phase because they contributed the most to the tensile properties of the membrane.

7.2.2 T-peel test

A t-peel test was performed to verify the intended cohesion promotion between the hydrophilic alginate and the lipophilic PLA through a solution electrospun polymer mesh as intermediate layer for a better fixation of the bioadhesive alginate layer on the PLA film. The test was conducted with rectangular test specimens (1 cm × 5 cm) of the trilayers with PLA-PEG-PLA meshes and compared to the performance of samples of the PLA/alginate bilayers. The resulting load – distance diagrams of the bilayers (***Figure 7.7***) revealed a load maximum at the beginning of the test, followed by a load plateau over the main distance of the measurements and a second load maximum right before the final separation of the layers indicating a very even alginate coating on top of the PLA film. Because of the peaks of the load maximums, standardly the load values of the plateau after the initial load maximum peak are averaged for peel strength calculations.[248]

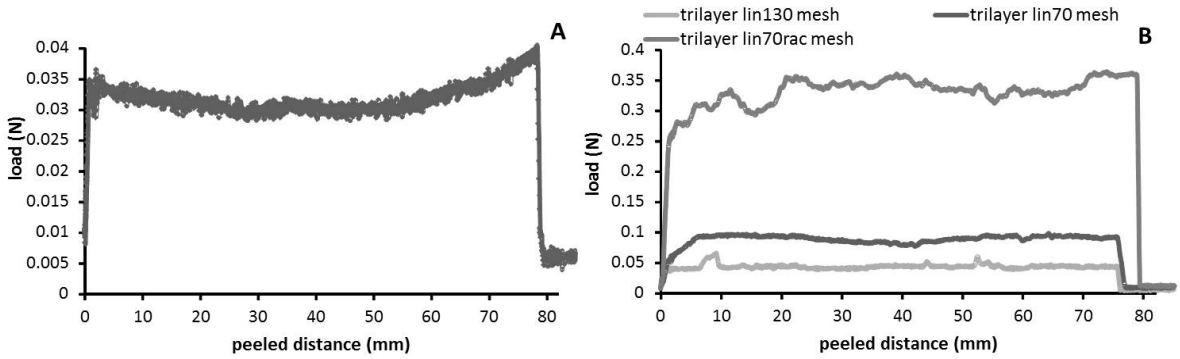

Figure 7.7 *Load – distance diagrams of the t-peel test of the bilayer (A) and the trilayers with various PLA-PEG-PLA mesh (B) with 3 % alginate.*

The load – distance diagrams of the trilayers showed more inequalities during the load plateau in comparison to the bilayers due to naturally occurring irregularities in the fiber distribution and merging of the fibers with the film during the electrospinning process and in case of the lin130 probably additionally because of the uneven infiltration of the alginate solutions and consequently an inhomogenous membrane. However, the measurements confirmed significantly higher necessary peel strengths to separate the alginate/mesh layer from the PLA film than to separate the bilayers (***Figure 7.8***). Moreover, the cohesion between the layers was stronger the higher the PEG content of the intermediate mesh was and was further increased by the use of the copolymer with racemic PLA chains compared to the PLA-PEG-PLA synthesized with 70:30 L-lactide:D, L-lactide. Although the PLA-PEG-PLA copolymer with 70:30 L-lactide:D, L-lactide PLA is totally amorphous like the copolymer synthesized with completely racemic PLA, a still higher flexibility of the racemic polymer chains[317] may lead to a more flexible orientation of the PEG blocks and consequently enable a more consistent infiltration of the hydrophilic alginate solutions. Furthermore, the trilayers prepared with 3 % alginate solutions showed always higher peel strengths than the trilayers prepared with 5 % solutions, which may be attributed to a significantly better infiltration of the alginate solution into the mesh due to the lower viscosity of the solution and consequently a more stable connection of the different layers. In conclusion, the conducted t-peel test nicely illustrated the successful realization of the desired cohesion promotion between PLA film and alginate by means of an intermediate electrospun mesh layer and confirmed the best results for the trilayer consisting of a PLA film with the PLA-PEG-PLA

mesh with the highest investigated PEG content and racemic PLA chains and an alginate layer prepared with a 3 % solution.

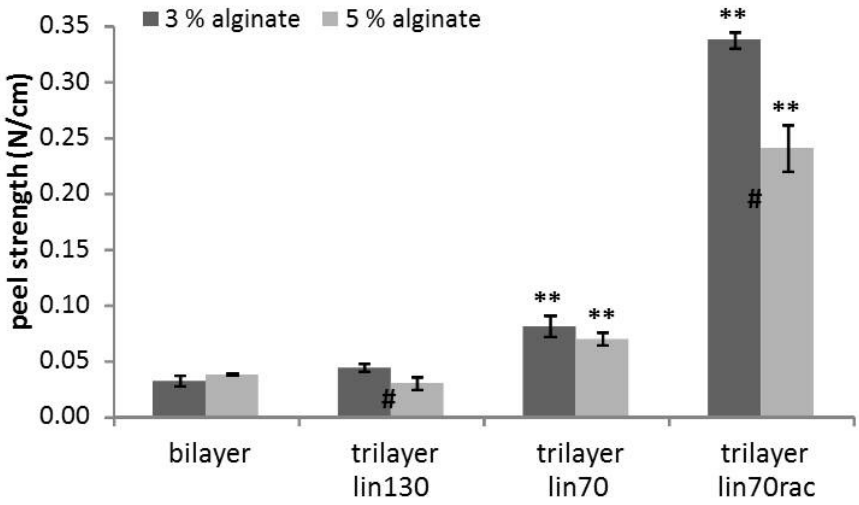

Figure 7.8 *Peel strengths of bilayers and trilayers.*
******** *indicates a significant difference to the bilayer with similar alginate coating.*
# *indicates a significant difference between coatings with 3 % and 5 % alginate.*

7.2.3 Bioadhesion test

A specially designed bioadhesion test was performed to evaluate the desired better adhesion to tissue surfaces of a side made of alginate, which is known for its mucoadhesiveness due to the formation of hydrogen bonds with mucin-type glycoproteins,[318] in comparison to the smooth PLA surface. As bioadhesive polymeric systems have been widely investigated especially for targeted drug delivery formulations through mucosal membranes like for buccal, ophthalmic, vaginal, nasal or intestinal delivery,[319] the implementation of a comparable standardized test setup to evaluate the bioadhesive strength is of high interest. However, despite the findings of Wong et al.[243] that the outcomes of adhesion measurements depend on instrument variables such as contact force, contact time and speed of the probe during removal, up to now there is no agreed standard test method.[249,319] As a consequence, an appropriate test method was developed that was tailored to the intended application as physical barrier device for the prevention of postsurgical adhesions. Since adhesions often affect the small intestine and lead to small bowel obstructions,[20] the outside of a small intestine of a male domestic pig was chosen as test surface for the mucoadhesive properties of the prepared membranes and the alginate sides of the trilayers were tested in comparison to a simple PLA film. During the test, no

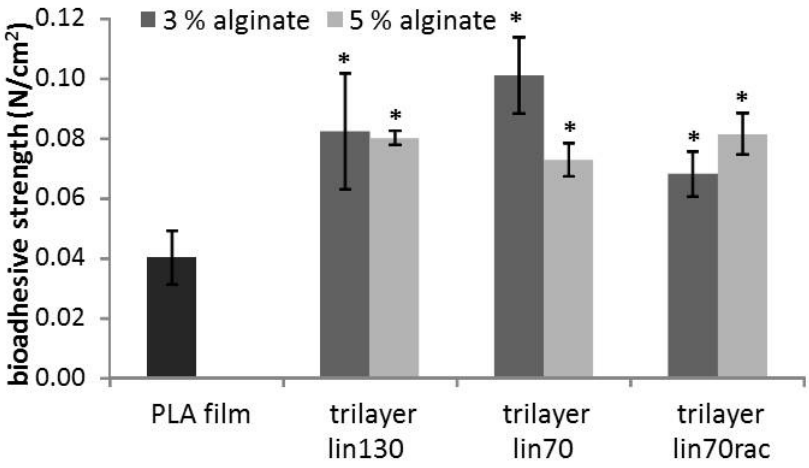

Figure 7.9 *Results of the bioadhesion test.*
******* *indicates a significant difference to the PLA film.*

separation of the individual layers of the trilayers was observed but only the detachment forces of the alginate layer from the small intestine were determined indicating that the achieved cohesion forces between the layers were sufficient for the mechanical stability of the whole construct. Thereby, all investigated alginate sides of the trilayers resulted in bioadhesive strengths around twice as high as the unmodified PLA film, which illustrates a significantly better adhesion to the intestine for the trilayers (***Figure 7.9***). The results confirm the bioadhesive properties of the alginate and that the PLA film becomes stickier to tissue surfaces by a modification with this natural polysaccharide on one side. The higher bioadhesive strength may lead to a prolongation of the residence time of the membrane on the site of injury and successfully facilitate the application by the surgeon as the membrane does not slip out of place during suturing. However, the here utilized un-cross-linked alginate is highly water soluble and consequently potentially quickly washed away so that persistence during the entire time of wound healing without any fixation is questionable without further adaptions. A possible cross-linking of the alginate can improve the stability and persistence by making the layer less water soluble but with increasing cross-linking the mucoadhesive properties are also diminished.[239] As a consequence, following studies for an eventual necessary further improvement of the bilateral PLA/alginate membranes will have to deal both with the nontrivial development of an appropriate test set-up for the quantification of the residence time of the membrane on tissue surfaces and with the achievement of an appropriate balance between layer stability and bioadhesive strength at the application site.

7.3 Summary and conclusions

In conclusion, promising bilateral PLA/alginate membranes for the prevention of post-surgical adhesions were established. Thereby, the aim was to cover a smooth PLA film, that keeps the affected tissues and organs glidingly separated, on one side with the mucoadhesive natural polysaccharide alginate to achieve a one-sided attachment of the membrane on the site of injury to facilitate surgical handling or ideally make an additional fixation redundant. Solution electospun PLA-PEG-PLA copolymer meshes as intermediate layer proved to be versatile tools to promote the cohesion between the otherwise easily separable layers of PLA film and alginate, while a mere surface modification with a PLA mesh without chemical modification did not improve the cohesion. With increasing PEG content of the mesh, infiltration of the alginate solution during the manufacturing process was facilitated which led to uniform membranes with improved mechanical properties, adequate peel strengths proving a good cohesion between the layers and enhanced bioadhesive properties that may prolong the residence time on tissue surfaces. Since solutions with lower alginate concentration (3 %) led to a better embedding of the fibers because of an easier infiltration due to a lower viscosity, a PLA film with an electrospun mesh of the PLA-PEG-PLA with the highest PEG content and racemic PLA chains (lin70rac) as cohesion promoter and an alginate coating with a 3 % solution turned out to be the best suited combination of the investigated trilayers. Apart from an enhanced bioadhesiveness, the achieved combination of lipophilic with hydrophilic polymer layers could be further beneficial with regard to a modified drug release. For a final evaluation of the actual effectiveness of the developed trilayers, with or without drug loading, subsequent animal studies are necessary.

Chapter 8
Summary, conclusions and outlook

In this chapter, the main points of the thesis are summarized in English as well as in German. Furthermore, the main conclusions from the results of the conducted experiments with an outlook on further necessary steps for the development of an ideal barrier device are given.

8.1 Summary/Zusammenfassung

8.1.1 Summary

An ideal barrier device for the prevention of postsurgical adhesions should fulfill several requirements in order to effectively perform in a patient. At first it should be highly biocompatible causing as little foreign body reactions and inflammation as possible. Second, the device should efficiently separate the affected tissues and completely and stably cover the site of injury over the time of wound healing. Then, it should be easy to handle both in open procedures and in laparoscopic surgery. Ideally, the applied material is biodegradable and can be completely absorbed and remodeled by the body so that no further surgical intervention is necessary to remove it from the patient.[1] Regardless of the size of the injury peritoneal wound healing typically takes place within only five to ten days[15–16] so that this time period would represent the required minimum for an ideal barrier to stay intact. However, since a too fast degradation can also promote inflammation and adhesiogenicity,[76] a slightly longer degradation time clinically seems to be more appropriate. A further preferred property of an ideal barrier device is that it stays in place without further fixation by sutures, since suturing additionally enhances adhesion formation.[11] By loading the barrier with pharmacologically active substances depending on the nature of the drug an additional positive effect such as reduction of infection and subsequent inflammation or alternatively a promotion of the wound healing process can be anticipated.

The aim of this thesis was to develop new barrier devices that show improved properties compared to the clinically applied PLA films (Surgiwrap®) and fulfill most of the above described requirements. Therefore, apart from biodegradable PLA, different custom-made PEG-PLA copolymers were used in this thesis as base materials for the subsequent barrier preparation. Commercial PLA (Resomer® LR708) was used and analyzed as purchased. PEG-PLA copolymers with various architecture and composition were synthesized via standard ring opening polymerization using tin(II) 2-ethylhexanoate as catalyst. A subsequent characterization via ^{1}H-NMR, GPC and DSC confirmed the desired polymer compositions and molecular weights as well as the amorphous nature of the synthesized polymers (***Chapter 4***). The polymers were then further processed into solvent cast films as well as solution electrospun meshes of different thickness and dimensions.

Investigations on 20 µm thick solvent cast films confirmed that through the copolymerization of PLA with hydrophilic PEG the barrier properties can successfully be tailored. Due to a higher water uptake, the degradation time was significantly shorter for PEG-PLA films than for PLA films and with an appropriate PEG content could be adjusted to the desired time frame. Moreover, potentially adequate mechanical properties for surgical handling as well as for the performance within the patient's body were achieved. Thereby, shorter degradation times were obtained for star-shaped than for linear copolymers due to smaller initial degradation products which can be washed out faster, but a longer persistence of the mechanical properties over time was achieved for star-shaped copolymers due to a better anchorage of the plasticizing PEG. *In vitro* release studies and an agar diffusion test with triclosan loaded films demonstrated further that due to a higher water uptake the release rate and the antibacterial efficacy were also enhanced for PEG-PLA films in contrast to pure PLA films (***Chapter 5***).

The experiments with solution electrospun meshes revealed a massively higher water uptake of the meshes than of the solid films due to their high initial porosity. Moreover, shorter degradation times for most of the tested polymers in comparison to films with similar thickness made of the same polymer were observed which can be attributed to the higher specific surface and the overall smaller polymer content. Nevertheless, for some of the polymers still the desired mesh degradation time was obtained. The meshes shrank to different extents during the degradation study but kept their morphology of separated fibers without occurring coalescence over the investigated time. Mechanical tests demonstrated the high flexibility of the solution electrospun meshes but also revealed that the forces, which 20 µm thick meshes withstand until they rupture or until a surgical suture is pulled out, are too low for a successful application as a monolayer. However, already with 40 µm thick electrospun meshes similar values as for the stable applicable solid films for the suture pullout test indicate appropriate properties with increased mesh thickness. Cell adhesion and viability tests showed the non-toxicity of the clinically used PLA films as well as of PEG-PLA films and meshes. Moreover, the experiments confirmed that L929 cells adhered even less on the PEG-PLA devices than on the purely lipophilic PLA surfaces. A long-term agar diffusion test with drug loaded devices revealed a longer and higher antibacterial efficacy for triclosan loaded meshes than for triclosan loaded films especially if drug loading of the

meshes is realized after the electrospinning process by adding the drug on top and in the pores of the mesh. With an antibacterial efficacy over more than one week especially the prepared meshes appear a quite promising device for a drug eluting membrane, alone or in combination with a burst release layer (***Chapter 6***).

Apart from film and mesh monolayers, bilayered and trilayered membranes with PLA on one side and the mucoadhesive polysaccharide alginate on the other side were prepared with the intention to achieve a device that stays in place without the further need for suturing. With a bioadhesion test on a small intestine of a domestic pig the benefit of an additional alginate side towards the pure PLA film was successfully demonstrated. Optical evaluations and a t-peel test gave proof that the cohesion between the chemically completely different layers was distinctly enhanced and a separation successfully made more difficult by the use of an appropriate PEG-PLA mesh as intermediate cohesion promoting layer where the alginate solution can efficiently infiltrate (***Chapter 7***).

8.1.2 Zusammenfassung

Eine ideale Barrieremembran zur Prävention postoperativer Adhäsionen sollte mehrere Anforderungen erfüllen, um eine effektive Anwendung im Patienten zu gewährleisten. Zunächst sollte sie biokompatibel sein und so wenig Fremdkörper- und Entzündungsreaktionen wie möglich hervorrufen. Außerdem sollte die Barriere die verletzte Stelle während der Heilungsdauer der Wunde komplett bedecken und eine effiziente Trennung der betroffenen Gewebe sicherstellen. Weiterhin sollte die Membran einfach zu handhaben sein und sowohl bei offenen Operationen als auch bei laparoskopischen Eingriffen eingesetzt werden können. Um die Notwendigkeit eines weiteren Eingriffs, bei dem die eingesetzte Membran wieder entfernt wird, zu vermeiden, sollte das verwendete Material idealerweise bioabbaubar sein und vom Körper komplett resorbiert und anschließend verstoffwechselt werden können.[1] Da die peritoneale Wundheilung unabhängig von der Größe der verletzten Stelle innerhalb von fünf bis zehn Tagen abläuft,[15–16] stellt dieser Zeitraum die minimal notwendige Dauer dar, über die eine physikalische Barriere intakt bleiben sollte. Da jedoch ein zu schneller Materialabbau wieder selbst Entzündungsreaktionen und damit verbunden eine Adhäsionsbildung hervorrufen kann,[76] erscheint eine etwas längere Abbauzeit klinisch sinnvoll. Eine weitere erwünschte Eigenschaft einer idealen Barrieremembran ist, dass sie ohne weitere chirurgische Fixierung mit Nahtmaterialien an der betroffenen Stelle verbleibt, da Annähen zusätzlich zur Bildung von Adhäsionen führen kann.[11] Durch eine zusätzliche Beladung der Membran mit pharmakologisch aktiven Substanzen kann, abhängig von der Beschaffenheit des verwendeten Arzneistoffs, ein zusätzlicher positiver Effekt wie die Reduktion von Infektionen und damit verbundener Entzündung oder alternativ die Förderung des Wundheilungsprozesses erzielt werden.

Ziel dieser Arbeit war es, neue Barrieremembranen zu entwickeln, die im Vergleich zu bereits in der Klinik angewendeten PLA-Filmen (Surgiwrap®) verbesserte Eigenschaften zeigen und die meisten der oben beschriebenen Anforderungen erfüllen. Hierzu wurden neben bioabbaubarem PLA verschieden geartete PEG-PLA-Copolymere als Basismaterial für die Herstellung von Barrieremembranen verwendet. Dabei wurde handelsübliches PLA (Resomer® LR708) wie vom Hersteller erhalten benutzt und analysiert. PEG-PLA-Copolymere mit verschiedener Struktur und Zusammensetzung wurden mittels

Ringöffnungspolymerisation unter Einsatz von Zinn(II)-2-ethylhexanoat als Katalysator synthetisiert. Die durchgeführte Charakterisierung per ^{1}H-NMR, GPC und DSC bestätigte die angestrebten Molekulargewichte und Zusammensetzung der synthetisierten Polymere sowie ihre amorphe Beschaffenheit (***Kapitel 4***). Die Polymere wurden anschließend mittels Lösemittel-Gießverfahren zu Filmen und mittels Elektrospinnen zu Vliesen verschiedener Dicke und Größe weiterverarbeitet.

Untersuchungen zu 20 µm dicken Filmen bestätigten, dass durch die Copolymerisation von PLA mit hydrophilem PEG die Eigenschaften der Barriere erfolgreich optimiert werden konnten. Aufgrund höherer Wasseraufnahme war die Abbauzeit von PEG-PLA-Filmen signifikant kürzer als von PLA-Filmen und konnte mit geeignetem PEG-Gehalt auf den gewünschten Zeitraum eingestellt werden. Darüber hinaus wurden adäquate mechanische Eigenschaften sowohl für die Handhabung durch den Chirurgen als auch für das Verhalten im Körper des Patienten erreicht. Dabei wurden aufgrund von initial kleineren Abbauprodukten, die schneller ausgewaschen werden können, für sternförmige Copolymere kürzere Abbauzeiten festgestellt als für lineare, wobei aber durch eine bessere Verankerung des weich-machenden PEGs eine zeitlich längere Aufrechterhaltung der vorteilhaften mechanischen Eigenschaften für sternförmige als für lineare Copolymere erreicht wurde. *In vitro*-Freisetzungsuntersuchungen sowie Agardiffusionstests mit Triclosan-beladenen Filmen zeigten weiterhin, dass aufgrund von höherer Wasseraufnahme die Freisetzungsrate und die antibakterielle Wirksamkeit von PEG-PLA-Filmen gegenüber reinen PLA-Filmen ebenfalls erhöht wurden (***Kapitel 5***).

In den Experimenten mit elektrogesponnenen Vliesen wurde aufgrund ihrer hohen Porosität eine deutlich höhere Wasseraufnahme festgestellt als für die massiven Filme. Darüber hinaus wurden für die meisten Polymere kürzere Abbauzeiten für Vliese als für die entsprechenden Filme aus demselben Polymer beobachtet, was der höheren spezifischen Oberfläche sowie dem generell niedrigeren Polymergehalt der Vliese zugeschrieben werden kann. Dennoch lag die Abbauzeit der Vliese für manche der untersuchten Polymere noch im gewünschten Bereich. Die Vliese schrumpften während des Abbauversuchs in unterschiedlichem Ausmaß, wobei die ursprüngliche Morphologie mit getrennten Fasern dabei jedoch erhalten blieb, ohne dass ein Verschmelzen der Fasern über den Untersuchungszeitraum beobachtet wurde. Mechanische Tests demonstrierten die hohe

Flexibilität der elektrogesponnenen Vliese, zeigten jedoch auch, dass die Kräfte, denen 20 µm dicke Vliese standhalten bis sie reißen oder bis ein chirurgischer Faden ausgerissen wird, zu niedrig sind, als dass die Vliese allein sinnvoll als einschichtige Barriere angewendet werden können. Allerdings konnten mit 40 µm dicken elektrogesponnenen Vliesen bei einem Fadenausreißtest ähnliche Werte erzielt werden wie für die klinisch eingesetzten Filme, was für das Erreichen von zweckmäßigen Eigenschaften für Vliese mit erhöhter Dicke spricht. Zelladhäsions- und Zellviabilitätstests bestätigten darüber hinaus sowohl die Ungiftigkeit der klinisch angewendeten PLA-Filme als auch der PEG-PLA-Filme und -Vliese. Außerdem zeigten die Experimente, dass L929-Zellen schlechter an den hydrophilen PEG-PLA-Membranen haften als an lipophilen PLA-Oberflächen. Ein Langzeit-Agardiffusionstest mit arzneistoffbeladenen Membranen ergab eine länger andauernde und höhere antibakterielle Wirksamkeit für Triclosan-beladene Vliese als für Triclosan-beladene Filme, insbesondere wenn die Arzneistoffbeladung der Vliese erst im Anschluss an den Elektrospinnprozess durch oberflächliches Aufbringen des Arzneistoffs erfolgte. Mit einer antibakteriellen Wirksamkeit über mehr als eine Woche erwiesen sich vor allem die gefertigten Vliese als vielversprechendes Freisetzungssystem, ob alleine oder in Kombination mit einer sehr schnell freisetzenden Schicht (***Kapitel 6***).

Abgesehen von Filmen und Vliesen zur Anwendung als Einzelschicht wurden zweischichtige sowie dreischichtige Membranen hergestellt, die aus einem PLA-Film auf der einen Seite und einer Schicht aus dem mucoadhäsiven Polysaccharid Alginat auf der anderen Seite bestehen, um eine Barrieremembran zu entwickeln, die ohne zusätzliche Fixierung mit chirurgischem Nahtmaterial von alleine am Gewebe haftet. Mit einem Bioadhäsionstest auf einem Stück Schweinedünndarm konnte der Nutzen einer zusätzlichen Alginatschicht gegenüber einem reinen PLA-Film erfolgreich gezeigt werden. Visuelle Begutachtungen und ein T-Peeltest bewiesen, dass die Kohäsion zwischen den chemisch komplett unterschiedlichen Polymerschichten deutlich verbessert und ihre Trennung erfolgreich erschwert wurde, was durch den Einsatz eines geeigneten PEG-PLA-Vlieses als kohäsionsfördernde Zwischenschicht erreicht wurde, in die die Alginatlösung effektiv einsickern kann (***Kapitel 7***).

8.2 Conclusions and outlook/Schlussfolgerungen und Ausblick

8.2.1 Conclusions and outlook

In conclusion, by processing PEG-PLA copolymers to solvent cast films and solution electrospun meshes, promising barrier devices for the prevention of postsurgical adhesions with improved properties compared to PLA films were successfully developed. With an appropriate PEG content and polymer architecture barrier devices were achieved that fulfill the requirements currently postulated for an ideal physical barrier during *in vitro* testing. The prepared devices are biocompatible and biodegradable in an appropriate time frame and possess adequate mechanical properties both for surgical handling and for a decent performance within the patient's body. Moreover, drug release behavior could also be adjusted by varying the PEG content of the used polymer, the morphology of the barrier and the applied procedure of drug loading. By preparing a barrier with a layer of bioadhesive alginate on one side additionally a device was developed that effectively sticks to tissues by itself. However, additional *in vivo* studies are without a doubt necessary to conclusively evaluate the suitability of the developed membranes for adhesion prevention since naturally occurring factors such as the patient's body movement, the actual composition of peritoneal fluids, the presence of other cells or enzymatic activities highly influence the integrity and performance of the device and cannot be mimicked *in vitro*. Moreover, efforts in the development of a modification of the electrospinning process to prevent mesh shrinkage during application or of a feasible preshrink process before usage have to be made to ensure constant mesh dimensions and the coverage of the entire wound area after mesh application. Further investigations are also recommended for the also promising approach of bilateral membranes with one bioadhesive side. Since the utilized un-cross-linked alginate is very bioadhesive but potentially quickly washed away due to its good water solubility, a suitable test system for the determination of the endurance of adhesive properties has to be established and the composition of the adhesive layer as far as necessary adjusted. Moreover, it is advisable to evaluate if the use of PEG-PLA films instead of PLA films as basic layer can also in this case be further beneficial regarding cohesion between the layers and the overall mechanical properties of the device to get a further optimized *in vivo* performance.

8.2.2 Schlussfolgerungen und Ausblick

Durch die Verarbeitung von PEG-PLA-Copolymeren zu aus Lösemittel gegossenen Filmen und elektrogesponnenen Vliesen wurden schlussendlich vielversprechende Barrieremembranen zur Prävention von postoperativen Adhäsionen erfolgreich entwickelt, die verbesserte Eigenschaften im Vergleich zu PLA Filmen aufweisen. Mit geeignetem PEG-Gehalt und Polymerarchitektur wurden Barrieremembranen erzeugt, die den Anforderungen gerecht werden, die aktuell für eine ideale physikalische Barriere für *in vitro*-Untersuchungen angenommen werden. Die hergestellten Membranen sind biokompatibel und bioabbaubar innerhalb eines angemessenen Zeitraums und besitzen geeignete mechanische Eigenschaften sowohl für die Handhabung durch den Chirurgen als auch für eine angemessene Leistung im Körper des Patienten. Darüberhinaus konnte das Freisetzungsverhalten von Arzneistoffen durch die Variation des PEG-Gehalts des verwendeten Polymers, der Morphologie der Barriere und der angewendeten Methode zur Arzneistoffbeladung passend eingestellt werden. Durch die Herstellung einer Barriere mit einer Schicht aus bioadhäsivem Alginat auf einer Seite wurde zusätzlich eine Membran entwickelt, die von selbst am Gewebe haftet. Jedoch sind zweifellos zusätzlich *in vivo*-Studien notwendig, um abschließend die Eignung der entwickelten Membranen für die Prävention von Adhäsionen zu beurteilen, da natürlich vorkommende Faktoren wie Körperbewegungen des Patienten, die tatsächliche Zusammensetzung von peritonealen Flüssigkeiten, die Gegenwart anderer Zellen oder enzymatische Aktivitäten die Integrität und Leistung der Membran stark beeinflussen und *in vitro* nicht nachgeahmt werden können. Daneben sollten Anstrengungen unternommen werden in Richtung einer Modifikation des Elektrospinningprozesses, um ein Schrumpfen des Vlieses während der Applikation zu vermeiden oder in Richtung eines praktikablen Vorschrumpfprozesses vor Gebrauch, um konstante Vliesdimensionen und die Bedeckung der kompletten Wundfläche nach Applikation des Vlieses sicherzustellen. Weitere Untersuchungen sind außerdem empfehlenswert im Hinblick auf den ebenfalls vielversprechenden Ansatz von bilateralen Membranen mit einer bioadhäsiven Seite. Da das verwendete unvernetzte Alginat stark bioadhäsiv ist, aber aufgrund seiner guten Wasserlöslichkeit potenziell schnell weggewaschen wird, sollte ein passendes Testsystem für die Bestimmung der Dauer der adhäsiven Eigenschaften etabliert werden und die Zusammensetzung der adhäsiven Schicht

so gut wie möglich eingestellt werden. Darüberhinaus ist es ratsam zu bewerten, ob die Verwendung von PEG-PLA-Filmen anstelle von PLA-Filmen als Basisschicht auch in diesem Fall von weiterem Nutzen ist in Bezug auf den Zusammenhalt der Schichten und die gesamten mechanischen Eigenschaften des Konstruktes, um eine noch weiter optimierte *in vivo* Leistung zu erreichen.

Bibliography

1. Brochhausen C.; Schmitt V. H.; Rajab T. K.; Planck C. N. E.; Krämer B.; Wallwiener M., et al.: Intraperitoneal adhesions-an ongoing challenge between biomedical engineering and the life sciences. *J. Biomed. Mater. Res.* **2011,** *98,* 143–156.
2. Weibel M.-A.; Majno G.: Peritoneal adhesions and their relation to abdominal surgery. *The American Journal of Surgery* **1973,** *126,* 345–353.
3. Menzies D.; Ellis H.: Intestinal obstruction from adhesions-how big is the problem? *Annals of The Royal College of Surgeons of England* **1990,** *72,* 60–63.
4. Tingstedt B.; Isaksson K.; Andersson E.; Andersson R.: Prevention of Abdominal Adhesions – Present State and What's beyond the Horizon? *Eur Surg Res* **2007,** *39,* 259–268.
5. Koninckx P. R.; Binda M. M.; Corona R.; Molinas C. R.: Postoperative adhesions and their prevention: *Reconstructive and Reproductive Surgery in Gynecology,* Boca Raton, Florida, USA: CRC Press, **2010,** 8–17.
6. Lauder C. I.; Garcea G.; Strickland A.; Maddern G. J.: Abdominal Adhesion Prevention: Still a Sticky Subject. *Dig Surg* **2010,** *27,* 347–358.
7. Awonuga A. O.; Fletcher N. M.; Saed G. M.; Diamond M. P.: Postoperative Adhesion Development Following Cesarean and Open Intra-Abdominal Gynecological Operations: A Review. *Reproductive Sciences* **2011,** *18,* 1166–1185.
8. Diamond M. P.; Freeman M. L.: Clinical implications of postsurgical adhesions. *Hum. Reprod. Update* **2001,** *7,* 567–576.
9. Li Y.; Kissel T.: Synthesis, characteristics and in vitro degradation of star-block copolymers consisting of l-lactide, glycolide and branched multi-arm poly(ethylene oxide). *Polymer* **1998,** *39,* 4421–4427.
10. Godara P.; Milthorpe B.: Surgical Adhesion and Its Prevention: *Comprehensive Biomaterials,* **2011,** 561–572.
11. Wallwiener C. W.; Kraemer B.; Wallwiener M.; Brochhausen C.; Isaacson K. B.; Rajab T. K.: The extent of adhesion induction through electrocoagulation and suturing in an experimental rat study. *Fertility and Sterility* **2010,** *93,* 1040–1044.
12. Bristow R. E.; Montz F.: Prevention of adhesion formation after radical oophorectomy using a sodium hyaluronate-carboxymethylcellulose (HA-CMC) barrier. *Gynecologic Oncology* **2005,** *99,* 301–308.
13. Freedman R. S.; Deavers M.; Liu J.; Wang E.: Peritoneal inflammation - A microenvironment for Epithelial Ovarian Cancer (EOC). *J Transl Med* **2004,** *2,* 23.
14. Epstein F. H.; Singer A. J.; Clark R. A.: Cutaneous Wound Healing. *N Engl J Med* **1999,** *341,* 738–746.
15. Hubbard T. B.; Khan M. Z.; Carag V. R.; Albites V. E.; Hricko G. M.: The pathology of peritoneal repair: its relation to the formation of adhesions. *Ann. Surg.* **1967,** *165,* 908–916.

16. Raftery A. T.: Regeneration of parietal and visceral peritoneum: an electron microscopical study. *Journal of Anatomy* **1973,** *115,* 375–392.
17. Ellis H.; Harrison W.; Hugh T. B.: The healing of peritoneum under normal and pathological conditions. *Br. J. Surg.* **1965,** *52,* 471–476.
18. Boland G. M.; Weigel R. J.: Formation and prevention of postoperative abdominal adhesions. *J. Surg. Res.* **2006,** *132,* 3–12.
19. Liakakos T.; Thomakos N.; Fine P. M.; Dervenis C.; Young R. L.: Peritoneal adhesions: etiology, pathophysiology, and clinical significance. Recent advances in prevention and management. *Dig Surg* **2001,** *18,* 260–273.
20. Attard J.-A. P.; MacLean A. R.: Adhesive small bowel obstruction: epidemiology, biology and prevention. *Can J Surg (Canadian Journal of Surgery)* **2007,** *50,* 291–300.
21. van der Wal J. B. C.; Jeekel J.: Biology of the peritoneum in normal homeostasis and after surgical trauma. *Colorectal Dis* **2007,** *9 Suppl 2,* 9–13.
22. Miller G.; Boman J.; Shrier I.; Gordon P. H.: Etiology of small bowel obstruction. *The American Journal of Surgery* **2000,** *180,* 33–36.
23. Al-Took S.; Platt R.; Tulandi T.: Adhesion-related small-bowel obstruction after gynecologic operations. *American Journal of Obstetrics and Gynecology* **1999,** *180,* 313–315.
24. Swank D. J.; Swank-Bordewijk S. C. G.; Hop W. C. J.; van Erp W. F. M.; Janssen I. M. C.; Bonjer H. J.; Jeekel J.: Laparoscopic adhesiolysis in patients with chronic abdominal pain: a blinded randomised controlled multi-centre trial. *Lancet* **2003,** *361,* 1247–1251.
25. Peters A. A.; Trimbos-Kemper G. C.; Admiraal C.; Trimbos J. B.; Hermans J.: A randomized clinical trial on the benefit of adhesiolysis in patients with intraperitoneal adhesions and chronic pelvic pain. *BJOG:An international journal of O&G* **1992,** *99,* 59–62.
26. Rapkin A. J.: Adhesions and pelvic pain: a retrospective study. *Obstet Gynecol* **1986,** *68,* 13–15.
27. The Practice Committee of the American Society for Reproductive Medicine: Control and prevention of peritoneal adhesions in gynecologic surgery. *Fertility and Sterility* **2006,** *86,* S1–S5.
28. Kresch A. J.; Seifer D. B.; Sachs L. B.; Barrese I.: Laparoscopy in 100 women with chronic pelvic pain. *Obstet Gynecol* **1984,** *64,* 672–674.
29. Ellis H.; Moran B. J.; Thompson J. N.; Parker M. C.; Wilson M. S.; Menzies D., et al.: Adhesion-related hospital readmissions after abdominal and pelvic surgery: a retrospective cohort study. *Lancet* **1999,** *353,* 1476–1480.
30. Lower A. M.; Hawthorn R. J. S.; Emeritus H. E.; O'Brien F.; Buchan S.; Crowe A. M.: The impact of adhesions on hospital readmissions over ten years after 8849 open gynaecological operations: an assessment from the Surgical and Clinical Adhesions Research Study. *BJOG:An international journal of O&G* **2000,** *107,* 855–862.
31. Lower A.: Adhesion-related readmissions following gynaecological laparoscopy or laparotomy in Scotland: an epidemiological study of 24 046 patients. *Human Reproduction* **2004,** *19,* 1877–1885.

32. Parker M. C.; Wilson M. S.; Menzies D.; Sunderland G.; Clark D. N.; Knight A. D.; Crowe A. M.: The SCAR-3 study: 5-year adhesion-related readmission risk following lower abdominal surgical procedures. *Colorect Dis* **2005,** *7,* 551–558.
33. Coleman M. G.; McLain A. D.; Moran B. J.: Impact of previous surgery on time taken for incision and division of adhesions during laparotomy. *Dis. Colon Rectum* **2000,** *43,* 1297–1299.
34. Ray N. F.; Denton W. G.; Thamer M.; Henderson S. C.; Perry S.: Abdominal adhesiolysis: inpatient care and expenditures in the United States in 1994. *J. Am. Coll. Surg.* **1998,** *186,* 1–9.
35. Tingstedt B.; Isaksson J.; Andersson R.: Long-term follow-up and cost analysis following surgery for small bowel obstruction caused by intra-abdominal adhesions. *Br J Surg* **2007,** *94,* 743–748.
36. Menzies D.; Parker M.; Hoare R.; Knight A.: Small bowel obstruction due to postoperative adhesions: treatment patterns and associated costs in 110 hospital admissions. *Ann R Coll Surg Engl* **2001,** *83,* 40–46.
37. van den Tol M. P.; Haverlag R.; van Rossen M. E. E.; Bonthuis F.; Marquet R. L.; Jeekel J.: Glove powder promotes adhesion formation and facilitates tumour cell adhesion and growth. *Br J Surg* **2001,** *88,* 1258–1263.
38. Sjösten A. C.; Ellis H.; Edelstam G. A.: Post-operative consequences of glove powder used pre-operatively in the vagina in the rabbit model. *Hum. Reprod.* **2000,** *15,* 1573–1577.
39. Luijendijk R. W.; Lange D. C. de; Wauters C. C.; Hop W. C.; Duron J. J.; Pailler J. L., et al.: Foreign Material in Postoperative Adhesions. *Annals of Surgery* **1996,** *223,* 242–248.
40. Dowson H. M.; Bong J. J.; Lovell D. P.; Worthington T. R.; Karanjia N. D.; Rockall T. A.: Reduced adhesion formation following laparoscopic versus open colorectal surgery. *Br J Surg* **2008,** *95,* 909–914.
41. Garrard C. L.; Clements R. H.; Nanney L.; Davidson J. M.; Richards W. O.: Adhesion formation is reduced after laparoscopic surgery. *Surg Endosc* **1999,** *13,* 10–13.
42. Luciano A. A.; Maier D. B.; Koch E. I.; Nulsen J. C.; Whitman G. F.: A comparative study of postoperative adhesions following laser surgery by laparoscopy versus laparotomy in the rabbit model. *Obstet Gynecol* **1989,** *74,* 220–224.
43. Gutt C. N.; Oniu T.; Schemmer P.; Mehrabi A.; Büchler M. W.: Fewer adhesions induced by laparoscopic surgery? *Surg Endosc* **2004,** *18,* 898–906.
44. Molinas C. R.; Mynbaev O.; Pauwels A.; Novak P.; Koninckx P. R.: Peritoneal mesothelial hypoxia during pneumoperitoneum is a cofactor in adhesion formation in a laparoscopic mouse model. *Fertil. Steril.* **2001,** *76,* 560–567.
45. Molinas C. R.; Koninckx P. R.: Hypoxaemia induced by CO(2) or helium pneumoperitoneum is a co-factor in adhesion formation in rabbits. *Hum. Reprod.* **2000,** *15,* 1758–1763.
46. Jansen R. P.: Failure of intraperitoneal adjuncts to improve the outcome of pelvic operations in young women. *American Journal of Obstetrics and Gynecology* **1985,** *153,* 363–371.

47. Avsar F. M.; Sahin M.; Aksoy F.; Avsar A.; Aköz M.; Hengirmen S.; Bilici S.: Effects of diphenhydramine HCl and methylprednisolone in the prevention of abdominal adhesions. *The American Journal of Surgery* **2001,** *181,* 512–515.

48. Kucukozkan T.; Ersoy B.; Uygur D.; Gundogdu C.: Prevention of adhesions by sodium chromoglycate, dexamethasone, saline and aprotinin after pelvic surgery. *ANZ Journal of Surgery* **2004,** *74,* 1111–1115.

49. Muzii L.; Marana R.; Brunetti L.; Margutti F.; Vacca M.; Mancuso S.: Postoperative adhesion prevention with low-dose aspirin: effect through the selective inhibition of thromboxane production. *Hum. Reprod.* **1998,** *13,* 1486–1489.

50. Montz F.; Monk B. J.; Lacy S. M.; Fowler J.: Ketorolac Tromethamine, a Nonsteroidal Anti-inflammatory Drug: Ability to Inhibit Post-radical Pelvic Surgery Adhesions in a Porcine Model. *Gynecologic Oncology* **1993,** *48,* 76–79.

51. Nishimura K.; Nakamura R. M.; DiZerega G. S.: Ibuprofen inhibition of postsurgical adhesion formation: A time and dose response biochemical evaluation in rabbits. *Journal of Surgical Research* **1984,** *36,* 115–124.

52. Guvenal T.; Cetin A.; Ozdemir H.; Yanar O.; Kaya T.: Prevention of postoperative adhesion formation in rat uterine horn model by nimesulide: a selective COX-2 inhibitor. *Hum. Reprod.* **2001,** *16,* 1732–1735.

53. Greene A. K.; Alwayn I. P. J.; Nose V.; Flynn E.; Sampson D.; Zurakowski D., et al.: Prevention of Intra-abdominal Adhesions Using the Antiangiogenic COX-2 Inhibitor Celecoxib. *Annals of Surgery* **2005,** *242,* 140–146.

54. Doody K. J.; Dunn R. C.; Buttram V. C.: Recombinant tissue plasminogen activator reduces adhesion formation in a rabbit uterine horn model. *Fertil. Steril.* **1989,** *51,* 509–512.

55. Dörr P.; Vemer H.; Brommer E.; Willemsen W.; Veldhuizen R.; Rolland R.: Prevention of postoperative adhesions by tissue-type plasminogen activator (t-PA) in the rabbit. *European Journal of Obstetrics & Gynecology and Reproductive Biology* **1990,** *37,* 287–291.

56. Vipond M. N.; Whawell S. A.; Scott-Coombes D. M.; Thompson J. N.; Dudley H. A.: Experimental adhesion prophylaxis with recombinant tissue plasminogen activator. *Ann R Coll Surg Engl* **1994,** *76,* 412–415.

57. Dunn R. C.; Mohler M.: Effect of varying days of tissue plasminogen activator therapy on the prevention of postsurgical adhesions in a rabbit model. *J. Surg. Res.* **1993,** *54,* 242–245.

58. Gehlbach D. L.; O'Hair K. C.; Parks A. L.; Rosa C.: Combined effects of tissue plasminogen activator and carboxymethylcellulose on adhesion reformation in rabbits. *Int J Fertil Menopausal Stud* **1994,** *39,* 172–176.

59. Irkorucu O.; Ferahköşe Z.; Memiş L.; Ekinci O.; Akin M.: Reduction of postsurgical adhesions in a rat model: a comparative study. *Clinics (Sao Paulo)* **2009,** *64,* 143–148.

60. Hellebrekers B. W.; Trimbos-Kemper T. C.; Trimbos J. B.; Emeis J. J.; Kooistra T.: Use of fibrinolytic agents in the prevention of postoperative adhesion formation. *Fertil. Steril.* **2000,** *74,* 203–212.

61. Kamel R. M.: Prevention of postoperative peritoneal adhesions. *European Journal of Obstetrics & Gynecology and Reproductive Biology* **2010,** *150,* 111–118.
62. Arikan S.; Adas G.; Barut G.; Toklu A. S.; Kocakusak A.; Uzun H., et al.: An evaluation of low molecular weight heparin and hyperbaric oxygen treatment in the prevention of intra-abdominal adhesions and wound healing. *The American Journal of Surgery* **2005,** *189,* 155–160.
63. Bahadir I.; Oncel M.; Kement M.; Sahip Y.: Intra-Abdominal Use of Taurolidine or Heparin as Alternative Products to an Antiadhesive Barrier (Seprafilm®) in Adhesion Prevention: An Experimental Study on Mice. *Diseases of the Colon & Rectum* **2007,** *50,* 2209–2214.
64. Kutlay J.; Ozer Y.; Isik B.; Kargici H.: Comparative effectiveness of several agents for preventing postoperative adhesions. *World J Surg* **2004,** *28,* 662–665.
65. Ward B. C.; Panitch A.: Abdominal Adhesions: Current and Novel Therapies. *Journal of Surgical Research* **2011,** *165,* 91–111.
66. Bothin C.; Midtvedt T.; Perbeck L.: Orally delivered antibiotics which lower bacterial numbers decrease experimental intra-abdominal adhesions. *Langenbecks Arch Surg* **2003,** *388,* 112–115.
67. Rappaport W. D.; Holcomb M.; Valente J.; Chvapil M.: Antibiotic irrigation and the formation of intraabdominal adhesions. *The American Journal of Surgery* **1989,** *158,* 435–437.
68. Oncel M.; Kurt N.; Remzi F. H.; Sensu S. S.; Vural S.; Gezen C. F., et al.: The Effectiveness of Systemic Antibiotics in Preventing Postoperative, Intraabdominal Adhesions in an Animal Model. *Journal of Surgical Research* **2001,** *101,* 52–55.
69. Flessner M. F.: The transport barrier in intraperitoneal therapy. *Am. J. Physiol. Renal Physiol.* **2005,** *288,* F433-42.
70. Guilak F.; Butler D. L.; Goldstein S. A.; Baaijens F. P.: Biomechanics and mechanobiology in functional tissue engineering. *Journal of Biomechanics* **2014,** *47,* 1933–1940.
71. Moutos F. T.; Freed L. E.; Guilak F.: A biomimetic three-dimensional woven composite scaffold for functional tissue engineering of cartilage. *Nat Mater* **2007,** *6,* 162–167.
72. Hutmacher D. W.: Scaffolds in tissue engineering bone and cartilage. *Biomaterials* **2000,** *21,* 2529–2543.
73. Wilson M. S.; Menzies D.; Knight A. D.; Crowe A. M.: Demonstrating the clinical and cost effectiveness of adhesion reduction strategies. *Colorectal Dis* **2002,** *4,* 355–360.
74. Wilson M. S.: Practicalities and costs of adhesions. *Colorectal Dis* **2007,** *9 Suppl 2,* 60–65.
75. Yeo Y.; Kohane D. S.: Polymers in the prevention of peritoneal adhesions. *European Journal of Pharmaceutics and Biopharmaceutics* **2008,** *68,* 57–66.
76. Yamaoka T.; Takahashi Y.; Fujisato T.; Lee C. W.; Tsuji T.; Ohta T., et al.: Novel adhesion prevention membrane based on a bioresorbable copoly(ester-ether) comprised of poly-L-lactide and Pluronic: in vitro and in vivo evaluations. *J. Biomed. Mater. Res.* **2001,** *54,* 470–479.

77. Wiseman D. M.; Trout J.; Diamond M. P.: The rates of adhesion development and the effects of crystalloid solutions on adhesion development in pelvic surgery. *Fertility and Sterility* **1998,** *70,* 702–711.

78. Sites C. K.; Jensen B. A.; Glock J. L.; Blackman J. A.; Badger G. J.; Johnson J. V.; Brumsted J. R.: Transvaginal ultrasonographic assessment of Hyskon or lactated Ringer's solution instillation after laparoscopy: randomized, controlled study. *J Ultrasound Med* **1997,** *16,* 195–199.

79. Ricaurte E.; Hilgers T. W.: Safety of intraperitoneal 32% dextran 70 as an antiadhesion adjuvant. *J Reprod Med* **1989,** *34,* 535–539.

80. Larsson B.; Lalos O.; Marsk L.; Tronstad S. E.; Bygdeman M.; Pehrson S.; Joelsson I.: Effect of intraperitoneal instillation of 32% dextran 70 on postoperative adhesion formation after tubal surgery. *Acta Obstet Gynecol Scand* **1985,** *64,* 437–441.

81. Watson A.; Vandekerckhove P.; Lilford R.: Liquid and fluid agents for preventing adhesions after surgery for subfertility. *Cochrane Database Syst Rev* **2000,** CD001298.

82. Schnüriger B.; Barmparas G.; Branco B. C.; Lustenberger T.; Inaba K.; Demetriades D.: Prevention of postoperative peritoneal adhesions: a review of the literature. *The American Journal of Surgery* **2011,** *201,* 111–121.

83. Brown C. B.; Luciano A. A.; Martin D.; Peers E.; Scrimgeour A.; DiZerega G. S.: Adept (icodextrin 4% solution) reduces adhesions after laparoscopic surgery for adhesiolysis: a double-blind, randomized, controlled study. *Fertility and Sterility* **2007,** *88,* 1413–1426.

84. Burns J. W.; Skinner K.; Colt J.; Sheidlin A.; Bronson R.; Yaacobi Y.; Goldberg E. P.: Prevention of Tissue Injury and Postsurgical Adhesions by Precoating Tissues with Hyaluronic Acid Solutions. *Journal of Surgical Research* **1995,** *59,* 644–652.

85. Diamond M. P.: Reduction of de novo postsurgical adhesions by intraoperative precoating with Sepracoat (HAL-C) solution: a prospective, randomized, blinded, placebo-controlled multicenter study. The Sepracoat Adhesion Study Group. *Fertil. Steril.* **1998,** *69,* 1067–1074.

86. Dunn R.; Lyman M. D.; Edelman P. G.; Campbell P. K.: Evaluation of the SprayGel™ adhesion barrier in the rat cecum abrasion and rabbit uterine horn adhesion models. *Fertility and Sterility* **2001,** *75,* 411–416.

87. Mettler L.; Audebert A.; Lehmann-Willenbrock E.; Schive-Peterhansl K.; Jacobs V. R.: A randomized, prospective, controlled, multicenter clinical trial of a sprayable, site-specific adhesion barrier system in patients undergoing myomectomy. *Fertility and Sterility* **2004,** *82,* 398–404.

88. Johns D. A.; Ferland R.; Dunn R.: Initial feasibility study of a sprayable hydrogel adhesion barrier system in patients undergoing laparoscopic ovarian surgery. *J Am Assoc Gynecol Laparosc* **2003,** *10,* 334–338.

89. Mais V.: Reduction of postoperative adhesions with an auto-crosslinked hyaluronan gel in gynaecological laparoscopic surgery: a blinded, controlled, randomized, multicentre study. *Human Reproduction* **2006,** *21,* 1248–1254.

90. Mais V.; Cirronis M. G.; Peiretti M.; Ferrucci G.; Cossu E.; Melis G. B.: Efficacy of auto-crosslinked hyaluronan gel for adhesion prevention in laparoscopy and hysteroscopy: a

systematic review and meta-analysis of randomized controlled trials. *European Journal of Obstetrics & Gynecology and Reproductive Biology* **2012,** *160,* 1–5.

91. Lundorff P.: Clinical evaluation of a viscoelastic gel for reduction of adhesions following gynaecological surgery by laparoscopy in Europe. *Human Reproduction* **2004,** *20,* 514–520.
92. Young P.; Johns A.; Templeman C.; Witz C.; Webster B.; Ferland R., et al.: Reduction of postoperative adhesions after laparoscopic gynecological surgery with Oxiplex/AP Gel: a pilot study. *Fertility and Sterility* **2005,** *84,* 1450–1456.
93. FDA Safety Alert - INTERGEL Adhesion Prevention Solution. Silver Spring, MD 20993, USA, April 16, **2003**. Retrieved from http://www.fda.gov/Safety/MedWatch/SafetyInformation/SafetyAlertsforHumanMedicalProducts/ucm169519.htm
94. Gao X.; Deng X.; Wei X.; Shi H.; Wang F.; Ye T., et al.: Novel thermosensitive hydrogel for preventing formation of abdominal adhesions. *Int J Nanomedicine* **2013,** *8,* 2453–2463.
95. Zhang Z.; Ni J.; Chen L.; Yu L.; Xu J.; Ding J.: Biodegradable and thermoreversible PCLA–PEG–PCLA hydrogel as a barrier for prevention of post-operative adhesion. *Biomaterials* **2011,** *32,* 4725–4736.
96. Zhang Y.; Gao C.; Li X.; Xu C.; Zhang Y.; Sun Z., et al.: Thermosensitive methyl cellulose-based injectable hydrogels for post-operation anti-adhesion. *Carbohydrate Polymers* **2014,** *101,* 171–178.
97. Li L.; Wang N.; Jin X.; Deng R.; Nie S.; Sun L., et al.: Biodegradable and injectable in situ cross-linking chitosan-hyaluronic acid based hydrogels for postoperative adhesion prevention. *Biomaterials* **2014,** *35,* 3903–3917.
98. Seprafilm Package Insert, Genzyme Biosurgery, Cambridge, MA, USA, December 2008. Retrieved from http://www.seprafilm.com/SeprafilmPackageInsert.pdf
99. Diamond M. P.; Burns E. L.; Accomando B.; Mian S.; Holmdahl L.: Seprafilm® adhesion barrier: (2) a review of the clinical literature on intraabdominal use. *Gynecol Surg* **2012,** *9,* 247–257.
100. Hirschelmann A.; Tchartchian G.; Wallwiener M.; Hackethal A.; Wilde R. L. de: A review of the problematic adhesion prophylaxis in gynaecological surgery. *Arch. Gynecol. Obstet.* **2012,** *285,* 1089–1097.
101. Franklin R. R.: Reduction of ovarian adhesions by the use of Interceed. Ovarian Adhesion Study Group. *Obstet Gynecol* **1995,** *86,* 335–340.
102. Reid R. L.; Hahn P. M.; Spence J. E.; Tulandi T.; Yuzpe A. A.; Wiseman D. M.: A randomized clinical trial of oxidized regenerated cellulose adhesion barrier (Interceed, TC7) alone or in combination with heparin. *Fertility and Sterility* **1997,** *67,* 23–29.
103. Mais V.; Ajossa S.; Marongiu D.; Peiretti R. F.; Guerriero S.; Melis G. B.: Reduction of adhesion reformation after laparoscopic endometriosis surgery: a randomized trial with an oxidized regenerated cellulose absorbable barrier. *Obstet Gynecol* **1995,** *86,* 512–515.

104. González-Quintero V. H.; Cruz-Pachano F. E.: Preventing adhesions in obstetric and gynecologic surgical procedures. *Rev Obstet Gynecol* **2009,** *2,* 38–45.

105. CollaGUARD Inresa Informationsbroschüre, Inresa Arzneimittel GmbH, Freiburg, Germany, 2012. Retrieved from http://www.inresa.de/sites/default/files/downloads_free/CollaGUARD_Inresa_Broschüre_Juni12.pdf

106. Avital S.; Bollinger T. J.; Wilkinson J. D.; Marchetti F.; Hellinger M. D.; Sands L. R.: Preventing Intra-Abdominal Adhesions With Polylactic Acid Film: An Animal Study. *Diseases of the Colon & Rectum* **2005,** *48,* 153–157.

107. Ersoy E.; Ozturk V.; Yazgan A.; Ozdogan M.; Gundogdu H.: Comparison of the two types of bioresorbable barriers to prevent intra-abdominal adhesions in rats. *J. Gastrointest. Surg.* **2009,** *13,* 282–286.

108. Ersoy E.; Ozturk V.; Yazgan A.; Ozdogan M.; Gundogdu H.: Effect of Polylactic Acid Film Barrier on Intra-Abdominal Adhesion Formation. *Journal of Surgical Research* **2008,** *147,* 148–152.

109. SurgiWrap® Bioresorbable Adhesion Barrier Film Brochure, Mast Biosurgery, USA, 2006. Retrieved from http://www.mastbio.com/pdf/INT-SW-LT-100A_loRes.pdf

110. Lamoutte H.; Chatterji R.: SurgiWrap® MAST Bioresorbable Sheet Usefor the Prevention of Soft Tissue Attachment/Adhesions; A Two Year Experience., 2005.

111. Lamoutte H.; Chatterji R.: Application of SurgiWrap® Bioresorbable Sheet in Laparoscopic Surgery, Cesarean Section, and Findings during Secondary Pelvic Surgery, 2006.

112. Haney A. F.; Hesla J.; Hurst B. S.; Kettel L. M.; Murphy A. A.; Rock J. A., et al.: Expanded polytetrafluoroethylene (Gore-Tex Surgical Membrane) is superior to oxidized regenerated cellulose (Interceed TC7+) in preventing adhesions. *Fertil. Steril.* **1995,** *63,* 1021–1026.

113. The Myomectomy Adhesion Multicenter Study Group: An expanded polytetrafluoroethylene barrier (Gore-Tex Surgical Membrane) reduces post-myomectomy adhesion formation. *Fertil. Steril.* **1995,** *63,* 491–493.

114. Hellebrekers B. W.; Trimbos-Kemper G. C.; van Blitterswijk C. A.; Bakkum E. A.; Trimbos J. B.: Effects of five different barrier materials on postsurgical adhesion formation in the rat. *Hum. Reprod.* **2000,** *15,* 1358–1363.

115. Esser E.; Tessmar J. K. V.: Preparation of well-defined calcium cross-linked alginate films for the prevention of surgical adhesions. *J. Biomed. Mater. Res.* **2013,** *101,* 826–839.

116. Vogels R. R. M.; Bosmans J. W. A. M.; van Barneveld K. W. Y.; Verdoold V.; van Rijn S.; Gijbels M. J. J., et al.: A new poly(1,3-trimethylene carbonate) film provides effective adhesion reduction after major abdominal surgery in a rat model. *Surgery* **2015,** *157,* 1113–1120.

117. Chang J.-J.; Lee Y.-H.; Wu M.-H.; Yang M.-C.; Chien C.-T.: Electrospun anti-adhesion barrier made of chitosan alginate for reducing peritoneal adhesions. *Carbohydrate Polymers* **2012,** *88,* 1304–1312.

118. Zhang J.; Liu H.; Xu H.; Ding J.-X.; Zhuang X.-L.; Chen X.-S., et al.: Molecular weight-modulated electrospun poly(ε-caprolactone) membranes for postoperative adhesion prevention. *RSC Adv* **2014,** *4,* 41696–41704.
119. Dinarvand P.; Hashemi S. M.; Seyedjafari E.; Shabani I.; Mohammadi-Sangcheshmeh A.; Farhadian S.; Soleimani M.: Function of Poly(lactic-co-glycolic acid) Nanofiber in Reduction of Adhesion Bands. *Journal of Surgical Research* **2012,** *172,* e1–e9.
120. Rodgers K. E.; Johns D. B.; Girgis W.; diZerega G. S.: Prevention of adhesion formation with intraperitoneal administration of tolmetin and hyaluronic acid. *J Invest Surg* **1997,** *10,* 367–373.
121. Hill-West J. L.; Dunn R. C.; Hubbell J. A.: Local Release of Fibrinolytic Agents for Adhesion Prevention. *Journal of Surgical Research* **1995,** *59,* 759–763.
122. Liu Y.; Li H.; Shu X. Z.; Gray S. D.; Prestwich G. D.: Crosslinked hyaluronan hydrogels containing mitomycin C reduce postoperative abdominal adhesions. *Fertil. Steril.* **2005,** *83 Suppl 1,* 1275–1283.
123. Yeo Y.; Bellas E.; Highley C. B.; Langer R.; Kohane D. S.: Peritoneal adhesion prevention with an in situ cross-linkable hyaluronan gel containing tissue-type plasminogen activator in a rabbit repeated-injury model. *Biomaterials* **2007,** *28,* 3704–3713.
124. Chowdhury S. M.; Hubbell J. A.: Adhesion Prevention with Ancrod Released via a Tissue-Adherent Hydrogel. *Journal of Surgical Research* **1996,** *61,* 58–64.
125. Hubbell J. A.: Hydrogel systems for barriers and local drug delivery in the control of wound healing. *Journal of Controlled Release* **1996,** *39,* 305–313.
126. Yeo Y.; Adil M.; Bellas E.; Astashkina A.; Chaudhary N.; Kohane D. S.: Prevention of peritoneal adhesions with an in situ cross-linkable hyaluronan hydrogel delivering budesonide. *Journal of Controlled Release* **2007,** *120,* 178–185.
127. Kim K.; Luu Y. K.; Chang C.; Fang D.; Hsiao B. S.; Chu B.; Hadjiargyrou M.: Incorporation and controlled release of a hydrophilic antibiotic using poly(lactide-co-glycolide)-based electrospun nanofibrous scaffolds. *Journal of Controlled Release* **2004,** *98,* 47–56.
128. Bölgen N.; Vargel I.; Korkusuz P.; Menceloğlu Y. Z.; Pişkin E.: In vivo performance of antibiotic embedded electrospun PCL membranes for prevention of abdominal adhesions. *J. Biomed. Mater. Res. Part B Appl. Biomater.* **2007,** *81,* 530–543.
129. Wang H.; Li M.; Hu J.; Wang C.; Xu S.; Han C. C.: Multiple Targeted Drugs Carrying Biodegradable Membrane Barrier: Anti-Adhesion, Hemostasis, and Anti-Infection. *Biomacromolecules* **2013,** *14,* 954–961.
130. Zong X.; Li S.; Chen E.; Garlick B.; Kim K.-S.; Fang D., et al.: Prevention of Postsurgery-Induced Abdominal Adhesions by Electrospun Bioabsorbable Nanofibrous Poly(lactide-co-glycolide)-Based Membranes. *Annals of Surgery* **2004,** *240,* 910–915.
131. Oh S. H.; Kim J. K.; Song K. S.; Noh S. M.; Ghil S. H.; Yuk S. H.; Lee J. H.: Prevention of postsurgical tissue adhesion by anti-inflammatory drug-loaded pluronic mixtures with sol-gel transition behavior. *J. Biomed. Mater. Res.* **2005,** *72,* 306–316.
132. Lee J. H.; Go A. K.; Oh S. H.; Lee K. E.; Yuk S. H.: Tissue anti-adhesion potential of ibuprofen-loaded PLLA–PEG diblock copolymer films. *Biomaterials* **2005,** *26,* 671–678.

133. Corrales F.; Corrales M.; Schirmer C. C.: Preventing intraperitoneal adhesions with vitamin E and sodium hyaluronate/carboxymethylcellulose: a comparative study in rats. *Acta Cir Bras* **2008,** *23,* 36–41.
134. Kaptanoglu L.; Kucuk H.; Yegenoglu A.; Uzun H.; Eser M.; Mentes C.; Kurt N.: Effects of Seprafilm and Heparin in Combination on Intra-Abdominal Adhesions. *Eur Surg Res* **2008,** *41,* 203–207.
135. Dechy-Cabaret O.; Martin-Vaca B.; Bourissou D.: Controlled Ring-Opening Polymerization of Lactide and Glycolide. *Chem. Rev.* **2004,** *104,* 6147–6176.
136. Gupta A.; Kumar V.: New emerging trends in synthetic biodegradable polymers – Polylactide: A critique. *European Polymer Journal* **2007,** *43,* 4053–4074.
137. Thakur K. A. M.; Kean R. T.; Hall E. S.; Kolstad J. J.; Munson E. J.: 1 H NMR Spectroscopy in the Analysis and Characterization of Poly(lactide). *International Journal of Polymer Analysis and Characterization* **1998,** *4,* 379–391.
138. John R. P.; Nampoothiri K. M.; Pandey A.: Fermentative production of lactic acid from biomass: an overview on process developments and future perspectives. *Appl Microbiol Biotechnol* **2007,** *74,* 524–534.
139. Ajioka M.; Suizu H.; Higuchi C.; Kashima T.: Aliphatic polyesters and their copolymers synthesized through direct condensation polymerization. *Polymer Degradation and Stability* **1998,** *59,* 137–143.
140. Ajioka M.; Enomoto K.; Suzuki K.; Yamaguchi A.: The basic properties of poly(lactic acid) produced by the direct condensation polymerization of lactic acid. *J Environ Polym Degr* **1995,** *3,* 225–234.
141. Carothers W. H.; Dorough G. L.; van Natta F. J.: Studies of polymerization and ring formation. X. The reversible polymerization of six-membered cyclic esters. *J. Am. Chem. Soc.* **1932,** *54,* 761–772.
142. Spinu M.; Jackson C.; Keating M. Y.; Gardner K. H.: Material Design in Poly(Lactic Acid) Systems: Block Copolymers, Star Homo- and Copolymers, and Stereocomplexes. *Journal of Macromolecular Science, Part A* **2006,** *33,* 1497–1530.
143. Kricheldorf H. R.; Kreiser-Saunders I.: Polylactones, 19. Anionic polymerization of L-lactide in solution. *Makromol. Chem.* **1990,** *191,* 1057–1066.
144. Kricheldorf H. R.: Syntheses and application of polylactides. *Chemosphere* **2001,** *43,* 49–54.
145. Jedliński Z.; Wałach W.; Kurcok P.; Adamus G.: Polymerization of lactones, 12. Polymerization of L-dilactide and L,D-dilactide in the presence of potassium methoxide. *Makromol. Chem.* **1991,** *192,* 2051–2057.
146. Dittrich V. W.; Schulz R. C.: Kinetik und Mechanismus der ringöffnenden Polymerisation von L(—)-Lactid. *Angew. Makromol. Chemie* **1971,** *15,* 109–126.
147. Kricheldorf H. R.; Dunsing R.: Polylactones, 8. Mechanism of the cationic polymerization of L,L-dilactide. *Makromol. Chem.* **1986,** *187,* 1611–1625.
148. Kricheldorf H. R.; Berl M.; Scharnagl N.: Poly(lactones). 9. Polymerization mechanism of metal alkoxide initiated polymerizations of lactide and various lactones. *Macromolecules* **1988,** *21,* 286–293.

149. Dubois P.; Jacobs C.; Jerome R.; Teyssie P.: Macromolecular engineering of polylactones and polylactides. 4. Mechanism and kinetics of lactide homopolymerization by aluminum isopropoxide. *Macromolecules* **1991,** *24,* 2266–2270.

150. Moon S.-I.; Lee C.-W.; Taniguchi I.; Miyamoto M.; Kimura Y.: Melt/solid polycondensation of l-lactic acid: an alternative route to poly(l-lactic acid) with high molecular weight. *Polymer* **2001,** *42,* 5059–5062.

151. Middleton J. C.; Tipton A. J.: Synthetic biodegradable polymers as orthopedic devices. *Biomaterials* **2000,** *21,* 2335–2346.

152. Nair L. S.; Laurencin C. T.: Biodegradable polymers as biomaterials. *Progress in Polymer Science* **2007,** *32,* 762–798.

153. Södergård A.; Stolt M.: Properties of lactic acid based polymers and their correlation with composition. *Progress in Polymer Science* **2002,** *27,* 1123–1163.

154. Engelberg I.; Kohn J.: Physico-mechanical properties of degradable polymers used in medical applications: A comparative study. *Biomaterials* **1991,** *12,* 292–304.

155. Li S. M.; Garreau H.; Vert M.: Structure-property relationships in the case of the degradation of massive aliphatic poly-(α-hydroxy acids) in aqueous media, Part 3: Influence of the morphology of poly(L-lactic acid). *J Mater Sci: Mater Med* **1990,** *1,* 198–206.

156. Tsuji H.; Ikada Y.: Crystallization from the melt of poly(lactide)s with different optical purities and their blends. *Macromol. Chem. Phys.* **1996,** *197,* 3483–3499.

157. Fukushima K.; Kimura Y.: Stereocomplexed polylactides (Neo-PLA) as high-performance bio-based polymers: their formation, properties, and application. *Polym. Int.* **2006,** *55,* 626–642.

158. Li S. M.; Garreau H.; Vert M.: Structure-property relationships in the case of the degradation of massive aliphatic poly-(α-hydroxy acids) in aqueous media, Part 1: Poly(DL-lactic acid). *J Mater Sci: Mater Med* **1990,** *1,* 123–130.

159. Shih C.: Chain-end scission in acid catalyzed hydrolysis of poly (d,l-lactide) in solution. *Journal of Controlled Release* **1995,** *34,* 9–15.

160. Gunatillake P. A.; Adhikari R.: Biodegradable synthetic polymers for tissue engineering. *Eur Cell Mater* **2003,** *5,* 1-16; discussion 16.

161. Göpferich A.: Mechanisms of polymer degradation and erosion. *Biomaterials* **1996,** *17,* 103–114.

162. Han X.; Pan J.: Polymer chain scission, oligomer production and diffusion: a two-scale model for degradation of bioresorbable polyesters. *Acta Biomater* **2011,** *7,* 538–547.

163. Grizzi I.; Garreau H.; Li S.; Vert M.: Hydrolytic degradation of devices based on poly(DL-lactic acid) size-dependence. *Biomaterials* **1995,** *16,* 305–311.

164. Li S.: Hydrolytic degradation characteristics of aliphatic polyesters derived from lactic and glycolic acids. *J. Biomed. Mater. Res.* **1999,** *48,* 342–353.

165. Tracy M. A.; Ward K. L.; Firouzabadian L.; Wang Y.; Dong N.; Qian R.; Zhang Y.: Factors affecting the degradation rate of poly(lactide-co-glycolide) microspheres in vivo and in vitro. *Biomaterials* **1999,** *20,* 1057–1062.

166. Vert M.; Li S.; Garreau H.: New insights on the degradation of bioresorbable polymeric devices based on lactic and glycolic acids. *Clin Mater* **1992,** *10,* 3–8.

167. Zhang L.; Xiong C.; Deng X.: Miscibility, crystallization and morphology of poly(β-hydroxybutyrate)/poly(d,l-lactide) blends. *Polymer* **1996,** *37,* 235–241.

168. Gajria A. M.; Davé V.; Gross R. A.; P. McCarthy S.: Miscibility and biodegradability of blends of poly(lactic acid) and poly(vinyl acetate). *Polymer* **1996,** *37,* 437–444.

169. Suyatma N. E.; Copinet A.; Tighzert L.; Coma V.: Mechanical and Barrier Properties of Biodegradable Films Made from Chitosan and Poly (Lactic Acid) Blends. *Journal of Polymers and the Environment* **2004,** *12,* 1–6.

170. Correlo V.; Boesel L.; Bhattacharya M.; Mano J.; Neves N.; Reis R.: Properties of melt processed chitosan and aliphatic polyester blends. *Materials Science and Engineering: A* **2005,** *403,* 57–68.

171. Wang N.; Yu J.; Ma X.: Preparation and characterization of thermoplastic starch/PLA blends by one-step reactive extrusion. *Polym. Int.* **2007,** *56,* 1440–1447.

172. Martin O.; Avérous L.: Poly(lactic acid): plasticization and properties of biodegradable multiphase systems. *Polymer* **2001,** *42,* 6209–6219.

173. Li H.; Huneault M. A.: Comparison of sorbitol and glycerol as plasticizers for thermoplastic starch in TPS/PLA blends. *J. Appl. Polym. Sci.* **2011,** *119,* 2439–2448.

174. Tsuji H.; Ikada Y.: Blends of aliphatic polyesters. II. Hydrolysis of solution-cast blends from poly(L-lactide) and poly(ε-caprolactone) in phosphate-buffered solution. *Journal of Applied Polymer Science* **1998,** *67,* 405–415.

175. Simões C. L.; Viana J. C.; Cunha A. M.: Mechanical properties of poly(ε-caprolactone) and poly(lactic acid) blends. *J. Appl. Polym. Sci.* **2009,** *112,* 345–352.

176. Wang L.; Ma W.; Gross R.; McCarthy S.: Reactive compatibilization of biodegradable blends of poly(lactic acid) and poly(ε-caprolactone). *Polymer Degradation and Stability* **1998,** *59,* 161–168.

177. Jain R. A.: The manufacturing techniques of various drug loaded biodegradable poly(lactide-co-glycolide) (PLGA) devices. *Biomaterials* **2000,** *21,* 2475–2490.

178. Singh L.; Kumar V.; Ratner B. D.: Generation of porous microcellular 85/15 poly (dl-lactide-co-glycolide) foams for biomedical applications. *Biomaterials* **2004,** *25,* 2611–2617.

179. Li W.-J.; Laurencin C. T.; Caterson E. J.; Tuan R. S.; Ko F. K.: Electrospun nanofibrous structure: A novel scaffold for tissue engineering. *J. Biomed. Mater. Res.* **2002,** *60,* 613–621.

180. Deng X.; Zhu Z.; Xiong C.; Zhang L.: Synthesis and characterization of biodegradable block copolymers of ε-caprolactone and D,L-lactide initiated by potassium poly(ethylene glycol)ate. *J. Polym. Sci. A Polym. Chem.* **1997,** *35,* 703–708.

181. Huang M.-H.; Li S.; Coudane J.; Vert M.: Synthesis and Characterization of Block Copolymers of ε-Caprolactone and DL-Lactide Initiated by Ethylene Glycol or Poly(ethylene glycol). *Macromol. Chem. Phys.* **2003,** *204,* 1994–2001.

182. Zhu Y.; Leong M. F.; Ong W. F.; Chan-Park M. B.; Chian K. S.: Esophageal epithelium regeneration on fibronectin grafted poly(L-lactide-co-caprolactone) (PLLC) nanofiber scaffold. *Biomaterials* **2007,** *28,* 861–868.

183. Kumar N.; Ravikumar M. N.; Domb A.: Biodegradable block copolymers. *Advanced Drug Delivery Reviews* **2001,** *53,* 23–44.

184. Ruan G.; Feng S.-S.: Preparation and characterization of poly(lactic acid)–poly(ethylene glycol)–poly(lactic acid) (PLA–PEG–PLA) microspheres for controlled release of paclitaxel. *Biomaterials* **2003,** *24,* 5037–5044.

185. Xiao R. Z.; Zeng Z. W.; Zhou G. L.; Wang J. J.; Li F. Z.; Wang A. M.: Recent advances in PEG-PLA block copolymer nanoparticles. *Int J Nanomedicine* **2010,** *5,* 1057–1065.

186. Matsumoto J.; Nakada Y.; Sakurai K.; Nakamura T.; Takahashi Y.: Preparation of nanoparticles consisted of poly(l-lactide)–poly(ethylene glycol)–poly(l-lactide) and their evaluation in vitro. *International Journal of Pharmaceutics* **1999,** *185,* 93–101.

187. Dong Y.; Feng S.-S.: Methoxy poly(ethylene glycol)-poly(lactide) (MPEG-PLA) nanoparticles for controlled delivery of anticancer drugs. *Biomaterials* **2004,** *25,* 2843–2849.

188. Metters A.: Fundamental studies of a novel, biodegradable PEG-b-PLA hydrogel. *Polymer* **2000,** *41,* 3993–4004.

189. Kim S. W.; Jeong B.; Bae Y. H.; Lee D. S.: Biodegradable block copolymers as injectable drug-delivery systems. *Nature* **1997,** *388,* 860–862.

190. Lieb E.; Tessmar J.; Hacker M.; Fischbach C.; Rose D.; Blunk T., et al.: Poly(D,L-lactic acid)-Poly(ethylene glycol)-Monomethyl Ether Diblock Copolymers Control Adhesion and Osteoblastic Differentiation of Marrow Stromal Cells. *Tissue Engineering* **2003,** *9,* 71–84.

191. Lee J. H.; Go A. K.; Oh S. H.; Lee K. E.; Yuk S. H.: Tissue anti-adhesion potential of ibuprofen-loaded PLLA–PEG diblock copolymer films. *Biomaterials* **2005,** *26,* 671–678.

192. Wang B.-Y.; Fu S.-Z.; Ni P.-Y.; Peng J.-R.; Zheng L.; Luo F., et al.: Electrospun polylactide/poly(ethylene glycol) hybrid fibrous scaffolds for tissue engineering. *J. Biomed. Mater. Res.* **2012,** *100,* 441–449.

193. Yang D.-J.; Zhang L.-F.; Xu L.; Xiong C.-D.; Ding J.; Wang Y.-Z.: Fabrication and characterization of hydrophilic electrospun membranes made from the block copolymer of poly(ethylene glycol-co-lactide). *J. Biomed. Mater. Res.* **2007,** *82,* 680–688.

194. Cui W.; Zhu X.; Yang Y.; Li X.; Jin Y.: Evaluation of electrospun fibrous scaffolds of poly(dl-lactide) and poly(ethylene glycol) for skin tissue engineering. *Materials Science and Engineering: C* **2009,** *29,* 1869–1876.

195. Sheth M.; Kumar R. A.; Dave V.; Gross R. A.; McCarthy S. P.: Biodegradable polymer blends of poly(lactic acid) and poly(ethylene glycol). *J. Appl. Polym. Sci.* **1997,** *66,* 1495–1505.

196. Reintjes T.: Optimization of biodegradable barrier films for the Prevention of post surgical Adhesions: Dissertation, University of Regensburg, Germany, 2011.

197. Cohn D.; Younes H.: Biodegradable PEO/PLA block copolymers. *J. Biomed. Mater. Res.* **1988,** *22,* 993–1009.

198. Kissel T.; Li Y.; Unger F.: ABA-triblock copolymers from biodegradable polyester A-blocks and hydrophilic poly(ethylene oxide) B-blocks as a candidate for in situ forming hydrogel delivery systems for proteins. *Advanced Drug Delivery Reviews* **2002,** *54,* 99–134.

199. Caliceti P.: Pharmacokinetic and biodistribution properties of poly(ethylene glycol)–protein conjugates. *Advanced Drug Delivery Reviews* **2003,** *55,* 1261–1277.

200. Choi Y. K.; Bae Y. H.; Kim S. W.: Star-Shaped Poly(ether−ester) Block Copolymers: Synthesis, Characterization, and Their Physical Properties. *Macromolecules* **1998,** *31,* 8766–8774.

201. Calhoun CJ, Holmes RE, Kleinhenz KK: Resorbable Thin Membranes (US7947300 B2), May 24, **2011.**

202. Jenkins W. A.; Osborn K. R.: Plastic films: Technology and packaging applications. Boca Raton, Florida, USA: CRC Press LLC, **1992**.

203. Felton L. A.: Mechanisms of polymeric film formation. *International Journal of Pharmaceutics* **2013,** *457,* 423–427.

204. Banker G. S.: Film coating theory and practice. *J. Pharm. Sci.* **1966,** *55,* 81–89.

205. Wicks Z. W.; Jones F. N.; Pappas S. P.; Wicks D. A.: Organic coatings: Science and technology. Hoboken, N.J: John Wiley & Sons, **2007**.

206. Siemann U.: Solvent cast technology – a versatile tool for thin film production: *Scattering Methods and the Properties of Polymer Materials,* Berlin Heidelberg, Germany: Springer, **2005,** 1–14.

207. Preis M.; Knop K.; Breitkreutz J.: Mechanical strength test for orodispersible and buccal films. *International Journal of Pharmaceutics* **2014,** *461,* 22–29.

208. Formhals A: Process and apparatus for preparing artificial threads (US1975504), October 2, **1934.**

209. Doshi J.; Reneker D. H.: Electrospinning process and applications of electrospun fibers. *Journal of Electrostatics* **1995,** *35,* 151–160.

210. Reneker D. H.; Chun I.: Nanometre diameter fibres of polymer, produced by electrospinning. *Nanotechnology* **1996,** *7,* 216–223.

211. Baji A.; Mai Y.-W.; Wong S.-C.; Abtahi M.; Chen P.: Electrospinning of polymer nanofibers: Effects on oriented morphology, structures and tensile properties. *Composites Science and Technology* **2010,** *70,* 703–718.

212. Li D.; Xia Y.: Electrospinning of Nanofibers: Reinventing the Wheel? *Adv. Mater.* **2004,** *16,* 1151–1170.

213. Taylor G.: Electrically Driven Jets. *Proceedings of the Royal Society A: Mathematical, Physical and Engineering Sciences* **1969,** *313,* 453–475.

214. Sill T. J.; Recum H. A. von: Electrospinning: Applications in drug delivery and tissue engineering. *Biomaterials* **2008,** *29,* 1989–2006.

215. Teo W. E.; Ramakrishna S.: A review on electrospinning design and nanofibre assemblies. *Nanotechnology* **2006,** *17,* R89–R106.

216. Meinel A. J.; Germershaus O.; Luhmann T.; Merkle H. P.; Meinel L.: Electrospun matrices for localized drug delivery: Current technologies and selected biomedical applications. *European Journal of Pharmaceutics and Biopharmaceutics* **2012,** *81,* 1–13.

217. Agarwal S.; Wendorff J. H.; Greiner A.: Use of electrospinning technique for biomedical applications. *Polymer* **2008,** *49,* 5603–5621.

218. Lannutti J.; Reneker D.; Ma T.; Tomasko D.; Farson D.: Electrospinning for tissue engineering scaffolds. *Materials Science and Engineering: C* **2007,** *27,* 504–509.

219. Triclosan - GESTIS Substance database, Institut für Arbeitsschutz der Deutschen Gesetzlichen Unfallversicherung (IFA). Retrieved from http://gestis-en.itrust.de/nxt/gateway.dll?f=templates$fn=default.htm$vid=gestiseng:sdbeng

220. Orvos D. R.; Versteeg D. J.; Inauen J.; Capdevielle M.; Rothenstein A.; Cunningham V.: Aquatic toxicity of triclosan. *Environ Toxicol Chem* **2002,** *21,* 1338–1349.

221. Gilbert P.; McBain A. J.: Literature-Based Evaluation of the Potential Risks Associated with Impregnation of Medical Devices and Implants with Triclosan. *Surgical Infections* **2002,** *3,* s55–s63.

222. Levy C. W.; Roujeinikova A.; Sedelnikova S.; Baker P. J.; Stuitje A. R.; Slabas A. R., et al.: Molecular basis of triclosan activity. *Nature* **1999,** *398,* 383–384.

223. McMurry L. M.; Oethinger M.; Levy S. B.: Triclosan targets lipid synthesis. *Nature* **1998,** *394,* 531–532.

224. Stewart M. J.; Parikh S.; Xiao G.; Tonge P. J.; Kisker C.: Structural basis and mechanism of enoyl reductase inhibition by triclosan. *J. Mol. Biol.* **1999,** *290,* 859–865.

225. Fang J.-L.; Stingley R. L.; Beland F. A.; Harrouk W.; Lumpkins D. L.; Howard P.: Occurrence, Efficacy, Metabolism, and Toxicity of Triclosan. *Journal of Environmental Science and Health, Part C* **2010,** *28,* 147–171.

226. Sanches-Silva A.; Sendón-García R.; López-Hernández J.; Paseiro-Losada P.: Determination of triclosan in foodstuffs. *J. Sep. Science* **2005,** *28,* 65–72.

227. Agüera A.; Fernández-Alba A. R.; Piedra L.; Mézcua M.; Gómez M.: Evaluation of triclosan and biphenylol in marine sediments and urban wastewaters by pressurized liquid extraction and solid phase extraction followed by gas chromatography mass spectrometry and liquid chromatography mass spectrometry. *Analytica Chimica Acta* **2003,** *480,* 193–205.

228. Bhargava H.; Leonard P. A.: Triclosan: Applications and safety. *American Journal of Infection Control* **1996,** *24,* 209–218.

229. Barbolt T. A.: Chemistry and safety of triclosan, and its use as an antimicrobial coating on Coated VICRYL* Plus Antibacterial Suture (coated polyglactin 910 suture with triclosan). *Surg Infect (Larchmt)* **2002,** *3 Suppl 1,* S45-53.

230. Galal I.; El-Hindawy K.: Impact of using triclosan-antibacterial sutures on incidence of surgical site infection. *The American Journal of Surgery* **2011,** *202,* 133–138.

231. Rothenburger S.; Spangler D.; Bhende S.; Burkley D.: In Vitro Antimicrobial Evaluation of Coated VICRYL* Plus Antibacterial Suture (Coated Polyglactin 910 with Triclosan) using Zone of Inhibition Assays. *Surgical Infections* **2002,** *3,* s79–s87.

232. Jones R. D.; Jampani H. B.; Newman J. L.; Lee A. S.: Triclosan: A review of effectiveness and safety in health care settings. *American Journal of Infection Control* **2000,** *28,* 184–196.

233. Suller M. T. E.: Triclosan and antibiotic resistance in Staphylococcus aureus. *Journal of Antimicrobial Chemotherapy* **2000,** *46,* 11–18.

234. Yueh M.-F.; Taniguchi K.; Chen S.; Evans R. M.; Hammock B. D.; Karin M.; Tukey R. H.: The commonly used antimicrobial additive triclosan is a liver tumor promoter. *Proc Natl Acad Sci USA* **2014,** *111,* 17200–17205.

235. Fukuhira Y.; Ito M.; Kaneko H.; Sumi Y.; Tanaka M.; Yamamoto S.; Shimomura M.: Prevention of postoperative adhesions by a novel honeycomb-patterned poly(lactide) film in a rat experimental model. *J. Biomed. Mater. Res. Part B Appl. Biomater.* **2008,** *86,* 353–359.

236. Weis C.; Odermatt E. K.; Kressler J.; Funke Z.; Wehner T.; Freytag D.: Poly(vinyl alcohol) membranes for adhesion prevention. *J. Biomed. Mater. Res.* **2004,** *70,* 191–202.

237. Medisse Medical Technology: FlexiSurge Adhesion Barrier [Online]. Netherlands, 2015 Retrieved from http://www.medisse.com/products/adhesion-barrier/.

238. Park S.-N.; Jang H. J.; Choi Y. S.; Cha J. M.; Son S. Y.; Han S. H., et al.: Preparation and characterization of biodegradable anti-adhesive membrane for peritoneal wound healing. *J Mater Sci: Mater Med* **2007,** *18,* 475–482.

239. Cho W. J.; Oh S. H.; Lee J. H.: Alginate Film as a Novel Post-Surgical Tissue Adhesion Barrier. *Journal of Biomaterials Science, Polymer Edition* **2010,** *21,* 701–713.

240. Cho W. J.; Oh S. H.; Kim In Gul; Lee C. S.; Lee J. H.: Prevention of Postsurgical Tissue Adhesion by a Bi-layer Membrane Consisting of Adhesion and Lubrication Layers. *Tissue Engineering and Regenerative Medicine* **2010,** *7,* 49–56.

241. Smidsrød O.; Draget K. I.: Alginate gelation technologies: *Food Colloids: Proteins, Lipids and Polysaccharides,* Cambridge, UK: The Royal Society of Chemistry, **1997,** 279–293.

242. Pawar S. N.; Edgar K. J.: Alginate derivatization: A review of chemistry, properties and applications. *Biomaterials* **2012,** *33,* 3279–3305.

243. Wong C. F.; Yuen K. H.; Peh K. K.: An in-vitro method for buccal adhesion studies: importance of instrument variables. *International Journal of Pharmaceutics* **1999,** *180,* 47–57.

244. ASTM International: Standard Test Method for Tensile Properties of Thin Plastic Sheeting. West Conshohocken, PA, **2002** (ASTM D882-02) [Online]. Retrieved from www.astm.org.

245. Radebaugh G. W.; Murtha J. L.; Julian T. N.; Bondi J. N.: Methods for evaluating the puncture and shear properties of pharmaceutical polymeric films. *International Journal of Pharmaceutics* **1988,** *45,* 39–46.

246. Bodmeier R.; Paeratakul O.: Dry and wet strengths of polymeric films prepared from an aqueous colloidal polymer dispersion, Eudragit RS30D. *International Journal of Pharmaceutics* **1993,** *96,* 129–138.

247. Yamada K.; Miyamoto S.; Nagata I.; Kikuchi H.; Ikada Y.; Iwata H.; Yamamoto K.: Development of a dural substitute from synthetic bioabsorbable polymers. *J. Neurosurg.* **1997,** *86,* 1012–1017.

248. ASTM International: Standard Test Method for Peel Resistance of Adhesives (T-Peel Test). West Conshohocken, PA, **2008** (ASTM D1876-08) [Online]. Retrieved from www.astm.org.

249. Nair A. B.; Kumria R.; Harsha S.; Attimarad M.; Al-Dhubiab B. E.; Alhaider I. A.: In vitro techniques to evaluate buccal films. *Journal of Controlled Release* **2013,** *166,* 10–21.

250. Lardner A.: The effects of extracellular pH on immune function. *J. Leukoc. Biol.* **2001,** *69,* 522–530.

251. Steen K. H.; Steen A. E.; Reeh P. W.: A dominant role of acid pH in inflammatory excitation and sensitization of nociceptors in rat skin, in vitro. *J. Neurosci.* **1995,** *15,* 3982–3989.

252. Latch D. E.; Packer J. L.; Stender B. L.; VanOverbeke J.; Arnold W. A.; McNeill K.: Aqueous photochemistry of triclosan: Formation of 2,4-dichlorophenol, 2,8-dichlorodibenzo-p-dioxin, and oligomerization products. *Environ Toxicol Chem* **2005,** *24,* 517.

253. Grove C.; Liebenberg W.; Du Preez J. L.; Yang W.; Villiers M. M. de: Improving the aqueous solubility of triclosan by solubilization, complexation, and in situ salt formation. *J Cosmet Sci* **2003,** *54,* 537–550.

254. Chedgzoy P.; Winckle G.; Heard C. M.: Triclosan: release from transdermal adhesive formulations and in vitro permeation across human epidermal membranes. *International Journal of Pharmaceutics* **2002,** *235,* 229–236.

255. Youxin L.; Kissel T.: Synthesis and properties of biodegradable ABA triblock copolymers consisting of poly(l-lactic acid) or poly (l-lactic-co-glycolic acid) A-blocks attached to central poly (oxyethylene) B-blocks. *Journal of Controlled Release* **1993,** *27,* 247–257.

256. Fox T. G.; Flory P. J.: Second-Order Transition Temperatures and Related Properties of Polystyrene. I. Influence of Molecular Weight. *J. Appl. Phys.* **1950,** *21,* 581.

257. Nagahama K.; Ohya Y.; Ouchi T.: Synthesis of Star-shaped 8 arms Poly(ethylene glycol)-Poly(L-lactide) Block Copolymer and Physicochemical Properties of Its Solution Cast Film as Soft Biomaterial. *Polym J* **2006,** *38,* 852–860.

258. Bourges-Monnier C.; Shanahan M. E. R.: Influence of Evaporation on Contact Angle. *Langmuir* **1995,** *11,* 2820–2829.

259. Roth C. B.; Dutcher J. R.: Glass transition and chain mobility in thin polymer films. *Journal of Electroanalytical Chemistry* **2005,** *584,* 13–22.

260. Bunsell A. R.: Handbook of tensile properties of textile and technical fibres. Oxford: Woodhead Publishing, **2009**.

261. Eyerer P.; Hirth T.; Elsner P. (eds): Polymer Engineering. Berlin, Heidelberg: Springer **2008**.

262. Huang C.; Chen S.; Reneker D. H.; Lai C.; Hou H.: High-Strength Mats from Electrospun Poly(p-Phenylene Biphenyltetracarboximide) Nanofibers. *Adv. Mater.* **2006,** *18,* 668–671.

263. McKee M. G.; Wilkes G. L.; Colby R. H.; Long T. E.: Correlations of Solution Rheology with Electrospun Fiber Formation of Linear and Branched Polyesters. *Macromolecules* **2004,** *37,* 1760–1767.

264. McKee M. G.; Unal S.; Wilkes G. L.; Long T. E.: Branched polyesters: recent advances in synthesis and performance. *Progress in Polymer Science* **2005,** *30,* 507–539.

265. Jaenigen B. M.; Weis C.; Odermatt E. K.; Hopt U. T.; Obermaier R.: The new adhesion prophylaxis membrane A-part®-From in vitro testing to first in vivo results. *J. Biomed. Mater. Res.* **2009,** *89,* 293–299.

266. Nguyen C. T.; Vu-Khanh T.; Dolez P. I.; Lara J.: Puncture of elastomer membranes by medical needles. Part I: Mechanisms. *Int J Fract* **2009,** *155,* 75–81.

267. Zdunek A.; Frankevych L.; Konstankiewicz K.; Ranachowski Z.: Comparison of puncture test, acoustic emission and spatial-temporal speckle correlation technique as methods for apple quality evaluation. *Acta Agrophysica* **2008,** *11,* 303–315.

268. Letaief H.; Rolle L.; Zeppa G.; Gerbi V.: Assessment of grape skin hardness by a puncture test. *J. Sci. Food Agric.* **2008,** *88,* 1567–1575.

269. Bourne M. C.: Texture measurement of individual cooked dry beans by the puncture test. *J Food Science* **1972,** *37,* 751–753.

270. Bussemer T.; Peppas N. A.; Bodmeier R.: Time-Dependent Mechanical Properties of Polymeric Coatings Used in Rupturable Pulsatile Release Dosage Forms. *Drug Development and Industrial Pharmacy* **2003,** *29,* 623–630.

271. ASTM International: Standard Test Method for High Speed Puncture Properties of Plastics Using Load and Displacement Sensors. West Conshohocken, PA, **2000** (ASTM D3763-00) [Online], Retrieved from www.astm.org.

272. Mendes G. C. C.; Brandão T. R. S.; Silva C. L. M.: Ethylene oxide sterilization of medical devices: a review. *Am J Infect Control* **2007,** *35,* 574–581.

273. Plikk P.; Odelius K.; Hakkarainen M.; Albertsson A.: Finalizing the properties of porous scaffolds of aliphatic polyesters through radiation sterilization. *Biomaterials* **2006,** *27,* 5335–5347.

274. Odelius K.; Plikk P.; Albertsson A.-C.: The influence of composition of porous copolyester scaffolds on reactions induced by irradiation sterilization. *Biomaterials* **2008,** *29,* 129–140.

275. Dånmark S.; Finne-Wistrand A.; Schander K.; Hakkarainen M.; Arvidson K.; Mustafa K.; Albertsson A.-C.: In vitro and in vivo degradation profile of aliphatic polyesters subjected to electron beam sterilization. *Acta Biomaterialia* **2011,** *7,* 2035–2046.

276. Martin O.; Avérous L.: Poly(lactic acid): plasticization and properties of biodegradable multiphase systems. *Polymer* **2001,** *42,* 6209–6219.

277. Omelczuk M. O.; McGinity J. W.: The influence of polymer glass transition temperature and molecular weight on drug release from tablets containing poly(DL-lactic acid). *Pharm. Res.* **1992,** *9,* 26–32.

278. Park T. G.; Cohen S.; Langer R.: Poly(L-lactic acid)/Pluronic blends: characterization of phase separation behavior, degradation, and morphology and use as protein-releasing matrixes. *Macromolecules* **1992,** *25,* 116–122.

279. Kim K.; Yu M.; Zong X.; Chiu J.; Fang D.; Seo Y.-S., et al.: Control of degradation rate and hydrophilicity in electrospun non-woven poly(d,l-lactide) nanofiber scaffolds for biomedical applications. *Biomaterials* **2003,** *24,* 4977–4985.

280. Ma D.; McHugh A. J.: The interplay of membrane formation and drug release in solution-cast films of polylactide polymers. *International Journal of Pharmaceutics* **2010,** *388,* 1–12.

281. Lao L. L.; Venkatraman S. S.; Peppas N. A.: Modeling of drug release from biodegradable polymer blends. *European Journal of Pharmaceutics and Biopharmaceutics* **2008,** *70,* 796–803.

282. Jeong B.; Bae Y. H.; Kim S. W.: Drug release from biodegradable injectable thermosensitive hydrogel of PEG–PLGA–PEG triblock copolymers. *Journal of Controlled Release* **2000,** *63,* 155–163.

283. Zong X.; Kim K.; Fang D.; Ran S.; Hsiao B. S.; Chu B.: Structure and process relationship of electrospun bioabsorbable nanofiber membranes. *Polymer* **2002,** *43,* 4403–4412.

284. Gupta P.; Elkins C.; Long T. E.; Wilkes G. L.: Electrospinning of linear homopolymers of poly(methyl methacrylate): exploring relationships between fiber formation, viscosity, molecular weight and concentration in a good solvent. *Polymer* **2005,** *46,* 4799–4810.

285. Lee K.; Kim H.; Bang H.; Jung Y.; Lee S.: The change of bead morphology formed on electrospun polystyrene fibers. *Polymer* **2003,** *44,* 4029–4034.

286. Fong H.; Chun I.; Reneker D.: Beaded nanofibers formed during electrospinning. *Polymer* **1999,** *40,* 4585–4592.

287. Bock N.; Woodruff M. A.; Hutmacher D. W.; Dargaville T. R.: Electrospraying, a Reproducible Method for Production of Polymeric Microspheres for Biomedical Applications. *Polymers* **2011,** *3,* 131–149.

288. Shenoy S. L.; Bates W. D.; Frisch H. L.; Wnek G. E.: Role of chain entanglements on fiber formation during electrospinning of polymer solutions: good solvent, non-specific polymer–polymer interaction limit. *Polymer* **2005,** *46,* 3372–3384.

289. Koombhongse S.; Liu W.; Reneker D. H.: Flat polymer ribbons and other shapes by electrospinning. *J. Polym. Sci. B Polym. Phys.* **2001,** *39,* 2598–2606.

290. Bognitzki M.; Czado W.; Frese T.; Schaper A.; Hellwig M.; Steinhart M., et al.: Nanostructured Fibers via Electrospinning. *Adv. Mater.* **2001,** *13,* 70–72.

291. Megelski S.; Stephens J. S.; Chase D. B.; Rabolt J. F.: Micro- and Nanostructured Surface Morphology on Electrospun Polymer Fibers. *Macromolecules* **2002,** *35,* 8456–8466.

292. Sigma-Aldrich: N,N-Dimethylformamide (Product Number: 227056, Material Safety Data Sheet, Version 7.2) **2015,** January 17 [Online]. Retrieved from https://www.sigmaaldrich.com

293. Sigma-Aldrich: Acetone (Product Number: 650501, Material Safety Data Sheet, Version 5.10) **2015,** January 15 [Online]. Retrieved from http://www.sigmaaldrich.com

294. Sigma-Aldrich: Dichloromethane (Product Number: 32222, Material Safety Data Sheet, Version 7.0) **2015,** February 05 [Online]. Retrieved from http://www.sigmaaldrich.com
295. Wenzel R. N.: Resistance of solid surfaces to wetting by water. *Ind. Eng. Chem.* **1936,** *28,* 988–994.
296. Cassie A. B. D.; Baxter S.: Wettability of porous surfaces. *Trans. Faraday Soc.* **1944,** *40,* 546.
297. Lafuma A.; Quéré D.: Superhydrophobic states. *Nat Mater* **2003,** *2,* 457–460.
298. Yoshimitsu Z.; Nakajima A.; Watanabe T.; Hashimoto K.: Effects of Surface Structure on the Hydrophobicity and Sliding Behavior of Water Droplets. *Langmuir* **2002,** *18,* 5818–5822.
299. Puppi D.; Piras A. M.; Detta N.; Dinucci D.; Chiellini F.: Poly(lactic-co-glycolic acid) electrospun fibrous meshes for the controlled release of retinoic acid. *Acta Biomaterialia* **2010,** *6,* 1258–1268.
300. Lee K.; Kim H.; Khil M.; Ra Y.; Lee D.: Characterization of nano-structured poly(ε-caprolactone) nonwoven mats via electrospinning. *Polymer* **2003,** *44,* 1287–1294.
301. Zussman E.; Rittel D.; Yarin A. L.: Failure modes of electrospun nanofibers. *Appl. Phys. Lett.* **2003,** *82,* 3958.
302. Liu L.-Q.; Tasis D.; Prato M.; Wagner H. D.: Tensile Mechanics of Electrospun Multiwalled Nanotube/Poly(methyl methacrylate) Nanofibers. *Adv. Mater.* **2007,** *19,* 1228–1233.
303. He S.; Li X.; Yang Y.; Jia G.; Zou J.: Correlations of in vitro and in vivo degradation tests on electrospun poly- DL -lactide-poly(ethylene glycol) fibers. *J. Appl. Polym. Sci.* **2012,** *125,* 2207–2215.
304. Zong X.; Ran S.; Kim K.-S.; Fang D.; Hsiao B. S.; Chu B.: Structure and morphology changes during in vitro degradation of electrospun poly(glycolide-co-lactide) nanofiber membrane. *Biomacromolecules* **2003,** *4,* 416–423.
305. Tsuji H.: Autocatalytic hydrolysis of amorphous-made polylactides: effects of l-lactide content, tacticity, and enantiomeric polymer blending. *Polymer* **2002,** *43,* 1789–1796.
306. El-Amin S. F.; Lu H. H.; Khan Y.; Burems J.; Mitchell J.; Tuan R. S.; Laurencin C. T.: Extracellular matrix production by human osteoblasts cultured on biodegradable polymers applicable for tissue engineering. *Biomaterials* **2003,** *24,* 1213–1221.
307. Makadia H. K.; Siegel S. J.: Poly Lactic-co-Glycolic Acid (PLGA) as Biodegradable Controlled Drug Delivery Carrier. *Polymers* **2011,** *3,* 1377–1397.
308. Badami A. S.; Kreke M. R.; Thompson M. S.; Riffle J. S.; Goldstein A. S.: Effect of fiber diameter on spreading, proliferation, and differentiation of osteoblastic cells on electrospun poly(lactic acid) substrates. *Biomaterials* **2006,** *27,* 596–606.
309. Liu H.-C.; Lee I.-C.; Wang J.-H.; Yang S.-H.; Young T.-H.: Preparation of PLLA membranes with different morphologies for culture of MG-63 Cells. *Biomaterials* **2004,** *25,* 4047–4056.

310. Yamaguchi M.; Shinbo T.; Kanamori T.; Wang P.-c.; Niwa M.; Kawakami H., et al.: Surface modification of poly(l-lactic acid) affects initial cell attachment, cell morphology, and cell growth. *J Artif Organs* **2005,** *7,* 187–193.

311. Matlin N. A.; Nuessle A. C.: Dimensional Stabilization of Textile Fabrics. *Ind. Eng. Chem.* **1955,** *47,* 1729–1739.

312. Zilberman M.; Elsner J. J.: Antibiotic-eluting medical devices for various applications. *J Control Release* **2008,** *130,* 202–215.

313. Nosonovsky M.; Bhushan B.: Roughness optimization for biomimetic superhydrophobic surfaces. *Microsyst Technol* **2005,** *11,* 535–549.

314. Chen G.; Liu H.: Electrospun cellulose nanofiber reinforced soybean protein isolate composite film. *J. Appl. Polym. Sci.* **2008,** *110,* 641–646.

315. Wu M.; Wu Y.; Liu Z.; Liu H.: Optically transparent poly(methyl methacrylate) composite films reinforced with electrospun polyacrylonitrile nanofibers. *Journal of Composite Materials* **2012,** *46,* 2731–2738.

316. Tang C.; Liu H.: Cellulose nanofiber reinforced poly(vinyl alcohol) composite film with high visible light transmittance. *Composites Part A: Applied Science and Manufacturing* **2008,** *39,* 1638–1643.

317. Bero M.; Kasperczyk J.: Coordination polymerization of lactides, 5. Influence of lactide structure on the transesterification processes in the copolymerization with ε-caprolactone. *Macromol. Chem. Phys.* **1996,** *197,* 3251–3258.

318. Davidovich-Pinhas M.; Bianco-Peled H.: Alginate–PEGAc: A new mucoadhesive polymer. *Acta Biomaterialia* **2011,** *7,* 625–633.

319. Andrews G. P.; Laverty T. P.; Jones D. S.: Mucoadhesive polymeric platforms for controlled drug delivery. *European Journal of Pharmaceutics and Biopharmaceutics* **2009,** *71,* 505–518.

Danksagung

Zu guter Letzt möchte ich mich bei allen Menschen bedanken, die zum Gelingen dieser Arbeit beigetragen haben.

Großer Dank gebührt in erster Linie Prof. Dr. Achim Göpferich und Prof. Dr. Jürgen Groll, die mir erst die Möglichkeit zur Durchführung dieser Doktorarbeit gegeben haben und vor allem den kurzfristigen und dennoch reibungslosen Wechsel von Regensburg nach Würzburg ermöglicht haben, was nicht selbstverständlich war.

Ferner gilt mein herzlicher Dank Dr. Jörg Teßmar, der mich durchgehend über die ganzen Jahre betreut, unterstützt und motiviert hat. Vor allem dafür, dass ich bei ihm stets nur eine offene Tür einrennen musste um auf ebenso offene Ohren zu stoßen, was hauptsächlich viele lange, fachliche Diskussionen anging, aber auch darüber hinaus.

Des Weiteren möchte ich mich ganz herzlich bei sämtlichen Mitarbeitern der beiden Arbeitskreise aus Regensburg und Würzburg bedanken (auch den hier nicht namentlich erwähnten), wo ich meine Doktorandenzeit verbracht habe. Dafür, dass ich in beiden Arbeitskreisen mehr als herzlich aufgenommen wurde und sie dafür gesorgt haben, dass ich mich sehr wohl gefühlt habe und eine alles in allem schöne Zeit in sehr angenehmer und humorvoller Arbeitsatmosphäre verbringen durfte. Insbesondere die allseits sofortige Hilfsbereitschaft, Verlässlichkeit und Kollegialität sowie die überaus unterhaltsamen Mittagspausen werden mir in guter Erinnerung bleiben.

Im Einzelnen gilt mein Dank dabei besonders allen technischen Mitarbeitern, die stets für gut funktionierende Arbeitsabläufe und zügige Problemlösungen gesorgt haben. Insbesondere möchte ich mich dabei bei Harald Hümpfer, Anton Hofmann und Stefan Kolb bedanken, die gesägt, gezimmert, ausgefräst, etc. und damit geschaffen haben, was ich für diverse Versuche neben Standardequipment benötigt habe. Ferner möchte ich Maria Aniolek und Simone Werner danken, die mich zusammen mit Dr. Andrea Ewald bei den Zellkultur- und mikrobiologischen Untersuchungen unterstützt haben. Mein Dank geht außerdem an Judith Friedlein für die Unterstützung am REM sowie an Isabell Biermann, die in sämtlichen organisatorischen Fragen rund um das Arbeiten im Labor stets eine große Hilfe war.

Mein ganz besonderer Dank gilt meinen Bürokollegen Eva Esser, Michael Schmitz und Matthias Kuhlmann, die viel mehr waren als nur Unterstützung in fachlicher Hinsicht. Eva für ihre aufrichtige Freundschaft und dass sie ihre anfänglich zugeteilt bekommene Rolle der „großen Schwester“ über die Jahre beibehalten und mehr als ausgefüllt hat, indem ich mich immer auf sie verlassen konnte und sie mir stets geholfen hat, wenn an irgendeiner Stelle Hilfe nötig war. Bei Matthias und Michael möchte ich mich v.a. für ihre Unterstützung während der letzten, für mich gesundheitlich bedingt nicht ganz so leichten, Monate bedanken. Dafür, dass sie mit ihrem Humor und Zuspruch diese Zeit für mich wesentlich erträglicher gemacht haben.
Großer Dank gebührt außerdem Susanne Feineis, Simone Stichler, Laura Wistlich und Dr. Ana Sancho, die mich ebenfalls immer aufgebaut haben, als es mir nicht so gut ging und auf die ich mich sowohl in fachlichen als auch in freundschaftlichen Belangen immer verlassen konnte.

Weiterhin möchte ich mich bedanken bei Prof. Dr. Dirk Kurth, Prof. Dr. Gerhard Sextl, Matthias Geist, Bastian Christ und Stephanie Maaß vom Lehrstuhl für Chemische Technologie der Materialsynthese für die Unterstützung bei Messungen am Rheometer und an der DSC. Außerdem gilt mein Dank Prof. Dr. Frank Würthner und Jana Gershberg vom Institut für Organische Chemie für die Hilfsbereitschaft bzgl. GPC-Messungen.
Für die Durchführung und Auswertung von GPC-Messungen mit Verzweigungsanalytik möchte ich mich bei Dr. Bassem Sabagh und Dr. Bernd Tartsch von Malvern Instruments bedanken.
Mein Dank für die finanzielle Unterstützung dieser Arbeit gilt dem BMBF und der Mast Biosurgery AG.

Des Weiteren möchte ich mich noch ganz herzlich bei meiner Familie, insbesondere bei meinen Eltern, und bei meinen Freunden bedanken, die immer ein offenes Ohr für mich hatten und mich immer unterstützt haben.